

NATÁLIA FERNANDA DO COUTO

**CONTRIBUTION OF ENDOTHELIAL CELLS MECHANICAL PROPERTIES,
VESICLE TRAFFICKING AND MEMBRANE REPAIR ABILITY TO THE
DEVELOPMENT OF ATHEROSCLEROSIS: AN *IN VITRO* AND *IN VIVO* STUDY**

Institute of Biological Sciences
Universidade Federal De Minas Gerais

August/2020

NATÁLIA FERNANDA DO COUTO

**CONTRIBUTION OF ENDOTHELIAL CELLS MECHANICAL PROPERTIES,
VESICLE TRAFFICKING AND MEMBRANE REPAIR ABILITY TO THE
DEVELOPMENT OF ATHEROSCLEROSIS: AN *IN VITRO* AND *IN VIVO* STUDY**

Thesis presented to the Graduate Program in Cell Biology of the Morphology Department, Institute of Biological Sciences, Universidade Federal de Minas Gerais, as a partial requirement for obtaining the doctorate degree.

Research field: Cell and structural biology

Advisor: Dra. Luciana de Oliveira Andrade

Co-advisor: Dr. Thiago Castro Gomes

Institute of Biological Sciences

Universidade Federal De Minas Gerais

August/2020

043 Couto, Natália Fernanda do.
Contribution of endothelial cells mechanical properties, vesicle trafficking and membrane repair ability to the development of atherosclerosis: an *in vitro* and *in vivo* study [manuscrito] / Natália Fernanda do Couto. - 2020.

141 f. : il. ; 29,5 cm.

Orientadora: Dra. Luciana de Oliveira Andrade. Coorientador: Dr. Thiago Castro Gomes.

Tese (doutorado) - Universidade Federal de Minas Gerais, Instituto de Ciências Biológicas. Programa de Pós-Graduação em Biologia Celular.

1. Aterosclerose. 2. Receptores de LDL Oxidado. 3. Células Endoteliais. 4. Membrana Celular. I. Andrade, Luciana de Oliveira. II. Gomes, Thiago Castro. III. Universidade Federal de Minas Gerais. Instituto de Ciências Biológicas. IV. Título.

CDU: 576



ATA DA DEFESA DE TESE DE DOUTORADO DE

NATÁLIA FERNANDA DO COUTO

228/2020
entrada
1º/2016
2016706036

Às treze horas do dia 28 de agosto de 2020, reuniu-se, no Instituto de Ciências Biológicas da UFMG, a Comissão Examinadora da Tese, indicada pelo Colegiado do Programa, para julgar, em exame final, o trabalho final intitulado: "CONTRIBUTION OF ENDOTHELIAL CELLS MECHANICS PROPERTIES AND THEIR CONSEQUENCES TO THE DEVELOPMENT OF ATHEROSCLEROSIS: AN IN VITRO AND IN VIVO STUDY", requisito final para obtenção do grau de Doutora em Biologia Celular. Abrindo a sessão, a Presidente da Comissão, **Dra. Luciana de Oliveira Andrade**, após dar a conhecer aos presentes o teor das Normas Regulamentares do Trabalho Final, passou a palavra à candidata, para apresentação de seu trabalho. Seguiu-se a arguição pelos examinadores, com a respectiva defesa da candidata. Logo após, a Comissão se reuniu, sem a presença da candidata e do público, para julgamento e expedição de resultado final. Foram atribuídas as seguintes indicações:

Prof./Pesq.	Instituição	Indicação
Dra. Luciana de Oliveira Andrade	UFMG	APROVADA
Dra. Juliana Alves Silva	UFMG	APROVADA
Dra. Irena Levitan	University of Illinois at Chicago	APROVADA
Dra. Debora Levy	FM / USP	APROVADA
Dra. Virgínia Soares Lemos	UFMG	APROVADA

Pelas indicações, a candidata foi considerada: APROVADA

O resultado final foi comunicado publicamente à candidata pela Presidente da Comissão. Nada mais havendo a tratar, a Presidente encerrou a reunião e lavrou a presente ATA, que será assinada por todos os membros participantes da Comissão Examinadora. **Belo Horizonte, 28 de agosto de 2020.**

Dra. Luciana de Oliveira Andrade (Orientadora) _____

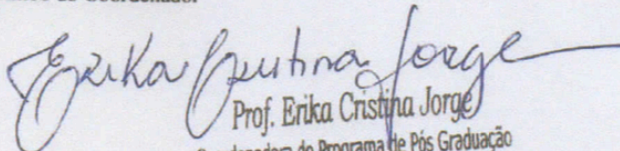
Dra. Juliana Alves Silva _____

Dra. Irena Levitan _____

Dra. Debora Levy _____

Dra. Virgínia Soares Lemos _____

Obs: Este documento não terá validade sem a assinatura e carimbo do Coordenador


Prof. Erika Cristina Jorge
Coordenadora do Programa de Pós Graduação
em Biologia Celular ICB/UFMG

ACKNOWLEDGMENTS

I would like to thank all the funding Agencies: Conselho Nacional de Desenvolvimento Científico e Tecnológico (CNPq), Fundação de Amparo à Pesquisa do Estado de Minas Gerais (FAPEMIG) and, in special, Coordenação de Aperfeiçoamento de Pessoal de Nível Superior (CAPES). To CAPES I acknowledge for granting me with research costs and living expenses during the entire length of my PhD studies and the research exchange fellowship at École Polytechnique Fédérale de Lausanne (EPFL), Switzerland. I am also grateful to INCT-FCx for the scientific collaborations and financial support.

A special thank you to my advisor Prof. Luciana Andrade for the intellectual and personal support through this important phase of my career. I can't thank you enough. Also, to my co-advisor Prof. Thiago Castro Gomes, my sincere acknowledgments for all the discussions and insights on this project. To all LBCM and LGI members for sharing with me innumerable joyful moments at the lab.

I am thankful to Prof. Nikolaos Stergiopoulos for opening the doors of his lab for me and for providing incredible experiences during my one-year research exchange. To my collaborators Dr. Augusto Martins and Dr. Rodrigo Fraga-Silva who intensely helped me with the *in vivo* study. To them and all LHTC members my special thank you for the fantastic year I had over there.

I am also grateful to Centro de Aquisição e Processamento de Imagens (CAPI/ICB) and BioImaging and Optics Platform (BIOP/EPFL) for the use of microscopes and imaging processing systems, to the Histology Core Facility (EPFL) for the use of the cryostat and histological staining solutions, as well as to Centro de Laboratórios Multiusuários do ICB (CELAM – ICB)/UFMG and Center for Gastrointestinal Biology in the name of Dr. Gustavo Batista de Menezes for the use of FACS equipment.

Last but not least, I am specially grateful to my family and friends for all the love and support, for believing in my potential, sometimes even more than I believed myself, and for being there for me in the moments I needed the most. Thank you all!

ABSTRACT

Atherosclerosis is an inflammatory disease caused by subendothelial retention of oxidized LDL (oxLDL), leading to the formation of a plaque. It preferentially develops at areas of vessel bifurcation or curvature, revealing that hemodynamic forces, such as the shear stress generated by blood flow, also work as local risk factors, likely leading to endothelium mechanical injury. It is known that oxLDL modifies cellular biomechanics, inducing cytoskeleton reorganization in cell cortex. This may compromise membrane trafficking events between cytoplasm and cell surface, which in turn can affect cellular functions such as plasma membrane repair. The latter depends on lysosomal fusion with plasma membrane and the subsequent recycling of vesicles. Using *in vitro* and *in vivo* approaches, we evaluated the influence of endothelial cells exposure to oxLDL and hyperlipidemia in cells mechanical modulation, vesicle trafficking, plasma membrane repair and cell susceptibility to injury. Additionally, we evaluated possible contributions of these mechanical alterations together with variations in blood flow shear stress for the development of the atherosclerotic plaque *in vivo*. Our *in vitro* data shows that, in a human umbilical vein endothelial cell line (EAhY926), oxLDL exposure led to actin reorganization and *de novo* polymerization, as well as an increase in cell rigidity and lysosomal exocytosis. Additionally, there was an initial increase in endocytic events rates, likely triggered by the peak of exocytosis induced by both treatments. However, no further endocytic events were observed, suggesting that constitutive endocytosis is blocked upon treatment and that the reorganized cytoskeleton function as a mechanical barrier to membrane traffic. Moreover, the increase in cell rigidity renders cells more prone to mechanical injury. In order to evaluate whether the same was true *in vivo* and if alterations on shear stress pattern would influence these effects, we surgically implanted a shear stress modifier device (cast) on the right carotid (RC) artery of ApoE-knock out (ApoE^{-/-}) mice, an animal model for atherosclerosis studies. The particular shape of the device causes a gradual stenosis in the vessel, resulting in increased shear stress (HSS) in the vessel segment inside the device, a decrease in blood flow and consequently a low shear stress (LSS) region downstream, and a vortex in the upstream region (oscillatory shear stress, OSS). Wild type C57BL/6 mice, as well as the left carotid (LC) of each animal, were used as controls. The data obtained in the present work indicates a tendency of actin fibers accumulation in areas with higher lipid deposition, corroborating with our *in vitro* study. Furthermore, shear stress alone was able to increase cell injury in areas of HSS in the RC of both ApoE^{-/-} and C57BL/6 mice. In this analysis, hyperlipidemia was not determinant to vascular cells susceptibility to injury. However, we speculate that exposing cells to excess of lipids can be prejudicial to their ability in repairing from damage, since lysosomal exocytosis, an important step for PMR, is compromised in ApoE^{-/-} mice. Together, these data show that mechanical modulation induced by oxLDL exposure *in vitro*, as well as hyperlipidemia and variations on shear stress patterns *in vivo*, not only alters membrane traffic in cells, but also makes them more susceptible to mechanical injury, which may likely contribute to endothelial fragility and thus to the initial steps of atherosclerosis development.

Key-words: oxLDL, atherosclerosis, endothelial cells, shear stress, plasma membrane repair

LIST OF FIGURES

Figure 1: Schematic model of Plasma Membrane Repair.....	20
Figure 2: OxLDL and nLDL SDS-PAGE electrophoresis gel.....	28
Figure 3: Membrane injury and repair assay.....	33
Figure 4: Animal Experimentation.....	35
Figure 5: Experimental timeline.....	36
Figure 6: Methodology used for the quantification of fluorescence intensity in the carotid artery cross-sections.....	39
Figure 7: Actin cytoskeleton organization of endothelial cells upon treatment with oxLDL.....	42
Figure 8: Defocusing microscopy of endothelial cells upon oxLDL treatment.....	44
Figure 9: Quantification of lysosomal exocytosis through activity of β -hexosaminidase in cell culture supernatant.....	45
Figure 10: Quantitative analysis of endocytic events induced by the treatment alone.....	49
Figure 11: Quantitative analysis of compensatory endocytosis, injury level and PMR ability of ECs submitted to mechanical injury.....	53
Figure 12: Schematic illustration of the hypothesis.....	54
Figure 13: Timeline of plaque formation in ApoE ^{-/-} mice.....	57
Figure 14: Actin cytoskeleton staining in carotid artery wall of ApoE ^{-/-} and C57BL/6 mice.....	58
Figure 15: Actin cytoskeleton staining in the endothelium of ApoE ^{-/-} and C57BL/6 mice.....	59
Figure 16: Actin cytoskeleton organization in the vascular wall of ApoE ^{-/-} and C57BL/6 mice.....	60
Figure 17: Level of injury in carotid artery wall of ApoE ^{-/-} and C57BL/6 mice.....	62
Figure 18: Level of injury in the endothelium of ApoE ^{-/-} and C57BL/6 mice.....	63
Figure 19: Lysosomal exocytosis in carotid artery wall of ApoE ^{-/-} and C57BL/6 mice.....	65
Figure 20: Lysosomal exocytosis in the endothelium of ApoE ^{-/-} and C57BL/6 mice...	66
Figure 21: Schematic illustration of vascular cells' response to Hyperlipidaemia and disturbed shear stress patterns.....	77

LIST OF ABBREVIATIONS

ApoE	Apolipoprotein E	PFA	Paraformaldehyde
ApoE ^{-/-}	Apolipoprotein E - knockout	PI	Propidium Iodide
ASM	Acid Sphingomyelinase	PIP2	Phosphatidylinositol (3,4) biphosphate
BAECs	Bovine Aortic Endothelial Cells	PMR	Plasma Membrane Repair
DM	Defocusing Microscopy	RC	Right Carotid Artery
DMEM	Dulbecco's Modified Eagle Medium	ROS	Reactive Oxygen Species
EC	Endothelial Cell	SLO	Streptolysin O
ECM	Extracellular matrix	SMC	Smooth Muscle Cell
eNOS	Endothelial Nitric Oxide Synthase	tSNARE	Target membrane SNARE
F-actin	Filamentous actin	vSNARE	Vesicle membrane SNARE
FBS	Fetal Bovine Serum	VCAM-1	Vascular Adhesion Molecule 1
FI	Fluorescence Intensity	VLDL	Very Low Density Lipoprotein
HBSS	Hank's Balanced Salt Solution	WGA	Wheat Germ Agglutinin
HDL	High Density Lipoprotein	Wpci	Week(s) post cast implantation
HSS	High Shear Stress	WT	Wild Type
HUVEC	Human Umbilical Vein Endothelial Cell		
ICAM-1	Intercellular Adhesion Molecule 1		
LAMP-2	Lysosome Associate Membrane Protein		
Lat-A	Latrunculin-A		
LC	Left Carotid Artery		
LDL	Low Density Lipoprotein		
LOX-1	Lectin-like Oxidized LDL receptor 1		
LSS	Low Shear Stress		
MDA	Malondialdehyde		
MMP	Metalloproteinases		
M β CD	Methyl-beta-cyclodextrin		
nLDL	Native Low Density Lipoprotein		
NO	Nitric Oxide		
ORO	Oil Red O		
OSS	Oscillatory Shear Stress		
oxLDL	Oxidized Low Density Lipoprotein		

SUMMARY

1. LITERATURE REVIEW	8
Cholesterol and membrane microdomains	9
Membrane rafts in membrane-cytoskeleton interaction and cellular biomechanical control	11
Cholesterol, cytoskeleton organization and vesicle exocytosis	12
Lipoproteins, rafts and cell cytoskeleton.....	14
Endothelial dysfunction and its role in atherogenesis.....	16
Mechanism of plasma membrane repair	18
Shear stress and atherosclerosis	20
Shear stress and plaque vulnerability.....	21
2. RATIONALE	23
3. MAIN GOAL.....	26
Specific goals	26
4. MATERIALS AND METHODS	27
5. RESULTS	40
6. DISCUSSION	67
7. CLOSING REMARKS	76
8. ANNEX.....	79
9. REFERENCES.....	134

1. LITERATURE REVIEW

Plasma membrane is a complex structure formed by a lipid bilayer that confers fluidity and restricted permeability, acting as a barrier between the extracellular environment and the cytosol. Lipids are the major components of the plasma membrane and make up about 50% of the bilayer structure (Alberts, 2002). The remainder of this structure consists of proteins and carbohydrates that modify lipids and proteins. Among the lipids that compose the membrane, phospholipids are the most abundant, of which the main ones are phosphoglycerides (phosphatidylethanolamine, phosphatidylserine and phosphatidylcholine) and sphingomyelin. Two other classes of lipids, glycolipids and cholesterol, also have important functions conferring structural and functional characteristics to the lipid bilayer (Alberts, 2002; Head *et al.*, 2014). The amount and disposition of each of these lipids will depend on the type of membrane (plasma or intracellular) and the cell type (Alberts, 2002; Pomorski *et al.*, 2001).

Plasma membrane presents a heterogeneous distribution of lipids along its bilayer, forming an asymmetric arrangement with sphingomyelin and glycolipids abundant on the outer leaflet and phosphoglycerides on the cytosolic leaflet (Van Meer *et al.*, 2009, Pomorski *et al.*, 2001). This distribution is maintained by an active transport of lipids through the lipid bilayer. However, the same does not apply for cholesterol. The movement of cholesterol across the membrane seems not to be related to its concentration in each of the layers, but rather to its high affinity for sphingolipids, being therefore enriched in the non-cytosolic leaflet of the plasma membrane, where they can associate forming ordered membrane microdomains (Van Meer *et al.*, 2009; Lange and Steck, 2016).

The maintenance of this asymmetric arrangement of lipids is important for plasma membrane functions. In addition to acting as a barrier, the lipids that compose the membrane provide other important characteristics, such as the potential for budding, fission and fusion of vesicles, which are fundamental for cell division, reproduction and membrane intracellular trafficking (Van Meer *et al.*, 2009). Furthermore, lipids can act directly on signal transduction processes, as well as recruiting and organizing membrane proteins in microdomains. The latter will participate in cell signalling processes or as effector mechanisms (Van Meer *et al.*, 2009). Thus, changes in lipid distribution generally lead to a physiological response (Pomorski *et al.*, 2001).

Cholesterol and membrane microdomains

The lipid molecules of the plasma membrane can naturally aggregate as specialized regions in the form of microdomains, responsible for important membrane functions. Cholesterol-rich membrane domains, also called membrane rafts, are small domains (10-200nm), rich in sterols and sphingolipids, which cover a large part of the cell surface and are responsible for several cellular functions (Ikonen, 2008; Pike, 2006).

It is assumed that membrane rafts are lipids in an ordered liquid phase, in which sphingolipids associate laterally with each other through weak interactions among carbohydrate heads of glycosphingolipids and through hydrophobic interactions among their saturated fatty acid side chains. Cholesterol fits into free spaces in between sphingolipids lateral fatty acid chains, creating tightly packed regions that help segregating them from the rest of the plasma membrane lipid components (Cremesti *et al.*, 2002). Cholesterol is therefore an essential molecule for the organization and structure of these membrane rafts, conferring special biophysical properties to the cell membrane, forming platforms containing proteins they have affinity to (Ikonen, 2008).

Disorganization of these cholesterol enriched microdomains through their isolation or the use of drugs capable of sequestering cholesterol from plasma membrane have been used to study the role of these specialized regions and their components in several physiological processes (Allen *et al.*, 2007). It has been demonstrated that membrane rafts, due to their lipid composition and association with specific proteins, have different functions and are required in several cellular processes, ranging from cell signaling to membrane trafficking and fusion, as well as participating as a site of interaction and entry for different pathogens (Hanzal-Bayer and Hancock 2007 , Kwik *et al.*, 2003, Lafont and Van der Goot, 2005, Van Meer *et al.*, 2009).

Membrane fusion is a key mechanism in the endocytic and exocytic pathways, which are responsible for maintaining several cellular functions. As mentioned above, it may be also dependent on membrane cholesterol content, especially cholesterol enriched membrane microdomains (Gil *et al.*, 2005; Murray and Tamm, 2010). Membrane fusion is mediated by proteins of the SNARE complex, which are

transmembrane proteins found in both vesicle membrane (vSNARE) and target membrane (tSNARE). Upon pairing, v and tSNARE proteins strongly interact forming a four-helix bundle that leads to the approximation of the two membranes and “catalyzes” their fusion (Alberts, 2002; Murray and Tamm, 2010). The role of membrane rafts in membrane fusion processes was evidenced after observing that vesicle exocytosis was compromised in cholesterol-depleted cells. Also, several proteins from the SNARE complex were found to be associated with these microdomains and their clustering was sensitive to variations in cholesterol content (Lang *et al.*, 2001).

Rafts, in addition to their role in membrane fusion, are also important as sites of cytoskeleton anchorage, through direct or indirect interaction of the latter with these membrane domains. These interactions may work as platforms of communication with the extracellular matrix through integrins, cadherins and other cell adhesion molecules (Byfield *et al.*, 2004, Head *et al.*, 2014). Both microtubules and actin filaments interact with membrane rafts. The role of microdomains in the control of microtubule dynamics is still not well understood, but there are evidences showing the interaction of tubulins (microtubule constituent proteins) with membrane rafts, which seem to associate with caveolins, helping in their stabilization (Allen *et al.*, 2007).

The interaction between rafts and actin cytoskeleton seems to have different roles. First, these microdomains seem to modulate the dynamics of actin filaments. Some lipids, such as phosphatidylinositol (4,5) biphosphate and phosphatidylinositol (3,4) biphosphate (PIP2), are found enriched in membrane rafts and are known for their binding to actin and for conducting the assembly of actin filaments, functioning as binding sites of these filaments to the plasma membrane (Allen *et al.*, 2007). On the other hand, actin also has an important role in the clustering of signaling molecules, such as G proteins (Rho-GTPases, for example), in the membrane rafts. These proteins control the shape of the cell in response to external signals by changing its position within the rafts and consequently modifying the actin cytoskeleton. They also control signaling pathways for cell development and survival (Allen *et al.*, 2007).

Membrane rafts in membrane-cytoskeleton interaction and cellular biomechanical control

As mentioned, cholesterol enriched membrane microdomains have lipid components and proteins that regulate the association between plasma membrane and the cytoskeleton, controlling the sites of cell adhesion and cytoskeletal organization (Allen *et al.*, 2007; Head *et al.*, 2014; Hong *et al.*, 2012; Levitan e Gooch, 2007).

In 1998, Pike and Miller showed that the disruption of membrane rafts by cholesterol depletion leads to a reduction in PIP2 levels, which in turn changes the cortical actin cytoskeleton organization. Later, Kwik and coworkers (2003) observed that acute treatment of fibroblasts with methyl-beta-cyclodextrin (M β CD) caused changes in the organization and activity of actin and actin modifying proteins. The authors found higher instability of cytoplasmic actin when compared to untreated controls, as well as an increase in actin fibers located at the cell cortex. Several sites of actin polymerization and cytoskeleton microprojections were also observed in treated cells. However, membrane cholesterol interference on actin cytoskeleton organization has been shown not to be solely dependent on its role in PIP2 distribution, but also by its regulation of Rho-GTPase family activation (reviewed by Levitan and Gooch, 2007). Qi and coworkers. (2009) evaluated the effect of MC3T3 cells treatment with M β CD on Rho-A activation. The authors observed that cholesterol depletion led to a substantial increase in active Rho-A after 30 minutes of treatment and this activation continued to increase up to 60 minutes of incubation with M β CD. The downstream effector of Rho-A, Rho-kinase, was also activated by M β CD treatment and its inhibition prevented the formation of stress fibers in treated cells.

It was also observed that membrane cholesterol depletion of bovine aortic endothelial cells (BAECS) by M β CD treatment, followed by the addition of exogenous PIP2, altered PIP2 membrane distribution to a more uniform pattern and increased cytoskeleton adhesion to cellular membrane (Hong *et al.*, 2012). The direct change in PIP2 levels did not result in any effect on membrane-cytoskeletal adhesion, indicating that the role of PIP2 in this interaction is regulated by plasma membrane cholesterol. Corroborating with these findings, Hissa and coworkers (2013) demonstrated that cholesterol depletion altered the organization of actin cytoskeleton via activation of Rho-A, with increased stress fiber formation. This increase in the

number of stress fibers induced by cholesterol depletion was shown to be due to both reorganization of preexisting filaments and polymerization of new actin filaments (Hissa *et al.*, 2013).

Since cholesterol-rich microdomains concentrate lipids and proteins involved in the organization, modulation and metabolism of actin cytoskeleton, several authors have investigated the participation of these regions in the dynamics of cellular mechanics. These studies have shown the effects of plasma membrane cholesterol sequestration on the mechanical modulation of different cell types. Byfield and coworkers (2004) observed that the decrease in membrane cholesterol content of BAECs, by the action of M β CD, resulted in increased membrane stiffness. When cholesterol was restored, the elastic properties of the membrane were completely recovered. The authors further showed that treatment of these cells with Latrunculin-A (Lat-A), a drug that compromise the association of actin in filaments, suppressed the effects of cholesterol depletion, suggesting that the effect on cell stiffness is dependent on the integrity of actin fibers. These results indicated that the observed increase in cell rigidity was due to changes in the properties of the cytoskeleton and its interaction with the membrane. The same cholesterol depletion effect on membrane stiffness was observed in fibroblasts. M β CD treatment altered the surface tension and elastic modulus of these cells. The evaluation of mechanical modulation during treatment with M β CD showed an increase in relaxation time and the membrane fluctuation range between 10-30 minutes after drug addition. These results indicate that removal of cholesterol from the membrane of these cells makes them more rigid than untreated controls (Hissa *et al.*, 2013).

As membrane-cytoskeletal interaction plays an essential role in the accomplishment of several functions, it is important to understand the role of membrane cholesterol content and, especially, of membrane rafts in the dynamics of this interaction and how these effects may interfere with other cellular processes.

Cholesterol, cytoskeleton organization and vesicle exocytosis

It has been demonstrated in the literature that the cortical actin cytoskeleton could act as a barrier to vesicle exocytosis or facilitate the exocytosis of preexisting lysosomes near the plasma membrane (Aunis and Bader, 1988; Muallen *et al.*, 1995; Nakata and Hirokawa, 1992, Pendleton and Koffer, 2001, Miklavc *et al.*, 2009).

In 1988, Aunis and Bader already evidenced the existence of two pools of secretory vesicles. A first pool of vesicles was located just below the plasma membrane by binding with elements of the cytoskeleton although its secretion was not regulated by the cytoskeleton. A second pool was attached to the actin filaments, slightly further away from the membrane, which could be mobilized when the first pool was depleted. This second pool of secretory vesicles was exocytosed after depolarization of the membrane. The depolarisation caused both actin filaments rearrangement and vesicles detachment from the cytoskeleton, leading to the dissolution of the cytoskeleton barrier and allowing these vesicles to have access to the exocytosis sites.

Koseoglu and coworkers. (2011) also demonstrated the existence of different pools of secretory vesicles and the influence of membrane cholesterol content on the exocytosis of these pools. The authors observed that membrane cholesterol sequestration from chromaffin cells of the adrenal medulla did not alter either the kinetics or the amount of release of the first pool of vesicles, which was already pre-anchored to the plasma membrane. However, the subsequent release of the remaining vesicles, belonging to the slow release pool, also called the reserve pool, was compromised by changes in membrane cholesterol levels. The authors further suggested that the change in the polymerization of actin filaments induced by cholesterol depletion could be compromising the mobilization of the slow release or reserve vesicles.

Hissa and collaborators (2012), studying the process of *Trypanosoma cruzi* (a protozoan parasite) entry into cardiomyocytes, showed that membrane cholesterol sequestration leads to decreased host cell invasion. Decrease in membrane cholesterol content interfered with lysosome recruitment and fusion during parasite host cell interaction, a key event for *T. cruzi* effective cell infection. However, in their work they observed that pre-treatment of cardiomyocytes with M β CD actually induced a 3.5-fold increase in the frequency of lysosome vesicle exocytosis, as early as 10 minutes upon exposure to the drug when compared to untreated controls. In addition, they observed that treatment with the drug altered lysosomal dispersion, in which lysosomes from M β CD-treated cells showed to be more restricted to the perinuclear area. Replacement of cholesterol was able to reverse this distribution, showing that this was indeed an effect of cholesterol removal from the plasma membrane (Hissa *et al.*, 2012). Together with these findings they showed that there was an increase in actin stress fiber formation in M β CD treated cells. Later, studying

the effect of cholesterol sequestration on fibroblasts, these authors showed that the observed changes in the actin cytoskeleton appear to be responsible for the exocytosis and depletion of the peripheral pool of lysosomes, which is likely the one recruited during parasite host cell entry (Hissa *et al.*, 2013). The analysis of the secretion and distribution of lysosomes after treatment with Lat-A, alone or in combination with M β CD, also indicated that there are probably at least two distinct pools of lysosome vesicles differentially regulated by actin cytoskeleton rearrangement (Hissa *et al.*, 2013).

Although at first Koseoglu's and Hissa's results seem to be contradictory to each other, the involvement of cortical actin cytoskeleton and SNARE proteins suggested by Koseoglu and coworkers seems to be still valid for Hissa's work. In the latter the pool of lysosomal vesicles localized to the cell periphery is exocytosed as the actin cytoskeleton is reorganized, while the following events of lysosomal exocytosis (after drug treatment and upon parasite exposure) are decreased, probably because the reorganized cytoskeleton and the polymerization of new actin filaments may act as a barrier for the mobilization of lysosome vesicles located at the perinuclear region.

Considering the existence of distinct pools of exocytic vesicles in different cell types and the above mentioned effect of actin cytoskeleton reorganization on vesicle fusion with the plasma membrane, it is possible to infer that cholesterol-rich membrane microdomains may also play an important role in the regulation of various membrane trafficking and exocytic events.

Lipoproteins, rafts and cell cytoskeleton

Outside the membrane context, cholesterol and other lipids are found associated with lipoproteins, forming lipoprotein particles, allowing these hydrophobic molecules to be transported through the blood stream and extracellular fluids. These lipoprotein particles are formed by an apolar central portion, consisting mainly of cholesterol ester and triglycerides, surrounded by a layer containing phospholipids, a small amount of non-esterified cholesterol and apoproteins (Walker *et al.*, 1990). Different forms of lipoprotein particles can be identified, among which there are the Very Low Density Lipoproteins (VLDL), Low Density Lipoproteins (LDL) and High Density Lipoproteins (HDL), depending on the amount of lipoproteins/lipids

associated with the particle. LDL, in particular, has been the focus of various studies. Its increase in blood plasma has been implicated as one of the main risk factors for the development of atherosclerosis, an important disease that is usually associated to heart failure. LDL atherogenicity seems to be attributed to modifications that may occur to this particle. These modifications range from changes in lipid composition/oxidation to changes in their conformation and aggregation of particles (Aviram, 1993). These seem to occur through interactions between lipoproteins and blood vessel wall cells, blood cells, plasma constituents and matrix components of the vessel wall. The oxidative modification of LDL (oxLDL) is accompanied by a number of structural and compositional changes that result in several alterations in their physical properties, which in turn increases its pathogenic level, including accelerated recruitment of macrophages, cytotoxicity and chemotactic activity for monocytes (Steinbrecher, Zhang, & Loughheed, 1990).

Recent studies have shown that exposure of endothelial cells to oxLDL in culture considerably alters biomechanical properties of these cells by triggering reorganization of its cytoskeleton, leading to increased cell rigidity (Byfield *et al.*, 2006; Chouinard *et al.*, 2008; Kowalsky *et al.*, 2008). This process occurs similarly to what happens when membrane cholesterol content is depleted by the action of M β CD (Byfield *et al.*, 2004, Hissa *et al.*, 2012).

Cell exposure to oxLDL, however, does not seem to induce significant changes in total amount of cholesterol content at the cell plasma membrane. In this case, it seems there may be small changes in cholesterol content specifically from membrane rafts regions, affecting the organization of lipids in these domains, which consequently alters the biophysical properties of these cells (Shentu *et al.*, 2010). It has been shown that this effect in disrupting membrane rafts come from the oxysterols present in oxLDL molecules. Depending on the amount and type of these oxysterols, the effects may be more or less evident (Shentu *et al.*, 2012). Similarly to cholesterol depletion, oxLDL increase in cell stiffness depends on the organization of the actin cytoskeleton (Byfield *et al.*, 2006), which is mediated by the RhoA/ROCK pathway (Oh *et al.*, 2016). Interestingly, preloading cells with cholesterol prevents these effects (Oh *et al.*, 2016).

Since endothelial cells are in constant mechanical stress generated by the blood flow, it is possible that biomechanical changes induced by endothelial cell exposure to oxLDL may significantly contribute to injuries and alterations in cell viability previously observed by Liao e Granger (1995). It is known that the

endothelium has the property of realigning by reorganizing its actin cytoskeleton, to adapt to the blood flow and distribute the hemodynamic forces, facilitating endothelial integrity (Liao and Granger, 1995). Interestingly, it has been demonstrated that endothelial cells exposed to oxLDL are more responsive to flow realignment than untreated cells, despite its increased cell stiffness. These findings suggest that increased cell rigidity and cytoskeletal stress due to disruption of the membrane rafts result in an increase in the response of these cells to mechanical stimuli, such as those generated by blood flow (Kowalsky *et al.*, 2008).

However, it is not yet known whether these biomechanical changes observed in response to oxLDL exposure, could lead to a greater propensity to injury, possibly affecting endothelial permeability and integrity, contributing to atherogenesis.

Endothelial dysfunction and its role in atherogenesis

Atherogenesis is a degenerative process involving several lesions in the arterial wall. The wall of the arteries is composed of three different layers. The outermost layer of the blood vessel, the adventitial tunica, is composed of connective tissue. The middle layer, or middle tunica, is composed of circularly arranged smooth muscle cells and varying amounts of elastic fibers. More internally there is the intima tunica, consisting of the endothelium, the subendothelial layer (formed by loose connective tissue) and the elastic lamina (Alberts, 2002; Van de Graaff, 2001).

This endothelium that covers the inner wall is responsible for regulating the exchange of substances, as well as blood cells, between the bloodstream and surrounding tissues. Under physiological conditions, endothelial cells prevent the transmigration of blood cells into tissues. However, under stress conditions, such as hyperlipidemia, hypertension or pro-inflammatory factors, these cells increase their permeability, promoting the transmigration of inflammatory cells and the accumulation of lipids in the arterial wall (Libby *et al.*, 2011).

High cholesterol, obesity, hypertension and smoking are four of the major risk factors associated with the development of atherosclerosis (Criqui, 1986; Rodriguez-Flores *et al.*, 2013). In Brazil, atherosclerosis is mainly responsible for the occurrence of cardiovascular diseases and, according to the World Health Organization (WHO), cardiovascular diseases are the leading cause of death in the world, with three-

quarters of these deaths occurring in underdeveloped or developing countries (WHO, 2015).

It is known that the subendothelial accumulation of low density lipoproteins in their native state (LDL) and its subsequent oxidative modification (oxLDL) plays a critical role in the early stages of the development of atherosclerosis through the induction of endothelial dysfunction (Pirillo *et al.*, 2013; Berliner and Watson 2005, Steinberg 2009, Steinberg and Witztum 2010). In endothelial cells, oxLDL is recognized by its receptor Lectin-like oxidative low-density lipoprotein receptor-1 (LOX-1), mainly expressed in endothelial cells and used as a marker for atherosclerosis. Under physiological conditions, LOX-1 expression is very low. However, its expression is increased in the vascular endothelium under stress conditions, such as hypercholesterolemia, oxidative stress, inflammatory cytokines and even shear stress (Hoffman, 2017; Balzan, 2018).

LOX-1, which is located in the regions of membrane rafts, binds to oxLDL and induces its internalization, causing endothelial dysfunction (Balzan, 2018). This endothelial dysfunction leads to an increase in vascular permeability and subendothelial retention of oxLDL (Pirillo *et al.*, 2013, Berliner and Watson, 2005, Steinberg, 2009, Steinberg and Witztum, 2010). As a consequence, there is an increase in the expression of adhesion molecules, as well as in the transmigration of monocytes, which then contribute to the progression of the inflammatory process (Suciu, 2018).

Studies with animal models have shown that, shortly after the onset of an atherogenic LDL-rich diet, endothelial cells begin to express selective adhesion molecules on their surface, such as VCAM-1 (Vascular cell adhesion molecule 1), ICAM-1 (Intercellular adhesion molecule 1) and also increase the production of proteoglycans by smooth muscle cells. The latter bind and retain lipoprotein particles, facilitating their oxidation and promoting inflammatory responses that contribute to the formation of atherosclerotic lesions (Libby *et al.*, 2002). Although LDL retention precedes and promotes endothelial activation and monocyte uptake, monocyte-derived macrophages in the lesion may also secrete LDL-binding proteoglycans, contributing to the amplification of the atherosclerotic process (Moore and Tabas, 2011).

After transmigration to the subendothelial space, monocytes differentiate into macrophages driven by macrophage colony stimulating factor (M-CSF) and other differentiation factors. These macrophages, in turn, phagocyte and process

lipoprotein aggregates retained in the subendothelial space, especially oxLDL, which accumulates in the cytoplasm in the form of lipid droplets, leading to the formation of foam cells (Hansson, 2006; Moore and Tabas, 2011, Pirillo, 2013). Foam cells will then release proinflammatory cytokines, reactive oxygen species (ROS) and proteolytic enzymes involved in the degradation of the extracellular matrix (Hansson, 2006; Pirillo, 2013).

This progressive inflammatory process is responsible for the atherosclerotic plaque formation, which is characterized by thickening of the vascular intima, accumulation of extracellular components, infiltration of inflammatory cells and uncontrolled proliferation of smooth muscle cells (De Flora *et al.*, 1997). The plaque may further cause thrombus formation, which is involved in impaired blood flow and generation of vascular accidents. Therefore, initial modifications triggered at the internal surface of the vessel, i.e. endothelium, are the key point for the development of the atherosclerosis.

As mentioned, exposure of endothelial cells to oxLDL plays a critical role in the early stages of the development of atherosclerosis through the induction of endothelial dysfunction and increased vascular permeability (Pirillo *et al.*, 2013; Steinberg and Witztum, 2010). In part, this increase in vascular permeability is due to the fact that exposure of endothelial cells to LDL seems to trigger the increase of adhesion molecules on their surface, facilitating cellular transmigration (Libby *et al.*, 2002). Nonetheless, as mentioned previously, it was also shown that endothelial cell cultures exposed to oxLDL were less efficient in recovering from mechanical injury when compared to control cells (Liao and Granger, 1995). The latter could also contribute to increased vessel permeability and formation of the atheromatous plaque. The reason why cell viability and recombination is compromised upon oxLDL exposure is not yet fully understood.

Mechanism of plasma membrane repair

When injured, plasma membrane repair is a rapid event that happens within a few seconds and therefore is an essential process for cell survival.

Previous studies have shown that when a cell suffers an injury, an important event of lysosome exocytosis is triggered for membrane repair to occur. This is an event dependent on extracellular Ca^{2+} , so that its influx through the lesion site

induces local exocytosis of lysosomes (Reddy *et al.*, 2001; McNeil *et al.*, 2003). However, the exact mechanism by which this lysosome exocytosis promoted repair of the cell membrane was unknown.

Later, Idone and collaborators. (2008) observed a compensatory endocytosis event following Ca^{2+} influx-induced exocytosis, capable of internalizing transmembrane pores. These endocytic events were observed a few seconds after membrane injury induced by Streptolysin O (SLO), a pore-forming toxin. The same sequence of events, exocytosis followed by endocytosis, was observed when cells were exposed to mechanical injury, linking the endocytosis to the membrane repair process. Also, it was suggested an important role for cholesterol-rich membrane domains in this endocytosis mechanism. The authors showed that the acute depletion of cholesterol had a dose dependent inhibitory effect on exocytosis-induced compensatory endocytosis, consequently interfering with membrane repair. In addition, the authors demonstrated that compensatory endocytosis was facilitated after treatment with drugs that negatively interfered with the organization of the actin cytoskeleton, such as Cytochalasin D and Latrunculin-A (Idone *et al.*, 2008).

To demonstrate the relationship between lysosomal exocytosis and compensatory endocytosis, Tam and coworkers (2010) evaluated the number of new endosomes formed after SLO pore formation in cells previously treated with Bromoenol Lactane, a drug capable of blocking lysosomal exocytosis. A 10-fold decrease in the number of new endosomes and a reduction in the ability of these treated cells to repair their membrane was observed. Furthermore, it was shown that injured cells secrete acid sphingomyelinase (ASM), a lysosome derived enzyme, in the extracellular milieu. ASM cleaves sphingomyelin, present in the plasma membrane, transforming it into ceramide and generating ceramide rich domains. These domains, in turn, appear to be capable of promoting membrane invagination and then vesicle formation in a process known as compensatory endocytosis. The important role of this enzyme in membrane repair was confirmed by inhibition of its activity. Upon ASM inhibition, compensatory endocytosis was severely compromised and consequently membrane repair, without compromising cell exocytic ability (Tam *et al.* 2010).

Based on these findings, a new model for plasma membrane repair, mediated by lysosomal secretion of ASM, was proposed. In this model, shown schematically in Fig. 1, when a cell undergoes an injury, an influx of Ca^{2+} from the extracellular

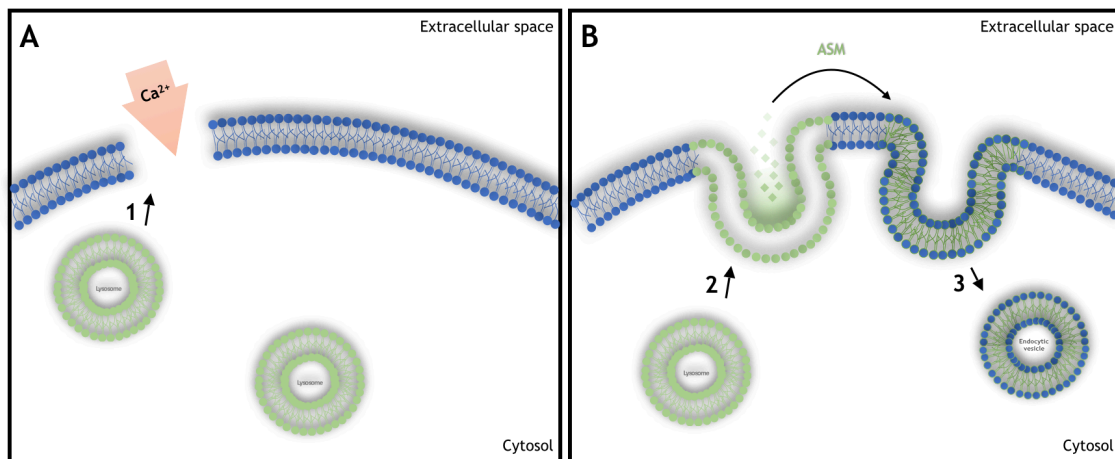


Figure 1: Schematic model of Plasma Membrane Repair. Model of PMR mediated by lysosomal secretion of ASM proposed by Tam et al. (2010).

medium into the cytoplasm occurs through the lesion sites (Fig. 1A). Increased cytoplasmic Ca^{2+} concentration induces lysosomal exocytosis (1). The lysosomal enzyme ASM is then released into the outer layer of the plasma membrane (2), where it converts sphingomyelin to ceramide (Fig. 1B). Ceramide tends to associate in microdomains that bud into the cytoplasm, generating endosomes that internalize the lesions (3) and leading to membrane repair (Tam *et al.*, 2010).

Shear stress and atherosclerosis

Atherosclerosis development is influenced by a variety of genetic and environmental factors. It is a geometrically focal disease in which lesions tend to appear in predisposed areas of the artery, such as side branches, curved areas of the vasculature and vessel bifurcations, where the blood-flow is non-uniform or blood velocity tends to be slower. The preferential development of atherosclerotic plaques at these predilection sites revealed that hemodynamic forces can act locally as a risk factor.

Wall shear stress, the frictional force generated by blood flow, is considered as one of the major hemodynamic forces acting on the endothelium. At “linear” areas of the vasculature blood flows in a laminar and unidirectional fashion with high mean shear stress values ($\text{HSS} > 15 \text{ dyne/cm}^2$) (reviewed by Malek *et al.*, 1999). These areas are relatively resistant to the development of early atherosclerosis. It has been shown that HSS areas results in a atheroprotective responses, for example by

expression of endothelial nitric oxide synthase (eNOS) (Ziegler, Silacci *et al.*, 1998; Cheng *et al.*, 2005).

In contrast, at arterial curvatures endothelial cells are often exposed to a unidirectional low shear stress value (LSS/ <4 dyne/cm²) (reviewed by Malek *et al.*, 1999) and at vessel bifurcations shear stress is low and oscillatory (OSS). These regions have been known for its atherogenic phenotype, such as the expression of leucocyte adhesion factors VCAM-1 and ICAM-1 and down regulation of eNOS (Sampath *et al.*, 1995; Walpola *et al.*, 1995; Ziegler, Bouzourene *et al.*, 1998). Therefore, these findings indicate that atherosclerotic plaque development is highly associated with the pattern of local shear stress.

Local shear stress patterns function as an important biomechanics factor for the modulation of atherogenesis and for plaque composition. They play an important role in modulating plaque size and stability, and can trigger endothelial dysfunction. Previous studies have shown that reduction of shear stress was associated with an increase in EC proliferation, followed by EC loss, change in morphology, decrease in actin stress fibers, greater monocyte attachment and migration through the endothelial layer (Walpola *et al.*, 1993).

Endothelial cells are able to sense the shear stress through several sensors that involves caveolae, G proteins, stretch-sensitive ion channels and cytoskeleton-coupled proteins (Fisher *et al.*, 2001). It is known that endothelial cells are able to respond to several external stimuli by altering their biomechanics properties e.g. reorganizing their cytoskeleton. In fact, it has already been shown that these cells adapt their morphology and phenotype in response to flow conditions (Fisher *et al.* 2001; Kowalsky *et al.*, 2008). Endothelial cells exposure to oxLDL in early atherosclerotic lesions can affect membrane rafts, as caveolae, and alter cytoskeleton organization (Shentu *et al.*, 2010; Byfield *et al.*, 2006; Chouinard *et al.*, 2008). It is possible that, in these abnormal conditions, ECs mechanical sensors could be somehow perturbed. Moreover, since endothelial cells are in constant mechanical stress generated by the blood flow, it is possible that these biomechanics changes are responsible for injuries and alterations in cell viability.

Shear stress and plaque vulnerability

Rupture of atherosclerotic plaque is an important cause of morbidity and mortality in the advanced stages of the disease. Vulnerability of these lesions are

associated with their morphological composition (Stary, 2000; Stary *et al.*, 1995). Vulnerable plaques display a large lipid core, thin fibrous cap, high activation of macrophages and metalloproteinases (MMPs) and a lower collagen content than stable lesions (Cheng, et al., 2006).

The importance of wall shear stress to the etiology of atherosclerosis is known for more than 20 years. Animal models, especially mice, have been widely used to study atherosclerosis. Apolipoprotein E knockout (ApoE^{-/-}) mice rapidly develop diet-induced plaques, which are morphologically similar to plaques developed in humans. However, only more recently an appropriate animal model was developed to study the cause-effect relationship between wall shear stress and plaque formation. In 2006, the group of Prof. Rob Krams has created a very elegant mice model of shear stress-induced atherogenesis and plaque vulnerability (Cheng *et al.*, 2006).

By using this model, it was demonstrated for the first time that specific patterns of wall shear stress applied in the carotid artery of ApoE^{-/-} mice can determine the size and the phenotype of the lesions. Atherosclerotic plaques induced by low values of shear stress present a vulnerable phenotype (Cheng *et al.*, 2006). In regions of vessel bifurcations and curvatures, LSS decreases nitric oxide (NO) availability, increase the production of ROS, adhesion molecules and chemoattractants cytokines. The imbalance of these molecules provokes endothelium dysfunction. As a consequence, the damaged endothelium becomes more sensitive to the local and systemic pro-atherogenic mediators, initiating early lesions.

With this animal model it was also shown the morphological heterogeneity of the developing plaque with a higher matrix degrading gelatinolytic activity in the proximal plaque segment. This related to the site where plaque rupture generally occurs, and colocalized with a subgroup of macrophages and smooth muscle cells (SMC) associated with oxLDL. The plaque morphology was also modulated by chemokine activation (Cheng *et al.*, 2007), in special CXCL10, which is expressed by distinct cell types as monocytes/macrophages, endothelial cells, fibroblasts and natural-killer cells. Inhibition of CXCL10 was able to reduce macrophage activation, increase SMC and consequently increase collagen content (Segers *et al.*, 2011).

2. RATIONALE

Endothelial cells are under constant mechanical stress due to the hemodynamic environment to which they are inserted. For this, several mechanisms are necessary for the maintenance of the endothelium integrity, such as the actin cytoskeleton realignment in relation to blood flow and most likely post-injury cell membrane repair mechanisms.

Membrane repair involves a sequence of Ca^{2+} -dependent mechanisms, including lysosomal exocytosis and subsequent compensatory endocytosis. Briefly, when a cell undergoes a micro-injury, its membrane must be sealed, otherwise it may compromise cellular viability. Upon injury, an influx of Ca^{2+} occurs, due to differences in the concentration of this ion between extracellular and intracellular environment, triggering the fusion of lysosomal vesicles with the plasma membrane (Reddy et al., 2001). This process leads to the addition of membrane to the cell surface, which is accompanied by the release of lysosomal enzymes capable of hydrolyzing sphingomyelin, the main sphingolipid present in the cell membrane (Idone et al., 2008). The hydrolysis of sphingomyelin generates ceramide that aggregates forming microdomains that are capable of inward budding and formation of new intracellular vesicles, a process called compensatory endocytosis. The newly formed endocytic vesicles carry with them the portion of the membrane containing the injury allowing the recovery of the original membrane (Idone et al., 2008; Tam et al., 2010; Andrews et al., 2014).

It has been demonstrated that the post-injury compensatory endocytosis can be affected by cholesterol depletion by decreasing the formation of new intracellular vesicles and inhibition of membrane repair, suggesting the direct link between injury induced endocytosis and membrane repair and the role of cholesterol and lipid rafts in the mechanisms of compensatory endocytosis (Idone et al., 2008).

Recent studies from our group have shown that the sequestration of cell membrane cholesterol by treatment with M β CD leads to a deregulated exocytosis of lysosomes located at the cellular periphery (Hissa et al., 2012). It has been demonstrated that this lysosomal exocytosis is due to changes in the polymerization and reorganization of the actin cytoskeleton, which in turn also reflects in changes of biomechanics properties of the cell (Hissa et al., 2013).

On the other hand, it is possible that the formation of a more rigid and organized cytoskeleton near the cell surface may function as a barrier to new

membrane traffic between the cell surface and intracellular vesicles, interfering with the maintenance of cellular integrity. Cells are continuously exposed to microinjuries, especially those subject to mechanical stress, such as endothelial cells. Since vesicle trafficking between the plasma membrane and the cellular interior is essential for maintenance of cellular integrity, changes in cellular biomechanics properties could compromise membrane repair ability and thus contribute to vascular endothelium fragility.

In previous studies, we observed that treatment of endothelial cells with M β CD, in addition to biomechanics changes and unregulated lysosomal exocytosis, induced an increase in endocytic events between 10 and 20 minutes after drug addition. These events occurred almost simultaneously with the peak of lysosomal exocytosis, suggesting that compensatory endocytosis events, triggered by the lysosomal exocytosis were not compromised. On the other hand, events of constitutive endocytosis, originating from pinocytic processes, common in endothelial cells, were blocked upon continuous exposure to the drug. We then suggested that the reorganized cytoskeleton functions as a mechanical barrier to new membrane trafficking events. Moreover, we showed that cells treated with M β CD presented a higher level of membrane injury, coincident with the peak of increase in cell stiffness, suggesting that these cells were more prone to injury when submitted to mechanical stress .

Due to the similarities observed in the literature between biomechanical changes induced by cholesterol depletion and treatment with oxLDL, it is possible that the exposure of endothelial cells to the latter can also cause the same effects on membrane trafficking between the periphery and cellular interior, as well as the level of injury susceptibility.

In this sense, we attempted to investigate whether changes in biomechanical properties of endothelial cells correlate with the cholesterol depletion results obtained previously. Additionally, we investigated whether it interferes with cells ability to perform membrane injury repair. Since increased exposure of endothelial cells to oxLDL is important for the development of atherosclerosis, it is important to conduct studies correlating the effects of mechanical modulation on cell membrane repair mechanisms in order to better understand how biomechanics changes may affect atherosclerotic plaque formation process.

Furthermore, atherosclerotic plaque development is highly associated to disturbance in local shear stress. The role of different patterns of shear stress on

atherosclerotic plaque composition, as well as on biomechanical elements of the artery, among other aspects, has been described in the literature (Cheng et al., 2006; Cheng et al., 2007; Fraga-Silva et al., 2014; De Wilde et al., 2015). However, it is not known how endothelial cells respond mechanically to these stimuli, especially considering *in vivo* models. Changes in biomechanics properties could increase the susceptibility of injury and/or compromise the ability of these cells to repair an injured membrane and, therefore, contribute to the vascular endothelium fragility and atherogenesis. For this, we proposed here to study the biological and mechanical properties of endothelial cells exposed to oxLDL and different hemodynamic environments, in order to assess the effects of different shear stress patterns on endothelial cell biomechanics and its impact in endothelial integrity and in the ability of cells to repair from injury during plaque development.

3. MAIN GOAL

Study the effect of biomechanical alterations caused by the treatment of endothelial cells with oxLDL in the mechanisms of post-injury membrane repair in order to understand the role of these lipoproteins on endothelial fragility and its contribution to atherosclerosis.

Specific goals

1. Evaluate changes in the mechanical properties of endothelial cells by defocusing microscopy after treatment with native or oxidized LDL (nLDL and oxLDL, respectively);
2. Evaluate the effect nLDL or oxLDL exposure on the structural organization of the actin cytoskeleton;
3. Evaluate the effect of nLDL or oxLDL exposure on lysosomal vesicle exocytosis;
4. Evaluate the effect of treatment with nLDL or oxLDL on constitutive and compensatory endocytosis events;
5. Evaluate the level of membrane injury under mechanical stress, as well as repair ability of endothelial cells previously treated with nLDL or oxLDL, and its role in cellular viability;
6. Evaluation of structural organization of the actin cytoskeleton of endothelial cells exposed to different patterns of shear stress in Apolipoprotein E knockout mice (ApoE^{-/-}) mice;
7. Evaluation of lysosomal distribution of endothelial cells exposed to different patterns of shear stress in ApoE^{-/-} mice;
8. Evaluate the level of membrane injury induced by the flow in endothelial cells exposed to different patterns of shear stress in ApoE^{-/-} mice.

4. MATERIALS AND METHODS

1. Cell Culture

The endothelial cell line EAHy926, derived from Human Umbilical Vein Endothelial Cells (HUVEC) was used for all experiments (*passages 2 – 10*). Endothelial cells (ECs) were maintained in high-glucose Dulbecco's Modified Eagle's Medium (DMEM; Gibco), supplemented with 10% fetal bovine serum (FBS; GIBCO) and 1% penicillin/streptomycin (100U/mL and 100µg/mL, respectively) (GIBCO) at 37°C in a humidified atmosphere containing 5% CO₂.

2. Isolation and oxidation of LDL

Blood from health individuals was collected and plasma separated by centrifugation. Potassium Bromide (KBr) solution at the density of 1.019g/ml was added to the plasma and the latter was submitted to ultracentrifugation at 236.500x g for 7h using Sorvall Ultra Pro 80 ultracentrifuge. Following, the supernatant containing VLDL was discarded. The infranatant was resuspended, its density was adjusted to 1.063 g/ml with KBr, and then submitted to a new ultracentrifugation cycle at 236.5x g for 6h. After this cycle, LDL was collected and dialyzed overnight in PBS with gentle agitation in a cold chamber. LDL concentration was determined by evaluating protein concentration using Lowry's method. After that, a cocktail of protease inhibitors and antioxidants composed of PMSF (5 µmol/L plasma), Benzamidine (10 µmol/L plasma), BHT (100 µmol/L plasma) and aprotinin (10 µmol/L plasma) was added to the LDL fraction. This portion of LDL, which will be referred to as nLDL, was filtered through a 0.22µm filter unity and held at -80°C, protected from light, until use.

For LDL oxidation (oxLDL), after determining protein concentration, LDL was incubated for 18h at 37°C with 20 µM CuSO₄/mg of protein. To stop the oxidation reaction, the cocktail of inhibitors and antioxidants was added only at the end. OxLDL was then filtered through a 0.22 µm filter unity and stored at -80°C, protected from light, until use. Lipid oxidation was detected by TBARS assay (in fresh and thawed samples) and the results expressed by the ratio of malondialdehyde (MDA) / protein concentration. Preparations used in the

experiments presented the following values: nLDL = 0.602 nmol of MDA/mg of protein; oxLDL = 24.401 nmol of MDA/mg of protein (extensively oxidized LDL). In order to ensure that LDL samples were not degraded with the freezing and thawing processes, we have performed SDS-PAGE electrophoresis of nLDL (1 mg/ml) and oxLDL (0.4 mg/ml) (Fig. 2).

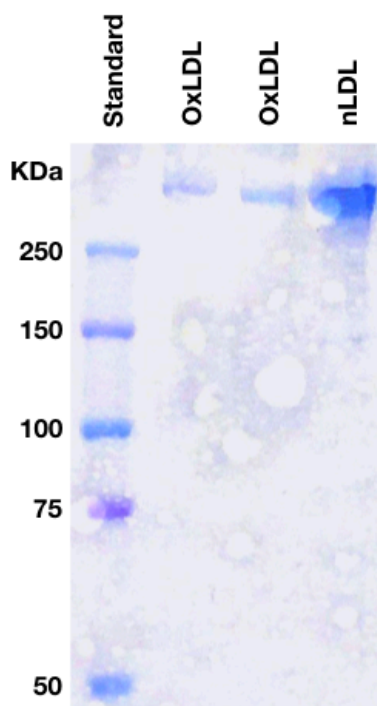


Figure 2: OxLDL and nLDL SDS-PAGE electrophoresis gel. Electrophoresis gel of Standard sample (Kaleidoscope, BioRad), oxLDL (0.4 mg/ml) in duplicate and nLDL (1 mg/ml).

3. Cell Treatment

ECs were washed three times with serum free DMEM and exposed to oxidized LDL for 24h in a working concentration of 50 $\mu\text{g/ml}$, a standard concentration used in several studies (Byfield et al., 2006; Oh et al., 2016; Zhang et al., 2017). In these assays, native LDL (50 $\mu\text{g/ml}$) was used as negative control. As an additional control, cells were washed and incubated with serum-free DMEM for 24h.

4. *In vitro* labeling of Polymerized Actin

Cells were plated onto 13 mm round coverslips inserted into wells of 24-well plates at a density of 4×10^4 cells/well, 24 h before the assay. Cells were then treated and fixed with formaldehyde 3.7% for 20 min at room temperature. To analyze *de novo* polymerization, cells were previously treated with 95 μM

Latrunculin-A (LAT-A; Sigma-Aldrich) for 1 hour, followed by the different treatments and fixation.

After fixation, coverslips with attached cells were washed three times in Phosphate Buffered Saline (PBS) and permeabilized with Triton X-100 0.5% (Sigma-Aldrich) for 15 min. For polymerized actin labeling, cells were incubated with Phalloidin-Alexa Fluor 546 (Invitrogen) using a 1:40 dilution in PBS at room temperature followed by three additional washes. Subsequently, the DNA of cells was stained for 1 min with DAPI (Sigma), mounted, and examined on a Zeiss ApoTome.2 microscope. Fluorescence intensity was measured using the image processing software FIJI (NIH, v. 2.0.0) as the mean gray value of the whole image normalized by the number of cells.

5. *Defocusing Microscopy*

In order to measure parameters able to characterize the biomechanical properties of the complex plasma-membrane-cytoskeleton of endothelial cells during treatment, we used Defocusing Microscopy (DM) technique as previously described (Agero et al, 2003). DM is an optical technique which has been applied to obtain quantitative parameters which characterize membrane surface dynamics of living cells using a bright field microscope (Agero et al, 2004; Coelho-Neto et al., 2006). Briefly, cells were plated on glass coverslips in 35mm dishes at a density of 8×10^4 cells/dish 24 hours before the assay. To evaluate the effects of oxLDL exposure, cells were treated for 24 hours and then recorded by DM in serum free DMEM for 10 minutes. For the experiments in which cholesterol sequestration was performed, ECs were recorded by DM in serum free DMEM for 10 minutes (control), then M β CD was added to the medium and cells continued to be recorded for another 40 minutes. These assays were performed in triplicate and at least 5 different cells were analyzed.

In order to obtain parameters that evaluate drug treatment as a function of time we analyzed slightly defocused captured movies. The contrast of the defocused images is proportional to cell surface curvature (Agero et al., 2003). The analysis has been done by the temporal autocorrelation of the contrast adjusted by a single exponential as a function of time, as shown in Eq(1),

$$\langle C(t_0)C(t_0 + t) \rangle = Ae^{\frac{-t}{\tau}} \quad \text{Eq. (1)}$$

The amplitude, A , is proportional to the oscillations amplitude, and τ , represents the relaxation time of membrane fluctuations. The mathematical model that describes the autocorrelation function to image contrast is shown by Agero and coworkers (2003).

All experiments were analyzed using ImageJ Plugins that correct for background and calculate the temporal autocorrelation function among frames. These temporal autocorrelation functions were adjusted in Kaleida Graph Software (Synergy Software, Essex Junction, VT, USA) using single exponential decay curves that carry information about their time characteristics (relaxation time) and amplitude of curvature. The experiments were performed in a Nikon Eclipse TI inverted microscope equipped with a 530 nm wavelength green filter, a stage-heated oil immersion objective Nikon Apo TIRF 100X, NA 1.49 (Nikon, Japan), and an environmental chamber (model ChamLide ICCU: 109, Live Cell Instrument, Nowan-gu, Korea) which provides a 5% CO₂ atmosphere, 37°C temperature and 50% humidity. The images were captured using a 12 bit monochrome Uniq camera (model 1800 CL) (Epix Inc, Buffalo Grove, IL, USA, 4096 gray levels and 0.064 mm of pixel square side), with a gain of 11.04 db and a capture rate of 1 frame per second. The focal distance was controlled during the entire experiment by a Nikon Perfect Focus System (PFS) apparatus and the camera gray level calibration was performed as previously described (Agero et al., 2004).

6. *In vitro* cell Viability Assay

Cells were plated on 6-well plates at a density of 1×10^5 cells/well. After 24 hours, cells were treated (in triplicates), washed twice with Ca²⁺ and Mg²⁺ free PBS, trypsinized, pelleted and incubated with a solution of Propidium Iodide (10 µg/mL) in Hanks' Balanced Salt Solution (HBSS; Sigma-Aldrich). The PI fluorescence of 30,000 individual cells in each replica was measured using a Becton Dickinson FACScan or Accuri C6 (BD Biosciences, USA). Data were analyzed using FlowJo v10.1 software (Tree Star, Inc.). Three independent experiments were performed.

7. *In vitro* β -hexosaminidase assay

To evaluate lysosomal exocytosis, a β -hexosaminidase secretion assay was performed according to previous work (Martinez et al., 2000). Briefly, EAhy. 926 cells were plated in triplicates in 24-well plates at a density of 4×10^4 cells/well 24 hours before the assay. ECs were then treated with oxLDL or nLDL (50 μ g/ml) for 24h or 10 μ M Ionomycin (Calbiochem) for 10 min at 37°C. After treatment, the supernatant was collected and attached cells were lysed with Triton x-100 (Sigma-Aldrich) 1% in PBS. Cell supernatant and cell lysates were incubated with 50 μ L of β -hexosaminidase substrate, 6mM 4-methylumbelliferyl-N-acetyl-B-D-glucosaminide (Sigma M2133), dissolved in Na-citrate-PO₂ buffer (pH4.5). After 15 min of incubation at 37°C, the reactions were stopped by adding 100 μ L of stop buffer solution (2M Na₂CO₃-H₂O, 1.1M glycine) followed by reading in a spectrofluorimeter at 365 nm excitation and 450 nm emission (Synergy 2, Biotek). Several independent experiments were performed.

8. *In vitro* compensatory endocytosis assay

Compensatory endocytic events triggered by lysosomal exocytosis as well as constitutive endocytosis were measured for each treatment.

In order to measure compensatory endocytosis upon M β CD treatment, 2×10^6 cells were kept in suspension and the outer leaflet of the plasma membrane was labeled with 1 μ g/ml wheat germ agglutinin (WGA) – Alexa Fluor 488 for 1 min at 4°C, followed by two washes with HBSS. After membrane labeling, cells were exposed or not to M β CD at 37°C (as described above), resuspended in 0.2% trypan blue (Sigma-Aldrich), washed with HBSS and fixed with formaldehyde 3.7% before FACS analysis. WGA-Alexa Fluor 488 fluorescence of 10,000 individual cells was measured using BD FACScan and analyzed using FlowJo v10.1 software. Due to WGA-Alexa Fluor 488 susceptibility to quenching by the membrane impermeable trypan blue, Alexa Fluor 488 fluorescence measurement will correspond to the amount of membrane endocytosed after trypan blue exposure.

For nLDL/oxLDL treatment, due to the long period of incubation and WGA degradation with time, we used an alternative method to evaluate compensatory endocytosis. For this, cells were plated onto 13 mm round coverslips, inserted into wells of 24-well plates, at a density of 4×10^4 cells/well

24h before the assay. Following, cells were submitted or not to treatment with nLDL or oxLDL for 0, 1, 4, 8, 12, 16 and 24 h in the presence of Texas-Red Dextran, a membrane impermeable fluorescent dye. At each time point, cells were washed to eliminate extracellular Texas-Red Dextran, fixed with paraformaldehyde 4% and cell nuclei labeled with DAPI. The fluorescence of the endocytosed fluorophore was evaluated by fluorescence microscopy using Zeiss Axio Vert.A1. To quantify the distribution of Texas-Red Dextran labeled vesicles in each cell, first the mean nucleus' radius (R) was measured in order to determine the perinuclear area. Next, the distances between labeled vesicles (D) and the center of cell nuclei were also measured, and the ratio D/R determined. Values closer to one indicate vesicles located closer to the perinuclear area, whereas values higher than one indicate locations further from the cell center and nearer the cell borders. Texas-Red Dextran distribution was measured using the image processing software FIJI (NIH, v. 2.0.0) as previously described (Couto et al., 2020).

For oxLDL treatment we also measured compensatory endocytosis induced by plasma membrane repair after injury. For this we used a scrape wound assay as previously described (Idone et al., 2008). ECs were grown in 10cm plates, subjected to oxLDL exposure, washed with HBSS containing or not 1.8mM Ca²⁺. Cells were then labeled on the plasma membrane with 1µg/ml WGA–Alexa Fluor 488 for 1 min at 4°C, washed twice with HBSS, wounded by scraping in the presence or absence of Ca²⁺ and incubated for 2 min at 37°C with 0.2% trypan blue before washing and FACS analysis. Internalized WGA–Alexa Fluor 488 fluorescence of 30,000 individual cells was measured using BD Accuri C6 and data analyzed using FlowJo v10.1 software.

9. *In vitro* membrane injury and repair assays

ECs were plated in 35 mm culture dishes (3x10⁵ cells/dish) in high glucose DMEM supplemented with 10% FBS and 1% penicillin/streptomycin at 37°C and 5% CO₂. After 24 hours, cell monolayers were subjected or not to oxLDL/nLDL treatments and washed with Calcium-free PBS. To measure the amount of membrane injury (hitting control), treated cells were incubated with Ca²⁺-free HBSS at 4°C, wounded by scraping in the presence of PI (10 µg/mL) and then incubated for 5 minutes at 37°C (Figure 3B). To measure membrane

resealing and injury recovery, treated cells were incubated with HBSS containing Ca^{2+} , wounded by scraping and incubated for 5 min in the presence of extracellular Ca^{2+} to allow for PM repair. Propidium iodide (10 $\mu\text{g}/\text{ml}$) was then added to the medium (Figure 3A). After that, 30,000 individual cells were analyzed by flow cytometry using BD Accuri C6 and data analyzed using FlowJo v10.1 software. The efficiency of membrane repair was calculated based on the level of injury using the equation below:

$$\text{Membrane repair (\%)} = \frac{(\text{PI negative cells in assay A} - \text{PI negative cells in assay B}) * 100}{\text{PI positive cells in assay B}}$$

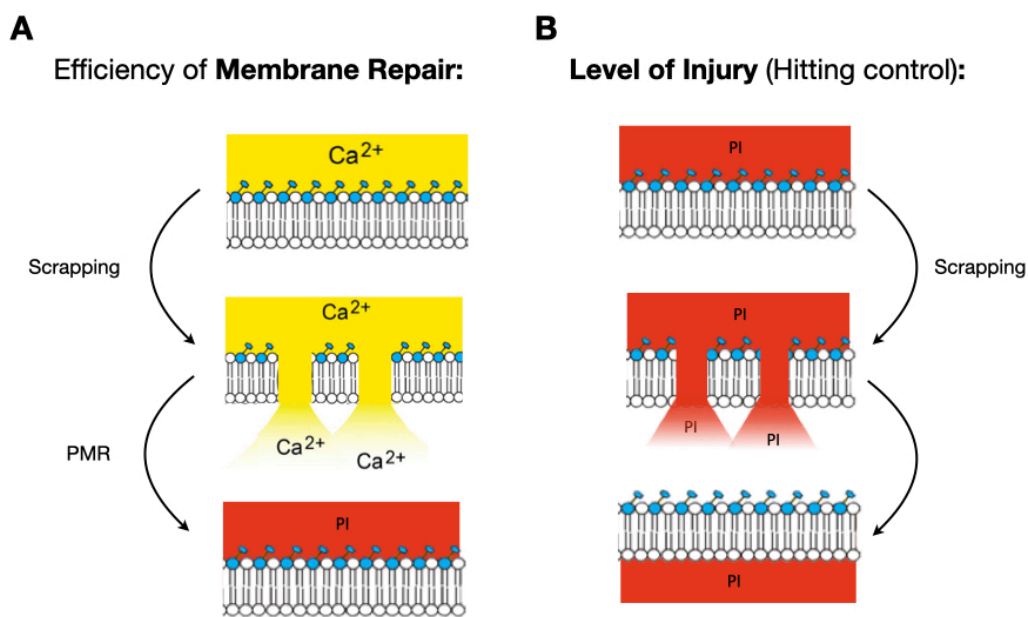


Figure 3: Membrane injury and repair assay. (A) In order to analyze whether the cells were able to repair from injury, cells were scrapped in the presence of extracellular Ca^{2+} , allowed to repair for 5 min and then PI was added. If the membrane was repaired, PI would not cross the membrane, so the amount of cells that repaired are shown as PI negative. (B) To address the amount of injury caused by scraping (hitting control), cells were scrapped in the presence of PI. Scrapping cause small ruptures in the membrane allowing PI to flow into the cell. Therefore, the level of injury is shown by the amount of PI positive cells.

10. *In vitro* orbital shear stress induced membrane injury assay

For this assay, 3×10^5 cells were seeded into wells of 6-well plates and incubated at 37°C and 5% CO_2 until reaching confluence. Cells were then submitted to treatment of oxLDL or nLDL and placed on a 37°C incubator with orbital shaker at 160 rpm and rotation radius of 1 cm^2 to obtain a shear stress of

approximately 7 dyne/cm². The shear stress was calculated as previously described (Dardik et al., 2005). After 1h of rotation in serum free media, PI was added to a concentration of 10 µg/ml. PI positive cells were counted within 16 fields at the well periphery.

11. Animal Experimentation

Mice are significantly less susceptible to the development of atherosclerotic plaque due to a significant increase of Apolipoprotein E (ApoE) in the arterial wall when fed with a high cholesterol diet. Based on that, ApoE knockout mice were developed and became one of the most used models for atherosclerosis. For that reason, we have chosen to use mice deficient in ApoE (ApoE^{-/-}) in a C57BL/6 background to investigate the role of shear stress in atherogenesis (Figure 4).

Wild type C57BL/6 (WT) and ApoE^{-/-} mice (15-20 weeks old) were exposed to different hemodynamic environments by using a shear stress modifier device (Figure 4C). The device (cast) was made of thermoplastic (polyetherketon). It consists of 2 longitudinal halves of a cylinder with a cone-shaped lumen (Figure 4A). Its particular shape allows to impose a fixed geometry on the vessel wall, thereby causing a gradual stenosis, resulting in increased shear stress in the vessel segment inside the cast, a decrease in blood flow and consequently a lower shear stress region downstream from the cast, and a vortex upstream from the cast (oscillatory shear stress region) (Cheng et al, 2006). Therefore, three types of shear stress can be applied for each mouse: high shear stress (HSS; 15 N/m²); low shear stress (LSS; 10 N/m²); oscillatory shear stress (OSS; 14 N/m² range 60 N/m²) (Figura 4B).

The animal experimentation was divided in two parts (see corresponding timeline on figure 5):

A) a pilot study to assess in which period of atherogenesis the study would be performed (Fig. 5A). ApoE^{-/-} mice were divided in 5 subgroups according to the number of weeks after cast implantation (1-5 weeks post cast implantation - wpci; n=4 per subgroup). C57BL/6 mice were separated only in 2 groups, 1 and 5 wpci (n=4 per subgroup). The samples from these groups were processed to Oil Red O staining and plaque size measurements.

B) In the second part, after determining the best period to perform the experiments, we investigated the impact of different patterns of shear stress on the mechanical properties of endothelial cells and on injury susceptibility during atherogenesis (Fig. 5B).

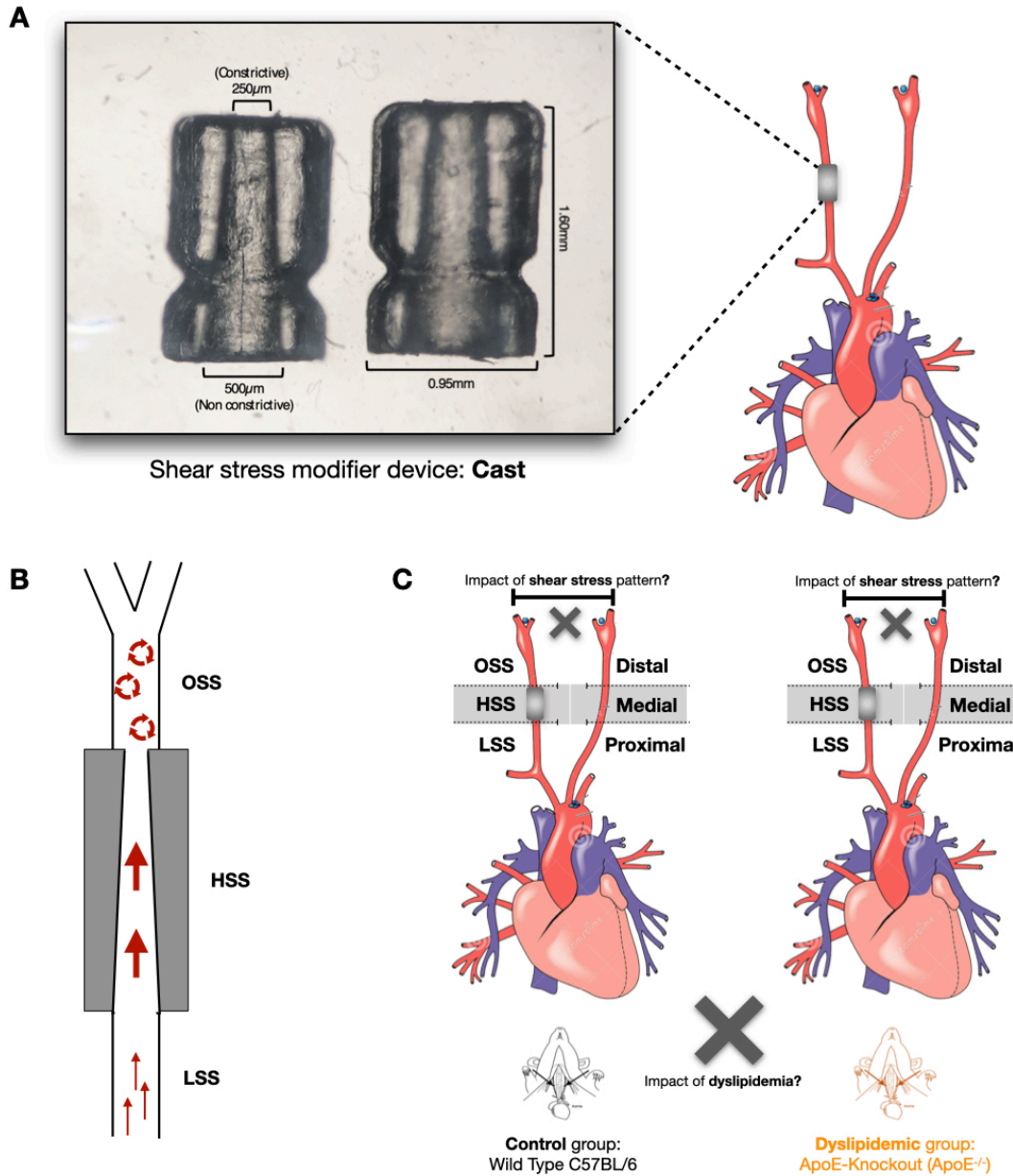


Figure 4: Animal experimentation. (A) Shear stress modifier device (cast). Device developed by Cheng et al. (2006), the cast consists of 2 longitudinal halves of a cylinder with a cone-shaped lumen, which imposes a fixed geometry of the vessel wall. (B) The geometry of the cast has been designed with computational flow dynamics software to produce vortices downstream of the cast when placed around the carotid artery. This downstream region therefore is expected to be exposed to spatio-temporal oscillations in shear stress (oscillatory shear stress region). The gradual decline in the inner diameter (from 500µm to 250µm) induces a gradual increase in shear stress (increased shear stress region). In addition, the constrictive stenosis decreases the blood flow, resulting in a relatively low (lowered) shear stress region upstream from the cast (approximately 30% reduction). (C) The left carotid (LC) of each animal was divided in three regions and used as an internal control in order to understand the impact of different shear stress patterns on the different aspects studied in this work. To understand the role of exposing cells to the excess of lipids, we used a ApoE-Knockout mice (ApoE^{-/-}) in the study.

In both studies, WT and ApoE^{-/-} mice were fed with a high fat diet (15% (w/w) cocoa butter and 1.25% (w/w) cholesterol, Research Diets D12108C) for 2 weeks (adaptation period for the diet) before cast implantation. After that, the animals continuously received the high cholesterol diet for the entire length of experiment: 1-5 weeks post cast implantation for the pilot study and 1 week post cast implantation for the experimental group.

The device was implanted as previously described (Olivon et al, 2013; Fraga-Silva, 2014; Fraga-Silva, 2015). Briefly, mice were anesthetized by isoflurane inhalation (3-5% for induction and 2% for maintenance). On anesthetized animals, we performed a longitudinal incision (0.8-1 cm) in the

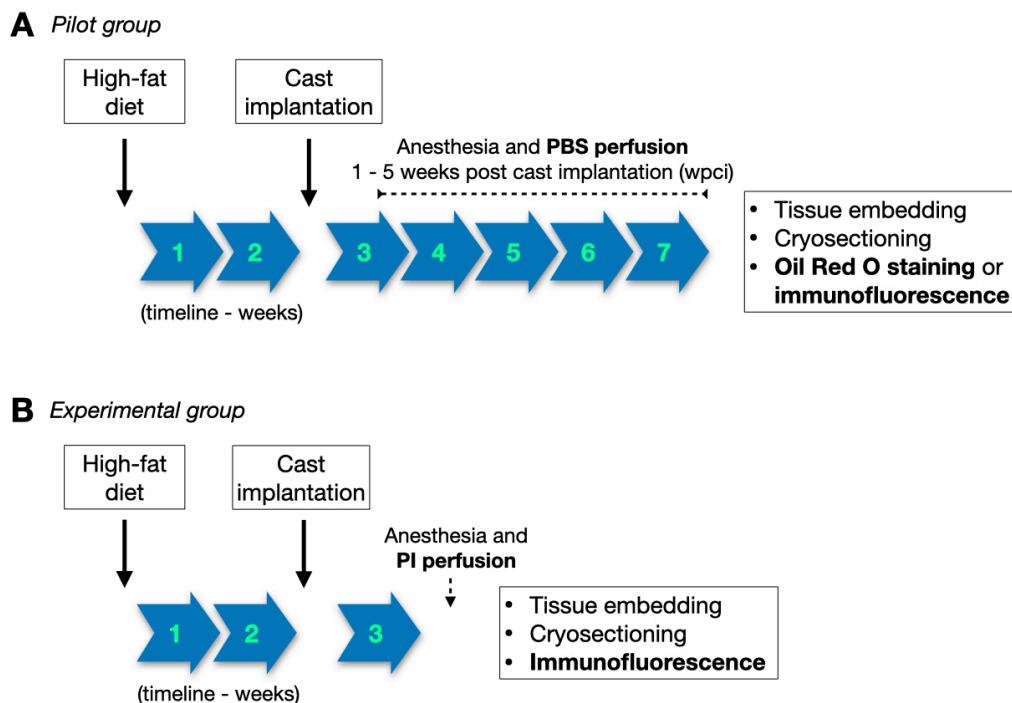


Figure 5: Experimental timeline. The animal experimentation was divided in two parts: (A) Pilot study: WT and ApoE^{-/-} mice were fed with a high fat diet for 2 weeks (adaptation period for the diet) before cast implantation in the right carotid artery. After that, in the end of each week following cast implantation (corresponding to weeks 3-7) 4 animals were anesthetized and perfused with 5ml PBS. Then left and right carotid arteries were collected, embedded in cryomatrix, frozen at -80°C until cryosectioning and then stained with Oil Red O or immunofluorescence. Animals continuously received the high cholesterol diet for the entire length of experiment. (B) Experimental group: WT and ApoE^{-/-} mice were fed with a high fat diet for 2 weeks, followed by cast implantation in the right carotid artery. 1 week post cast implantation (wpci), mice were anesthetized and perfused with 5ml PBS containing 500 µg/ml Propidium Iodide. After that, we performed a cardiac perfusion with PBS to wash the excess of PI. Right and left carotid arteries of each animal were then collected, included with cryomatrix, frozen and kept at -80°C until sectioning. Fresh tissue slices were then used for immunofluorescence. Animals continuously received the high cholesterol diet for the entire length of experiment.

sagittal anterior area of the neck in order to access the right carotid artery (RC). Once the right carotid artery was localized, the cast (Fig. 4A) was positioned around the artery and fixed with a layer of suture. The cast was kept for up to 5 weeks. The left carotid (LC) of each animal was used as an internal control. After cast implantation, the animals were treated with acetaminophen for 3 days in the drinking water (200-300 mg/kg).

The sacrifice was performed by anaesthesia (ketamine and xylazine, 100 mg/kg and 15 mg/kg) followed by cardiac perfusion of 5ml of PBS for the pilot group (Fig. 5A) or 5 ml of PBS containing 500 μ g/ml Propidium Iodide for the experimental group (Fig. 5B). Since cell membrane is impermeable to PI, PI labelling would happen only in the presence of plasma membrane rupture. Following PI exposure, cardiac perfusion with PBS was performed in order to wash the excess PI and guarantee complete blood removal. Right and left carotid arteries of each animal were then collected, included with cryomatrix, frozen and kept at -80°C until sectioning (20 μ m per slice) using the cryostat Leica CM3050S. Fresh tissue slices were collected in glass slides and stored at -20°C for later use in histology or immunostaining.

This animal study was performed at the Laboratory of Hemodynamic and Cardiovascular Technology and was approved by local ethics committee and Swiss Regulatory Authorities (license number 3395) and it is in accordance with the guidelines from Directive 2010/63/EU of the European Parliament on the protection of animals used for scientific purposes.

12. *Oil-Red O Staining of tissue sections*

Tissues samples from pilot group (mice 1-5 wpci) were stained with Oil Red O (ORO) in order to identify the presence of atherosclerotic plaques and to measure their sizes. For that, fresh frozen tissue sections were fixed in ice cold 10% formalin. Slides were pre-incubated in absolute propylene glycol at room temperature for 2-5 min, followed by incubation with 0.5% Oil Red O solution in absolute propylene glycol for 8-10 min in 60°C oven. Next, slides were differentiated in 85% propylene glycol solution at room temperature for 2-5 min, rinsed and stained in Mayer's hematoxylin solution. Images were acquired on a light microscope Zeiss Axiolab.A1 using a 10x objective. The wall area of each carotid artery section was measured using the image processing software FIJI

(NIH, v. 2.0.0). After qualitative identification of atherosclerotic plaques, plaque size was calculated as the difference between the total wall area and the mean wall area in the same region of the respective control (LC). Plaque sizes from subsequent tissue sections were added together in order to identify the total plaque size.

13. *Immunofluorescence of tissue sections*

Actin cytoskeleton: The actin cytoskeleton was stained with Phalloidin-Atto 565. Fresh frozen tissue sections were fixed with formaldehyde 4%, permeabilized with 0.5% Triton X-100 in PBS and incubated with phalloidin-atto 565 (1:40). Slides were then mounted with Fluoroshield containing DAPI. For these slides, the endothelium was labeled (as described below) previously to the actin cytoskeleton labelling. To calculate fluorescence intensity, images of each cross section were acquired on a fluorescence microscope Leica DM5500 using a 10x and 20x objective. For the qualitative analysis of actin cytoskeleton organization, images were captured in the Zeiss Axio Imager.Z2 (ApoTome.2 structured illumination system) fluorescence microscope using the 63x objective.

Lysosomes: To evaluate lysosomal vesicles distribution in the tissue, we stained LAMP-2, a transmembrane lysosomal protein, in the frozen sections. For this, tissue samples were fixed with PFA 4%, blocked with 3% BSA in PBS and incubated with rat anti-mouse LAMP 2 antibody (1:50) in PBS/1% BSA, at room temperature for 2 h. After rinsing with PBS/1% BSA, the sections were incubated at room temperature for 2 h with a secondary chicken α -rat antibody conjugated with Alexa Fluor 647, rinsed and processed for endothelium immunostaining. To calculate fluorescence intensity, images of each cross section were acquired on a fluorescence microscope Leica DM5500 using a 10x and 20x objective.

Endothelium: In order to label the endothelium, the tissue samples were incubated for 15 min with 0.01M Citrate Buffer, for antigen unmasking, followed by permeabilization with PBS/1% BSA/0.3% Triton x-100 (15 min) and blockage with PBS/3% BSA (30 min). Endothelial cells were then immunostained with rabbit anti-mouse CD31 antibody (Abcam, 1:100) in PBS/1% BSA at room temperature for 2 h and then incubated with secondary donkey anti-rabbit

antibody conjugated with Alexa Fluor 488 at room temperature for 2 h, rinsed and mounted with Fluoroshield containing DAPI.

Phalloidin, LAMP-2 and PI fluorescence intensity (FI) were measured in the vascular wall and in the endothelium (Figure 6 A and B, respectively) using the image processing software FIJI (NIH, v. 2.0.0). The integrated density of the selected area image was measured and applied to the equation in Figure 6C in order to correct for background and calculate the FI. Results were normalized by the FI of the DAPI channel in the same selection.

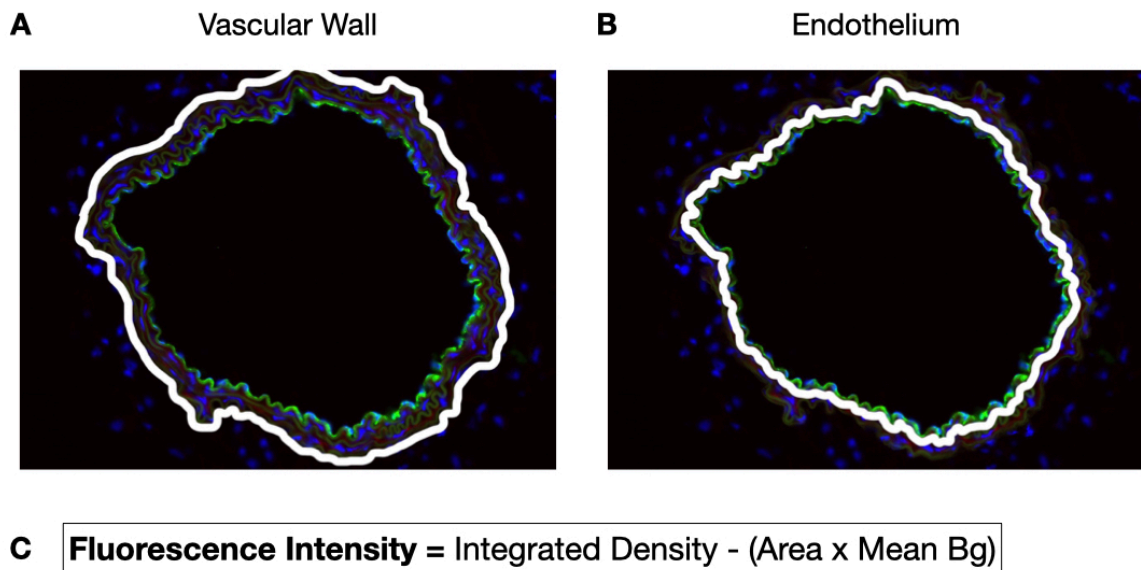


Figure 6: Methodology used for the quantification of fluorescence intensity in the carotid artery cross-sections. (A) Selection area for the analysis of the entire vascular wall. (B) Selection area for the analysis of the endothelium based on CD31-positive labelling. (C) Equation used to calculate the fluorescence intensity (FI) based on the integrated density measurements after correction for background. FI was calculated for phalloidin-Atto 565, LAMP-2 and Propidium Iodide and normalized by the respective DAPI FI in each image.

5. RESULTS

5.1. *OxLDL exposure, induces reorganization of cell actin, de novo polymerization and changes in cell mechanical properties*

Alterations in cell membrane cholesterol content and consequently membrane rafts disruption by treatment with a well-known cholesterol sequestering drug (M β CD) has been shown to have significant effects on actin cytoskeleton reorganization in different cell types, including endothelial cells (Hissa et al., 2013; Kwik et al., 2003; Byfield et al., 2004). Recently, our group has also shown that cholesterol sequestration and rafts disruption using M β CD, besides reorganizing cell actin cytoskeleton, also induce de novo actin polymerization in fibroblasts (Hissa et al., 2013). Both events lead to altered cell mechanical properties (Hissa et al., 2013; Byfield et al., 2004). Exposure of endothelial cells to oxLDL, similarly to cholesterol sequestration using M β CD, has also been shown to induce rafts disorganization and consequently change actin cytoskeleton organization (Chouinard et al., 2008; Shentu et al., 2010). We then decided to investigate whether oxLDL treatment would also induce de novo actin polymerization in ECs by using a cell lineage of human umbilical vein endothelial cells (EAhy926).

In order to confirm the effect of oxLDL on actin reorganization in this cell lineage we first submitted these ECs to treatment with oxLDL or nLDL and compared their effects on actin cytoskeleton organization by labelling cells with Alexa 546-conjugated phalloidin (Fig.7A). As expected, we observed considerable changes in actin filaments structural organization after treatment with oxLDL when compared to control groups. A significant increase in actin fluorescence intensity was observed upon oxLDL treatment in relation to control or nLDL treated cells (Fig. 7B). As a consequence of actin reorganization, we also observed changes in cell morphology. Similar results were obtained when this cell lineage was treated with M β CD. These results were described previously in my Master thesis and it has been shown here as an Annex Supplementary Fig. 1A).

In parallel, we analyzed the ability of these cells in polymerizing new actin filaments upon treatment. In this regard, cells were previously treated with Latrunculin-A (Lat-A), a toxin able to disrupt actin filaments through its binding

to actin monomers, blocking their association into microfilaments. After Lat-A exposure and cytoskeleton disruption, cells were washed and exposed or not to the different treatments.

As previously shown for fibroblasts (Hissa et al., 2013), treatment of ECs with M β CD, after Lat-A incubation, also induced de novo actin polymerization with reconstruction of actin fibers, whereas the same was not observed for cells pre-treated with Lat-A and incubated with serum-free medium (Annex: Supplementary Fig. 1B). We further tested if this was also the case for ECs pre-treated with Lat-A and then exposed to oxLDL. Similar to what was observed for M β CD, pre-treatment of these cells with Lat-A followed by treatment with oxLDL induced de novo actin polymerization (Fig. 7C and D). However, since the exposure to oxLDL is performed for an extended period of time (24 h) after treatment with Lat-A, new actin filaments were also observed in the control groups (non-treated and treated with nLDL for the same 24 h after Lat-A treatment). Nonetheless, when compared to oxLDL treated cells, the latter were still more efficient in reconstructing their cytoskeleton.

Additionally to cell actin reorganization, the literature shows that rafts disruption upon cholesterol depletion or oxLDL exposure also affects the biomechanical properties of the complex cytoskeleton-membrane, thereby increasing cell stiffness (Hissa et al., 2013; Byfield et al., 2006; Chouinard et al., 2008; Kowalsky et al., 2008). To confirm this, we evaluated actin reorganization effects on biomechanical properties of endothelial cells after oxLDL exposure. In order to characterize the mechanical dynamics on cell membrane we used DM technique to follow the treatment as a function of time.

The analysis of the autocorrelation function as a function of time allows us to measure relaxation time and the amplitude of membrane fluctuation, which characterize the changes on cellular membrane curvature over time, considering the interface cytoskeleton-membrane, as previously described (Agero et al., 2004).

In this assay, cells were exposed to oxLDL for 24 h and then recorded for 10 min (Supplementary Video 1). As control, cells were exposed to either nLDL treatment or serum free DMEM for 24 h and then recorded for 10 min (Supplementary Videos 2 and 3, respectively). All experiments were analyzed using ImageJ Plugins that correct for background and calculate the temporal autocorrelation function among frames, as described in the methods section.

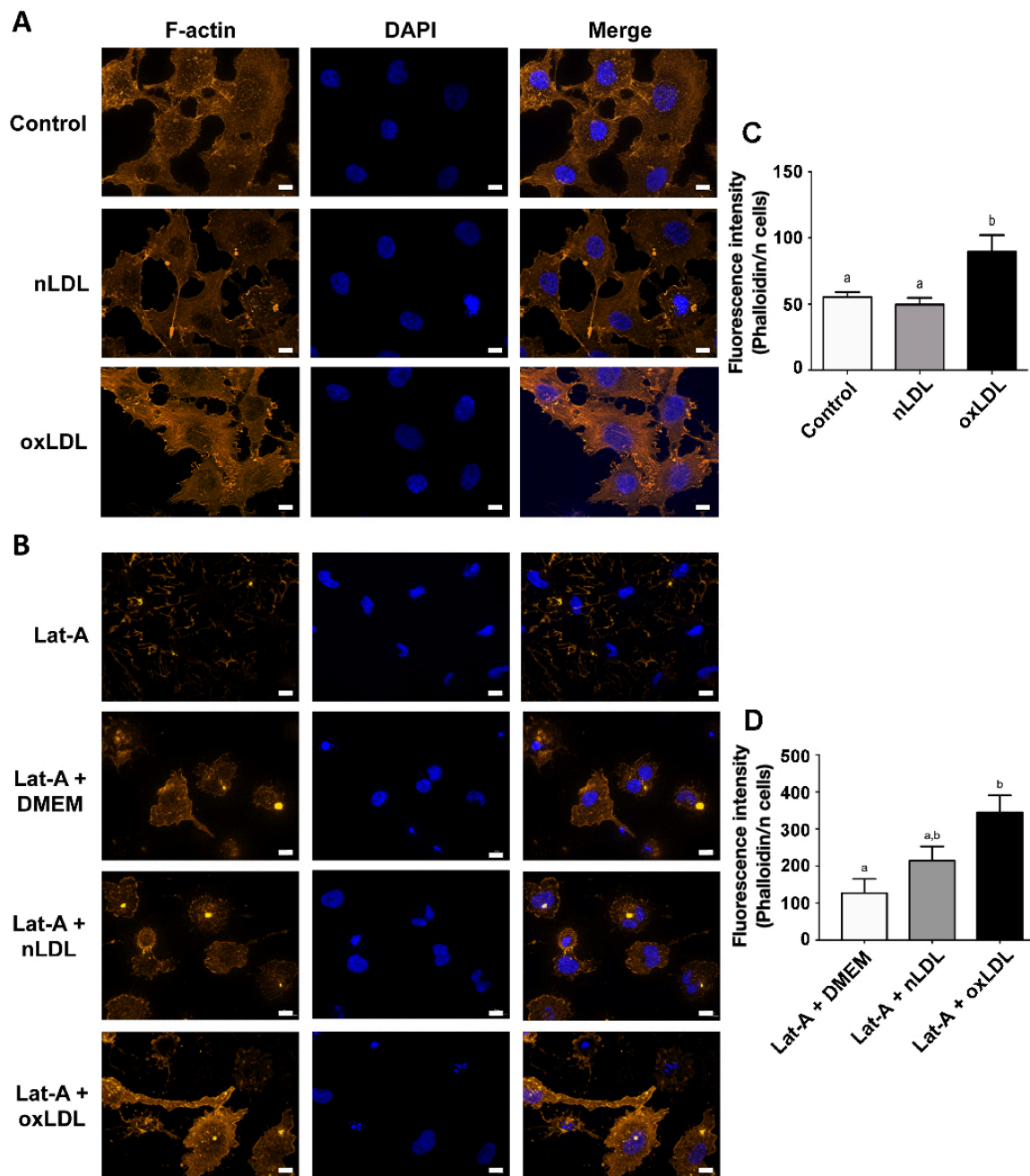


Figure 7: Actin cytoskeleton organization of endothelial cells upon treatment with oxLDL. (A) Representative images of cells treated or not with oxLDL or nLDL (50µg/ml) for 24 hours and labeled with Phalloidin-Alexa Fluor 546 to reveal F-actin filaments organization (left panels) and DAPI to reveal cell nuclei (middle panel). Right panels show a merge of the first two panels. Control cells were maintained in serum free DMEM for the same amount of time. (B) Representative images of cells treated with 95µM of Lat-A for 1 hour followed by treatment or not with oxLDL or nLDL (50µg/ml) for 24 hours. Cells were also labeled with Phalloidin-Alexa Fluor 546 (left panels), DAPI (middle panel). Right panels show a merge of the first two panels. Control cells were pre-treated with Lat-A and incubated with serum free DMEM for the same amount of time (24h). Images were captured in a Zeiss Axio Imager.Z2 (ApoTome.2 structured illumination system) fluorescence microscope using the 40x objective and the most representative images of the assay were shown. Scale bars: 20µm. (C) Graph shows Phalloidin- Alexa Fluor 546 fluorescence intensity of control non-treated cells, as well as oxLDL and nLDL treated cells. (D) Graph shows Phalloidin- Alexa Fluor 546 fluorescence intensity of

cells previously treated with Lat-A followed by treatment or not with oxLDL or nLDL. Different letters above bars indicate statistically significant differences ($p < 0,05$ using One-way ANOVA and Newman-Keuls post-test).

Representative frames are shown in Figure 8, revealing the non-treated control images and images from nLDL or oxLDL treated cells (Fig. 8A). Temporal correlation fits are shown below each frame and were used to determine the values of the relaxation time and amplitude of curvature (Fig. 8B and C, respectively). Similar to cholesterol depletion upon M β CD treatment of fibroblasts, cells exposed to oxLDL have an increase in cell stiffness, demonstrated by the increase in relaxation time (Fig. 8A-B and Supplementary Fig. 2A), which corroborates previous data from the literature Byfield et al., 2006; Chouinard et al., 2008; Kowalsky et al., 2008).

Exposure to nLDL (Supplementary Video 2) did not change cell stiffness, as observed by the similar values of relaxation time obtained for control and non-treated cells. We did not observe any changes on the amplitude of curvature among treatments (Figure 8C and Supplementary Fig. 2B and D). The absence of changes in membrane stiffness in nLDL treated cells confirmed previous results showing that this treatment is not able to induce stress fibers formation and therefore has no impact on cellular mechanical properties. This result reinforces that the effects observed for oxLDL treatment is due to rafts disruption, as described previously Byfield et al., 2006; Chouinard et al., 2008; Kowalsky et al., 2008).

5.2. *ECs exposure to oxLDL triggers deregulated lysosomal exocytosis*

It has been shown that changes in cell mechanical properties upon membrane cholesterol sequestration also triggers unregulated lysosomal exocytic events (Hissa et al., 2012). These exocytic events were shown to happen in the absence of extracellular Ca²⁺ and to be most likely induced by actin reorganization, which would push lysosomes against the cytosolic face of the plasma membrane contributing to its fusion. These events seem to compromise a peripheral pool of lysosomes, which are thought to be engaged with plasma membrane repair (PMR). Thus, we first tested whether this was also true for ECs treated with M β CD and then whether treatment with oxLDL would trigger the same effect.

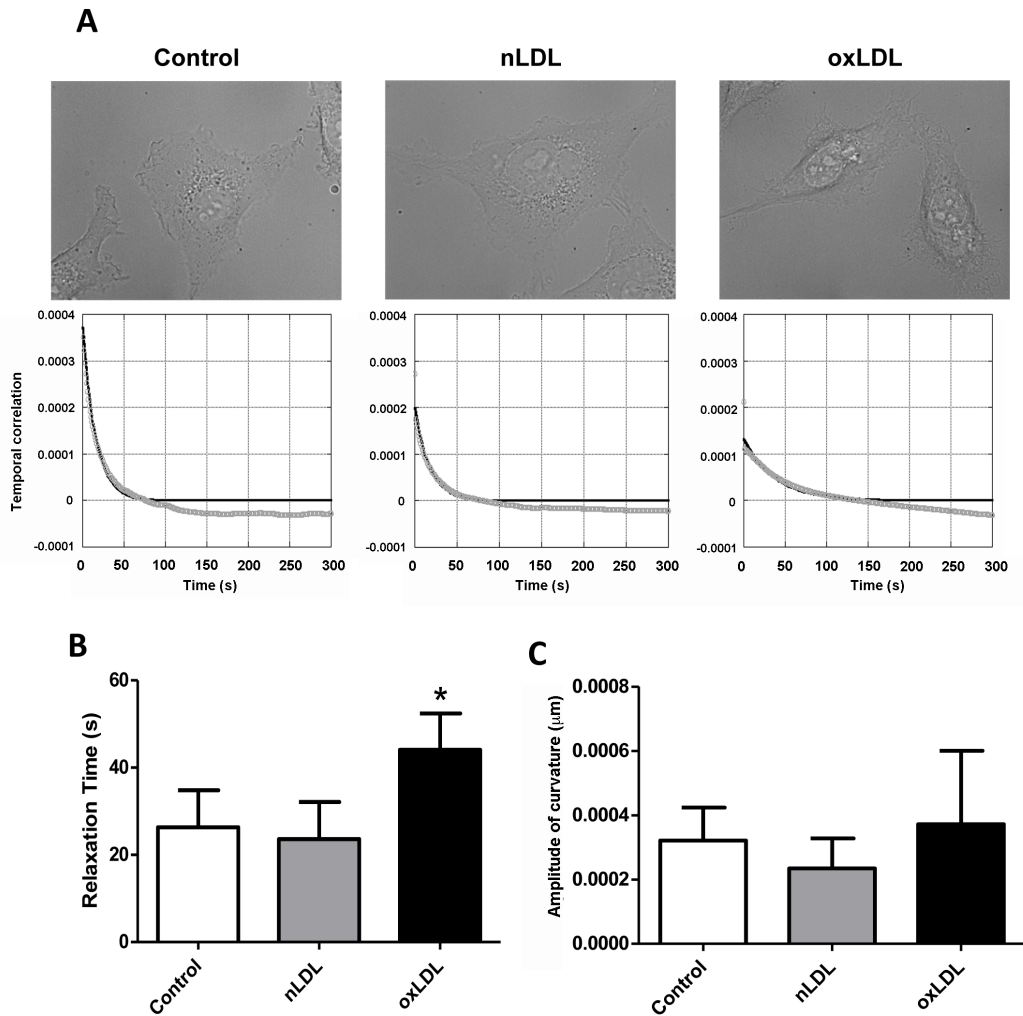


Figure 8: Defocusing microscopy of endothelial cells upon oxLDL treatment. (A) Representative DM images showing control untreated EC as well as nLDL and oxLDL treated cells (50 $\mu\text{g}/\text{ml}$ for 24h). Control cells were kept in serum-free medium for 24h before being recorded. Temporal correlation functions for each condition is also displayed under each representative images. (B) Relaxation time of control non-treated cells, as well as nLDL and oxLDL treated cells. (C) Amplitude of curvature of control non-treated cells, as well as treated cells. Different letters above bars indicate statistically significant differences ($p < 0,05$ using One-way ANOVA and Newman-Keuls post-test).

Lysosomal exocytosis upon treatment was quantified using a β -hexosaminidase secretion assay (Martinez et al., 2000). Briefly, cells were exposed to M β CD for 10-40 minutes or oxLDL/nLDL for 24h and β -hexosaminidase activity measured in the supernatant and cells lysates. As positive control, cells were exposed to 10mM Ionomycin for 10 minutes.

Exposure of ECs to both oxLDL (Fig. 9A) or M β CD (Fig. 9B) led to an increase in the levels of β -hexosaminidase activity in the cell supernatants. M β CD treatment doubled enzyme activity in the cell supernatant when compared to non-treated controls. These exocytic events were observed as early as 10 minutes of treatment (Fig. 9B). It is important to note that the

inactive analog of M β CD (H γ CD) did not show any effects on ECs exocytosis. For oxLDL treated cells, an increase of about 50% in β -hexosaminidase secretion in relation to control (non-treated) or nLDL treated cells was obtained (Fig. 9A).

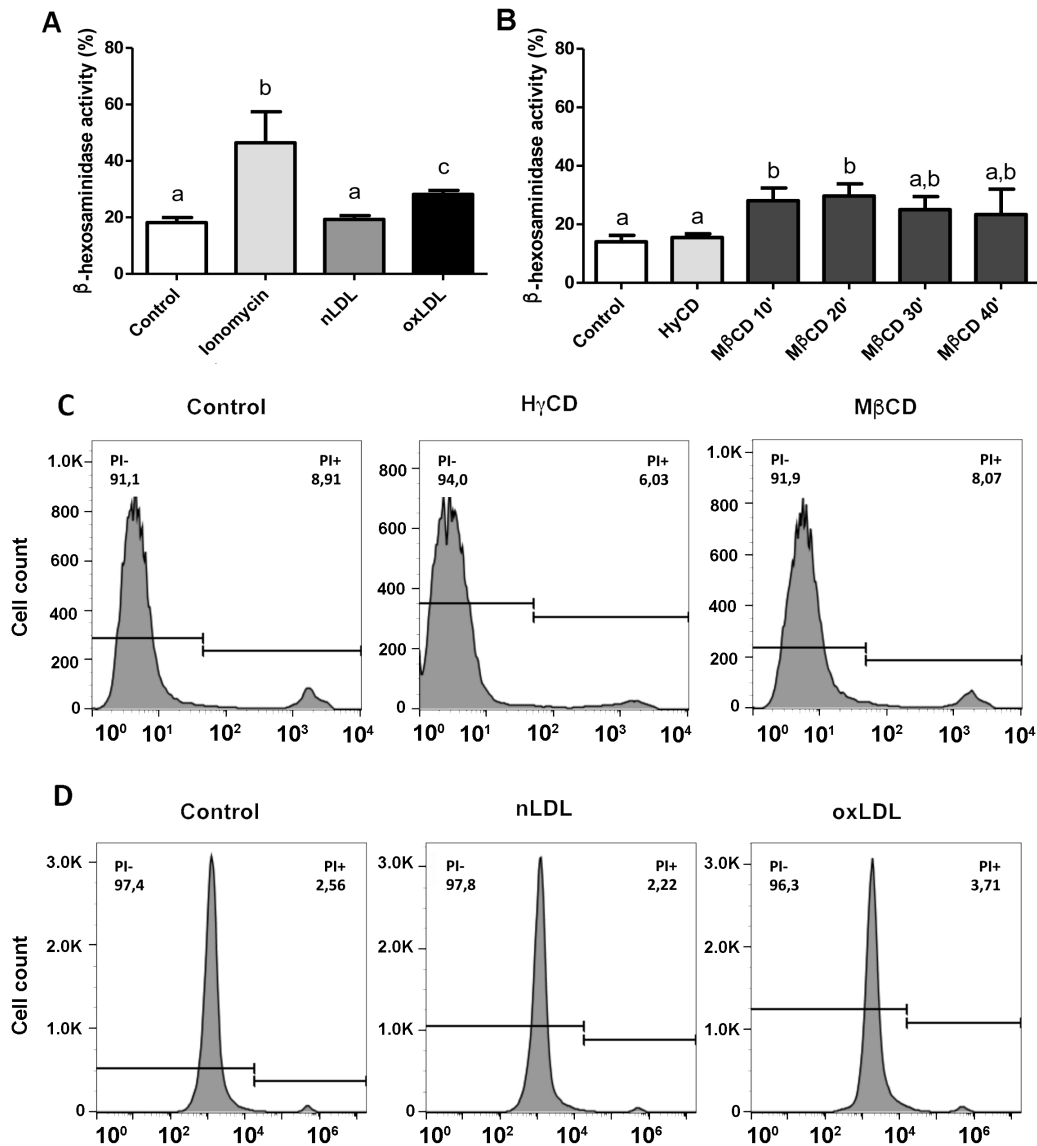


Figure 9: Quantification of lysosomal exocytosis through activity of β -hexosaminidase in cell culture supernatant. (A) Graph shows the percentage of β -hexosaminidase activity in the supernatant of EC cultures incubated for 24h in serum-free medium alone (non-treated control cells) or containing 50 μ g/ml nLDL or oxLDL. Results are expressed as percentage of the enzyme found in the supernatant in relation to total amount of the enzyme. (B) Graph shows the percentage of β -hexosaminidase activity found in supernatant of EC cultures incubated in serum-free medium alone (control non-treated cells) or containing HyCD (5mM) for 40 minutes, or serum-free medium containing M β CD (5mM) for different periods (10 to 40 min.). Different letters above bars indicate statistically significant differences ($p < 0,05$ using One-way ANOVA and Newman-Keuls post-test). (C-D) Analysis of cell viability through Propidium Iodide (PI) exclusion. ECs were treated with serum-free medium (control non-treated cells), M β CD or HyCD (5mM) for 40 min (C) and nLDL or oxLDL for 24h (D), then labeled with PI (10 μ g/mL) and

analyzed by flow cytometry. Histograms show the number of viable cells (PI-) and the number of non-viable cells (PI+).

In order to confirm that the increase in β -hexosaminidase activity observed for oxLDL treated cells was really due to lysosome exocytosis and not due to cell death, a cell viability assay was performed. The cell viability assay was performed by exposing control non-treated and treated (M β CD, nLDL or oxLDL) cells to Propidium Iodide. As expected, no significant differences in the percentage of PI labeled cells was observed between controls (non-treated and H γ CD treated cells) and M β CD treated cells (Fig. 9C). For assays, using LDL treated cells, non-treated controls showed less than 3% of PI labeled cells (2.56%), and similar values were observed for nLDL and oxLDL treated cells (2.22% and 3.71% of PI labeled cells, respectively) (Fig 9D). These results confirm that none of the treatments induce cell death and that the high amount of enzyme activity observed was indeed due to lysosomal exocytosis induced by M β CD and oxLDL treatment.

5.3. *OxLDL exposure impaired constitutive endocytosis in endothelial cells*

It is well known that every exocytic event is accompanied by compensatory endocytosis in order to maintain cell volume. Lysosomal exocytosis is no exception. On the other hand, cytoskeleton reorganization with an increase in peripheral actin stress fibers may compromise membrane trafficking especially at cell periphery (Aunis & Bader, 1988). We then evaluated whether actin rearrangements induced by ECs exposure to M β CD or oxLDL would compromise compensatory endocytic events following lysosome exocytosis.

We first evaluated compensatory endocytic events following lysosomal exocytosis induced by M β CD treatment. For this we performed a previously described compensatory endocytosis assay using a fluorophore conjugated Wheat Germ Agglutinin (WGA) (Idone et al., 2008). Briefly, the plasma membrane of a suspension of endothelial cells was labeled with WGA-Alexa Fluor 488, followed by treatment with M β CD for 10 to 40 minutes, after the quenching of the extracellular fluorescence with trypan blue, the intracellular fluorescence correspondent to the endocytosed dye was quantified by flow cytometry.

After 10 minutes of incubation with M β CD, non-treated cells showed higher levels of endocytosis when compared to cells treated with M β CD. However, between 10 to 20 minutes of treatment, a significant increase in compensatory endocytosis was observed for M β CD treated in relation to non-treated control cells, as indicated by the 1.37-fold increase in WGA-Alexa Fluor 488 fluorescence intensity in these cells when compared to non-treated controls (Fig. 10A). It is noteworthy that the increase in endocytic events occurs right after the peak of lysosomal exocytosis observed 10 minutes post treatment with M β CD in endothelial cells (see Fig. 9B). This result shows that compensatory endocytosis triggered by M β CD-induced exocytosis was not impaired.

Nonetheless, we have observed that constitutive endocytosis events in later time points, derived from pinocytosis, a very common process in ECs, are impaired in cells treated with the drug. Indeed, while control non-treated cells increased intracellular WGA-Alexa Fluor 488 fluorescence over time, M β CD-treated cells maintained a similar amount of fluorescence observed after 10 to 20 minutes of exposure to the drug.

In order to evaluate compensatory endocytic events following lysosomal exocytosis induced by oxLDL treatment we used an alternative assay. Because of the long period of exposure to oxLDL, endocytosis was evaluated by incubating cells for a period of 24h in the presence of Texas-Red Dextran, a fluorescent dye membrane impermeable. At determined time points during the 24-hour treatment, cells were washed to eliminate extracellular dextran-conjugated fluorophore, fixed and cell nuclei labeled with DAPI for further fluorescence microscopy analysis. Therefore, only the endocytosed fluorophore would be evaluated.

As shown in figure 10B and supplementary figure 3A, in all conditions it is possible to note a time-dependent increase in fluorescence intensity, indicating the occurrence of endocytic events. However the distribution of Texas-Red Dextran labeled vesicles seemed to differ when cells were exposed to oxLDL, when compared to control non-treated or nLDL treated cells (Fig. 10C and Supplementary Fig. 3A). While non-treated and nLDL-treated cells exhibit Texas-Red Dextran labeled vesicles disperse all over the cytoplasm throughout the different incubation times, vesicles from oxLDL-treated cells were accumulated in the perinuclear region, especially at later time points.

To further address this difference, we decided to perform a quantitative assay to measure vesicle dispersion using an approach previously described for lysosomes dispersion analyses (Hissa et al., 2013). Briefly, for each isolated nucleus it was calculated the mean distance between labeled vesicles (D) relative to the mean nucleus' radius (R), defined as the ratio D/R. Values closer to one indicated vesicles located closer to the perinuclear area, whereas values higher than one indicated locations further from the cell center and nearer the cell borders.

The graphs show the percentage of vesicles located at a specific D/R value (Fig. 10D). As shown in the graphs for control and nLDL treated cells it is possible to observe a high dispersion of vesicles throughout the cytoplasm in all times analyzed. This, as mentioned above, may indicate that these cells are able to endocytose during the entire period of the experiment. On the other hand, for oxLDL treated cells it is possible to observe a change in vesicle dispersion throughout time.

Eight hours post treatment, Texas-Red Dextran labeled vesicles seem less dispersed than vesicles from control and nLDL treated cells and show a very high percentage of vesicles close to the nuclei. This probably corresponds to endocytic events triggered by lysosomal exocytosis observed upon oxLDL treatment.

At 16h of oxLDL exposure, vesicle dispersion in these cells increase with a larger number of vesicles located at regions further from the cell nuclei and more similar to the distribution observed for control and nLDL treated cells. Then a shift back to cell nuclei is observed upon 24 hours of treatment, showing a noteworthy difference from their control and nLDL treated counterparts, even though not statistically significant. These results suggest that in oxLDL treated cells there are fewer events of endocytosis at later exposure times when compared to controls, indicating that new endocytic events might be compromised upon oxLDL treatment.

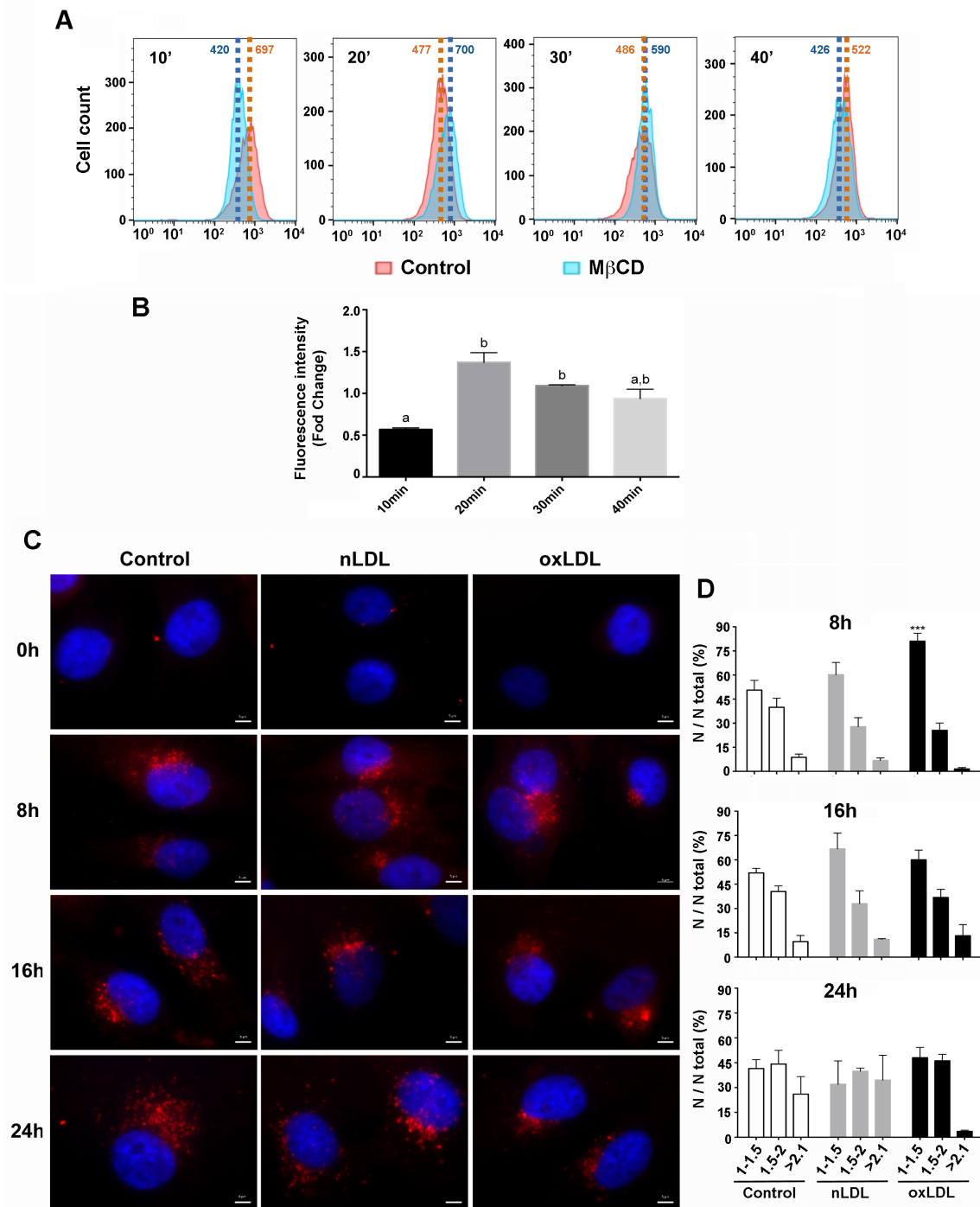


Figure 10: Quantitative analysis of endocytic events induced by the treatment alone. (A) ECs were labeled with WGA-Alexa Fluor 488 and treated with MβCD for 10 to 40 min. After treatment, plasma membrane fluorescence was quenched with trypan blue 0.2%, so that only fluorescence from endocytic vesicles would remain. Cells were then fixed and analyzed by flow cytometry. Histograms show the number, as well as WGA-Alexa Fluor 488 fluorescence intensity, of control non-treated (red) or MβCD treated cells (blue). The higher the fluorescence, the higher the number of endocytic events. (B) Graph shows the fold-change of WGA-Alexa Fluor 488 mean fluorescence intensity in MβCD treated cells in relation to non-treated control cells. Different letters above bars indicate statistically significant differences ($p < 0,05$ using One-way ANOVA and Newman-Keuls post-test). (C) ECs were exposed or not (control cells) to oxLDL or nLDL for 8, 16 or 24h in the presence of Texas-Red Dextran, a membrane impermeable fluorescent compound, washed, fixed, labeled with DAPI and analyzed in the fluorescence microscope Zeiss Axio Vert.A1 using a 100x objective. Panels show intracellular

vesicles containing Texas-Red Dextran (red) and cell nuclei (blue). (D) Quantitative analysis of Texas-Red Dextran labeled vesicle distribution, relative to cell nuclei, in control non-treated and nLDL or oxLDL treated cells. The mean distance between a vesicle and its respective nuclei center is represented by letter D and the mean vesicle distance relative to the mean nucleus' radius (R) was defined as the ratio D/R. Data are expressed as the percentage of vesicles from total (N/N total) located at a specific D/R. Asterisks indicate statistically significant differences ($p < 0,05$ using One-way ANOVA and Newman-Keuls post-test).

5.4. *OxLDL treated endothelial cells became more prone to mechanical injury*

It has been shown before by our group that M β CD induced cholesterol depletion leads to the exocytosis of a peripheral pool of lysosomes (Hissa et al., 2012), which has then been proposed to be the first one to exocytose upon signaling and thus more prone to participate in PMR (Hissa et al., 2013). Therefore both exocytosis and endocytosis are crucial steps for PMR. We have shown in the present work that cell exposure to oxLDL as well as to M β CD, leads to lysosomal exocytosis and compensatory endocytic events, likely triggered by the latter. However, we have also shown that cells exposure to oxLDL may compromise subsequent membrane trafficking events between cytoplasm and plasma membrane, likely due to the barrier formed by actin cytoskeleton rearrangement. This could then interfere with cells ability to perform PMR.

In fact, Idone, Tam & Andrews (2008) had shown that M β CD treatment inhibit plasma membrane repair by compromising compensatory endocytosis, in a concentration-dependent manner. Unexpectedly though, oxLDL-treated cells exhibited a significant increase in compensatory endocytosis upon scraping, indicating that these events are not impaired by the treatment with the lipoprotein (Supplementary Fig. 3B). However, it was also possible to observe in this experiment that cell counting was much smaller for oxLDL treated cells, when scraped in the absence of calcium, reflecting cell loss. This indicates that cells exposed to oxLDL are more prone to mechanical injury, which could be a consequence of the increase in cell stiffness upon treatment.

We then set out to investigate whether cells exposure to oxLDL would in fact affect cell's ability to perform plasma membrane repair. For this, we first performed a specific assay to address the amount of injury caused by cell scraping from the plate (see experimental design on figure 3), as described previously (Idone et al., 2008). Briefly, cells were treated with oxLDL for 24h and scraped from the surface they were adhered in the presence of PI. Next, cells

were allowed to recover from injury for 5 minutes at 37°C, followed by FACS analysis. In this model, since cell membrane is impermeable to PI, in the absence of plasma membrane rupture PI labeling would be prevented, characterizing the PI-negative peak in the histograms. In parallel, the PI-positive peak in the histograms provided the amount of cells injured by scraping from plates.

For non-treated cells, which rested in serum-free culture medium for the equivalent time as cells exposed to oxLDL (24h), about 30% of injured cells was obtained upon scraping (Fig. 11A and C). A similar amount of injured cells was found when cells were previously exposed to nLDL for 24h (33.5%) (Fig. 11A and C). However when cells were exposed to oxLDL for 24h and then scraped from the plate, approximately 50% of the cells were injured, representing an increase of 20% in the amount of injured cells when compared to control or nLDL treated cells (Fig. 11A and C). These results strongly suggest that oxLDL treatment makes cells more prone to mechanical injury.

We further investigated whether oxLDL treated cells were as efficient as non-treated or nLDL treated cells in performing PMR upon injury. For this, PI was only added after cells were scraped off the plate and allowed to repair. Using this approach, only cells that were not able to repair from injury would be labeled by PI. For control non-treated cells, 12.2% of injured cells were not able to repair (Fig. 11B and D). This result indicates that in control conditions about 58.5% of injured cells were able to recover from mechanical injury caused by scraping (Fig. 11E). Similar results were obtained for cells treated with nLDL. In the latter, about 12.8% of the cells were PI positive (Fig. 11B and D), which represents about 61,8% efficiency in repair (Fig. 11E). For oxLDL treated cells, the percentage of total cells that were not able to recover from injury was significantly higher (25.4%) when compared to the other two groups (Fig. 11B and C). Additionally, a smaller percentage of cells recovered from injury (about 48.6%) when compared to control non-treated or nLDL treated cells (Fig. 11E). These results reinforce that exposure to oxLDL make cells more susceptible to membrane injury.

Since cell scraping is very aggressive we decided to use also a less disruptive assay to measure cell susceptibility to injury and PMR in the different conditions. For this, cells (treated or not) were submitted to a shear stress of approximately 7 dyne/cm² in an orbital shaker. Subsequently, cells were

incubated with PI in order to stain cells that were not able to repair from injury. PI stained cells were then counted in a microscope. For control non-treated cells, we observed 290.25 ± 90.5 PI positive cells after orbital flow exposure. A similar amount of PI-positive cells were found in nLDL-treated cells (259 ± 57.7). Cells exposed to oxLDL, on the other hand, revealed to be significantly more susceptible to the flow-induced injury, showing a 2.4-fold increase in PI-positive cells (693.25 ± 200.6) when compared to the control group (Fig. 11F and G). Using this approach, cells exposed to oxLDL showed once again to be more susceptible to injury.

Even though the decrease in the relative efficiency of PMR was not statistically different when cells were exposed to oxLDL, our results indicate that cell susceptibility to mechanical injury is enhanced in this condition and the absolute values of cells that are not able to recover from this extensive injury is significantly higher.

Based on our results using this *in vitro* approach, we believe that at the early stages of oxLDL exposure, the treatment induces actin cytoskeleton rearrangements and de novo actin polymerization, leading to increased cell stiffness in endothelial cells. During this period of actin rearrangement, the cell is still able to realize lysosomal exocytosis, probably using the actin reorganisation and polymerisation as a physical stimuli to fusion with the plasma membrane. As a consequence, we observe a peak of endocytosis that might represent compensatory endocytosis events (Fig. 12A). As the time of oxLDL exposure increases, with actin cytoskeleton already rearranged, cells face a disturbance on vesicle trafficking events, such as the impairment on constitutive endocytosis, between cell cytoplasm and plasma membrane probably due to the cytoskeleton works as a barrier for new events (Fig. 12B).

The alterations in the mechanical properties of endothelial cells exposed to oxLDL, in special the increase in cell stiffness, enhance cell susceptibility to mechanical injury (Fig. 12C). We believe that with the injury, the barrier of the cytoskeleton is destroyed locally in the lesion site, allowing exocytosis and compensatory endocytosis to happen, resealing the injured membrane (Fig. 12D). Even though cells are still able to perform PMR, the absolute amount of cells that can not repair the injury is considerable and it might have a physiological impact, contributing to endothelial fragility and atherosclerotic plaque formation.

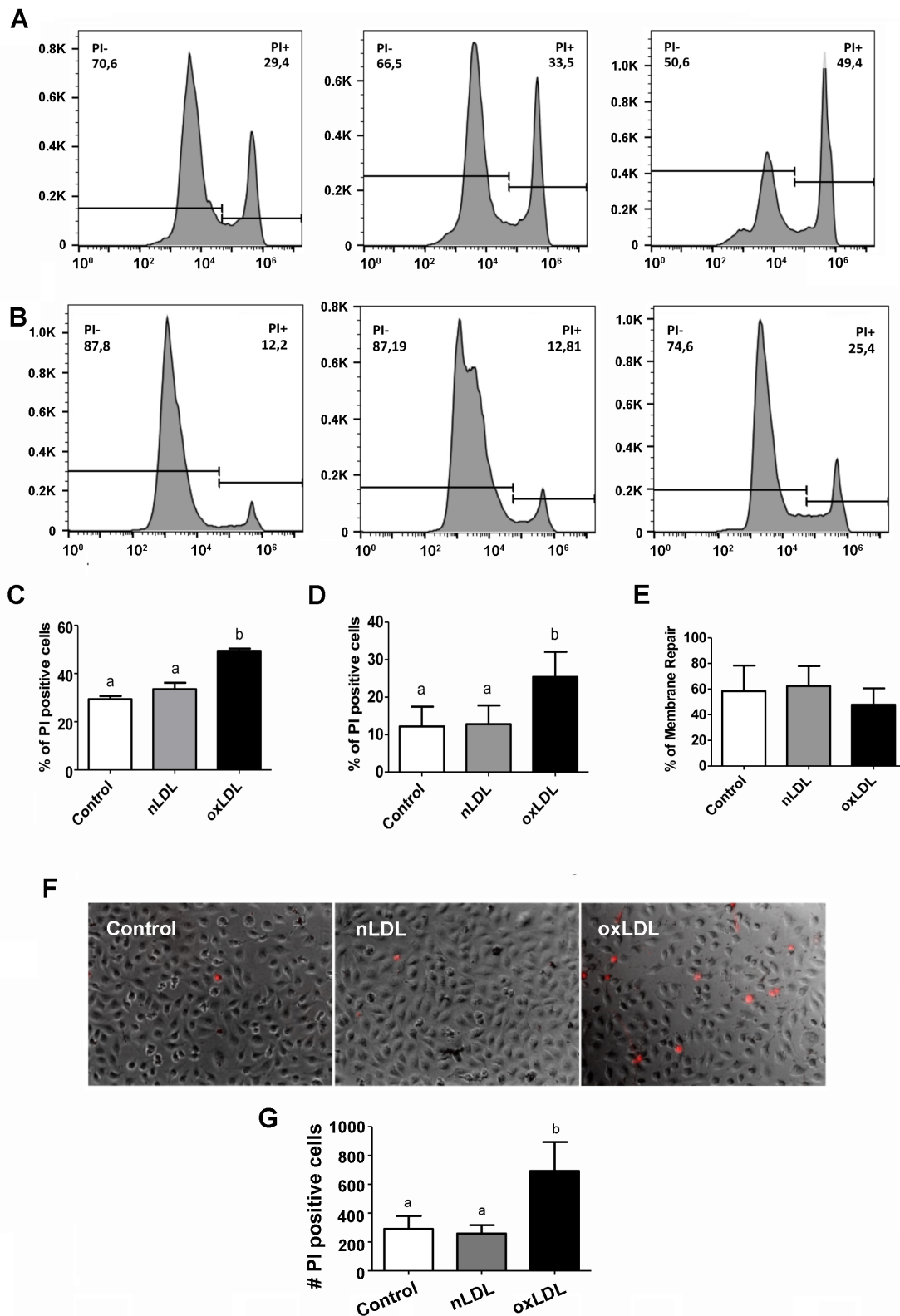


Figure 11: Quantitative analysis of compensatory endocytosis, injury level and PMR ability of ECs submitted to mechanical injury. (A) Analysis of injury level caused by cell scraping in the different conditions (control non-treated, 50 μ g/ml nLDL or oxLDL treated cells). ECs were incubated for 24h in serum-free medium alone (control non-treated cells) or containing 50 μ g/ml nLDL or oxLDL, submitted to injury by scraping in the presence of Propidium iodide (PI - 10 μ g/mL) and analyzed by flow cytometry. Histograms show the number of non-injured cells (PI-) and the number of injured cells (PI+). (B) Analysis of ECs PMR ability upon mechanical injury in the different conditions (control non-treated, 50 μ g/ml nLDL or oxLDL treated cells). ECs were incubated for 24h in serum-free medium alone (non-treated control

cells) or containing 50µg/ml nLDL or oxLDL, submitted to injury by scrapping, allowed to recover from injury and then incubated with PI (10µg/mL) before flow cytometry analysis. Histograms show the number of non-injured cells as well as cells that recovered from injury cells (PI-) and the number of injured cells that were not able to recover from injury (PI+). (C) Graph shows the quantitative analysis from three different experiments of the percentage of cells that were injured upon scrapping in the different conditions. (D) Graph shows the quantitative analysis from three different experiments of the percentage of cells that did not recover from injury upon scrapping in the different conditions. (E) Graph shows the percentage of membrane repair after injury in the different conditions relative to the total injury induced by scrapping. Different letters above bars indicate statistically significant differences ($p < 0,05$ using One-way ANOVA and Newman-Keuls post-test). (F) Analysis of the injured cells number upon orbital flow in the different conditions (control non-treated, 50µg/ml nLDL or oxLDL treated cells). ECs were incubated for 24h in serum-free medium alone (control non-treated cells) or containing 50µg/ml nLDL or oxLDL, submitted to injury by inducing a flow in a horizontal shaker for 1h. Cells were allowed to recover from injury and then incubated with PI (10µg/mL) before fluorescence microscope analysis. Panels show representative merged images of ECs in brightfield and PI+ cells (red). (G) Graph shows the number of injured cells (PI+) in each condition. Different letters above bars indicate statistically significant differences ($p < 0,05$ using One-way ANOVA and Newman-Keuls post-test).

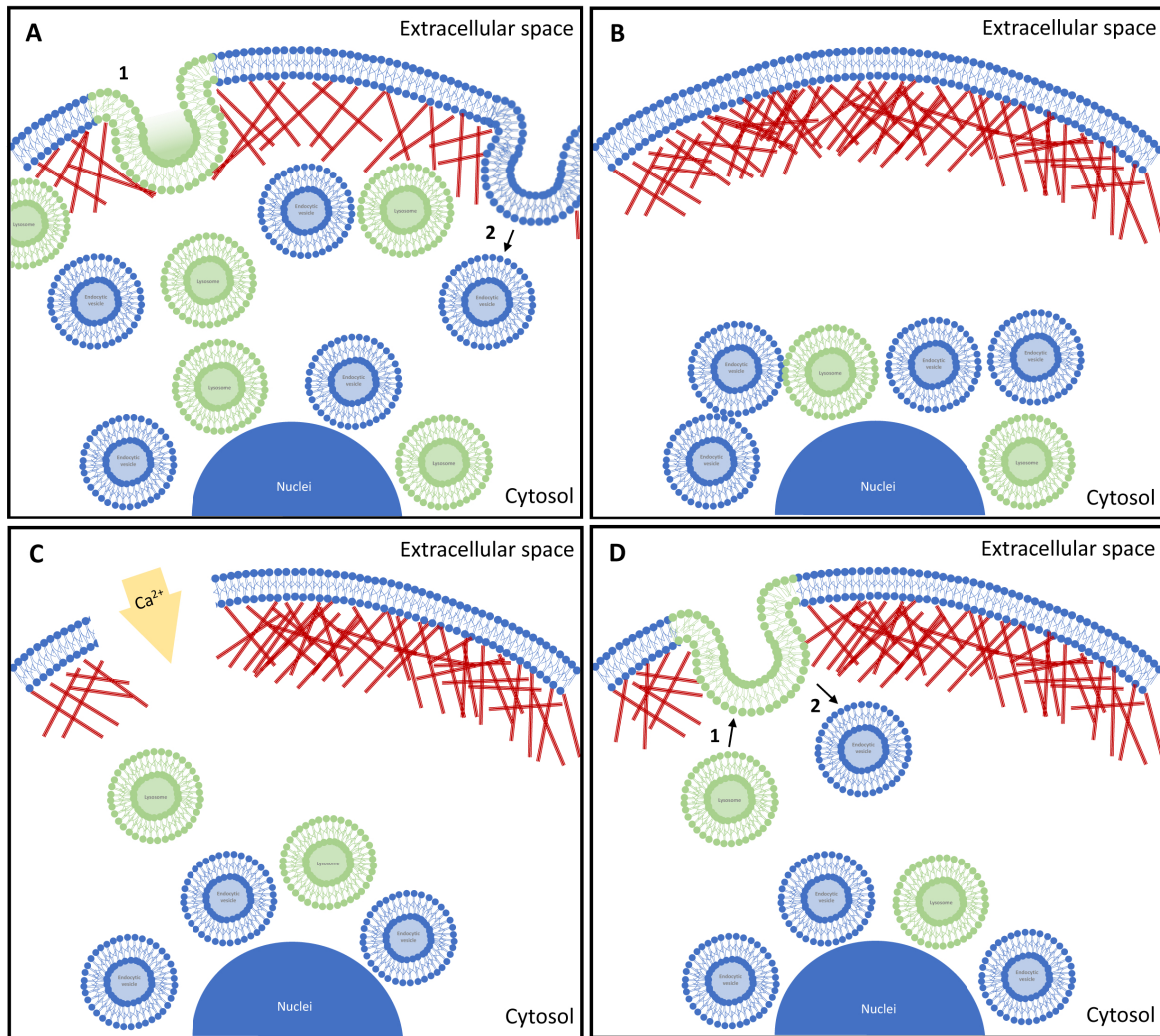


Figure 12: Schematic illustration of the *in vitro* study hypothesis. (A) During the first hours of oxLDL exposure, EC presents a window between the initial actin rearrangement, which stimulates lysosomal exocytosis (1), and its complete reorganization that allows for

compensatory endocytosis (2) to occur. (B) Once actin cytoskeleton is completely rearranged at the cell periphery, new membrane trafficking events are compromised. (C) Upon enhanced stiffness, mechanical injury causes disruption of local actin filaments, thereby breaking cytoskeleton barrier, allowing Ca^{2+} influx. (D) The increase in Ca^{2+} cytosolic concentration, stimulates the membrane trafficking at the cell periphery important to PMR, once lysosomal exocytosis (1) and its subsequent compensatory endocytosis (2) are allowed to happen, therefore resealing the plasma membrane.

5.5. *Accumulation of lipids in the arterial wall and alterations on cell actin labelling*

Our *in vitro* results indicated that ECs exposure to oxLDL, a key molecule during atherosclerosis development, lead to actin reorganization and *de novo* polymerization, increasing cell rigidity and turning cells more prone to mechanical injury. Additionally, constitutive endocytosis, arising from pinocytic processes, common in these cells, was blocked upon treatment, suggesting the reorganized cytoskeleton function as a mechanical barrier to membrane trafficking.

In order to address whether the observed *in vitro* ECs changes in mechanical properties, as well as their consequences (defects in vesicle trafficking or membrane susceptibility to injury) would also occur *in vivo* and whether these changes would in fact contribute to atherosclerotic plaque formation, we used a well known mouse model of atherosclerosis, ApoE^{-/-} mice fed with high cholesterol diet. Additionally, since shear stress is an important factor for atherogenesis, mice right carotid arteries were exposed to different hemodynamic environments by surgically implanting a shear stress modifier device (cast) (Fig. 4), as described in the methods. Wild Type C57BL/6 under the same diet and hemodynamic conditions were used as controls. Data obtained from cast implantation was compared not only among animals (WT and ApoE^{-/-}), but also with data obtained from the left carotid artery of the same animal, which was used as an internal control.

Once the results obtained from the *in vitro* model may represent the initial stages of atherosclerosis development, we decided to perform our *in vivo* experiments analysing a time point previous to plaque formation. For this, Oil Red O staining was used to label the accumulation of lipids in atherosclerotic plaques, 1-5 weeks post cast implantation (n=4).

Figure 13 shows the representative images of each group indicating the timeline of atherosclerosis development in the chosen model (Fig. 13A and B),

and the quantification of atherosclerotic plaque size in each region of both carotid arteries (Fig. 13 C and D). As expected, wild type C57BL/6 mice did not present any plaque formation (Fig. 13A, C and D), not even at 5wpci, the maximum extent of the study. Meanwhile, ORO staining revealed an early formation of atherosclerotic plaques in ApoE^{-/-} mice (Fig. 13B, D). Accumulation of lipids and plaque formation was observed as early as 1 wpci (1 mouse). Results of mice in the following week (2 wpci) revealed a slight increase in the number of plaque-positive animals (2 mice), but similarly to the 1 wpci group, it was not statistically significant due to the variability among animals. As shown in Figure 13 B and D, the number of plaque-positive mice and the atherosclerotic plaque size increased exponentially during the weeks post cast implantation.

Our results also indicates a major role of different shear stress patterns on atherosclerosis development as we identified a lower number of plaques, with smaller sizes, in the contralateral carotid artery which was not exposed to modified shear stress (Fig. 13A, B and C). Based on these results and considering the number of plaque-positive mice, we decided to continue our investigation at 1 week post cast implantation.

We then set out to investigate whether the accumulation of lipids in the arterial wall and/or changes in shear stress pattern was accompanied to changes in biomechanics properties of cells in the arterial wall and more specifically in the endothelium, as previously observed *in vitro*. For this we analyzed the actin cytoskeleton labelling in carotid arteries collected from 1-wpci ApoE^{-/-} and C56BL/6 mice using Phalloidin-Atto 565 (Figure 14A). The fluorescence intensity was quantified and compared between the two groups.

When considering Phalloidin-Atto 565 fluorescence intensity (FI) in the entire ApoE^{-/-} and C56BL/6 mice arterial walls, we noticed a subtle increase, although not statistically significant, in phalloidin labelling in LSS and OSS regions of ApoE^{-/-} mice in relation to C56BL/6 (Figure 14C). These regions are known for accumulating lipids and developing atherosclerotic plaques, compared to the proximal and distal regions of the contralateral artery.

When analysing only C57BL/6 mice, we observed a subtle decrease in phalloidin FI in LSS and HSS regions when compared with proximal and medial regions of its contralateral artery, but again this was not statistically different (Figure 14B). Our statistical analysis also did not indicate any differences when

comparing the FI of the different regions between ApoE^{-/-} and C56BL/6 mice (Figure 14D and E).

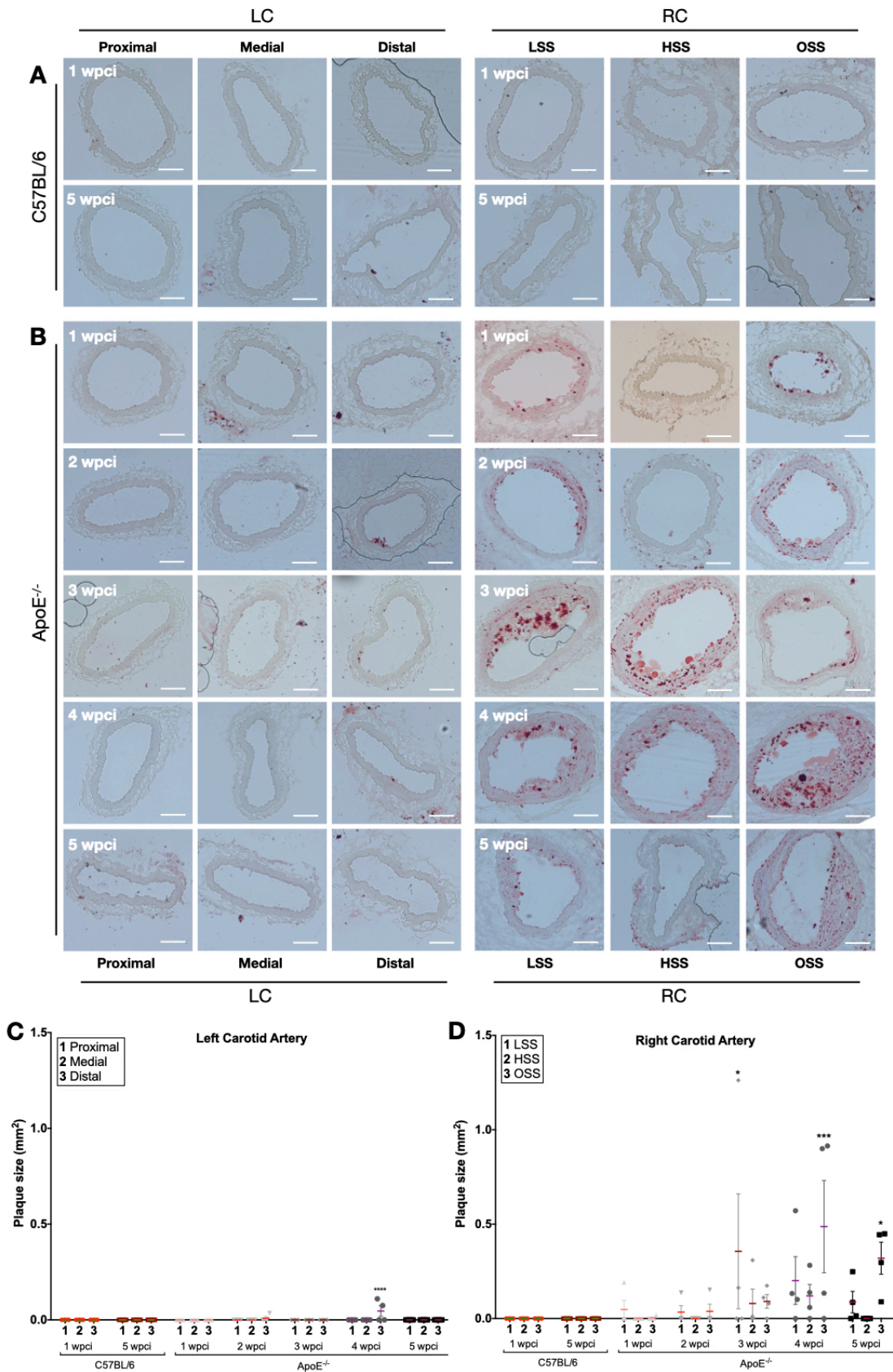


Figure 13: Timeline of plaque formation in ApoE^{-/-} mice. (A) Oil Red O staining of left and right carotids (LC and RC, respectively) of ApoE^{-/-} mice 1 to 5 weeks post cast implantation (wpci) (n=4). (B) Quantification of plaque size in the left carotid artery of ApoE^{-/-} mice 1 to 5 wpci

and C57BL/6 mice 1 and 5 wpci (n=4). (C) Quantification of plaque size in the right carotid artery of ApoE^{-/-} mice 1 to 5 wpci and C57BL/6 mice 1 and 5 wpci. Asterisks indicate statistic difference to the respective control C57BL/6 (p<0,05 using Two-way ANOVA).

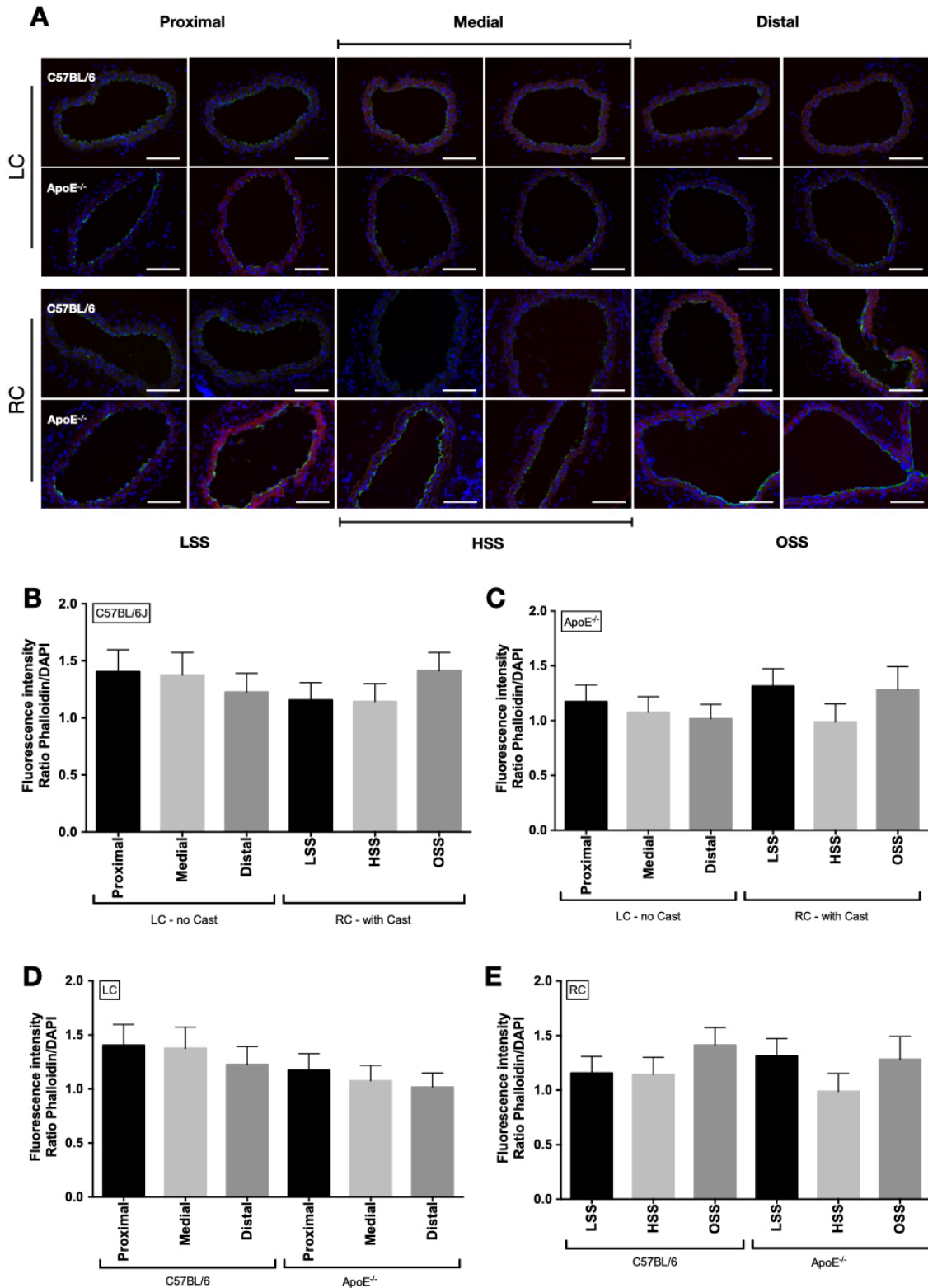


Figure 14: Actin cytoskeleton staining in carotid artery wall of ApoE^{-/-} and C57BL/6 mice. (A) Representative images of phalloidin-Atto 565 staining of left and right carotids (LC and RC, respectively) of C57BL/6 and ApoE^{-/-} mice. (B) Quantification of Phalloidin-Atto 565 FI in LC and RC of C57BL/6 mice. (C) Quantification of Phalloidin-Atto 565 FI in LC and RC of ApoE^{-/-} mice. (D) Comparison of Phalloidin-Atto 565 FI in LC between C57BL/6 and ApoE^{-/-} mice. (E) Comparison of Phalloidin-Atto 565 FI in RC between C57BL/6 and ApoE^{-/-} mice.

In the endothelium of both ApoE^{-/-} and C57BL/6 mice we observed a slight reduction in phalloidin FI in the RC, although this difference was not statistically significant (Figure 15). Actin FI seems to differ among the distinct regions in ApoE^{-/-} mice carotid arteries when compared to C57BL/6, suggesting a role of hyperlipidemia in actin cytoskeleton organization. Furthermore, even though not statistically different, we also observed a tendency in actin accumulation in ECs from the distal region of the LC and LSS and OSS regions of the RC of ApoE^{-/-} mice, which might be potentially associated with lipid accumulation in the arterial wall and with the following atherosclerotic lesions.

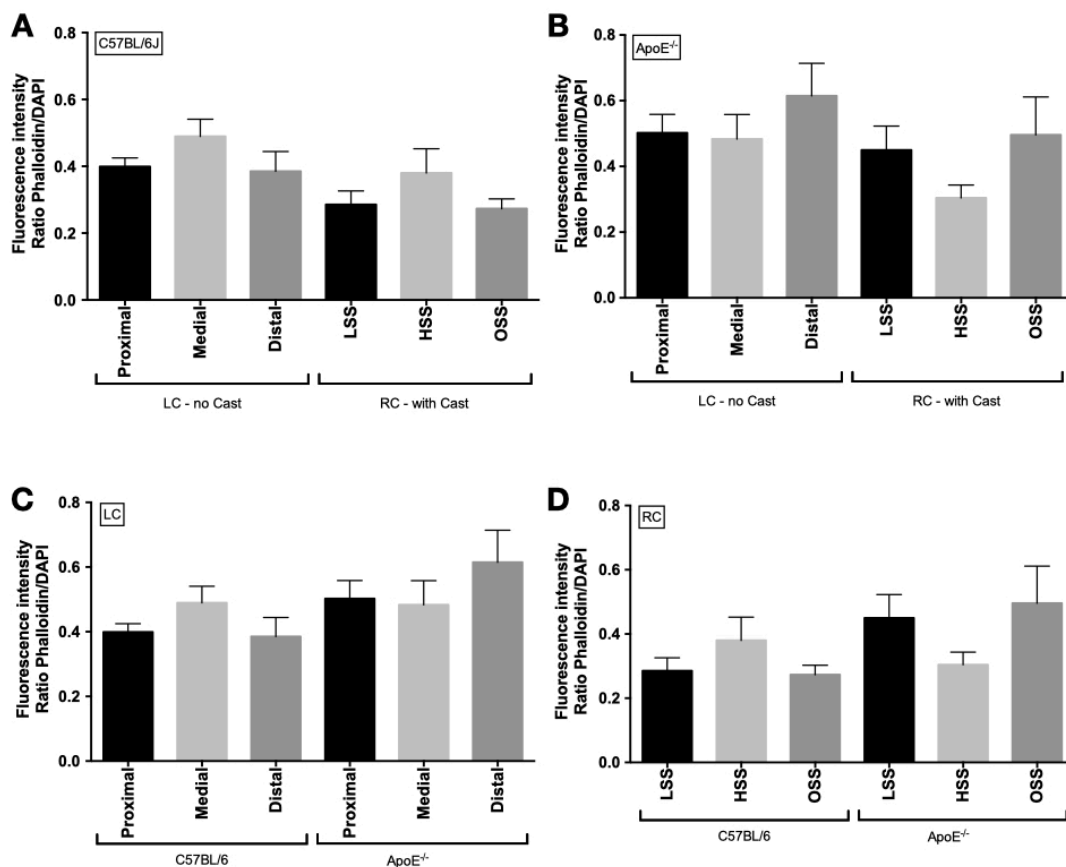


Figure 15: Actin cytoskeleton staining in the endothelium of ApoE^{-/-} and C57BL/6 mice. (A) Representative images of phalloidin-Atto 565 staining of left and right carotids (LC and RC, respectively) of C57BL/6 and ApoE^{-/-} mice. (B) Quantification of Phalloidin-Atto 565 FI in LC and RC of C57BL/6 mice. (C) Quantification of Phalloidin-Atto 565 FI in LC and RC of ApoE^{-/-} mice. (D) Comparison of Phalloidin-Atto 565 FI in LC between C57BL/6 and ApoE^{-/-} mice. (E) Comparison of Phalloidin-Atto 565 FI in RC between C57BL/6 and ApoE^{-/-} mice.

In order to further evaluate the role of hyperlipidemia in actin cytoskeleton organization of vascular cells, we performed a qualitative analysis of the carotid arteries cross sections. For that, images were captured in the Zeiss Axio Imager.Z2 (ApoTome.2 structured illumination system) fluorescence

microscope using the 63x objective. Representative images of LC and RC of both animal groups are shown in figure 16A and B, respectively.

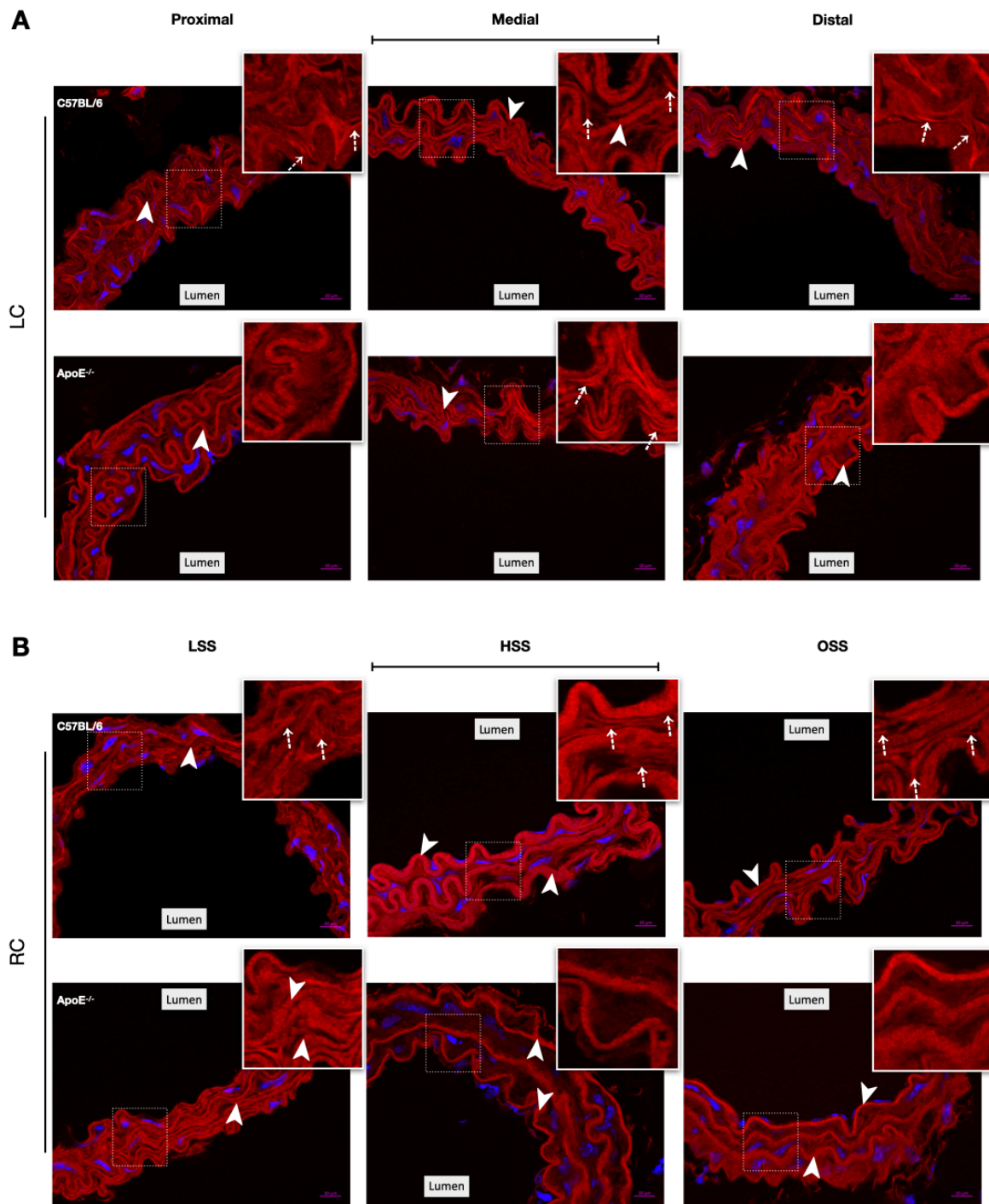


Figure 16: Actin cytoskeleton organization in the vascular wall of ApoE^{-/-} and C57BL/6 mice. Representative images of Phalloidin-Atto 565 staining in the different regions of (A) left carotids artery (LC) and (B) right carotid artery (RC) of C57BL/6 and ApoE^{-/-} mice. The cells were also stained with DAPI for nuclei (blue). Merged fluorescent images are shown. Scale bar, 10µm. Arrowheads: elastic fibers are evidenced by its autofluorescence. Dash arrows indicates filament-like structures. Insets show magnification images of the boxed regions. Images were captured in the Zeiss Axio Imager.Z2 (ApoTome.2 structured illumination system) fluorescence microscope using the 63x objective.

Insets show magnification images of the boxed regions for a better detailed examination. It is important to state that elastic fibers are strongly evidenced in the images due to its autofluorescence, as demonstrated by the arrowheads. In both carotid arteries (LC and RC) we could observe an alteration on actin cytoskeleton organization between the control C57BL/6 and ApoE^{-/-} mice as it can be seen by the presence of more filament-like structures (indicated by dashed arrows) in the control group, while ApoE^{-/-} mice display a more diffuse actin labelling, with exception to its medial-LC region. These qualitative differences still need to be quantified.

5.6. Effects of shear stress and hyperlipidemia in cell susceptibility to injury in the arterial wall and in the endothelium.

According to our *in vitro* results, endothelial cell exposure to excess oxLDL increased cell susceptibility to injury, which were much likely related to changes in cell biomechanics. Thus, we set out to investigate whether hyperlipidemia and/or alterations in patterns of shear stress would enhance cell susceptibility to mechanical injury caused by blood flow.

For that, 1 week after cast implantation, ApoE^{-/-} and C57BL/6 mice were perfused with PBS containing PI (500µg/ml). Since PI is a membrane impermeable fluorophore, it can only enter the cell upon membrane injury.

In both arterial wall and endothelium, shear stress alone was able to increase injury in areas of HSS in the RC either in ApoE^{-/-} and C57BL/6 mice (Figure 17 and 18). Furthermore, we observed an increase of injury in LSS region when analyzing the arterial wall of ApoE^{-/-} when compared to its contralateral control (Figure 17C).

5.6. Effects of shear stress and hyperlipidemia in lysosomal content in the arterial wall and in the endothelium.

Our *in vitro* data suggested that the biomechanics changes observed in endothelial cells exposed to oxLDL made them more prone to injury when compared to non-treated cells. OxLDL exposure also triggered lysosomal exocytic events (Fig. 9), as well as led to impaired constitutive endocytosis (Fig. 10). Under physiological conditions, cells are continuously exposed to situations that can generate microinjuries in the cell membrane, especially those subject

to mechanical stress, as endothelial cells. When unrepaired, these injuries lead to cell death. Since membrane repair depends on vesicle trafficking between the plasma membrane and the cell interior, any interference in this process, as is the case upon cell exposure to oxLDL or cholesterol depletion, could compromise membrane repair ability and thereby contribute to the initial events of atherosclerotic plaque formation.

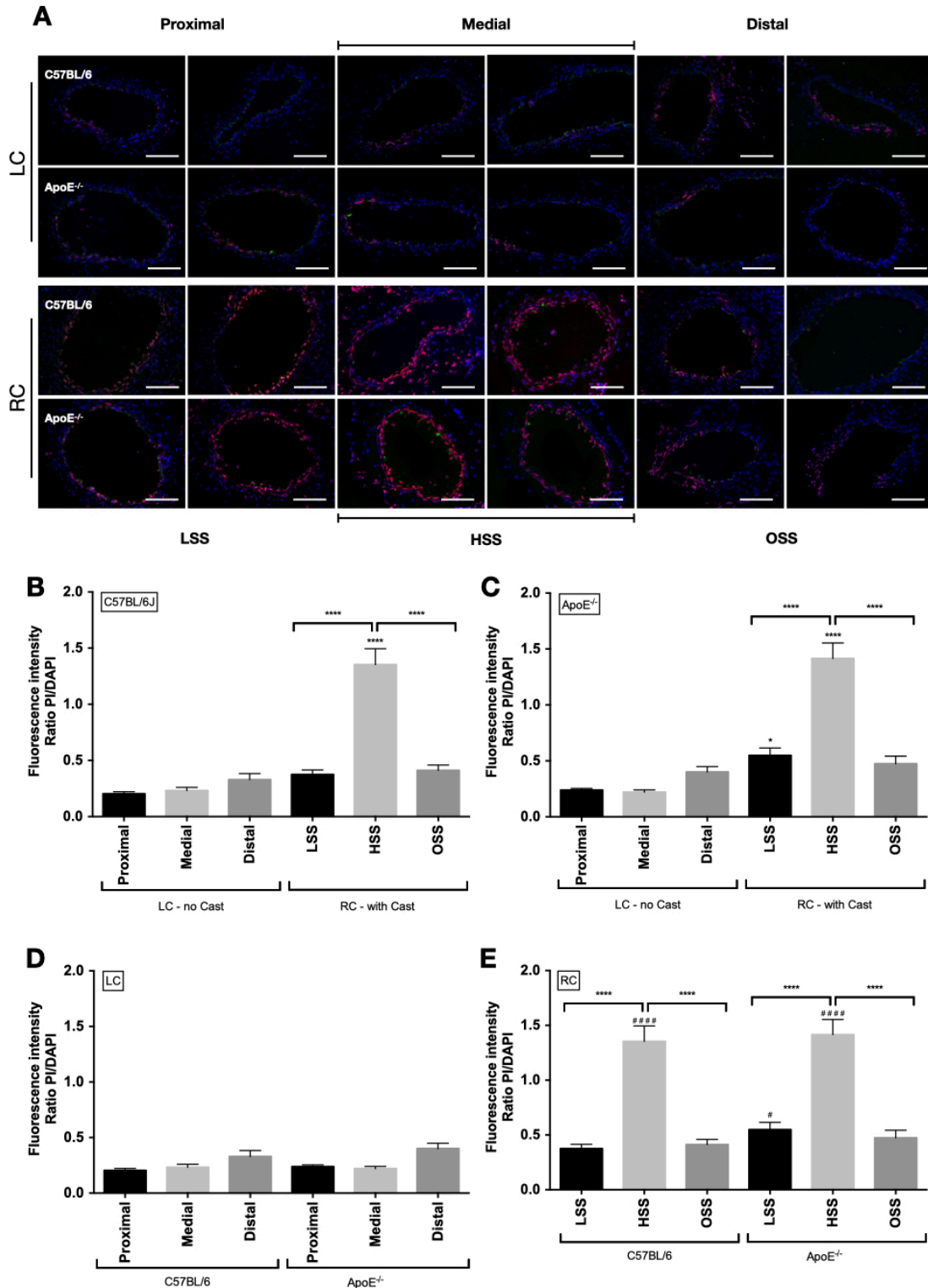


Figure 17: Level of injury in carotid artery wall of ApoE^{-/-} and C57BL/6 mice. (A) Representative images of Propidium Iodide (PI) staining of left and right carotids (LC and RC, respectively) of C57BL/6 and ApoE^{-/-} mice. (B) Quantification of PI FI in LC and RC of C57BL/6 mice. (C) Quantification of PI FI in LC and RC of ApoE^{-/-} mice. (D) Comparison of PI FI in LC between C57BL/6 and ApoE^{-/-} mice. (E) Comparison of PI FI in RC between C57BL/6 and ApoE^{-/-} mice. Asterisks above bars indicate statistic difference in comparison to the respective contralateral artery; asterisks brackets indicate statistic difference between regions of the same artery; in (E), hash above bars indicate statistic difference in comparison to the respective contralateral artery in graph (D) (p<0,05 using One-way ANOVA and Newman-Keuls post-test).

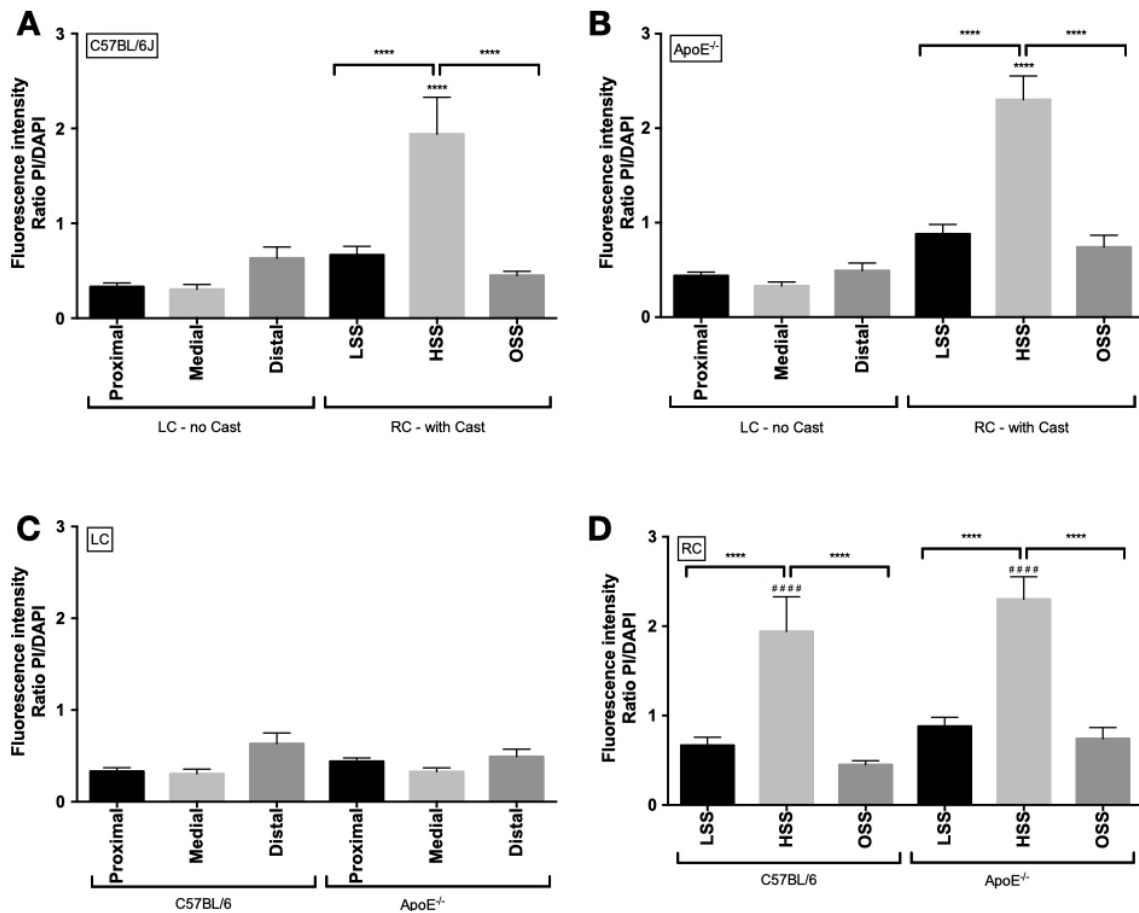


Figure 18: Level of injury in the endothelium of ApoE^{-/-} and C57BL/6 mice. (A) Quantification of PI FI in LC and RC of C57BL/6 mice. (B) Quantification of PI FI in LC and RC of ApoE^{-/-} mice. (C) Comparison of PI FI in LC between C57BL/6 and ApoE^{-/-} mice. (D) Comparison of PI FI in RC between C57BL/6 and ApoE^{-/-} mice. Asterisks above bars indicate statistic difference in comparison to the respective contralateral artery; asterisks brackets indicate statistic difference between regions of the same artery; in (D), hash above bars indicate statistic difference in comparison to the respective contralateral artery in graph (C) (p<0,05 using One-way ANOVA and Newman-Keuls post-test).

On account of being such an important step to PMR, and since we had seen an increase in cell injury after cast implantation, we decided to investigate whether any interference with lysosomal exocytosis would be observed in ApoE^{-/-} and C57BL/6 mice. To answer this question, after PI perfusion, we

measured the amount of LAMP-2 intracellular distribution and exposure to the plasma membrane in the carotid arteries of the different animals (Fig. 19A).

First, we evaluated LAMP2 FI in the entire arterial wall. In control C57BL/6 mice, the proximal and medial regions of the LC showed higher values of LAMP-2 FI when compared to the distal regions. Proximal and medial regions are known to have high shear stress while it is demonstrated an oscillatory shear stress in the distal region. In the RC, in which we implanted the cast, C57BL/6 mice presented a different profile of lysosomal distribution with higher LAMP-2 FI in the HSS region (Fig. 19B).

In ApoE^{-/-} mice, we did not observe any alterations in LAMP-2 staining neither in LC nor RC (Fig. 19C). In fact, when we compared the FI values in the LC between both groups, ApoE^{-/-} mice displayed a decrease in lysosomal vesicles in the proximal and medial regions (Fig. 19D), presenting values similar to the distal region. We did not find any difference in the RC when comparing both groups (Fig. 19E). It is important to notice that while C57BL/6 mice had an increase in HSS region, ApoE^{-/-} mice did not show any alteration in LAMP-2 FI, even with the increase in injury level in the region.

When considering just the endothelial layer, the results found in the LC of C57BL/6 mice were similar to the one found for the entire arterial wall showing an increase in LAMP-2 FI in proximal and medial regions. Surprisingly, the same profile was found in the RC were LSS and not only HSS showed a higher FI for LAMP-2 when compared to OSS region (Fig. 20A). There was no statistically significant difference when comparing the regions with their contralateral controls. In the endothelium of ApoE^{-/-} mice (Fig. 20B), we observed an increase in LAMP-2 FI in the proximal region of the LC compared to its distal region. In the RC, there was an increase in FI in HSS region in comparison to the other regions of the same artery and to the medial region of its contralateral artery.

When we compared LAMP-2 FI found in LC and RC between groups (Fig. 20C and D) we observed a decrease in lysosomal staining in ApoE^{-/-} mice specifically in the medial region of the LC and the LSS region of the RC. These results indicated a disturbance in vesicle trafficking in the arterial wall and endothelium of ApoE^{-/-} mice.

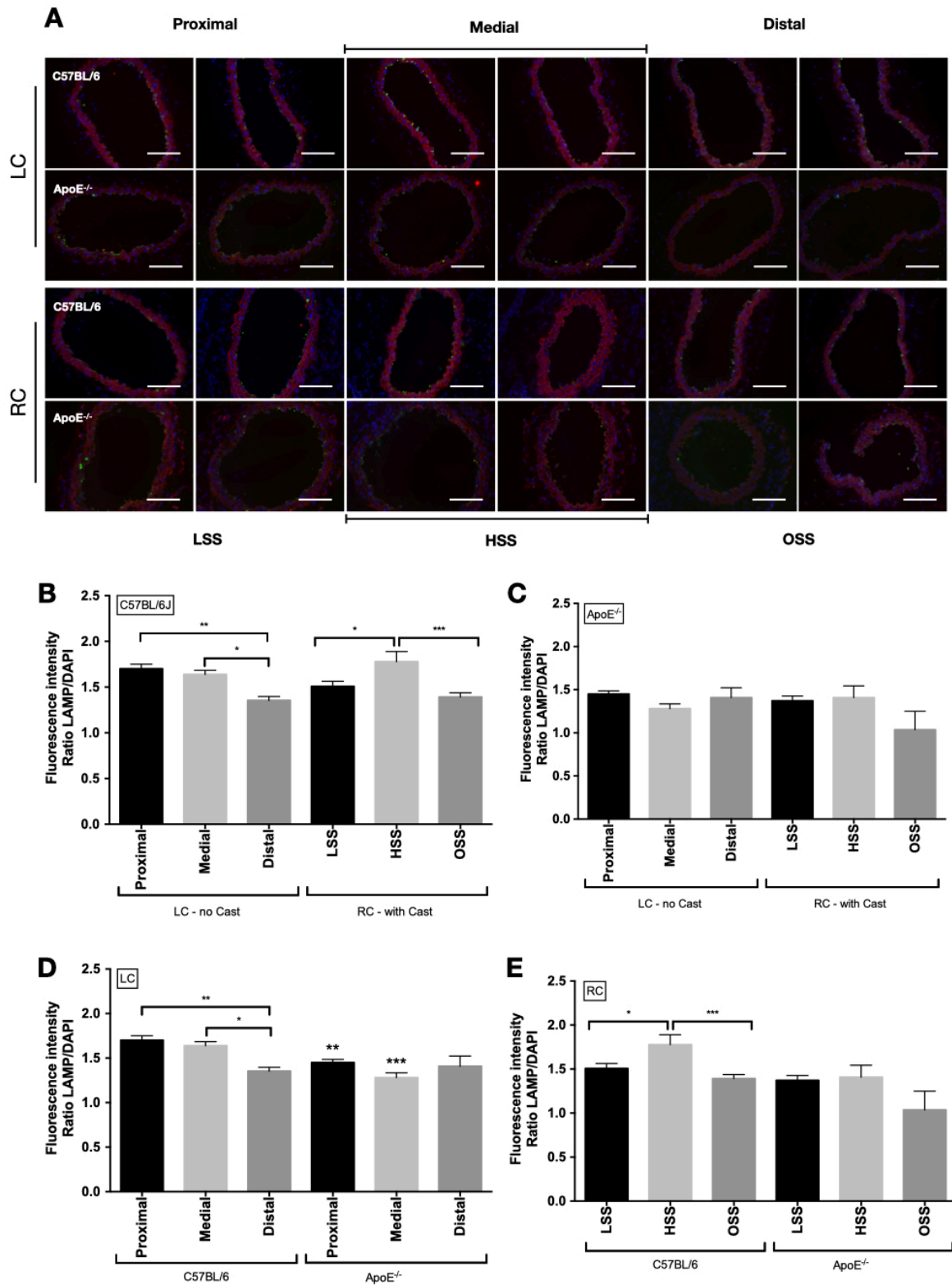


Figure 19: LAMP-2 staining in carotid artery wall of ApoE^{-/-} and C57BL/6 mice. (A) Representative images of LAMP-2 staining of left and right carotids (LC and RC, respectively) of C57BL/6 and ApoE^{-/-} mice. (B) Quantification of LAMP-2 FI in LC and RC of C57BL/6 mice. (C) Quantification of LAMP-2 FI in LC and RC of ApoE^{-/-} mice. (D) Comparison of LAMP-2 FI in LC between C57BL/6 and ApoE^{-/-} mice. (E) Comparison of LAMP-2 FI in RC between C57BL/6 and ApoE^{-/-} mice. Asterisks above bars indicate statistic difference in comparison to the respective contralateral artery and asterisks brackets indicate statistic difference between regions of the same artery ($p < 0,05$ using One-way ANOVA and Newman-Keuls post-test).

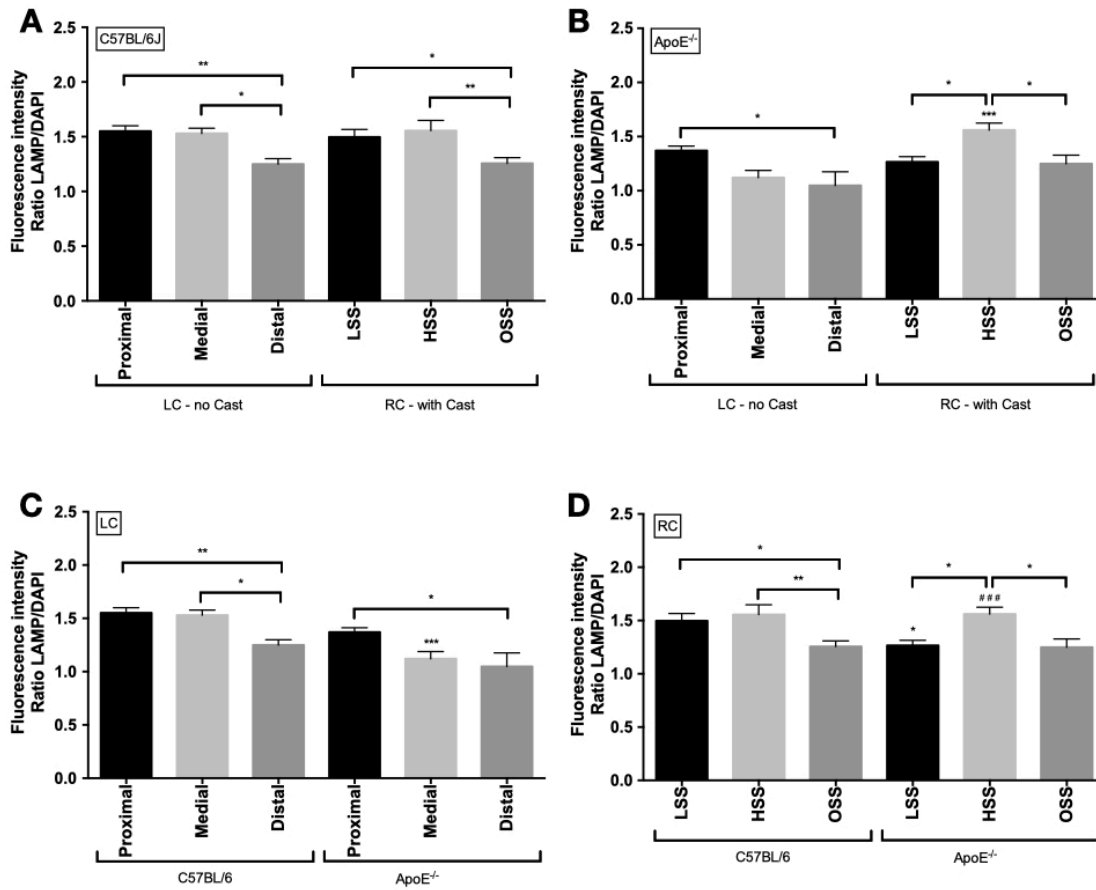


Figure 20: LAMP-2 staining in the endothelium of ApoE^{-/-} and C57BL/6 mice. (A) Quantification of LAMP-2 FI in LC and RC of C57BL/6 mice. (B) Quantification of LAMP-2 FI in LC and RC of ApoE^{-/-} mice. (C) Comparison of LAMP-2 FI in LC between C57BL/6 and ApoE^{-/-} mice. (D) Comparison of LAMP-2 FI in RC between C57BL/6 and ApoE^{-/-} mice. Asterisks above bars indicate statistic difference in comparison to the respective contralateral artery; asterisks brackets indicate statistic difference between regions of the same artery; in (D), hash above bars indicate statistic difference in comparison to the respective contralateral artery in graph (C) ($p < 0,05$ using One-way ANOVA and Newman-Keuls post-test).

6. DISCUSSION

Cholesterol content at the cell plasma membrane has long been known to interfere with membrane organization and consequently in diverse cellular processes (Brown & London, 2000; Chubisnkiy-Nadezhdin et al., 2011; Sun et al. 2007; Hissa et al., 2013). Most recently, a series of studies have implicated plasma membrane cholesterol levels and cholesterol enriched membrane microdomains, also known as membrane rafts, in actin cytoskeleton organization at the cell periphery, significantly controlling cellular biomechanics (Hissa et al., 2013; Shentu et al., 2010; Shentu et al., 2012). In parallel, previous studies from our group have shown that cholesterol sequestration induces a massive exocytosis of peripheral lysosomes, which was correlated to actin rearrangement and mechanical alterations at the cell surface (Hissa et al., 2013; Hissa et al., 2012). Localization of lysosomes throughout cell cytoplasm and more specifically its positioning at the cell periphery may influence their function in different cellular processes. Among them, the delivery of different molecules to the plasma membrane or to the extracellular space, as well as PMR, are particularly important for cell function and viability (Tam et al., 2010; Reddy et al., 2001; Pu et al., 2015; Encarnaçao et al., 2016; Andrews et al., 2014). Therefore comprehending membrane trafficking events at the cell surface level upon disorganization of rafts structures, especially when considering PMR, is of major importance.

ECs are continually submitted to mechanical stress due to blood flow and, consequently PMR mechanisms should be expected to play an important role for cell maintenance. Therefore, we used an EC model to study the effects of rafts disruption upon treatment with M β CD or the oxidized form of LDL particles in membrane trafficking events involved with PMR. In PMR, both exocytosis and endocytosis are primordial steps. The influx of Ca²⁺ through wound sites at plasma membrane stimulates local fusion and exocytosis of lysosomes. The delivery of lysosomal enzymes to the extracellular milieu induces and regulates a compensatory endocytic event responsible to reseal the membrane (Tam et al., 2010; Idone et al. 2008; Andrews et al., 2014; Castro-Gomes et al., 2016). Thereby, changes on cell cholesterol content and its consequent effect on exocytosis and actin organization could interfere with membrane repair mechanisms, affecting cell viability.

Our results confirmed previous reports showing that disruption of ECs rafts upon cholesterol sequestration or exposure to oxLDL leads to actin cytoskeleton reorganization, increased cell stiffness and lysosomal exocytosis (Hissa et al., 2013; Byfield et al., 2004; Hong et al., 2012). It has been shown before that oxLDL treatment interferes with rafts organization, especially regions enriched in cholesterol and caveolin (Shentu et al., 2010; Blair et al., 1999; Levitan & Shentu, 2011) reinforcing the role not only of cholesterol, but most importantly of rafts, in the regulation of these processes. Additionally, both treatments induced *de novo* actin polymerization, showing that disruption of membrane rafts without complete cholesterol sequestration is equally able to induce formation of new actin fibers. Although it has been shown that oxLDL treatment is able to induce Rho/Rock activation (Zhang et al., 2017), to the best of our knowledge, this is the first evidence for *de novo* actin polymerization, as well as lysosomal exocytosis upon treatment of ECs with oxLDL. Contrary to M β CD, we did not observe any difference in the amplitude of curvature upon oxLDL treatment when compared to control non-treated or nLDL treated cells. Interestingly though, for oxLDL treated cells we have observed a wider distribution of the amplitude of curvature values, which may indicate that oxLDL and M β CD effects on rafts organization may differ from each other. Nevertheless, both treatments lead to the same effect on actin polymerization and cell rigidity.

Previous studies demonstrated that actin cytoskeleton reorganization acts, on one hand, as a stimuli to vesicle fusion and exocytosis and, on the other hand, as a barrier to new traffic of vesicles localized more internally in the cell (Aunis & Bader, 1988; Nakata & Hirokawa, 1992; Muallen et al., 1995; Pedleton & Koffer, 2001; Miklavc et al., 2009). Here we showed that ECs treatment with oxLDL or M β CD induces a massive lysosome exocytosis, most likely due to actin rearrangement and polymerization as suggested before for M β CD treatment of cardiomyocytes (Hissa et al., 2012). In both oxLDL and M β CD treatments a peak of endocytosis following lysosome exocytic events is also observed, certainly corresponding to compensatory endocytosis induced by lysosome fusion with the plasma membrane. However, for both treatments it was also observed a reduction in new constitutive endocytic events, typical of these cells. It is plausible to suggest that there may be a window between the initial actin rearrangement, important for exocytosis, and its complete

reorganization that allows for compensatory endocytosis to occur. However, once actin is completely rearranged at the cell periphery, new membrane trafficking events are compromised. One evidence that corroborates this hypothesis is that non treated cells, as well as nLDL treated cells, continue to display small amounts of constitutive endocytic events, probably arising from pinocytosis, a common process in ECs. This is demonstrated by the presence of vesicles dispersed all over the cytosol even at later time points, indicating the existence of new endocytic events. These results suggest that, in contrast to what was previously proposed (Hissa et al., 2013), lysosomal exocytic events occur during the initial steps of actin remodeling and not after its complete rearrangement and that, in this last scenario, membrane trafficking is indeed compromised. In fact, this corroborates with the dual role, mentioned before, of actin cytoskeleton during secretion of vesicles in chromaffin cells. Although it was first demonstrated that actin formed a network at the cell periphery and vesicle secretion was seen only at sites of actin reorganization, later it was shown that there were secretory vesicles localized in between cortical actin filaments, which could also participate in vesicle transport during secretion (Aunis & Bader, 1988; Aunis et al., 1980; Cheek & Burgoyne, 1986; Burgoyne & Cheek, 1987; Lang et al., 2000; Rudolf et al., 2003). The same is observed for endocytosis, where actin might present as a barrier, but also work as active participants in endocytic pathways (reviewed by Smythe & Ayscough, 2006; Skruzny et al., 2012).

Interestingly, PMR evaluation through PI labeling after cell mechanical injury and repair showed that oxLDL treated cells do not lose their ability in repairing their membrane wounds. We speculate that, upon enhanced stiffness, mechanical injury causes disruption of local actin filaments, thereby breaking cytoskeleton barrier and allowing membrane trafficking at the cell periphery to occur and, therefore, PMR. It has been shown recently by Chen and coworkers (2014) that single-site sonoporation episodes induced by ultrasound-triggered collapse of a single targeted microbubble leads to rupture of filamentous actin (F-actin) at the sonoporation membrane injury site (Chen et al., 2014). Additionally, it has been shown that increase in calcium due to its influx from the extracellular to the intracellular milieu, caused by membrane rupture, may also contribute to actin depolymerization at the site of injury (Zechel, 1983; Boucher & Mandato, 2015). It is then plausible to assume that, even though actin

polymerization and reorganization induced by oxLDL treatment may interfere with membrane trafficking at cellular surface, upon mechanical injury actin cytoskeleton may be locally disrupted allowing new exocytic and endocytic events to occur. Nonetheless, it is noteworthy that the amount of injured cells after oxLDL exposure increases notoriously. Also, even though the relative efficiency of PMR in these cells is similar when compared to controls, the amount of PI positive cells after injury is significantly higher, which might have an important physiological impact in the endothelial barrier restoration. This is probably a result of the amount of injury caused by scraping in these mechanically stiffer cells.

The present work has a substantial impact in the understanding of cholesterol and rafts regulation in membrane trafficking events, especially membrane susceptibility to injury and PMR ability. Abnormal cholesterol metabolism and delivery to the plasma membrane has been implicated in various diseases (Simons & Ehelalt, 2002; Martins et al., 2009; Zhang & Liu, 2015; Li & Pfeffer, 2016). However, possible links between disease and defects in vesicle trafficking processes or with membrane susceptibility to injury have not been explored before. In this scenario, the effects of endothelial dysfunction in the first steps of atherosclerosis establishment, may be directly related to the mechanical alterations and injury susceptibility upon oxLDL exposure. Since endothelial cells are in constant mechanical stress generated by the blood flow, it is possible that biomechanics changes induced by endothelial cell exposure to oxLDL are responsible for injuries and alterations in cell viability previously observed by Liao & Granger (1995).

In order to evaluate whether biomechanics changes and their consequences observed for ECs exposed to oxLDL *in vitro* would contribute to atherosclerosis development, a mouse model of atherogenesis was used. Mice are well known to be significantly less susceptible to the development of atherosclerotic plaque due to a significant increase in ApoE-containing lipoproteins in the arterial wall when fed with a high cholesterol diet. Based on that, ApoE^{-/-} mice were developed and became one of the most used models for atherosclerosis. Additionally, since local shear stress patterns function as an important biomechanics factor for the modulation of atherogenesis, here we also used a shear stress modifier device (cast), which was introduced around

the right carotid artery of the animals in order to evaluate the role of shear stress forces in EC behavior.

Since we were interested in understanding the role of ECs changes in the first steps of disease development, we first evaluated the evolution of the atherosclerotic plaque formation along 5 wpci (7 weeks of high fat diet exposure). It was clear from our results the significative and exponential growth of atherosclerotic plaques from 3 to 5 wpci. Furthermore, lipid deposition started as early as 1 to 2 wpci with a precece plaque formation in a few of the animals studied in these groups, 1 and 2 plaque-positive mice, respectively (no statistical difference was found). Therefore, we decided to perform all experiments at 1 wpci, in which atherosclerotic plaques were present in the lowest number of animals.

In mice, ECs biomechanics properties were estimated by evaluating actin cytoskeleton organization. We have shown in the *in vitro* studies that actin reorganization induced by ECs exposure to oxLDL was accompanied by an increase in actin stress fibers and consequently in the intensity of fluorescently labeled actin. Thus we used actin fluorescence intensity (FI) to measure changes in actin cytoskeleton organization. No statistically significant differences in actin FI was observed for none of the carotids, right or left, in any of the shear stress conditions tested (low, high, oscillatory) or between control and ApoE^{-/-} mice. Neither when considering the entire artery wall nor when just ECs layer was evaluated. Nonetheless, some tendencies are worth mentioning, specially when considering those related to alterations in the pattern of shear stress.

When the entire vascular wall was taken into account, we observed a slight reduction in fluorescence intensity in the distal region of LC of both wild type C57BL/6 and ApoE^{-/-} mice. It has been shown that the distal region of carotid arteries present low to oscillatory shear stress, specially at vessel bifurcation, where the fluid shear stress on the outer vascular wall is lower in magnitude accompanied by directional changes in the flow (Malek et al., 1999). Therefore this tendency in decreasing actin FI might be related to less formation of stress fibers in regions of less physical stress. In fact, in 1993, Walpola and coworkers, using adult New Zealand white rabbits, reported that reduction in shear stress would lead to a reduction in cell elongation, as well as the

presence of fewer actin stress fibers when compared to cells exposed to the physiological shear stress.

When considering only EC layer, this tendency in reducing actin fibers at regions of less physical stress is even more pronounced in carotid arteries from WT animals. For these animals, lower and oscillatory shear stress regions of both left and right carotid arteries have a decrease in actin FI.

On the other hand, when we take hyperlipidemia into account (ApoE^{-/-} mice) this tendency in decreasing actin FI in ECs from low and oscillatory shear stress regions is not observed anymore. In fact, the opposite is seen. For these animals there was a tendency in increasing actin FI in low/oscillatory shear stress regions, especially at RC (where cast was inserted). Moreover, a better detailed analysis of ApoE^{-/-} actin cytoskeleton organization indicates a more diffuse labelling of actin and less filament-like structures when compared to the wild-type group. Beyond that, in both groups, variations on shear stress had also an impact on actin cytoskeleton organization.

Considering all the above, it is possible that for ApoE^{-/-} mice, effects of shear stress and oxLDL may be antagonistic. While the first (low/oscillatory shear stress) would lead to a decrease in actin stress fiber formation, the second (hyperlipidemia) would induce an increase. Corroborating this idea, LSS and OSS regions of carotid arteries are well known to accumulate lipids in the vascular wall, thus oxLDL, which *in vitro* induces actin rearrangement and *de novo* polymerization.

In this scenario, the outcome would be a reduction in the effect of hyperlipidemia in stress fiber formation due to a decrease in shear stress forces. The latter could then be the reason why in the *in vivo* model statistically significant increase in actin FI was not observed.

Additionally, while in our *in vitro* study cells were exposed to oxLDL for 24h, the *in vivo* investigation was performed in hyperlipidemic animals, 15-20 weeks-old, which received high fat diet for 3 weeks, thus presenting a chronic response. We presume that cells tend to reduce actin stress fibers in order to diminish subtle increases in cell tension, as the one caused by the acute exposure to oxLDL. In fact, it has been shown that cells present acute and chronic compensatory mechanisms to readapt from sudden changes in cytoskeleton organisation in order to buffer cell tension. Sinha et al. (2011) demonstrated, in ECs and muscle cells, a compensatory mechanism caveolae-

dependent in response to acute mechanical stress. They have observed caveolae flattening, upon cell stretching or osmotic swelling. This phenomena would release an amount of membrane stored in the invagination, providing additional membrane that was able to restore tension homeostasis. The authors then proposed a new role to caveolae as a membrane reservoir promptly available to respond to sudden increases in cell tension. Furthermore, they suggest the participation of other mechanisms (for instance endocytosis, exocytosis and actin dynamics) as additional compensatory mechanisms to prolong or complete the response to chronic mechanical stress and PMR (Sinha et al., 2011).

Other works have also demonstrated compensatory mechanism to reduce cell tension. It has been shown that during cell spreading, there is a local actin cytoskeleton reorganization to form lamellipodia protrusions, which flattens plasma membrane folds, increasing cell tension. Subsequently, the tension is reduced through the decrease in protrusions formation and exocytosis activating the contraction machinery which allows spreading to be completed (Batchelder et al. ,2011 and Gauthier et al., 2011).

Likewise stated, after different stimulus for cytoskeleton reorganization (i.e. flow-induced mechanical stress, cholesterol depletion, membrane rafts disruption or simply the formation of lamellipodia), the cells have compensatory mechanisms that assist in the readaptation of the cytoskeleton, reducing cell tension, so that its functions can return to physiological levels. This compensatory effect can be observed in cells during cholesterol depletion (Supplementary Fig. 2A), in which there is a reduction in cell tension after 30min of treatment. The same was observed in fibroblasts by Hissa and coworkers (2012).

Therefore, we hypothesize that, owing to the fact that it is a chronic model, greater statistical differences might not be detected, once these compensatory mechanisms would have already been taken place. This could also be the reason why we did not see an increase in cell injury neither in the arterial wall or the EC layer in regions of low/oscillatory shear stress, known to accumulate lipids, but only in induced high sheer stress regions. Nonetheless, contrary to our *in vitro* data, our *in vivo* results indicate that exposure to excess lipids seemed not to be crucial to the increase in cell injury susceptibility *in vivo*.

On the other hand, cytoskeleton reorganization and changes in biomechanics properties, induced by various conditions, have demonstrated to play an important role in promoting disturbances in vesicle trafficking, in particular in lysosomal exocytosis (Hissa et al., 2012; Koseoglu et al., 2011; Aunis & Bader, 1988; Lie & Nixon, 2018; Cabukusta & Neefjles, 2018). A docked pool of lysosomes and its interaction with actin cytoskeleton was evidenced by Ménasché and coworkers (2000) (reviewed by Cabukusta & Neefjles, 2018), when inhibiting actin-myosin contractile machinery through RAB27A mutations, compromised the secretion of a lysosome-related organelle, suggesting actin crucial role on vesicle fusion and lysosomal exocytosis.

Moreover, Hissa and coworkers (2013) and Hissa & Andrade (2015), studying the role of cholesterol depletion in fibroblast cell culture, have shown that, due to actin cytoskeleton reorganization and *de novo* polymerization, there was a peak of exocytosis of lysosomes pre-docked to the plasma membrane, while later exocytic events were blocked by the cytoskeleton barrier. When this barrier was removed by disrupting the cytoskeleton with Latrunculin-A, a perinuclear pool of lysosomes managed to be exocytosed. As detailed previously, a similar response was observed in the present study when evaluating the vesicle trafficking in our *in vitro* model. M β CD or oxLDL treated cells showed an endocytosis peak (likely arising from compensatory endocytosis induced by the lysosomal exocytic events) and then the endocytosis events ceases, probably due to the highly reorganized cytoskeleton.

Interestingly, ApoE^{-/-} vascular cells exhibit a significant reduction in lysosomal content when compared to the wild type counterpart as it can be seen by the reduction in LAMP-2 FI. As this is a chronic treatment, it is plausible to imagine that for ApoE^{-/-} mice vascular cells, the peak of lysosome exocytosis induced by cytoskeleton reorganization, proposed by Hissa and coworkers (2013), would have already occurred, and the peripheral pool of lysosomes would be depleted. In other words, while vessel cells from WT mice would be perfectly capable to perform new lysosomal exocytosis events, those from ApoE^{-/-} animals would be impaired due to the absence of the pre-docked pool of lysosomes.

It is noteworthy that lysosomal exocytosis is a crucial step to PMR and maintenance of cell integrity. The compromise in lysosomal distribution in both vascular wall and endothelial cells due to hyperlipidemia seen in the present study might have an impact on the response to injuries.

Furthermore, whether a massive and uncontrolled lysosome exocytosis is in fact happening in earlier time points *in vivo* still needs to be investigated. The excess of lysosomal secretions delivered to the extracellular matrix (ECM) might modulate the ECM environment triggering the initiation of a local inflammatory process.

As mentioned above, contrary to what we expected, hyperlipidemia itself was not a primordial factor in increasing the level of cell injury, neither considering the vessel wall, nor the endothelial cell layer. The change in shear stress pattern, however, had a critical impact on the induction of mechanical injury. Moreover, since in the *in vitro* model the increase in injury seems to be related to the increase in membrane stiffness (i.e. the higher the membrane rigidity, the higher is the susceptibility to injury), and in the *in vivo* model we may have the compensatory mechanism to reduce cellular tension chronically, it would be hard to identify the possible injury events arising specifically from the exposure to excess of lipids in the tissue.

We believe that the high increase in the level of injury suffered by the vascular cells in the HSS region of RC of both WT and ApoE^{-/-} animals, in comparison with regions of similar shear stress (contralateral carotid, proximal and medial regions - reviewed by Malek et al., 1999) might be justified by the reduction in the distension capacity of the vessel wall upon cast implantation. It is also worth not losing sight of the fact that, in advanced stages of atherosclerotic plaque development (as well as during vascular aging), there is increased collagen deposition and fragmentation of elastin fibers. The last-mentioned modifications culminate in enhanced arterial stiffness and thus reduction in the distention capacity of the vessel (reviewed by Palombo & Kozakova, 2015), perhaps leading to increased cell damage by mechanical injury in the region. Based on that, this data can be considered as an important factor for destabilization of the plaque and should be further studied.

Furthermore, we do not know how many of these cells are capable of repairing this damage, since lysosome exocytosis, a fundamental part of the

repair mechanisms, seems to be compromised in ApoE^{-/-} mice. Hence, the role of cell exposure to the excess of lipids in cell biomechanics, vesicle trafficking and membrane injury must be considered as an important factor to cell viability, endothelium integrity and to the development of atherosclerosis.

7. CLOSING REMARKS

Atherosclerosis is an inflammatory disease caused by LDL accumulation at the blood vessel wall, and its subsequently oxidation, leading to the formation of a plaque. It preferentially develops at areas of vessel bifurcation or curvature, revealing that hemodynamic forces, such as shear stress generated by blood flow, also work as local risk factors likely leading to cellular mechanical injury on the endothelium.

In this work, we have shown *in vitro* that oxLDL-induced changes in endothelial biomechanics properties also increase cell susceptibility to injury *in vitro*, compromising their ability to efficiently repair an injured membrane. The exposure to oxLDL also triggers an unregulated lysosomal exocytosis and impaired constitutive endocytosis. Similar results were also found upon cholesterol depletion from plasma membrane, indicating the role of cholesterol and membrane rafts to cell biomechanics, vesicle trafficking and PMR.

Under physiological conditions, cells are continuously exposed to situations that can generate microinjuries in the cell membrane, especially those subject to mechanical stress, as endothelial cells. When unrepaired, these injuries lead to cell death. Since membrane repair depends on vesicle trafficking between the plasma membrane and the cell interior, situations that interfere in this process, as is the case for cells exposure to oxLDL or cholesterol depletion, may compromise the repair ability and thereby contribute to the initial events of atherosclerotic plaque formation.

Since local shear stress patterns function as an important biomechanics factor for the modulation of atherogenesis, plaque composition and endothelial dysfunction, we decided to investigate the contribution of cellular biomechanics alterations together with variations in shear stress in the development of the atherosclerotic plaque *in vivo*. For this, we used an ApoE^{-/-} mouse model in

which we surgically implanted a shear stress modifier device on the carotid artery.

The results obtained in the *in vivo* work, summarised in figure 21, indicates a tendency of actin fibers accumulation in areas with higher lipid deposition, corroborating with our *in vitro* study. Furthermore, shear stress alone was able to increase cell injury in areas of HSS in the RC of both ApoE^{-/-} and C57BL/6 mice. In this analysis, hyperlipidemia was not determinant to vascular cells' susceptibility to injury. However, we speculate that exposing cells to excess lipids can be prejudicial to their ability in repairing from damage, since lysosomal content, an important organelle for PMR, is compromised in ApoE^{-/-} mice.

This study can contribute not only to the research field of atherosclerosis but to other scenarios that influence cholesterol metabolism, and its content at the plasma membrane level, which could also be affected by the events studied herein. Therefore, we believe that our results provide insights to better understand the biological and pathological roles of membrane cholesterol in cellular biomechanics, PMR and atherogenesis.

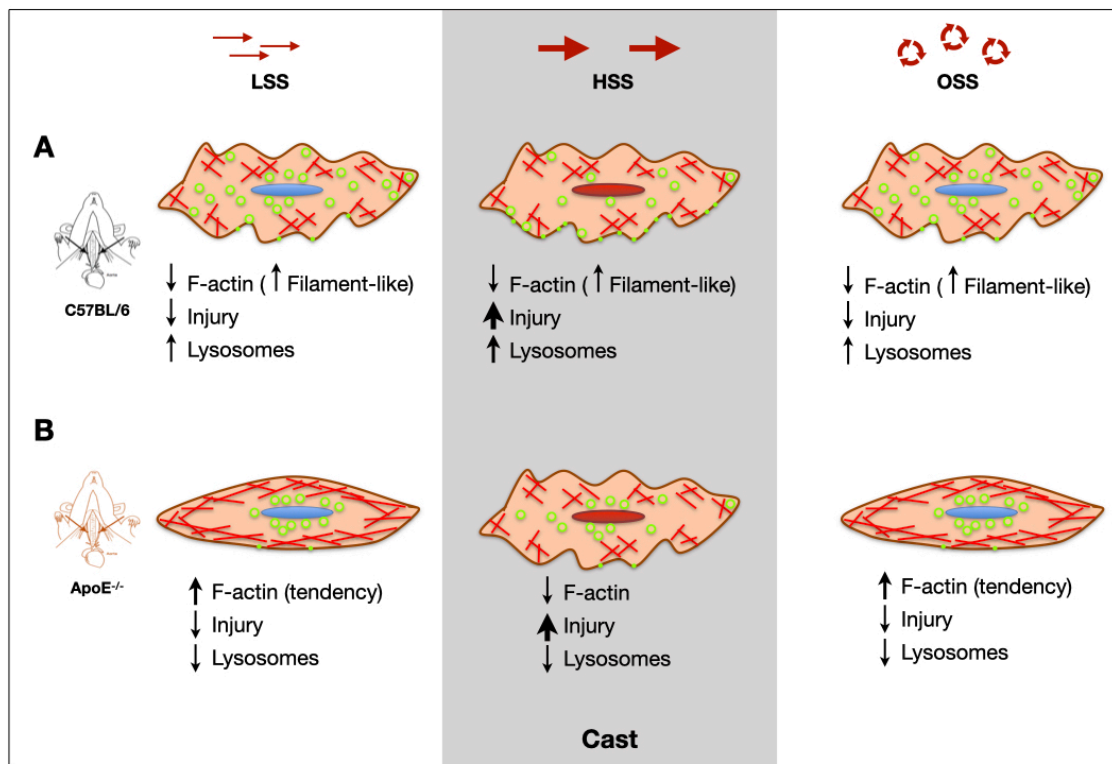
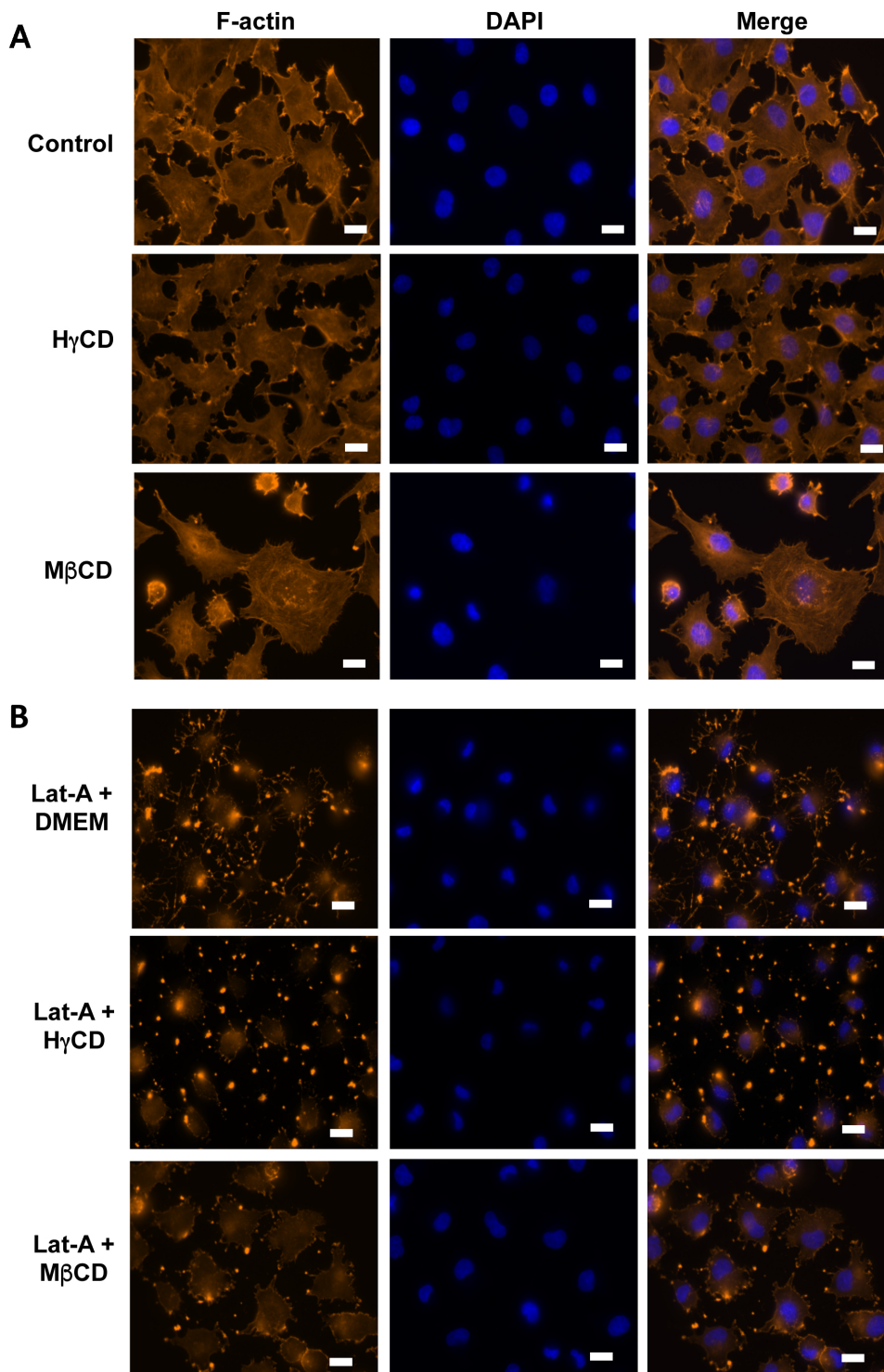


Figure 21: Schematic illustration of vascular cells' response to Hyperlipidaemia and disturbed shear stress patterns. Analysis of vascular cells' actin cytoskeleton, injury and lysosome content in the Low Shear Stress Region (LSS), High Shear Stress Region (HSS) and

Oscillatory Shear Stress Region (OSS) from Wild-type C57BL/6 (A) and ApoE-knockout (B) right carotid artery 1 week post cast implantation.

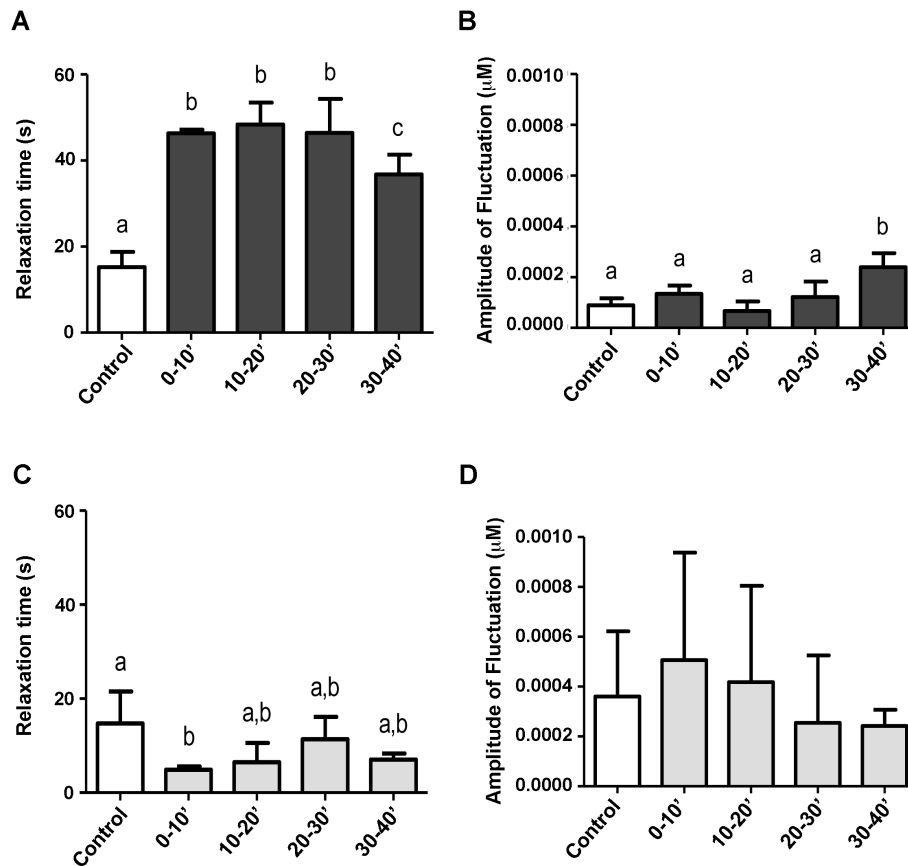
8. ANNEX

8.1 Supplementary Figures

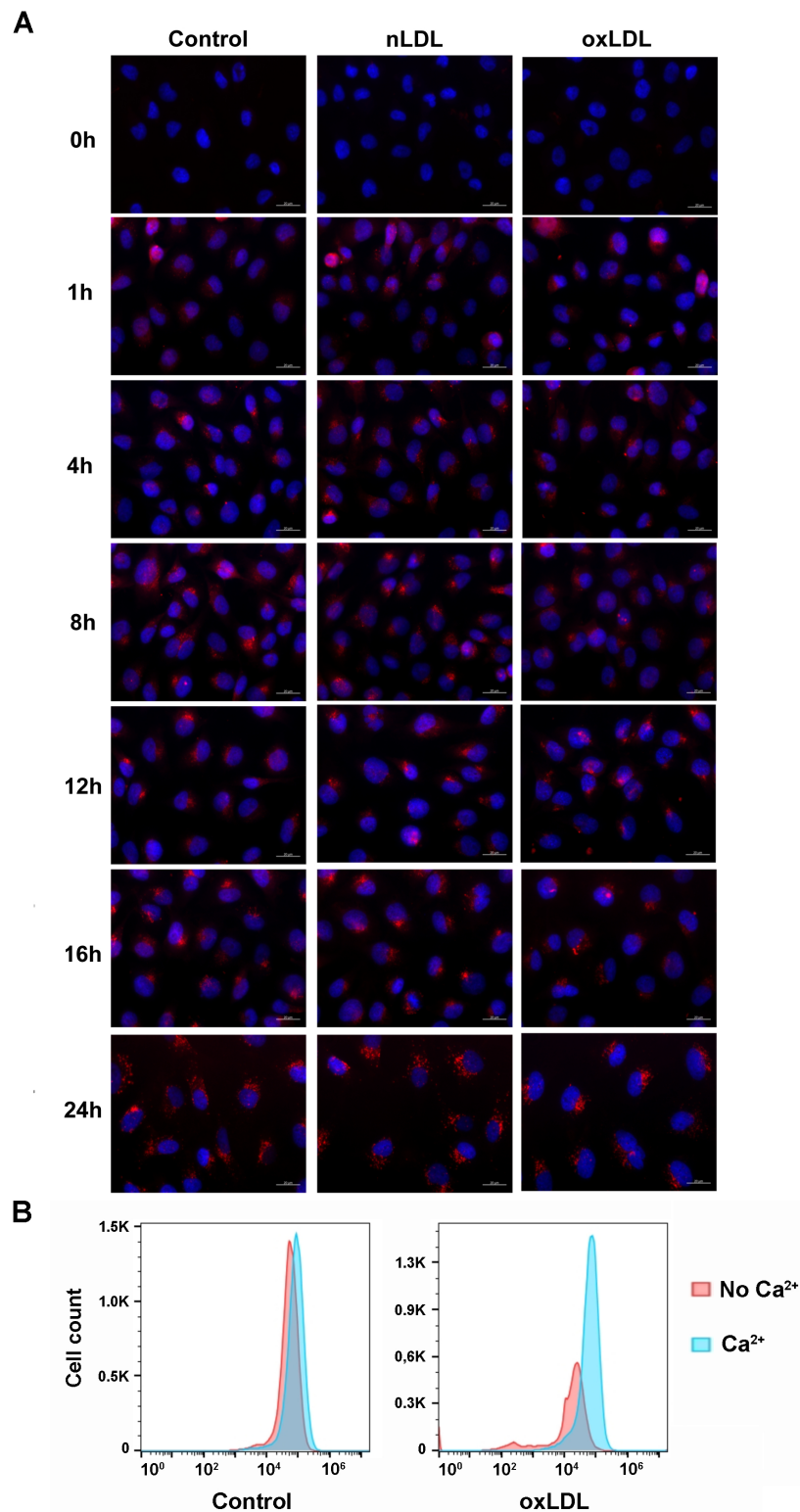


Supplementary Figure 1: Actin cytoskeleton organization of endothelial cells upon treatment with MβCD. (A) Representative images of cells treated or not with MβCD or HyCD (5mM) for 40 minutes and labeled with Phalloidin-Alexa Fluor 546 to reveal F-actin filaments organization (left panels), DAPI to reveal cell nuclei (middle panels). Right panels show a merge of the first two panels. (B) Representative images of cells treated with 95μM of Lat-A for 1 hour

followed by treatment or not with M β CD or HyCD (5mM) for 40 minutes. Cells were also labeled with Phalloidin-Alexa Fluor 546 (left panels), DAPI (middle panel). Right panels show a merge of the first two panels. Control cells were pre-treated with Lat-A and incubated with serum-free DMEM for the same amount of time. Control cells were maintained in serum-free DMEM for the same amount of time (40 min.). Images were captured in a Zeiss Axio Imager.Z2 (ApoTome.2 structured illumination system) fluorescence microscope using the 40x objective and the most representative images of the assay were shown. Scale bars: 20 μ m.

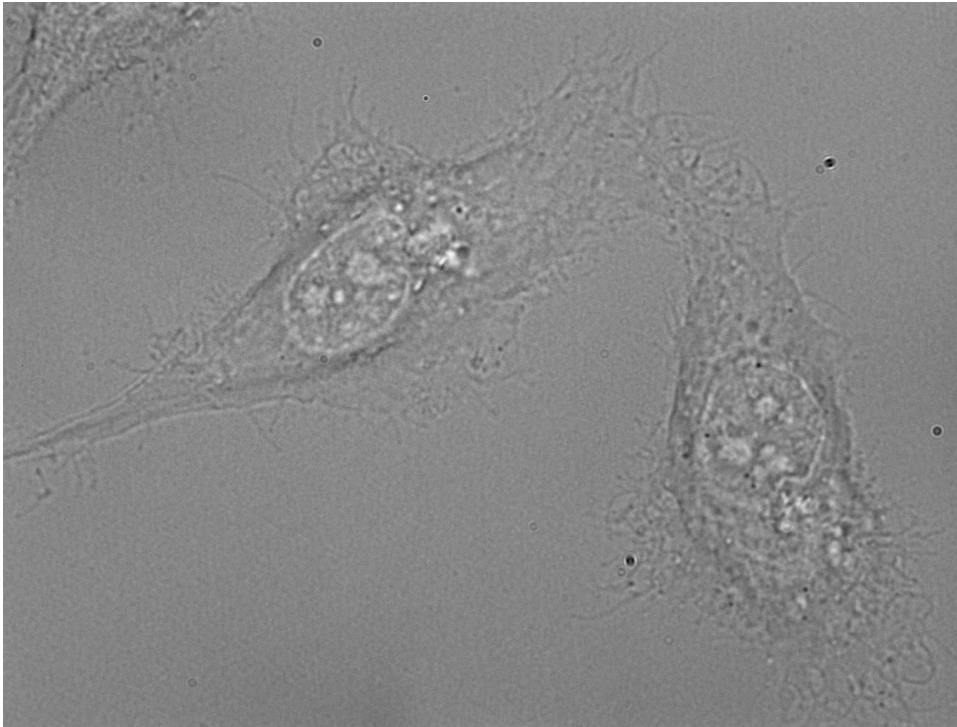


Supplementary Figure 2: Defocusing microscopy of endothelial cells upon M β CD treatment. (A) Relaxation time of control non-treated cells, as well as at different time points of M β CD treatment (5mM) (B) Amplitude of curvature of control non-treated cells, as well as during the 40 minutes of treatment with M β CD. (C) Relaxation time of control non-treated cells, as well as at different time points of HyCD treatment (5mM). (D) Amplitude of curvature of control non-treated cells, as well as during the 40 minutes of treatment with HyCD. Five independent experiments were performed and at least four regions of each one of the five cells were analyzed in each condition. Different letters above bars indicate statistically significant differences ($p < 0,05$ using One-way ANOVA and Newman-Keuls post-test).

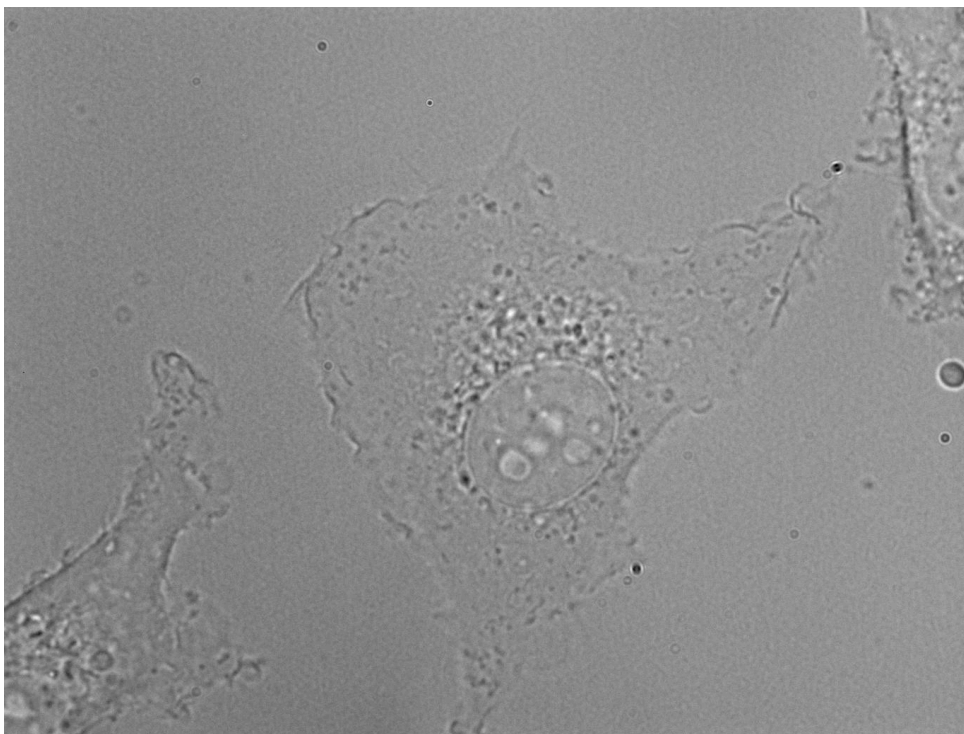


Supplementary Figure 3: Qualitative analysis of endocytic events induced by treatment with nLDL and oxLDL alone and compensatory endocytosis after injury. (A) ECs were exposed or not (control cells) to 50 μ g/ml oxLDL or nLDL for 0, 1, 4, 8, 12, 16 or 24h in the presence of Texas-Red Dextran, a membrane impermeable fluorescent compound, washed, fixed, labeled with DAPI and analyzed in the fluorescence microscope Zeiss Axio Vert.A1 using a 40x objective. Panels show intracellular vesicles containing Texas-Red Dextran (red) and cell nuclei (blue) in the different conditions. (B) Compensatory endocytosis assay of ECs incubated for 24h in serum-free medium alone (control non-treated cells) or containing 50 μ g/ml oxLDL. After treatment, cells were labeled with WGA-Alexa Fluor 488 and injured by scrapping in the

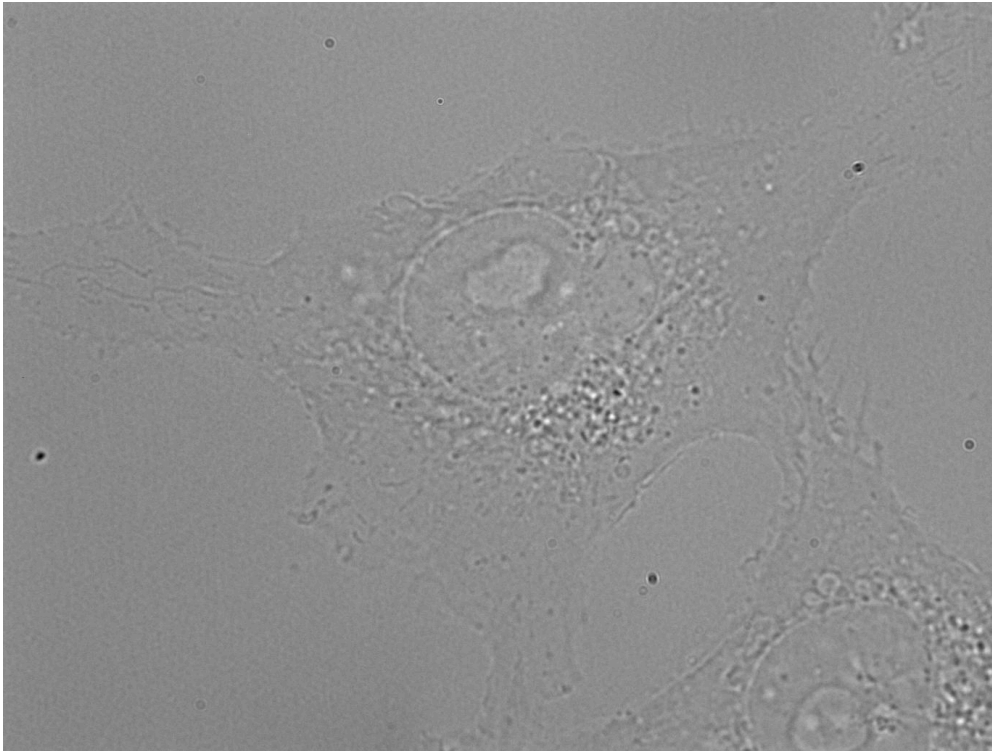
presence or absence of extracellular Ca^{2+} , followed by treatment with 0.2% trypan blue and flow cytometry analysis. Histograms show fluorescence intensity of cells treated or not with oxLDL in the absence (red) or the presence (blue) of Ca^{2+} .



Supplementary Video 1: Defocusing microscopy of endothelial cells upon oxLDL treatment. Cells were treated with oxLDL (50 $\mu\text{g}/\text{ml}$) for 24 hours and then recorded by DM in serum-free DMEM for 10 minutes.



Supplementary Video 2: Defocusing microscopy of control non-treated endothelial cells. Cells were incubated in serum-free DMEM for 24 hours and then recorded by DM for 10 minutes.



Supplementary Video 3: Defocusing microscopy of endothelial cells upon nLDL treatment. Cells were treated with nLDL (50 μ g/ml) for 24 hours and then recorded by DM in serum-free DMEM for 10 minutes.

8.2 Scientific productions related to thesis

Abstracts published in Annals of Events

Abstract presented at the XVIII Meeting of Brazilian Society for Cell Biology in 2016

EFFECTS OF MECHANICAL CHANGES INDUCED BY MEMBRANE CHOLESTEROL DEPLETION ON PLASMA MEMBRANE REPAIR

Natália F. do Couto, Ana Paula Alves, Luciana O. Andrade

Membrane repair after injury is an important process in retaining cell integrity, especially for cells, which are under constant physical stress, such as endothelial cells. However, changes in the mechanical properties of membranes could impair the ability of cells in repairing injured membrane, and contribute to endothelial fragility. The goal of this work was to evaluate the influence of the mechanical modulation induced by cholesterol depletion, upon M β CD treatment, on membrane repair mechanisms. All the experiments were performed using a human umbilical vein endothelial cell lineage. The absence of cholesterol leads to a reorganization of cellular actin and *de novo* polymerization, an increase in cell rigidity, as well as an induction of a rapid event of lysosomal exocytosis as early as 10 minutes after M β CD exposure. Additionally, during cholesterol sequestration, we observed an increase in endocytic events between 10-20 minutes, which coincided with the peak of exocytosis, indicating that these are most likely compensatory endocytic events. In parallel, we observed that constitutive endocytic events, arising from pinocytic processes, common in these cells, are blocked upon cell treatment with M β CD, suggesting that the reorganized cytoskeleton could function as a mechanical barrier to further pinocytosis. Also, coinciding with the peak of cell rigidity induced by M β CD treatment, cells become more prone to mechanical membrane injury in relation to non-treated cells. Together, these data show that mechanical modulation induced by cholesterol depletion not only alters membrane traffic in cells, but also makes cells more susceptible to mechanical injury.

Key-words: cholesterol, membrane repair, endothelial cell.

Abstract presented at the V SIBC – Simpósio de Integração dos Programas de Pós-Graduação em Biologia Celular – in 2017

EFFECTS OF OXIDIZED AND NATIVE LIPOPROTEINS IN MECHANICAL PROPERTIES AND MEMBRANE REPAIR ABILITY OF ENDOTHELIAL CELLS

Natália Fernanda do Couto, Wesley Fernandes Braga, Ana Paula Alves, Jaqueline Isaura Leite, Ubirajara Agero, Luciana de Oliveira Andrade.

Atherosclerosis is a chronic inflammatory vascular disease, having as ultimate outcome the atheromatous plaque, a focal lesion located within the intima of large and medium sized arteries. Subendothelial retention of native Low Density Lipoprotein (nLDL) and its oxidative modifications (oxLDL) represent the initial event in atherogenesis. It has been demonstrated that oxLDL, similar to the effects of cholesterol depletion through M β CD treatment, leads to reorganization of actin cytoskeleton and cell rigidity. Many studies have proposed that oxLDL-induced changes in cell biomechanics play an important role in endothelial physiology. The formation of a stiff and organized cytoskeleton in cell cortex could compromise membrane traffic between the cytoplasm and the cell surface, an important process for membrane repair that depends on lysosomal fusion with the plasma membrane and subsequent recycling of vesicles to the cytoplasm. Therefore, changes in mechanical properties could impair or alter the ability of cells in repairing their membrane. OxLDL can be divided into two groups the Minimally and the Extensively modified LDL, here called MoxLDL and EoxLDL, respectively. In this study, we attempted to observe the effect of MoxLDL or nLDL, in biomechanical properties and membrane repair ability of endothelial cells (ECs). For this, we used a cell line derived from human umbilical vein endothelial cells, EAhy.926. Analysis of fluorescence microscopy showed that MoxLDL treatment induces actin cytoskeleton reorganization with a higher amount of actin stress fibers when compared to non-treated or nLDL treated cells. To evaluate the mechanical properties of ECs upon treatment with MoxLDL, we used the Defocusing Microscopy technique. We have previously shown alterations in cell mechanical behavior using this technique in cells treated with M β CD. Surprisingly, contrary to what was previously shown in the literature for oxLDL, using this technique we were not able to observe an increase in stiffness in cells treated with MoxLDL, even though we saw reorganization of the actin cytoskeleton. This might be due to either the use of a mildly oxidized form of LDL or due to the fact that oxLDL seems to not extensively deplete membrane cholesterol content, as does M β CD, but to only disorganize rafts in membranes. In fact we showed that MoxLDL treatment does not significantly change the amount of cholesterol in cell membranes. Then we evaluated how MoxLDL or nLDL treated cells respond to mechanical injury, such as cell scrapping, as well as the ability of these cells to repair from injury. We observed that, even though treated cells suffered more injury, the cells were still able to repair their membranes after mechanical injury, such as non-treated cells. Our results indicate that the actin reorganization in ECs during oxLDL treatment does not impair their ability in repairing injured membrane but it makes cells more prone to injury.

Abstract presented at the I Summer School INCT/FCx

EFFECTS OF OXIDIZED AND NATIVE LIPOPROTEINS IN MECHANICAL PROPERTIES AND MEMBRANE REPAIR ABILITY OF ENDOTHELIAL CELLS

PhD student: Natália Fernanda do Couto

Advisor: Luciana de Oliveira Andrade.

Atherosclerosis is a chronic inflammatory vascular disease, having as ultimate outcome the atheromatous plaque. Subendothelial retention of Low Density Lipoprotein (nLDL) and its oxidative modifications (oxLDL) represent the initial event in atherogenesis. It has been demonstrated that oxLDL leads to reorganization of actin cytoskeleton and cell rigidity. Many studies have proposed that oxLDL-induced changes in cell biomechanics play an important role in endothelial physiology. The formation of a stiff and organized cytoskeleton in cell cortex could compromise membrane traffic between the cytoplasm and the cell surface, an important process for membrane repair that depends on lysosomal fusion with the plasma membrane and subsequent recycling of vesicles to the cytoplasm. In this study, we attempted to observe the effect of oxLDL or nLDL, in biomechanical properties and membrane repair ability of endothelial cells (ECs). For this, we used a cell line derived from human umbilical vein endothelial cells, EAhy.926. Analysis of fluorescence microscopy showed that oxLDL treatment induces actin cytoskeleton reorganization with a higher amount of actin stress fibers when compared to non-treated or nLDL treated cells. Analysis of vesicle trafficking showed that oxLDL-treated cells have an increase in lysosomal exocytosis that may have been stimulated by cytoskeleton reorganization. To evaluate the mechanical properties of ECs upon treatment with oxLDL, we used the Defocusing Microscopy technique. For this, we treated cells with oxLDL or nLDL for 24 hours and recorded cells for 10 minutes and temporal correlation were analyzed between frames. Analysis showed an increase in stiffness of oxLDL-treated cells when compared to non-treated or nLDL-treated cells. Since we observed that oxLDL-treated cells had their mechanical properties altered, together with an increase of lysosomal exocytosis, we attempted to observe how cells respond to mechanical injury, such as cell scrapping, and whether those cells were able to repair the injured membrane. We observed that, even though treated cells suffered more injury, the cells were still able to repair their membranes after mechanical injury, such as non-treated cells. Our results indicate that the actin reorganization in ECs during oxLDL treatment does not impair their ability in repairing injured membrane but it makes cells more prone to injury.

Abstract presented at the Annual Meeting INCT/FCx

ROLE OF SHEAR STRESS IN THE BIOMECHANICAL PROPERTIES AND SUSCEPTIBILITY TO INJURY IN *IN VIVO* MODEL OF ATHEROSCLEROSIS

Natalia F. Do Couto¹, Augusto Martins Lima², Rodrigo Fraga-Silva², Nikolaos Stergiopoulos², Thiago Castro-Gomes³, Luciana de Oliveira Andrade¹.

1 – Laboratory of Molecular and Cell Biology. Morphology Department. Institute of Biological Sciences, UFMG, Belo Horizonte, Brazil.

2 - Laboratory of Hemodynamics and Cardiovascular Technology. Institute of Bioengineering, EPFL, Lausanne, Switzerland.

3 - Parasitology Department. Institute of Biological Sciences, UFMG, Belo Horizonte, Brazil.

Atherosclerosis is influenced by a variety of genetic and environment factors. The preferential development of atherosclerotic plaques at vessel bifurcation and curved areas of the vasculature revealed that hemodynamic forces can act locally as a risk factor. Wall shear stress, the frictional force generated by blood flow, is considered as one of the major hemodynamic forces acting on the endothelium, which can lead to mechanical injury. However, it is not well known how the cells from the vessel wall respond mechanically to these stimuli, especially considering *in vivo* models. Changes in biomechanical properties could increase the susceptibility of injury and/or compromise the ability of these cells to repair an injured membrane and, therefore, contribute to the vascular fragility and consequently to the atherogenic process. In order to understand whether different patterns of shear stress induce vascular fragility enhancing the susceptibility to injury in vascular cells, in special in endothelial cells (ECs), we surgically implanted a modifier device on the right carotid (RC) artery of ApoE^{-/-} mice, a well-known model of atherosclerosis. Wild type C57BL/6 mice was used as a control using the same conditions and the left carotid (LC) of each animal was used as an internal control. The particular shape of the device causes a gradual stenosis in the vessel, resulting in increased shear stress (HSS) in the vessel segment inside the device, a decrease in blood flow and consequently a lowered shear stress (LSS) region downstream, and a vortex upstream (oscillatory shear stress, OSS). After 1 week, the animals were perfused with Propidium Iodide (PI; 500µg/ml in PBS) in order to estimate the level of injury caused by the flow. Since cell membrane is impermeable to PI, PI labeling would happen only in the presence of plasma membrane rupture. Cell actin cytoskeleton were then stained with phalloidin-Alexa Fluor 647. So far, our results indicate no statistical difference in biomechanical properties due to dyslipidemia nor to shear stress when analyzing the phalloidin staining in the entire vascular wall. When analyzing ECs, we could observe a tendency of ApoE^{-/-} samples to have a higher actin fluorescence intensity in regions known for accumulating lipids and for developing atherosclerotic plaques, as the distal region of the LC and in both HSS and OSS regions of the RC. When evaluating susceptibility to injury, we observed that modification in shear stress alone was able to increase it in both ApoE^{-/-} and C57BL/6 mice. We observed a higher PI labeling in areas of HSS in the RC of both groups. When we compared LC's PI labeling between groups, we observed that dyslipidemia was also able to induce changes in vascular cells' susceptibility to injury since there was an increase of injury level at LC distal region of ApoE^{-/-} mice, where actin fluorescence is higher and plaques are mostly formed. These results suggest that not only the modifications in shear stress but the excess of lipids in the vascular wall, and its consequent alteration in ECs biomechanical properties, makes cells more prone to injury, which can contribute to the endothelial fragility important in atherogenesis.

Research articles published in Journals

RESEARCH ARTICLE

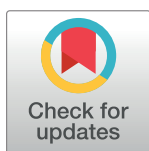
LAMP-2 absence interferes with plasma membrane repair and decreases *T. cruzi* host cell invasion

Natália Fernanda Couto¹✉, Dina Pedersane¹✉, Luisa Rezende¹, Patrícia P. Dias¹, Tayanne L. Corbani¹, Lívia C. Bentini¹, Anny C. S. Oliveira¹, Ludmila F. Kelles¹, Thiago Castro-Gomes², Luciana O. Andrade¹*

1 Department of Morphology/Federal University of Minas Gerais, Belo Horizonte, MG, Brazil, **2** Department of Biochemistry and Immunology/Federal University of Minas Gerais, Belo Horizonte, MG, Brazil

✉ These authors contributed equally to this work.

* lucianaandrade@ufmg.br



OPEN ACCESS

Citation: Couto NF, Pedersane D, Rezende L, Dias PP, Corbani TL, Bentini LC, et al. (2017) LAMP-2 absence interferes with plasma membrane repair and decreases *T. cruzi* host cell invasion. *PLoS Negl Trop Dis* 11(6): e0005657. <https://doi.org/10.1371/journal.pntd.0005657>

Editor: Carlos A. Buscaglia, Instituto de Investigaciones Biotecnológicas, ARGENTINA

Received: July 22, 2016

Accepted: May 22, 2017

Published: June 6, 2017

Copyright: © 2017 Couto et al. This is an open access article distributed under the terms of the [Creative Commons Attribution License](https://creativecommons.org/licenses/by/4.0/), which permits unrestricted use, distribution, and reproduction in any medium, provided the original author and source are credited.

Data Availability Statement: All relevant data are contained within the paper and its Supporting Information files.

Funding: This work has been funded by Fundação de Amparo à Pesquisa do Estado de Minas Gerais (FAPEMIG- APQ-02269-14) and Conselho Nacional de Desenvolvimento Científico e Tecnológico (CNPq- 479623/2009-0, INCT/CNPq Proc. 465259/2014-6). I would like to add that the funders had no role in study design, data collection and analysis,

Abstract

Trypanosoma cruzi enters host cells by subverting the mechanism of cell membrane repair. In this process, the parasite induces small injuries in the host cell membrane leading to calcium entry and lysosomal exocytosis, which are followed by compensatory endocytosis events that drive parasites into host cells. We have previously shown that absence of both LAMP-1 and 2, major components of lysosomal membranes, decreases invasion of *T. cruzi* into host cells, but the mechanism by which they interfere with parasite invasion has not been described. Here we investigated the role of these proteins in parasitophorous vacuole morphology, host cell lysosomal exocytosis, and membrane repair ability. First, we showed that cells lacking only LAMP-2 present the same invasion phenotype as LAMP1/2^{-/-} cells, indicating that LAMP-2 is an important player during *T. cruzi* invasion process. Second, neither vacuole morphology nor lysosomal exocytosis was altered in LAMP-2 lacking cells (LAMP2^{-/-} and LAMP1/2^{-/-} cells). We then investigated the ability of LAMP-2 deficient cells to perform compensatory endocytosis upon lysosomal secretion, the mechanism by which cells repair their membrane and *T. cruzi* ultimately enters cells. We observed that these cells perform less endocytosis upon injury when compared to WT cells. This was a consequence of impaired cholesterol traffic in cells lacking LAMP-2 and its influence in the distribution of caveolin-1 at the cell plasma membrane, which is crucial for plasma membrane repair. The results presented here show the major role of LAMP-2 in caveolin traffic and membrane repair and consequently in *T. cruzi* invasion.

Author summary

Trypanosoma cruzi is the etiological agent of Chagas disease, a very debilitating illness that has no efficient treatment to date. Better knowledge of the mechanisms involved with host cell infection is important to change this scenario. *T. cruzi* enters host cells by subverting the mechanism by which cells repair small injuries in their plasma membrane. In this

decision to publish, or preparation of the manuscript.

Competing interests: The authors have declared that no competing interests exist.

process, parasites interact with host cells causing membrane injuries. These injuries lead to secretion of lysosomal content to the extracellular media, which in turn causes the internalization of plasma membrane wounds via endocytosis. During this endocytic process the parasite is internalized by the host cell. We have previously shown that absence of two proteins located at the lysosomal membrane, LAMP-1 and 2, severely interferes with *T. cruzi* entry into host cells. In the present manuscript we show that absence of LAMP-2 alone is enough to compromise *T. cruzi* entry into host cells and it does so by compromising the endocytic events that follow lysosome secretion, which in turn is responsible for driving *T. cruzi* into the host cell interior.

Introduction

Trypanosoma cruzi is the causative agent of Chagas disease. This parasite is naturally transmitted through the feces of an infected vector, a triatomine bug, but transmission may also occur through contaminated food, blood transfusion, placenta or organ transplantation [1]. Therefore, although originally endemic to Latin America, where the vector is widespread, Chagas disease is now found in non-endemic countries, especially in the southern part of the United States and Europe due to human migration [2–5]. Chagas disease is a serious and debilitating illness with a variable clinical course, ranging from asymptomatic to very serious cardiac and/or gastrointestinal disease [6]. Available treatment is not efficient, especially considering the chronic phase of the infection [7]. In order to survive and replicate in the vertebrate host, *T. cruzi* needs to interact with and invade host cells. Therefore the comprehension of the mechanisms involved in these processes is extremely important for the development of more efficient treatment and disease control.

The parasite is able to invade a wide variety of cell lines, professional and non-professional phagocytic cells. In order to gain entry into host cells, *T. cruzi* subverts the mechanism by which cells repair small injuries in their plasma membrane. These small membrane tears lead to extracellular calcium influx into the cell cytoplasm. Increase in intracellular calcium induces lysosome recruitment and fusion at the site of injury, which leads to the release of an enzyme called acid sphingomyelinase. This enzyme cleaves sphingomyelin, generating ceramide, which induces a compensatory endocytosis event that carries the damaged site to the cell interior, resealing the plasma membrane. In the case of *T. cruzi*, intracellular calcium increase may occur through a series of molecules released by the parasite or located at its surface, which will trigger host signaling events that promote a rise in intracellular calcium [8–12]. In parallel, *T. cruzi* is also able to induce microinjuries at the host cell membrane, leading to calcium influx from the extracellular media into the cells [13]. In both cases, calcium leads to lysosomal exocytosis at the site of parasite attachment/injury [14, 15], followed by compensatory endocytosis events that pull *T. cruzi* into host cells [13]. To the newly formed parasitophorous vacuole, more lysosomes fuse until the entire vacuole is covered with lysosomal membrane markers. Lysosomal association and fusion during *T. cruzi* host cell invasion is essential for the formation of a viable parasitophorous vacuole, without which parasites could exit host cells [15]. Lysosomes could be contributing to anchor and drag parasite into host cells. In fact, we have previously shown that cells lacking Lysosomal Associated Membrane Proteins 1 and 2 (LAMP1/2^{-/-} cells), the major integral membrane proteins of lysosomes, are less susceptible to *T. cruzi* infection [16]. However, the mechanism by which these proteins interfere with invasion is still unclear.

LAMPs are highly glycosylated proteins, rich in sialic acid, and estimated to cover approximately 80% of the lysosome luminal surface [17, 18]. Due to its high sialic acid content and the

previously reported role of host cell sialic acid in *T. cruzi* invasion process [19–22], it has been suggested that LAMP's sialic acid moieties could be contributing to the invasion phenotype in LAMP knock out cells [16]. However, despite being heavily sialylated and structurally very similar, LAMP-1 and 2 have only around 37% similarity in amino acid sequence [23, 24] and differ in function, as revealed by the generation of LAMP1 and 2 single knock out mice [18, 25–27]. Therefore we were interested in evaluating the real role of LAMP during *T. cruzi* invasion of host cells. In order to evaluate the mechanism by which LAMP proteins participate in *T. cruzi* host cell invasion, we decided to investigate the role of these proteins in known important events involved in this process: parasitophorous vacuole morphology, host cell lysosomal exocytosis, and membrane repair ability. For this, we used LAMP1/2^{-/-} cells in comparison to WT cells. In parallel, we performed the same assays using LAMP2 single knock out fibroblast (LAMP2^{-/-}), since the lack of LAMP-2 caused a more severe alteration in cells and mice [28, 29].

Materials and methods

Antibodies and reagents

Anti-mouse LAMP-1 mAb (1D4B), as well as anti-mouse LAMP-2 mAb (ABL-93), were obtained from the Developmental Studies Hybridoma Bank. Anti-*T. cruzi* polyclonal antibodies were obtained from serum of rabbits immunized with *T. cruzi* trypomastigotes as described previously [30, 31]. Secondary antibodies, anti-rat IgG-Alexa fluor 488, anti-mouse-Alexa fluor 488 and anti-rabbit IgG-Alexa fluor 546 were obtained from Thermo Fischer Scientific.

Cells and parasites

Mouse fibroblasts cell lines, derived from wild type (WT), LAMP1 and 2 (LAMP1/2^{-/-}) or LAMP2 (LAMP2^{-/-}) knock out C57BL6 mice, were obtained from a collection of cell lines from Dr. Paul Saftig's laboratory (Biochemisches Institut / Christian-Albrechts-Universität Kiel, Germany), which were previously generated by spontaneous immortalization of primary fibroblasts in culture around passages 10–20 [18, 29, 32]. The cells were maintained in high-glucose DMEM (Thermo Fischer Scientific) supplemented with 10% fetal bovine serum (FBS), 1% penicillin/streptomycin (100U/mL and 100µg/mL, respectively) and 1% glutamine (DMEM 10%).

Tissue culture trypomastigotes (TCTs) from the *T. cruzi* Y strain were obtained from the supernatant of infected LLC-MK2 monolayers and purified as described by Andrews *et al.* (1987) [30].

T. cruzi invasion assay

For invasion assays, 4x10⁴ cells (WT, LAMP1/2^{-/-} and LAMP2^{-/-} fibroblasts) in high glucose DMEM 10% were plated in each well of a 24-well plate, containing 13mm round glass coverslips. Cells were plated 24 h before the experiment and incubated at 37°C and 5% CO₂. Cells were then exposed to *T. cruzi* TCTs Y strain for 20 min at 37°C at a multiplicity of infection (MOI) of 100. After parasite exposure, the monolayers were washed 4 times with phosphate buffered saline containing Ca²⁺ and Mg²⁺ (PBS+/+), in order to remove the non internalized parasites, and fixed in paraformaldehyde 4% overnight. After fixation, cells were processed for immunofluorescence.

Immunofluorescence and quantification of parasite invasion

After fixation, coverslips with attached cells were washed three times in PBS, incubated for 20 min with PBS containing 2% BSA and processed for an inside/outside immunofluorescence

invasion assay as described previously [30]. Briefly, extracellular parasites were immunostained with rabbit anti-*T. cruzi* polyclonal antibodies in a 1:500 dilution in PBS/BSA for 1h at room temperature, washed and labeled with Alexa Fluor-546 conjugated anti-rabbit IgG antibody (Thermo Fischer Scientific) in a proportion of 1:500 in PBS/BSA for 45min.

After the inside/outside immunofluorescence staining, host cell lysosomes were also immunostained using a 1:50 dilution of either rat anti-mouse LAMP-1 hybridoma supernatant (1D4B) or rat anti-mouse LAMP-2 hybridoma supernatant (Abl 93) in PBS/BSA/saponin and the appropriate fluorescent labeled secondary antibody anti-rat IgG-Alexa fluor 488, as described previously [15, 30]. After that, the DNA of host cells and parasites was stained for 1 min with DAPI (4',6-Diamidino-2-Phenylindole, Dihydrochloride—Sigma), 0,1μM in PBS, mounted, and examined on an Olympus BX51 microscope equipped with a Q color 3 camera controlled by the ImagePro Express Software (Olympus).

Transmission Electron Microscopy and analyses of parasitophorous vacuole morphology

WT, LAMP1/2^{-/-} and LAMP2^{-/-} fibroblasts were infected with *T. cruzi* TCTs at a MOI of 100 for 20 min, washed in PBS+/+ and then fixed with 2.5% Glutaraldehyde in 0.1M PHEM buffer (5mM MgCl₂.6H₂O, 70mM KCl, EGTA 10mM, HEPES 20mM, PIPES 60mM), pH7.2. After fixation cells were gently scraped off with a rubber policeman, harvested by centrifugation and incubated in 3% low melting agarose. The hardened agarose with the sample was cut into small pieces and washed in PHEM buffer. All samples were post-fixed with 2% osmium tetroxide containing 1.5% potassium ferrocyanide in PHEM buffer for 1h at room temperature. The cells were dehydrated using increasing concentrations of graded acetone before embedding the pellet in Araldite. Ultrathin sections in 200 mesh copper grids were stained with lead citrate and analyzed on Tecnai G2-12 –SpiritBiotwin FEI electron microscope. Quantification of vacuole volume density was performed by the ratio between the total area of the vacuole and the parasite area, using the Image J software. Values closer to 1 indicate a tight vacuole, while values greater than 1 indicate looser vacuoles.

β-hexosaminidase assay

To evaluate the lysosomal exocytosis, a β-hexosaminidase secretion assay was performed according to previous work [31]. Briefly, WT, LAMP1/2^{-/-} and LAMP2^{-/-} cells were treated with Ionomycin (Calbiochem) 5 and 10 μM for 10 min at 37°C. After treatment, cell extracellular media was collected and cells were lysed with Triton x-100 (Sigma) 1% in PBS. Extracellular media and cell lysates were incubated with 50μL of β-hexosaminidase substrate, 6mM 4 methylumbelliferyl-N-acetyl-B-D-glucosaminide (Sigma-Aldrich), dissolved in Na-citrate-PO₂ buffer (pH4.5). After 15–20 min of incubation at 37° the reactions were stopped by adding 100μL of stop solution (2M Na₂CO₃-H₂O, 1.1M glycine). 100μL of this solution was used for reading at 365nm of excitation and 450 nm of emission in a spectrofluorimeter (Synergy 2, Biotek in the Center of Flow Cytometry and Fluorimetry, Department of Biochemistry and Immunology, ICB-UFGM).

Compensatory endocytosis assay after cell injury

Compensatory endocytosis after injury was measured using a scrape wound assay followed by trypan blue fluorescence quenching, as previously described [33]. Briefly, WT cells were grown in 10cm plates, washed with HBSS at 4°C containing or not containing 1.8mM Ca²⁺ and labeled on the plasma membrane with 1μg/mL wheat germ agglutinin (WGA)–Alexa Fluor 488 (Invitrogen) for 1 minute at 4°C, followed by two more washes in HBSS. Cells were then wounded

by scraping in the presence or absence of Ca^{2+} and incubated for 2 minutes at 37°C with 0.2% trypan blue before washing and FACS analysis. Due to WGA-Alexa Fluor 488 susceptibility to quenching by the membrane impermeable trypan blue, Alexa Fluor 488 fluorescence measurement will correspond to the amount of membrane endocytosed after trypan blue exposure.

Acid sphingomyelinase exocytosis and detection

WT, LAMP1/2 and LAMP2 knockout cells were plated on 10 cm round dishes 24 hours prior to experiments at 2×10^6 cells/dish. Cell monolayers were washed 3 X with PBS and incubated at 4°C with 2 mL of cold HBSS media containing Ca^{2+} . To induce PM damage, exocytosis of lysosomes and PM repair each cell type was scrapped at 4°C, gently re-suspended with a serological pipette and incubated at 37°C for 5 minutes to induce lysosomal secretion and plasma membrane repair. As controls, non-scraped cells were incubated for 5 minutes at 37°C and the media were collected to assess constitutive exocytosis. The suspensions containing the exocytosed content from lysosomes were transferred to ice and centrifuged for 30 minutes at 10,000 g in order to remove possible detached cells. The supernatants containing the enzymes released from lysosomes were concentrated 20 times using 3 kDa Amicon Ultra filter units and analyzed by SDS-PAGE and Western Blot. Immunoblot assay was performed using rabbit polyclonal anti-ASM (Abcam ab83354). Protein samples were prepared with reducing sample buffer, boiled, separated on 10% SDS-PAGE and blotted onto nitrocellulose membranes (Bio-Rad) using the Trans-Blot transfer system (Bio-Rad) for 1 hour and 30 minutes at 100 V. The membrane was blocked for 1 h with 5% milk solution. After incubation with the primary antibody and peroxidase conjugated secondary antibody, detection was performed using Lumina Forte Western HRP Substrate (Millipore) and a Fuji LAS-4000 Imaging System with Image Reader LAS-4000 software (Fuji).

Membrane injury and repair assays

WT, LAMP1/2^{-/-} and LAMP2^{-/-} cells were cultured in 35mm culture dishes (3×10^5 cells/dish) at 37°C in 5% CO₂ in DMEM 10%. After 24 hours, cell monolayers, treated or not with MβCD, were washed at 4°C with Ca^{2+} -free PBS followed by two more washes in Ca^{2+} -free PBS. Cells were then incubated with HBSS containing Ca^{2+} at 4°C, wounded by scraping and incubated for 5 minutes at 37°C, to allow plasma membrane repair. Afterwards, cells were incubated at 4°C for 5 minutes with Propidium Iodide (PI) (10μg/mL in HBSS). For hitting control, cells were incubated with Ca^{2+} -free HBSS at 4°C, wounded by scraping in the presence of PI and incubated for 5 minutes at 37°C. Alternatively, cell monolayers were injured by incubation with DMEM 10% containing PI (10μg/mL) in the presence or absence of *T. cruzi* TCT's Y strain for 30 min at 37°C at a multiplicity of infection (MOI) of 100. After flow cytometry (FACS Scan; Becton Dickinson), the data were analyzed using FlowJo v10.1 software (Tree Star, Inc.).

Actin cytoskeleton labeling

WT, LAMP1/2^{-/-} and LAMP2^{-/-} cells were plated on 24 well plates containing 13 mm round coverslips at a density of 5×10^4 cells/well 24 hours before the assay. Cells were then fixed with paraformaldehyde (PFA) 4% for 1 hour at 4°C. After fixation, coverslips with attached cells were washed three times in PBS+/+, permeabilized with Triton X-100 0.1% (Sigma-Aldrich) and incubated for 30 min with PBS+/+ containing 1% BSA (PBS/BSA 1%). For labeling polymerized actin, cells were incubated with Phalloidin-Alexa Fluor 546 (Thermo Fischer Scientific) using a dilution 1:40 in PBS/BSA 1% at room temperature, followed by three additional washes. Labeled coverslips were mounted on glass slides and examined on a Zeiss Axio Imager.Z2 (ApoTome.2 structured illumination system) microscope.

Plasma membrane cholesterol quantification

Plasma membranes (PM) from WT, LAMP1/2^{-/-} and LAMP2^{-/-} cells were separated from nuclei and large granule fraction through differential centrifugation and subsequently isolated from endoplasmatic reticulum using equilibrium density ultracentrifugation as previously described [34], with few modifications. After isolation, PM subfraction was saponified with 25 ml ethanolic sodium hydroxide (1M) under heating. The unsaponifiable phase (enriched in cholesterol) was extracted with ethyl acetate and dried out overnight. The unsaponifiable matter was treated with *N,O*-Bis(trimethylsilyl)trifluoroacetamide (BSTFA) to obtain trimethylsilyl (TMS) derivatives [35]. Gas chromatography (GC) analyses were performed in a gas chromatograph HP7820A (Agilent) equipped with a flame ionization detector. An HP5 column (Agilent; 30 m x 0.32 mm x 0.25μm) was used following a ramp protocol starting from 250°C at a rate of 10°C/min for 5 min, with an injector (split 1:30) at 300°C and a detector at 300°C. Hydrogen was used as the carrier gas (3 ml/min); and an injection volume of 3μl. Peak identification and cholesterol concentration were obtained comparing peak areas with a standard curve using known concentration of cholesterol (Sigma-Aldrich) derivatized under same conditions as samples. The final content of cholesterol was normalized by total protein concentration taken from particle free supernatant obtained during PM subfraction isolation and protein concentration was determined according to Lowry et al. using bovine serum albumin as standard [36].

Caveolin detection

For Western blot detection of total caveolin-1 content, WT, LAMP1/2^{-/-} and LAMP2^{-/-} cells were plated the day before, scraped and lysed with RIPA buffer (25mM Tris-HCl pH 7.6, 150mM NaCl, 1% NP-40, 1% sodium deoxycholate, 0.1% SDS). Protein content was measured, samples were prepared with reducing sample buffer, boiled and 50 μg of protein were loaded in each lane on a 12% SDS-PAGE. After transfer (see above—same as for acid sphingomyelinase (ASM) detection) the membrane was incubated with anti-Caveolin 1 (BD—cat. # 610406) diluted 1:2000. Detection and imaging were performed as described for ASM detection.

For immunofluorescence labeling, WT, LAMP1/2^{-/-} and LAMP2^{-/-} cells were plated onto round glass coverslips the day before, fixed in 4% paraformaldehyde for 10 min and washed 3 x in PBS, followed by incubation for 45 min at room temperature in PBS containing 2% BSA and 0.05% saponin (PBS/BSA/saponin). Cells were then incubated for 2 h with anti-Caveolin 1 (BD—cat. # 610406) antibody diluted 1:500 in PBS/BSA/saponin, washed, followed by 1 h incubation with secondary anti-mouse antibodies conjugated with Alexa Fluor 488 (Thermo Fischer Scientific) diluted 1:500 in PBS/BSA/saponin. Coverslips were mounted using Pro-Long1Gold antifade reagent (Thermo Fischer Scientific) and imaged using a Zeiss Axio Imager.Z2 (ApoTome.2 structured illumination system) microscope with an Axiocam 503 monochrome camera controlled by the Zen Blue Software (Zeiss). Alternatively, cells were imaged in a Zeiss Axio Imager.Z2 Microscope to create a 3D reconstruction, which has been made following capture of 16 optical sections with an approximate 0.93μm interval, using the 63x oil objective. The 3D imaging stack has been reconstructed using Zen Blue Software.

Results

LAMP2^{-/-} cells are as refractory to *T. cruzi* invasion as LAMP1/2^{-/-} cells

We first decided to test the influence of lysosomal integral membrane protein 2, LAMP-2, in *T. cruzi* cell infection, when compared to LAMP1/2^{-/-} deficient or WT control fibroblasts. It had been shown before that LAMP-1 deficiency had little effect on cell morphology,

metabolism or viability and led to overexpression of LAMP-2 in cells, suggesting that LAMP-2 might compensate for LAMP-1 deficiency [25]. On the other hand, LAMP-2 deficiency in mice led to a series of lysosomal defects, which together compromised mice viability [27, 28]. For this, we performed cell invasion assays using fibroblast cell lines generated from a LAMP2 knock out mouse (LAMP2^{-/-} fibroblasts) and compared to the invasion rates obtained from WT and LAMP1/2 double knock out mouse (LAMP1/2^{-/-} fibroblasts) [29]. The phenotypes of the cell lines were confirmed through immunolabeling with both anti LAMP-1 and LAMP-2 antibodies (S1 Fig).

As expected from previous data from our group [16], lack of both LAMP-1 and 2 led to a reduction in the invasion rate of *T. cruzi* TCTs when compared to WT fibroblasts (Fig 1A–1C). The number of internalized parasites per 100 counted cells (Fig 1A), as well as the percentage of infected cells (Fig 1B) in LAMP1/2^{-/-} fibroblast cultures are about 3 times lower when compared to their WT counterparts. The same was observed for LAMP2^{-/-} fibroblasts, revealing that absence of LAMP-2 alone was sufficient to reduce *T. cruzi* invasion rates to the

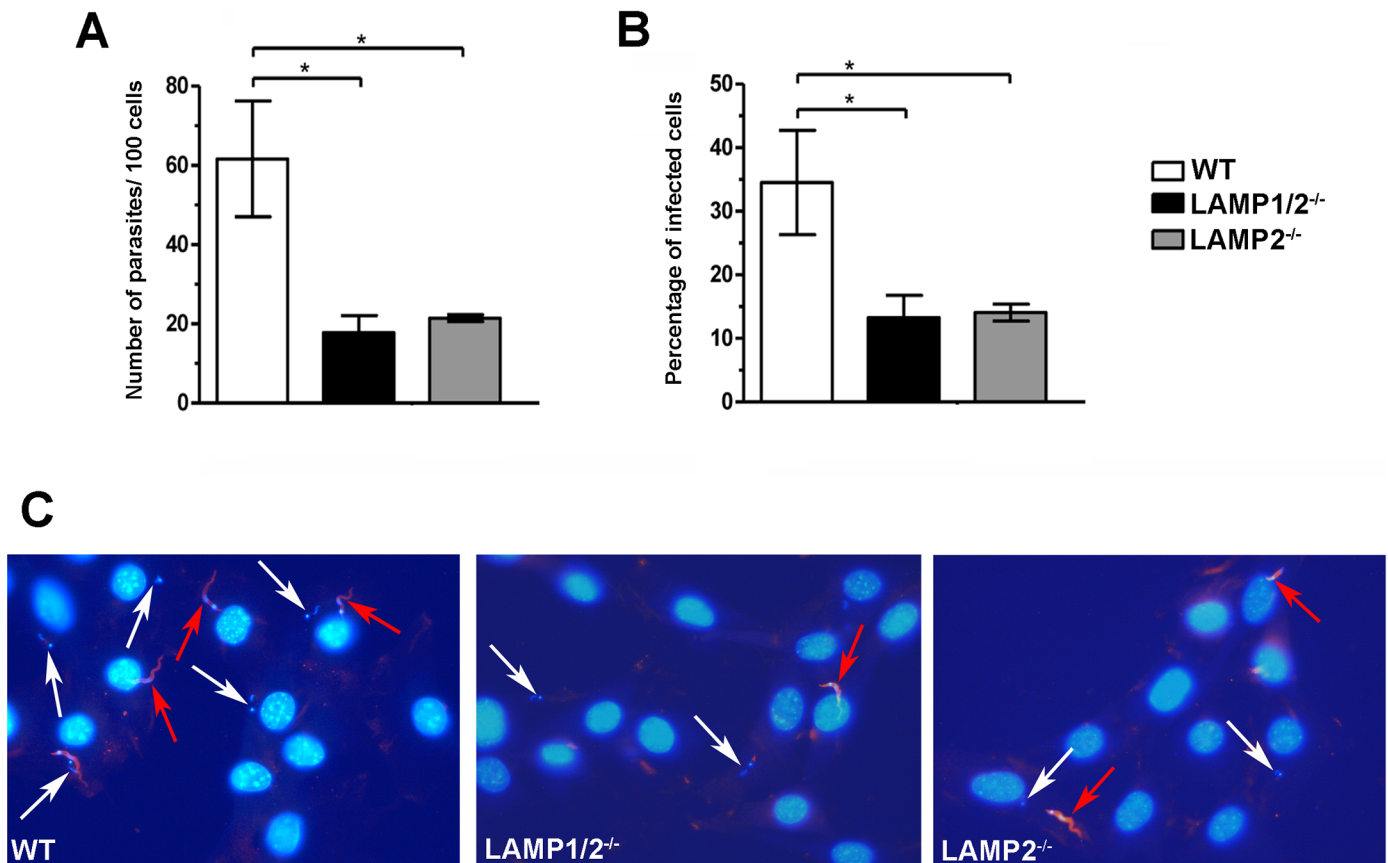


Fig 1. LAMP-2 deficiency is enough to compromise *T. cruzi* invasion in host cells. WT, LAMP1/2^{-/-} or LAMP2^{-/-} fibroblasts monolayers were exposed to Tissue Culture derived Trypomastigotes (TCT) from Y strain at a MOI of 50 for 20 minutes, washed, fixed and then processed for immunofluorescence detection of total intracellular parasites. Quantitative analysis of parasite infection rates in the three fibroblast cell lines was determined by the number of internalized parasites per 100 counted cells (A), as well as the percentage of infected cells (B). Data are shown as mean of triplicates ±SD. Asterisks indicate statistically significant differences (p<0.05, Student's t test) between WT and LAMP deficient cells. (C) Representative panels of *T. cruzi* invasion in the three different fibroblast cell lines revealed by immunofluorescence labeling. Cell and parasite nuclei, as well as parasite kinetoplast DNA, were labeled with DAPI (blue); extracellular parasites in the field were labeled with anti-*T. cruzi* antibody followed by secondary IgG labeled with Alexa Fluor 546 (red). White arrows indicate intracellular parasites, while red arrows indicate extracellular parasites. Data shown are representative of three independent experiments.

<https://doi.org/10.1371/journal.pntd.0005657.g001>

same level observed for LAMP1/2^{-/-} fibroblasts and indicating a primary role for this protein in the invasion process (Fig 1A–1C).

LAMP-2 deficiency does not affect *T. cruzi* parasitophorous vacuole morphology

Interaction of *T. cruzi* with its vacuolar membrane has been shown to interfere with parasite invasion ability [22]. Therefore, we decided to test whether, in the absence of LAMP proteins, parasite interaction with its vacuole was compromised, contributing to the decreased cell invasion observed in LAMP knock out cells. For this, we evaluated parasitophorous vacuole morphology in the different cell lines (WT, LAMP1/2^{-/-} and LAMP2^{-/-} fibroblasts) through Transmission Electron Microscopy (TEM). TEM images of parasitophorous vacuoles containing recently internalized trypomastigotes, in the different cell lines (Fig 2A–2C), were processed using the software Image J and the ratio between the parasitophorous vacuole and parasite areas were calculated (Fig 2D). As expected, membranes of parasite and vacuole were tightly apposed to each other in WT cells, showing almost no intravacuolar space between parasite plasma membrane and parasitophorous vacuolar membrane (Fig 2A). The same was observed for LAMP1/2^{-/-} or LAMP2^{-/-} fibroblasts (Fig 2B and 2C, respectively). Quantification of the ratio between vacuolar area and parasite area confirmed that presence or absence of LAMP did not interfere with vacuolar morphology (Fig 2D). The ratio between

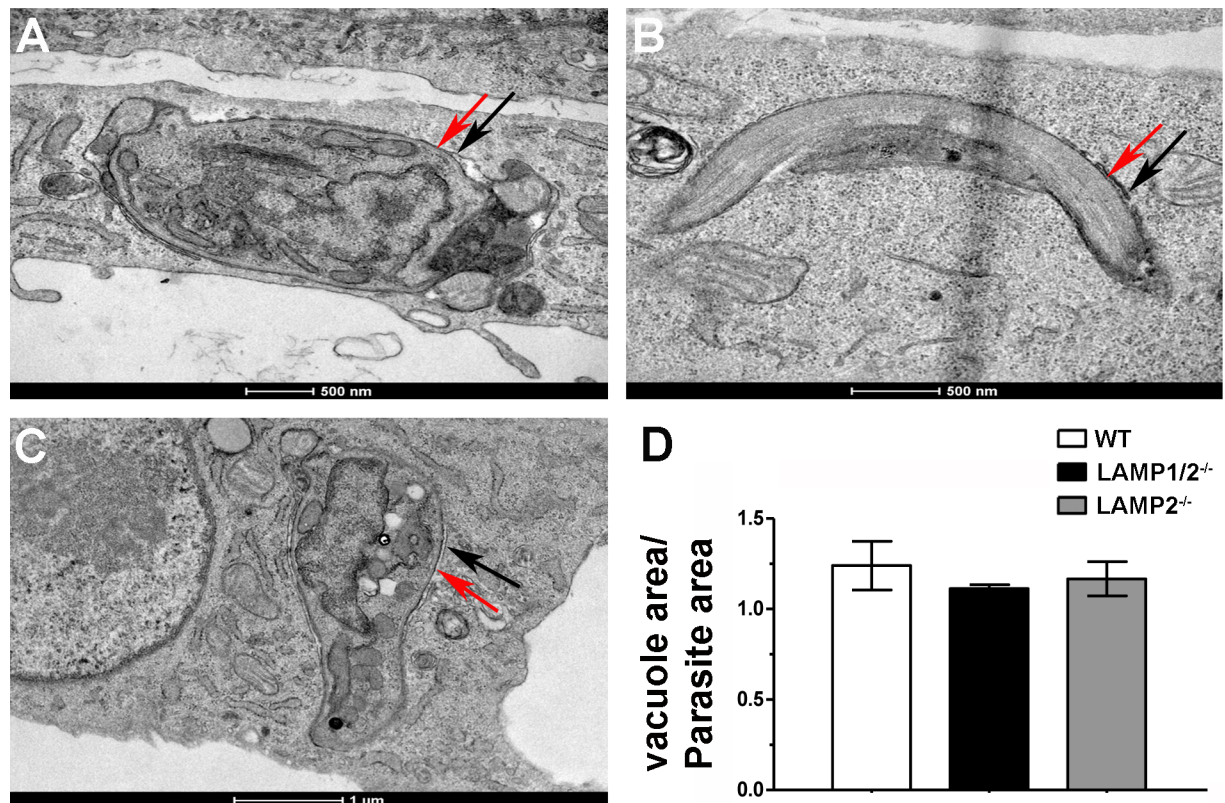


Fig 2. Absence of LAMP does not interfere with parasitophorous vacuole morphology. Transmission Electron Microscopy images of parasitophorous vacuoles from WT (A), LAMP1/2^{-/-} (B) e LAMP2^{-/-} (C) cells. Red arrows indicate parasite membrane and black arrows indicate parasitophorous vacuole membrane. (D) Graph shows the rate between parasitophorous vacuole and parasite areas. Data are shown as mean from 15 observed vacuoles ±SD from each cell line, WT, LAMP1/2^{-/-} and LAMP2^{-/-}. No statistically significant differences were observed (P < 0,05, Student's T test).

<https://doi.org/10.1371/journal.pntd.0005657.g002>

parasitophorous vacuole and parasite areas for all three cell lines were very close to one, showing that the two membranes, parasite and vacuolar, were intimately associated even in the absence of LAMP.

LAMP-2 deficiency does not impair lysosomal exocytosis

As it is well known, *T. cruzi* invasion depends on lysosomal secretion induced by calcium signaling events [14, 37], followed by compensatory endocytosis, which drives parasites into host cells [13]. To test whether impairment in *T. cruzi* entry was due to deficiency in lysosomal exocytosis in cells lacking LAMP-2, we performed a lysosomal exocytosis assay using WT, LAMP1/2^{-/-} and LAMP2^{-/-} fibroblasts stimulated with Ionomycin, a calcium ionophore. Cells were exposed to Ionomycin in two different concentrations, 5 and 10 μM and lysosomal exocytic events were measured by assaying β-hexosaminidase activity in cell culture supernatants. Supernatant of non-treated cells showed very little amounts of enzyme activity, as expected. On the other hand, treatment with Ionomycin did trigger lysosomal exocytosis in all cell lines, as it is demonstrated by the increase in β-hexosaminidase activity values in the cell supernatant upon treatment (Fig 3A). Treatment with 5 or 10 μM of the drug led to the same exocytic values in all cell lines. Additionally and most important, no difference in lysosomal content release was observed among the distinct cell lines either before or after cell stimulation with the drug, indicating that absence of LAMP does not affect host cell lysosomal exocytic ability and could not contribute to the invasion phenotype observed for LAMP-2 deficient cells.

LAMP-2 deficiency seriously affected compensatory endocytosis events induced by membrane injury

Once neither exocytosis nor vacuole morphology were compromised by LAMP deficiency, we decided to test whether compensatory endocytosis induced by these exocytic events, another important step of *T. cruzi* induced entry process [13], was affected. Compensatory endocytosis was measured by FACS analysis after scrape wounding using a trypan blue quantitative quenching assay [33, 38]. For this, WT, LAMP1/2^{-/-} and LAMP2^{-/-} fibroblasts were treated with WGA-Alexa Fluor 488, upon which cell membranes were fluorescently labeled, submitted to scrape wounding in the presence or absence of calcium and allowed to recover from injury. In this process, scrape wounding of plasma membrane will induce lysosome secretion, which will trigger compensatory endocytosis carrying the damaged WGA-Alexa Fluor 488 labeled membrane to cell interior. Cell external fluorescence was then quenched by trypan blue, to keep only fluorescence from internalized membranes, and cells were read using FACS. In the absence of calcium, endocytosis events were minimal, while in the presence of calcium endocytosis reached its maximum, enhancing intracellular WGA- Alexa Fluor 488 fluorescence. As observed in Fig 3B, a significant increase in intracellular WGA- Alexa Fluor 488 fluorescence is observed when WT cells were submitted to scrape wounding in the presence of calcium. However, no increase in intracellular WGA- Alexa Fluor 488 fluorescence was observed when LAMP1/2^{-/-} and LAMP2^{-/-} fibroblasts were submitted to the same procedure, indicating that LAMP-2 plays a critical role in the process of membrane repair by interfering with compensatory endocytosis after lysosome secretion (Fig 3B).

Since the endocytic process triggered by lysosomal secretion during membrane injury events is dependent on lysosomal acid sphingomyelinase (ASM) action on the extracellular leaflet of PM, we decided to evaluate whether ASM was present in the lysosomal secreted content during PM repair in WT, LAMP1/2^{-/-} and LAMP2^{-/-} cells. As shown in Fig 3C, the enzyme was normally exocytosed from lysosomes in all cell lines during resealing of mechanical wounds provoked by scraping. Thus, the defect in endocytosis observed in LAMP-2

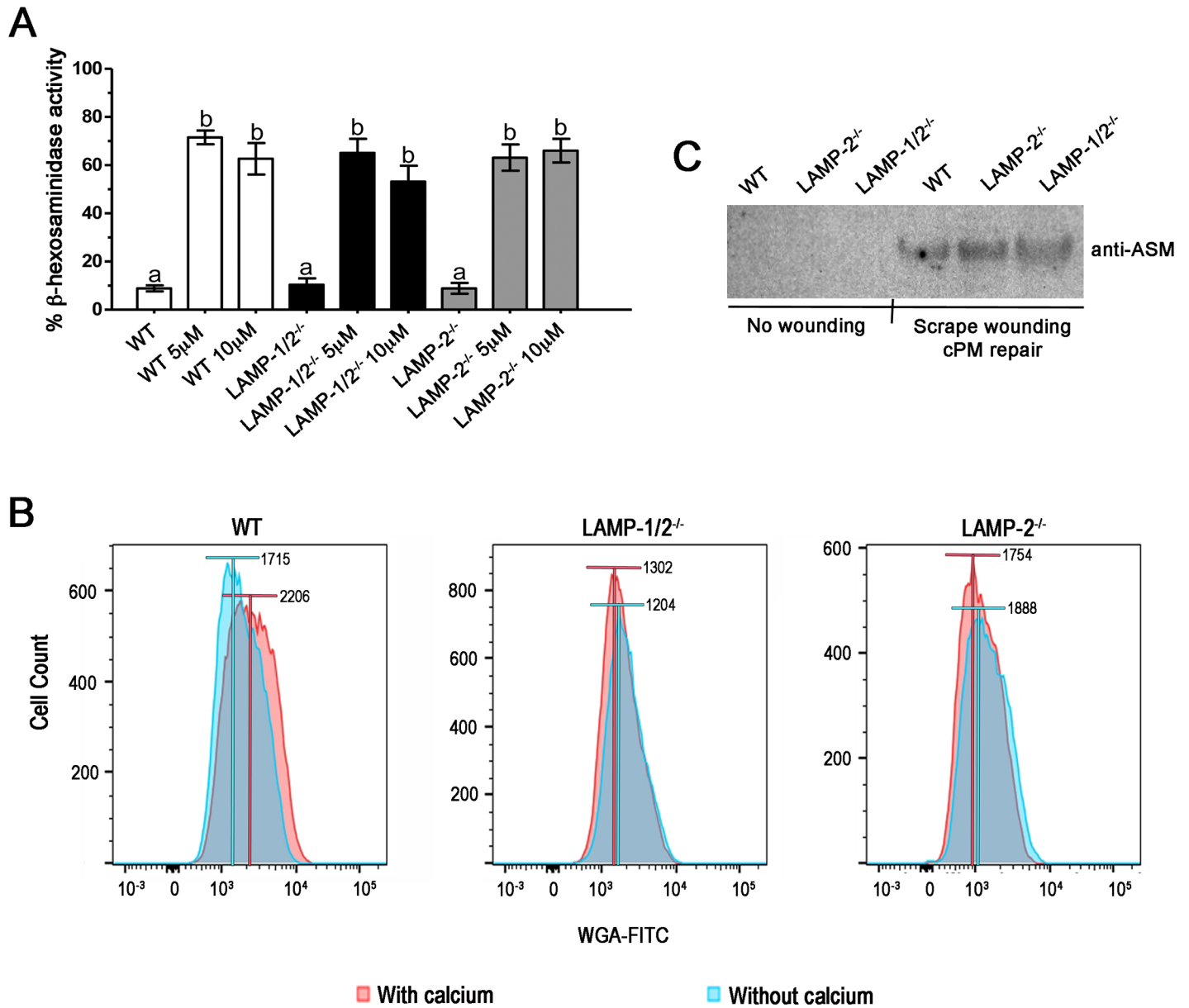


Fig 3. Absence of LAMP does not affect lysosomal exocytosis, but do interfere with compensatory endocytosis events. (A) Lysosome exocytosis assay. WT, LAMP1/2^{-/-} or LAMP2^{-/-} fibroblasts monolayers were exposed to 5 or 10 μ M Ionomycin for 10 minutes at 37°C, in the presence of calcium. Both extracellular media and lysates were collected and assayed for beta-hexosaminidase activity. Results are shown as the ratio between extracellular media β -hexosaminidase activity and total β -hexosaminidase activity (extracellular media plus cell lysate hexosaminidase activity). Non treated cells were used as lysosomal exocytosis negative control. Data are shown as mean of triplicates \pm SD. Asterisks indicate statistically significant differences ($p < 0.05$, Student's t test) between control and treated cells. (B) Measurement of compensatory endocytosis events induced by membrane injury. Cells were labeled with WGA-Alexa Fluor 488, submitted to membrane injury by cell scraping in the presence (red) or absence (blue) of calcium, and then incubated with trypan-blue to eliminate plasma membrane labeling. Only fluorescence from internalized membranes was preserved. The endocytosis was then quantified by FACS analysis. Histograms show the number of cells displaying WGA-Alexa Fluor labeling for the different fibroblast cell lines, WT, LAMP1/2^{-/-} and LAMP2^{-/-}. Bars above the curves indicate the median of the fluorescence for each condition (with or without calcium). Data shown are representative of three independent experiments. (C) Detection of ASM in the supernatant of control non-scraped cells, and cells that had been subjected to scrape wounding and membrane repair. Supernatants of WT, LAMP1/2^{-/-} and LAMP2^{-/-}, in the different conditions, were run on a gel, blotted onto nitrocellulose membranes and revealed using an anti-ASM antibody. The panel shows the presence of ASM in the supernatant of all three cells, only upon wounding and membrane repair.

<https://doi.org/10.1371/journal.pntd.0005657.g003>

deficient cells was not due to lack of ASM secretion and it is most likely due to events downstream of lysosomal secretion.

LAMP absence interferes with membrane repair efficiency

If endocytosis induced during plasma membrane repair was compromised in LAMP-2 deficient cells we should also observe a defect in these cells' ability to repair their plasma membrane. To test whether cells lacking LAMP were really deficient in repairing injured membranes, an event that requires compensatory endocytosis, we performed a plasma membrane repair assay using the membrane impermeable fluorophore propidium iodide (PI). For this, cells were exposed to PI during or after scraping. In the first experiment, cells were exposed to PI during scraping to measure the efficiency in mechanical wounding of plasma membrane. Therefore, PI labeled cells provided the total number of cells injured by scraping from plates (Fig 4A). Scraping in the presence of PI resulted in 94.7% of WT cells injured by scraping, while only 5.3% were not injured in this process. A similar amount of injured/non-injured cells was found for LAMP1/2^{-/-} and LAMP2^{-/-} (95.7% / 4.3% and 96.5% / 3.5%, respectively). In the second experiment, cells were exposed to PI after scraping in order to measure cells' ability in repairing injured membrane. In this case, PI labeled cells provided the total number of cells unable to recover from membrane injury. On the other hand, cells that excluded the fluorophore included the cells that were never injured and the ones that had been injured, but were able to repair their membranes (Fig 4B). In order to calculate the percentage of cells that recovered from injury by membrane repair, for each cell type, we subtracted the percentage of not injured cells given by the first experiment (Fig 4A, PI-) from the total percentage of viable cells given by the second experiment (Fig 4B, PI-). As shown in Fig 4A and 4B, 5.3% of cells were negative for PI when exposed to the fluorophore during scraping, while 36.8% of cells were negative for PI when exposed to the fluorophore after scraping, indicating that 31.5% of cells recovered from injury by plasma membrane repair. On the other hand, only 7.7% (12% - 4.3%) of LAMP1/2^{-/-} cells and 19% (22.5% - 3.5%) of LAMP2^{-/-} cells were able to recover from membrane injury. This result confirms the importance of LAMP-2 for the membrane repair process.

In order to confirm that the decreased invasion in cells lacking LAMP-2 was due to their deficiency in compensatory endocytosis and not an inability of these cells to be injured by *T. cruzi*, we have also measured membrane injury, using the parasite as the source of membrane tear. For this, cells were exposed to *T. cruzi* trypomastigotes for 30 minutes in the presence of PI. Cultures not exposed to the parasite, but incubated with PI for the same amount of time, were used as controls in order to measure membrane injuries that may occur even in the absence of the parasite. As shown in Fig 4C, upon parasite exposure, it was possible to observe an increase in the number PI positive events for all cell lines (WT, LAMP1/2^{-/-} and LAMP2^{-/-}) when compared to control condition (cell cultures without parasite exposure). WT cells exposed to *T. cruzi* showed about 7.3% more PI positive cells than its respective control, followed by LAMP1/2^{-/-} with 9.9% and LAMP2^{-/-} with 15.2% of PI positive cells (Fig 4D).

LAMP absence interferes with cholesterol content, as well as caveolin-1, at the plasma membrane

LAMP absence, especially LAMP-2, had been previously shown to induce cholesterol accumulation in lysosomes [26, 29]. The latter could compromise the levels of cholesterol delivered to the cell plasma membrane and consequently interfere with caveolin-1 distribution at the cell surface, which is important for the compensatory endocytosis process triggered during membrane repair [39]. Since plasma membrane cholesterol sequestration using M β CD has been shown to induce actin stress fiber formation [31], we first decided to evaluate the actin

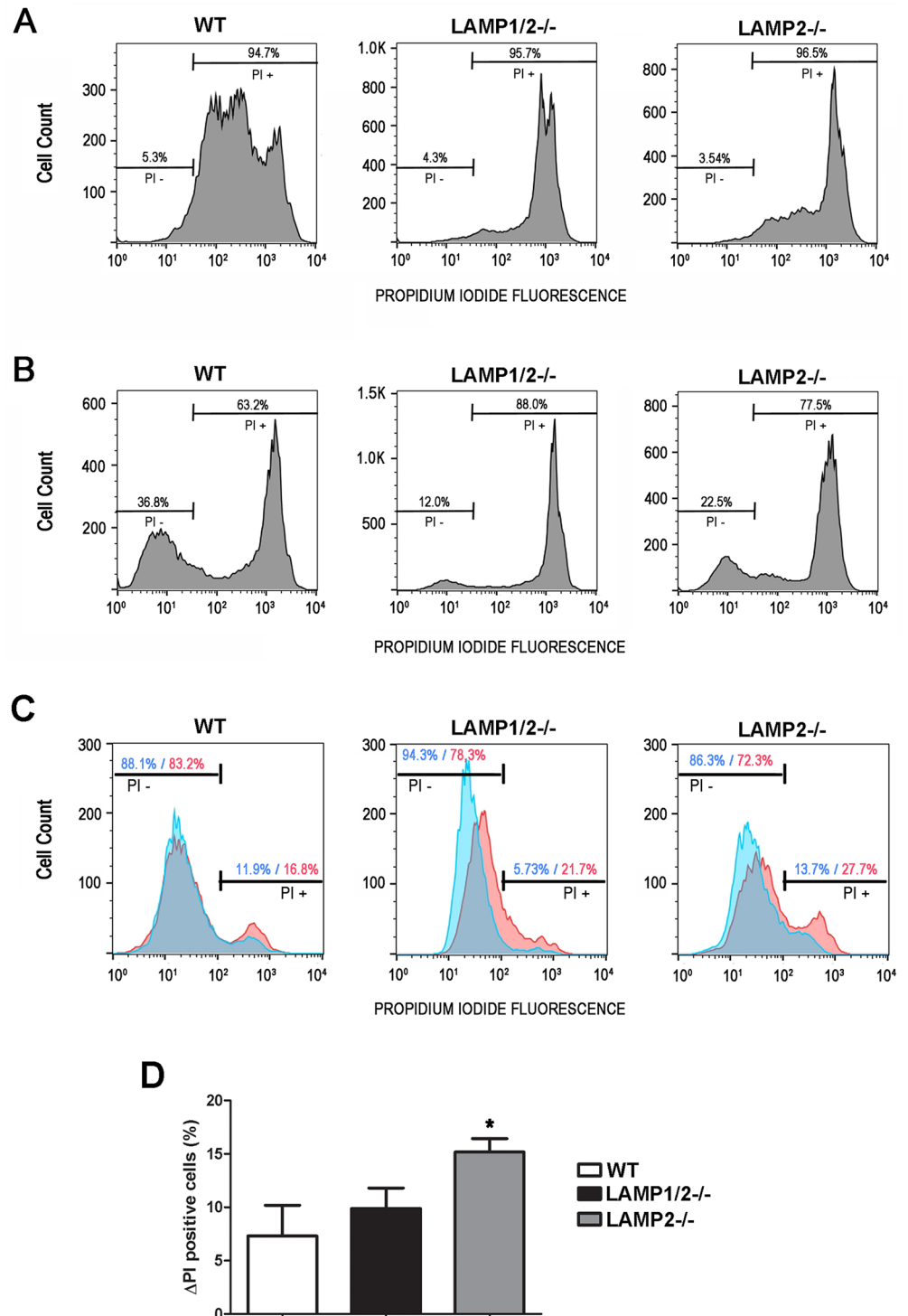


Fig 4. Absence of LAMP-2 does interfere with membrane repair. (A-B) WT, LAMP1/2^{-/-} or LAMP2^{-/-} were submitted to membrane injury by cell scraping. (A) Cells were scraped in the presence of Propidium Iodide (PI). Histograms show the number of cells presenting PI labeling (PI +), which represent the number of cells that suffered injury during scraping, while cells excluding PI represent those that didn't suffer membrane injury. Bars above the curve indicate the percentage of injured (PI +) and non-injured cells (PI -). (B) Cells were scraped in the absence of PI, allowed to reseal, and then exposed to PI. Histograms show the number of PI + and PI- cells, which represent the ones that did not or did recover from injury, respectively. Bars above the curve indicate the percentage of non-viable (PI +) and viable cells (PI -). (C) Cells were exposed or not to

T. cruzi trypomastigotes for 30 minutes in the presence of Propidium Iodide (PI). Blue curves represent control cultures, without parasite exposure, while red curves represent cell cultures exposed to *T. cruzi*. Histograms show the number of cells presenting PI labeling (PI +), which represent the number of cells that suffered injury, while cells excluding PI represent those that didn't suffer membrane injury. Bars above the curve indicate the percentage of injured (PI +) and non-injured cells (PI -) in the presence or absence of *T. cruzi*. (D) Difference in the percentage of PI+ cells between control and *T. cruzi* exposed cell cultures. Asterisks indicate statistically significant differences $p < 0.05$. Data shown are representative of three independent experiments.

<https://doi.org/10.1371/journal.pntd.0005657.g004>

cytoskeleton organization in WT, LAMP2^{-/-} and LAMP1/2^{-/-} using phalloidin staining of actin filaments. Analysis of the actin organization revealed that cells lacking LAMP-2 (LAMP2^{-/-} and LAMP1/2^{-/-}) showed a differential organization of actin stress fibers in their cytoplasm, especially at the cell periphery, strongly suggesting that cholesterol content at the plasma membrane level was compromised in these cells (Fig 5A). In order to prove that the cholesterol content at the plasma membrane of cells lacking LAMP-2 was in fact lower when compared to WT cells, we prepared lipid extracts from cell plasma membrane and measured the cholesterol content. Cells lacking LAMP-2 showed a reduction of 70% in the levels of cholesterol at the cell plasma membrane when compared to WT cells (Fig 5B).

We also labeled caveolin-1 using an anti-cav1 antibody and a secondary conjugated with Alexa-Fluor-488. WT cells show caveolin staining in cell interior, seen as small dots, as well as a very strong labeling at the cell surface (Fig 6A, S3 Fig and S1 Video). On the other hand, in cells lacking both LAMP-1 and 2 no surface labeling is observed, only the dotted labeling in cell interior (Fig 6A, S3 Fig and S1 Video). LAMP2^{-/-} cells show a profile similar to LAMP1/2^{-/-} cells, although in the first it is possible to see some labeling at the cell surface in few cells (Fig 6A, S3 Fig and S1 Video). In order to show that the amounts of caveolin produced by these cells were the same and only the distribution was different, we also evaluated by Western Blot the total amount of caveolin-1 in protein cell extracts. As it can be seen in Fig 6B and 6C, WT, LAMP1/2^{-/-} and LAMP2^{-/-} cells have the same amount of Caveolin-1.

Discussion

In order to gain entry into host cells, *T. cruzi* stimulates them by interacting with their proteins and/or producing small injuries in their plasma membrane [10, 12, 40–42]. These events lead to the increase in intracellular calcium, which will in turn trigger lysosome exocytosis [43–45]. The latter is followed by a compensatory endocytic event that carries the parasite into the host cell [13]. Lysosomes have also been shown to be important for parasite retention inside cells [15]. Therefore these organelles have a pivotal role during *T. cruzi* invasion.

Lysosomal proteins LAMP-1 and 2 have been shown before to interfere with parasite invasion, since LAMP1/2 knock out cells led to very low levels of cell infection. LAMPs are not only the most abundant, but also highly glycosylated proteins, rich in sialic acid, and estimated to cover about 80% of the luminal surface of this organelle [17, 18, 46, 47]. Since sialic acid had been shown to be important for *T. cruzi* entry into host cells, it had been proposed that those residues could contribute to the observed LAMP knock out phenotype [16, 21, 48]. However, cells lacking only LAMP-2 were able to reproduce the invasion defect produced by abrogation of both LAMP proteins, strongly suggesting that LAMP-2 alone was responsible for the LAMP1/2^{-/-} invasion phenotype and that sialic acid moieties, specifically from LAMPs, were most likely not important for this process. This was reinforced by the fact that parasitophorous vacuole morphology was not altered in LAMP2^{-/-} or LAMP1/2^{-/-} cells as compared to WT cells. It had been shown before by Lopez and co-workers (2002) that cells lacking sialic acid are less susceptible to infection and that this phenotype was a result of the formation of a looser

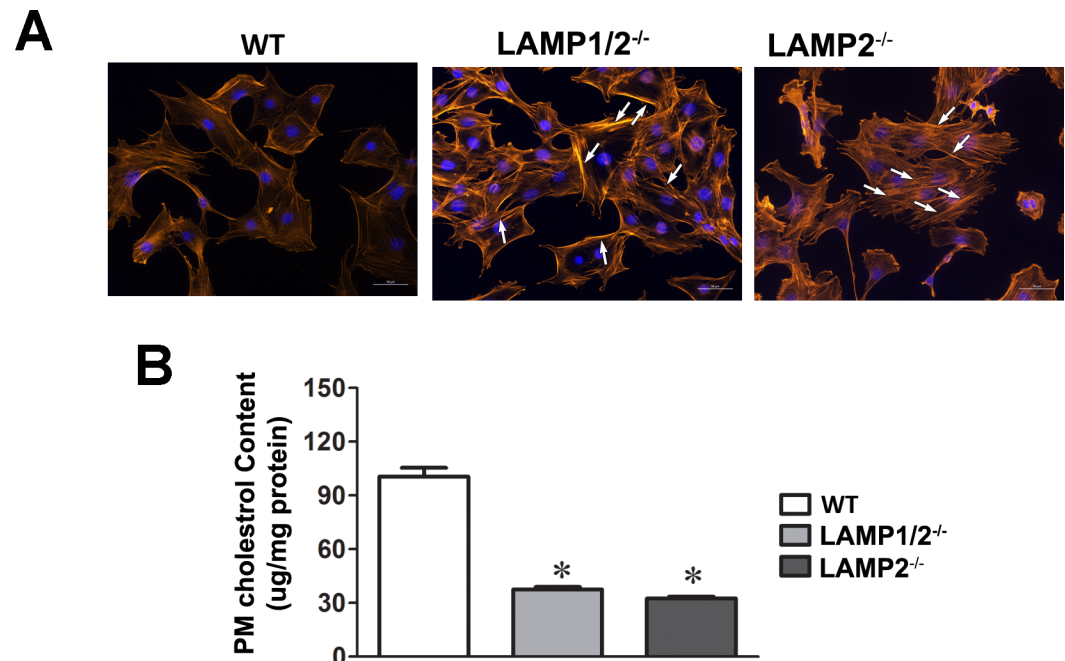


Fig 5. Absence of LAMP-2 leads to actin cytoskeleton rearrangement and decrease in cholesterol levels at the cell plasma membrane. (A) WT, LAMP1/2^{-/-} or LAMP2^{-/-} cells were submitted to phalloidin staining and analyzed in a fluorescence microscope. Arrows indicate the presence of the long actin stress fibers. (B) WT, LAMP1/2^{-/-} or LAMP2^{-/-} cells were submitted to lipid extraction from plasma membrane and the amount of cholesterol content evaluated. Plasma membrane cholesterol of LAMP2^{-/-} and LAMP1/2^{-/-} was measured as a percentage the plasma membrane content of WT cells, which was set as 100. Asterisk above bars indicate statistically significant differences.

<https://doi.org/10.1371/journal.pntd.0005657.g005>

vacuole, where membranes of parasite and vacuole were not tightly apposed [22]. Altogether these data reinforced that intrinsic characteristics of LAMP-2, other than its sialic acid residues were important for *T. cruzi* invasion of host cells.

In order to investigate how LAMP-2 was involved with *T. cruzi* host cell invasion, we evaluated the different steps involved with parasite internalization. First we investigated the ability of these LAMP2 knock out cells to perform lysosomal exocytosis. It had been shown before that lysosome fusion with phagosomes was somewhat disturbed in LAMP1/2^{-/-} cells [49], indicating that lysosome mobility could be affected upon loss of LAMP. We showed that this was not the case, since upon stimuli these LAMP knock out cells were able to induce lysosome exocytic events. These data corroborate previous work from our group, which had shown that no parasite loss was observed in LAMP1/2^{-/-} cells [16], as would be expected when lysosomal fusion is blocked [15].

On the other hand we showed that compensatory endocytosis triggered by lysosomal exocytosis is compromised in cells lacking LAMP-2 (LAMP2^{-/-} and LAMP1/2^{-/-}). These compensatory endocytic events are extremely important during membrane repair, since they are responsible for removing the injured membrane and promoting membrane resealing, without which cells would die [33, 38]. In fact, we showed here that LAMP-2 deficiency leads to more death of scraped injured cells. Although the latter could be explained by a compensatory endocytosis defect, it could also be a consequence of the fact that these cells are more prone to injury by scraping when compared to WT cells. The higher the number of injuries in one cell could lower its chance of membrane repair and recovery. In fact a larger number of cells presenting higher PI labeling values, was observed for cells lacking LAMP-2. The same was

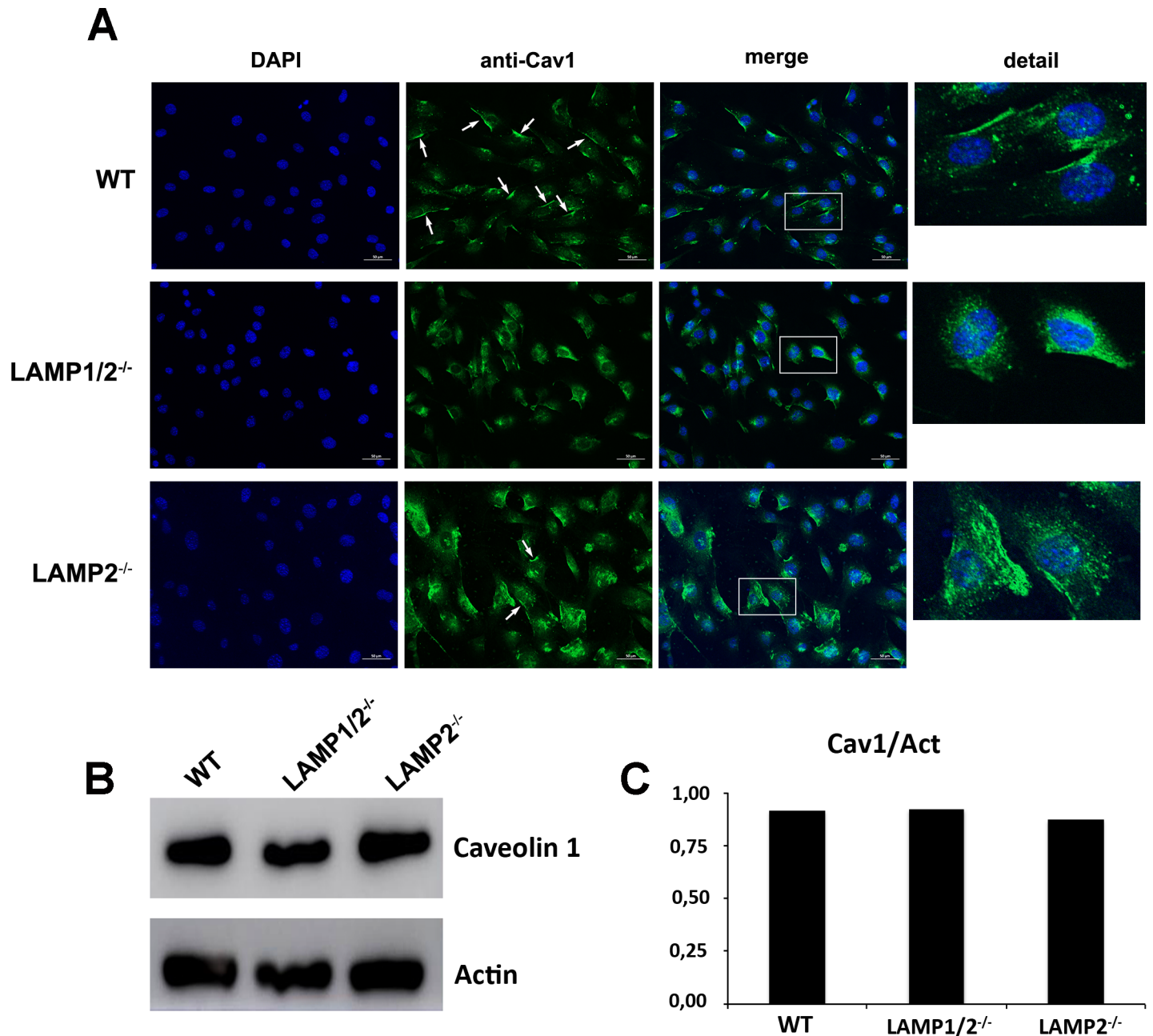


Fig 6. Absence of LAMP leads to decrease in caveolin associated with cell plasma membrane. (A) WT, LAMP1/2^{-/-}, or LAMP2^{-/-} cells were fixed, submitted to labeling with anti-caveolin 1 and analyzed in a fluorescence microscope. Arrows indicate the presence of caveolin-1 at the cell surface. Details of each image are shown on the side. (B) WT, LAMP1/2^{-/-} or LAMP2^{-/-} cells were submitted to total protein extraction. Extracts were run on a gel, blotted onto nitrocellulose membranes and revealed using an anti-caveolin 1 antibody. The panel shows the presence of caveolin in the protein extracts from all three cells. (C) Graph shows the quantification of the amount of total caveolin in the different cell types.

<https://doi.org/10.1371/journal.pntd.0005657.g006>

observed when we used the parasite as the source of injury. This susceptibility to membrane injury is probably linked to the fact that cells deficient in LAMP-2 retain cholesterol in lysosomes [29, 50]. LAMP-2 has been shown to bind cholesterol and help in its traffic to the plasma membrane [51], leading to less cholesterol at the cell surface, as demonstrated here. The decrease in the levels of cholesterol at the cell plasma membrane leads to actin cytoskeleton

reorganization and cell stiffening [31, 52], which could make cells more prone to mechanical injury. We then tested whether cells pre-treated with M β CD, a drug able to decrease cholesterol from cell plasma membrane and induce actin cytoskeleton rearrangement would also lead to increased cell injury and death. In the conditions tested here, even though M β CD treated cells were more prone to injury by scraping, they were almost as efficient as non-treated cells in recovering from injury (see S2 Fig). Therefore, the inability of LAMP-2 deficient cells in recovering from injury should really be due to their inability to endocytose the injured membrane and not due to the fact that they are excessively injured.

We further investigated why compensatory endocytosis events were compromised in cells lacking LAMP-2. Compensatory endocytosis triggered by lysosomal exocytic events are dependent on the secretion of Acid Sphingomyelinase (ASM), an enzyme that cleaves sphingomyelin into ceramide inducing its coalescence and membrane internalization [33]. The levels and secretion of ASM were not altered in LAMP-2 deficient cells. This corroborates previous data by Eskelinen and coworkers (2004), which showed that although these LAMP-2 deficient fibroblasts present an accumulation of autophagic vacuoles no deficiency in protein degradation was observed, indicating that lysosomal enzyme content seemed to be unaffected by LAMP-1 or 2 deficiency [29]. Additionally, contrary to other cellular models of cholesterol storage defects, such as NPC (Niemann-Pick type C) patient cells, it has been demonstrated that LAMP1/2^{-/-} cells do not show significant differences in the levels of sphingomyelin, ceramide and gangliosides at the cell surface when compared to WT cells. Therefore, not only ASM but also its substrate were available to trigger endocytosis in cells lacking LAMP-2 [50]. Thus subsequent events had to be responsible for the compensatory endocytosis defect. LAMP1/2^{-/-} fibroblasts had also been shown to have a marked defect in the maturation of autophagosomes and phagosomes to degradative autolysosomes and phagolysosomes, indicating an alteration in lysosome mobility in these cells [29, 49, 53]. In the work by Huynh and coworkers, late endosomes/lysosomes, as well as phagosomes, show reduced ability to move on microtubules towards the cell center in LAMP1/2^{-/-} cells, most likely due to impairment in the interaction between them. This reduced mobility could also be accounting for the reduction in the observed endocytic events. However, it has also been shown that in LAMP1/2^{-/-} cells the phagosomes acquired Rab5 and accumulated phosphatidylinositol 3-phosphate normally, suggesting that the first steps of the endocytic pathways had not been altered when LAMPs are not present [49]. Moreover Schneede and co-workers have described that the maturation defect of autophagosomes and phagosomes to degradative autolysosomes and phagolysosomes in LAMP1/2^{-/-} cells was not observed in MEFs lacking only LAMP-1 or 2. Therefore mobility was not likely to be responsible for the reduced compensatory events observed for LAMP-2 deficient cells.

Corrote and coworkers described that the endocytosis of PM wounds is dependent on caveolin-1 and caveolar structures, this being a major mechanism used by cells to reseal plasma membrane injuries [54]. Interestingly, our results showed that the distribution of caveolin-1 at the cell surface is seriously compromised in cells lacking LAMP-2. Since caveolin-1 associates with cholesterol to form caveole, cholesterol decrease in plasma membrane could be leading to dispersion of caveolin-1 as previously suggested [55]. Additionally, it has been shown that during caveolin traffic to the plasma membrane it accumulates in the medial Golgi, where it associates with cholesterol in order to be relocated to cell plasma membrane [56]. The altered intracellular traffic of cholesterol could be holding caveolin inside the cell and preventing its relocation to cell surface. In fact, we showed that the amount of caveolin produced in LAMP-2 deficient cells is the same as the one from WT cell. However, in LAMP-2 deficient cells caveolin is found only inside cells, apparently in small vesicles, most likely lysosomes as shown before [55]. Therefore, the lack of caveolin-1 at the plasma membrane could be responsible for

the defect in compensatory endocytosis phenotype of LAMP2 knock out cells. This would also consequently account for less parasite internalization, especially considering that we have shown that *T. cruzi* was able to promote membrane injuries in all three cell lines, but failed to efficiently invade cells lacking LAMP-2.

The results shown here not only demonstrate the importance and mechanism by which LAMP-2 interferes with *T. cruzi* host cell entry but also indicate a major role for this protein in regulating plasma membrane repair. Consequently, it may help to understand the mechanisms involved with other diseases, related not only to LAMP-2 deficiency, such as Danon disease, but also with some lysosomal storage maladies or any genetic disorder in which impairment in plasma-membrane repair is observed.

Supporting information

S1 Fig. LAMP-1 and 2 labeling in WT, LAMP1/2^{-/-} and LAMP2^{-/-} cells, through immunofluorescence with anti-LAMP-1 (A, C and E) or anti-LAMP-2 (B, D and F) antibodies and secondary labeled with Alexa Fluor 488® (as described in Material and Methods, 2.4). Cell nuclei are labeled with DAPI. LAMP-1 and 2 labeling is observed in WT cells (A and B), while no labeling of LAMP-1 or 2 is seen in LAMP1/2^{-/-} fibroblasts (C and D). LAMP2^{-/-} fibroblasts show labeling for only LAMP-1 (E and F). Nuclei can be seen in all panels. Details of each panel are shown on the side.

(TIF)

S2 Fig. Increased actin stress fibers make cells more susceptible to mechanical injury, but does not interfere with membrane repair. WT cells were treated with 5mM MβCD for 30 minutes in DMEM without serum and submitted to membrane injury by cell scraping. (A) Measurement of compensatory endocytosis events induced by membrane injury. Non-treated and MβCD-treated WT fibroblasts were labeled with WGA-Alexa Fluor 488, submitted to membrane injury by cell scraping, in the presence (red) or absence (blue) of extracellular calcium, and then incubated with trypan-blue to eliminate plasma membrane labeling. Only fluorescence from internalized membranes was preserved. The endocytosis was then quantified by FACS analysis. Histograms show the number of cells displaying WGA-Alexa Fluor 488 labeling. (B) Non-treated and MβCD-treated WT fibroblasts were either scraped in the absence of extracellular calcium and in the presence of Propidium Iodide (No Ca²⁺ + PI), to evaluate the amount of injury, or in the presence of extracellular calcium and absence of PI, allowed to reseal, and then exposed to PI (Ca²⁺ / PI), to evaluate the ability to recover from injury. For the “No Ca²⁺ + PI” condition, the number of PI+ cells represent the ones that suffered injury during scraping, while cells excluding PI represent those that didn’t suffer membrane injury. For the “Ca²⁺ / PI” condition, the number of PI- cells represent the ones did recover from injury and the PI+ cells the ones that did not recover from injury. Bars above the curve indicate the percentage of PI + and PI—cells. Data shown are representative of three independent experiments.

(TIF)

S3 Fig. Z-stack images of WT, LAMP1/2^{-/-} and LAMP2^{-/-} labeled with anti-caveolin 1 antibody. WT, LAMP1/2^{-/-}, or LAMP2^{-/-} cells were fixed, submitted to labeling with anti-caveolin 1 and imaged using a Zeiss Axio Imager Microscope. Eight optical slices with an approximate 1.86μm interval of each cell line were captured from bottom to top, using the 63x oil objective.

(TIF)

S1 Video. 3D reconstruction of wild type, LAMP1/2^{-/-}, and LAMP2^{-/-} cells. Cells were imaged in a Zeiss Axio Imager Microscope to create a 3D reconstruction, which has been

made following capture of 16 optical slices with an approximate 0.93µm interval, using the 63x oil objective. The 3D imaging stack has been reconstructed using Zen Blue software. (MP4)

Acknowledgments

We are especially grateful to Dr. Paul Saftig and Dr. Renato Mortara for providing the LAMP1/2 and LAMP2 knock out cells that have been used in this work, as well as Artur Miranda, Jader Santos and Vany Perpétua Ferraz for the help with the cholesterol quantification. We are also grateful to Centro de Aquisição e Processamento de Imagens (CAPI / ICB) and Centro de Microscopia da UFMG for the use of microscopes and imaging processing systems.

Author Contributions

Conceptualization: LOA TCG.

Data curation: LOA TCG.

Formal analysis: DP NFC LR TCG.

Funding acquisition: LOA.

Investigation: DP NFC LR PPD TLC LCB ACSO LFK TCG.

Methodology: LOA TCG NFC.

Project administration: LOA.

Resources: TCG LOA.

Supervision: LOA.

Validation: DP NFC LR TCG LOA.

Visualization: DP NFC LR LFK TCG.

Writing – original draft: NFC TCG LOA.

Writing – review & editing: TCG LOA.

References

1. Coura JR, Dias JC. Epidemiology, control and surveillance of Chagas disease—100 years after its discovery. *Mem Inst Oswaldo Cruz*. 2009; 104(4):31–40. Epub 2009/08/04. doi: S0074-02762009000900006 [pii]. PMID: 19649434.
2. Gascon J, Bern C, Pinazo MJ. Chagas disease in Spain, the United States and other non-endemic countries. *Acta Trop*. 2010; 115(1–2):22–7. Epub 2009/08/04. <https://doi.org/10.1016/j.actatropica.2009.07.019> PMID: 19646412.
3. Coura JR, Vinas PA. Chagas disease: a new worldwide challenge. *Nature*. 2010; 465(7301):S6–7. <https://doi.org/10.1038/nature09221> PMID: 20571554.
4. Albajar-Vinas P, Jannin J. The hidden Chagas disease burden in Europe. *Euro Surveill*. 2011; 16(38). Epub 2011/10/01. PMID: 21958529.
5. Gobbi F, Angheben A, Anselmi M, Postiglione C, Repetto E, Buonfrate D, et al. Profile of Trypanosoma cruzi infection in a tropical medicine reference center, Northern Italy. *PLoS Negl Trop Dis*. 2014; 8(12): e3361. <https://doi.org/10.1371/journal.pntd.0003361> PMID: 25502927; PubMed Central PMCID: PMC4263408.
6. Rassi A Jr., Rassi A, Marcondes de Rezende J. American trypanosomiasis (Chagas disease). *Infect Dis Clin North Am*. 2012; 26(2):275–91. Epub 2012/05/29. doi: S0891-5520(12)00011-6 [pii] <https://doi.org/10.1016/j.idc.2012.03.002> PMID: 22632639.

7. Bahia MT, Diniz Lde F, Mosqueira VC. Therapeutical approaches under investigation for treatment of Chagas disease. Expert opinion on investigational drugs. 2014; 23(9):1225–37. <https://doi.org/10.1517/13543784.2014.922952> PMID: 24855989.
8. Schenkman S, Ferguson MA, Heise N, de Almeida ML, Mortara RA, Yoshida N. Mucin-like glycoproteins linked to the membrane by glycosylphosphatidylinositol anchor are the major acceptors of sialic acid in a reaction catalyzed by trans-sialidase in metacyclic forms of *Trypanosoma cruzi*. Mol Biochem Parasitol. 1993; 59(2):293–303. Epub 1993/06/01. PMID: 8341326.
9. Ramirez MI, Ruiz Rde C, Araya JE, Da Silveira JF, Yoshida N. Involvement of the stage-specific 82-kilodalton adhesion molecule of *Trypanosoma cruzi* metacyclic trypomastigotes in host cell invasion. Infect Immun. 1993; 61(9):3636–41. Epub 1993/09/01. PMID: 8359886.
10. Caler EV, Vaena de Avalos S, Haynes PA, Andrews NW, Burleigh BA. Oligopeptidase B-dependent signaling mediates host cell invasion by *Trypanosoma cruzi*. EMBO J. 1998; 17(17):4975–86. <https://doi.org/10.1093/emboj/17.17.4975> PMID: 9724634; PubMed Central PMCID: PMC1170826.
11. Scharfstein J, Schmitz V, Morandi V, Capella MM, Lima AP, Morrot A, et al. Host cell invasion by *Trypanosoma cruzi* is potentiated by activation of bradykinin B(2) receptors. J Exp Med. 2000; 192(9):1289–300. Epub 2000/11/09. PMID: 11067878; PubMed Central PMCID: PMC2193362.
12. Yoshida N, Cortez M. *Trypanosoma cruzi*: parasite and host cell signaling during the invasion process. Subcell Biochem. 2008; 47:82–91. Epub 2008/06/03. PMID: 18512343.
13. Fernandes MC, Cortez M, Flannery AR, Tam C, Mortara RA, Andrews NW. *Trypanosoma cruzi* subverts the sphingomyelinase-mediated plasma membrane repair pathway for cell invasion. J Exp Med. 2011; 208(5):909–21. <https://doi.org/10.1084/jem.20102518> PMID: 21536739; PubMed Central PMCID: PMC3092353.
14. Rodriguez A, Martinez I, Chung A, Berlot CH, Andrews NW. cAMP regulates Ca²⁺-dependent exocytosis of lysosomes and lysosome-mediated cell invasion by trypanosomes. J Biol Chem. 1999; 274(24):16754–9. PMID: 10358016.
15. Andrade LO, Andrews NW. Lysosomal fusion is essential for the retention of *Trypanosoma cruzi* inside host cells. J Exp Med. 2004; 200(9):1135–43. PMID: 15520245. <https://doi.org/10.1084/jem.20041408>
16. Albertti LA, Macedo AM, Chiari E, Andrews NW, Andrade LO. Role of host lysosomal associated membrane protein (LAMP) in *Trypanosoma cruzi* invasion and intracellular development. Microbes Infect. 2010; 12(10):784–9. Epub 2010/06/22. <https://doi.org/10.1016/j.micinf.2010.05.015> S1286-4579(10)00154-1 [pii]. PMID: 20561595.
17. Howe C, Granger BL, Hull M, Green SA, Gabel CA, Helenius A, et al. Derived protein sequence, oligosaccharides, and membrane insertion of the 120 kDa lysosomal membrane glycoprotein (lgp120): identification of a highly conserved family of lysosomal membrane glycoproteins. Proc Natl Acad Sci USA. 1988; 85(7577–7581). PMID: 3174652
18. Eskelinen EL, Tanaka Y, Saftig P. At the acidic edge: emerging functions for lysosomal membrane proteins. Trends Cell Biol. 2003; 13(3):137–45. Epub 2003/03/12. doi: S0962892403000059 [pii]. PMID: 12628346.
19. Schenkman S, Jiang MS, Hart GW, Nussenzweig V. A novel cell surface trans-sialidase of *Trypanosoma cruzi* generates a stage-specific epitope required for invasion of mammalian cells. Cell. 1991; 65:1117–25. PMID: 1712251
20. Schenkman RP, Vandekerckhove F, Schenkman S. Mammalian cell sialic acid enhances invasion by *Trypanosoma cruzi*. Infect Immun. 1993; 61(3):898–902. PMID: 8381772.
21. Villalta F, Smith CM, Ruiz-Ruano A, Lima MF. A ligand that *Trypanosoma cruzi* uses to bind to mammalian cells to initiate infection. FEBS Lett. 2001; 505(3):383–8. PMID: 11576533.
22. Lopez M, Huynh C, Andrade LO, Pypaert M, Andrews NW. Role for sialic acid in the formation of tight lysosome-derived vacuoles during *Trypanosoma cruzi* invasion. Mol Biochem Parasitol. 2002; 119(1):141–5. PMID: 11755197
23. Chen JW, Chen GL, D'Souza MP, Murphy TL, August JT. Lysosomal membrane glycoproteins: properties of LAMP-1 and LAMP-2. Biochemical Society symposium. 1986; 51:97–112. PMID: 3101702.
24. Fukuda M, Viitala J, Matteson J, Carlsson SR. Cloning of cDNAs encoding human lysosomal membrane glycoproteins, h-lamp-1 and h-lamp-2. Comparison of their deduced amino acid sequences. J Biol Chem. 1988; 263(35):18920–8. PMID: 3198605.
25. Andrejewski N, Punnonen EL, Guhde G, Tanaka Y, Lullmann-Rauch R, Hartmann D, et al. Normal lysosomal morphology and function in LAMP-1-deficient mice. J Biol Chem. 1999; 274(18):12692–701. PMID: 10212251.
26. Schneede A, Schmidt CK, Holtta-Vuori M, Heeren J, Willenborg M, Blanz J, et al. Role for LAMP-2 in endosomal cholesterol transport. J Cell Mol Med. 2009. Epub 2009/11/26. doi: JCMM973 [pii] <https://doi.org/10.1111/j.1582-4934.2009.00973.x> PMID: 19929948.

27. Tanaka Y, Guhde G, Suter A, Eskelinen EL, Hartmann D, Lullmann-Rauch R, et al. Accumulation of autophagic vacuoles and cardiomyopathy in LAMP-2-deficient mice. *Nature*. 2000; 406(6798):902–6. <https://doi.org/10.1038/35022595> PMID: 10972293.
28. Eskelinen EL, Illert AL, Tanaka Y, Schwarzmann G, Blanz J, Von Figura K, et al. Role of LAMP-2 in lysosome biogenesis and autophagy. *Mol Biol Cell*. 2002; 13(9):3355–68. Epub 2002/09/11. <https://doi.org/10.1091/mbc.E02-02-0114> PMID: 12221139; PubMed Central PMCID: PMC124165.
29. Eskelinen EL, Schmidt CK, Neu S, Willenborg M, Fuertes G, Salvador N, et al. Disturbed cholesterol traffic but normal proteolytic function in LAMP-1/LAMP-2 double-deficient fibroblasts. *Mol Biol Cell*. 2004; 15(7):3132–45. Epub 2004/05/04. <https://doi.org/10.1091/mbc.E04-02-0103> E04-02-0103 [pii]. PMID: 15121881; PubMed Central PMCID: PMC452571.
30. Andrews NW, Hong KS, Robbins ES, Nussenzweig V. Stage-specific surface antigens expressed during the morphogenesis of vertebrate forms of *Trypanosoma cruzi*. *Exp Parasitol*. 1987; 64:474–84. PMID: 3315736
31. Hissa B, Pontes B, Roma PM, Alves AP, Rocha CD, Valverde TM, et al. Membrane cholesterol removal changes mechanical properties of cells and induces secretion of a specific pool of lysosomes. *PLoS One*. 2013; 8(12):e82988. <https://doi.org/10.1371/journal.pone.0082988> PMID: 24376622; PubMed Central PMCID: PMC3869752.
32. Aderem A. Signal transduction and the actin cytoskeleton: the roles of MARCKS and profilin. *TIBS*. 1992; 17:438–43. PMID: 1455513
33. Tam C, Idone V, Devlin C, Fernandes MC, Flannery A, He X, et al. Exocytosis of acid sphingomyelinase by wounded cells promotes endocytosis and plasma membrane repair. *J Cell Biol*. 2010; 189(6):1027–38. <https://doi.org/10.1083/jcb.201003053> PMID: 20530211; PubMed Central PMCID: PMC2886342.
34. Ferber E, Resch K, Wallach DF, Imm W. Isolation and characterization of lymphocyte plasma membranes. *Biochim Biophys Acta*. 1972; 266(2):494–504. PMID: 5038272.
35. Alonso L, Lozada L., Fontecha J., Juárez M. Determination of cholesterol in milk fat by gas chromatography with direct injection and sample saponification. *Cromatographia*. 1995; 41(5):6.
36. Lowry OH, Rosebrough NJ, Farr AL, Randall RJ. Protein measurement with the Folin phenol reagent. *J Biol Chem*. 1951; 193(1):265–75. PMID: 14907713.
37. Dorta ML, Ferreira AT, Oshiro ME, Yoshida N. Ca²⁺ signal induced by *Trypanosoma cruzi* metacyclic trypomastigote surface molecules implicated in mammalian cell invasion. *Mol Biochem Parasitol*. 1995; 73(1–2):285–9. Epub 1995/07/01. PMID: 8577342.
38. Idone V, Tam C, Goss JW, Toomre D, Pypaert M, Andrews NW. Repair of injured plasma membrane by rapid Ca²⁺-dependent endocytosis. *J Cell Biol*. 2008; 180(5):905–14. Epub 2008/03/05. doi: jcb.200708010 [pii] <https://doi.org/10.1083/jcb.200708010> PMID: 18316410; PubMed Central PMCID: PMC2265401.
39. Miller H, Castro-Gomes T, Corrotte M, Tam C, Mangel TK, Andrews NW, et al. Lipid raft-dependent plasma membrane repair interferes with the activation of B lymphocytes. *J Cell Biol*. 2015; 211(6):1193–205. <https://doi.org/10.1083/jcb.201505030> PMID: 26694840; PubMed Central PMCID: PMC4687878.
40. Burleigh BA, Andrews NW. A 120-kDa alkaline peptidase from *Trypanosoma cruzi* is involved in the generation of a novel Ca(2+)-signaling factor for mammalian cells. *J Biol Chem*. 1995; 270(10):5172–80. PMID: 7890627.
41. Andrade D, Serra R, Svensjo E, Lima AP, Ramos ES Jr., Fortes FS, et al. *Trypanosoma cruzi* invades host cells through the activation of endothelin and bradykinin receptors: a converging pathway leading to chagasic vasculopathy. *Br J Pharmacol*. 2012; 165(5):1333–47. Epub 2011/07/30. <https://doi.org/10.1111/j.1476-5381.2011.01609.x> PMID: 21797847.
42. Fernandes MC, Cortez M, Geraldo Yoneyama KA, Straus AH, Yoshida N, Mortara RA. Novel strategy in *Trypanosoma cruzi* cell invasion: implication of cholesterol and host cell microdomains. *Int J Parasitol*. 2007; 37(13):1431–41. Epub 2007/06/22. doi: S0020-7519(07)00149-X [pii] <https://doi.org/10.1016/j.ijpara.2007.04.025> PMID: 17582418.
43. Tardieux I, Webster P, Ravesloot J, Boron W, Lunn JA, Heuser JE, et al. Lysosome recruitment and fusion are early events required for trypanosome invasion of mammalian cells. *Cell*. 1992; 71(7):1117–30. PMID: 1473148.
44. Rodriguez A, Rioult MG, Ora A, Andrews NW. A trypanosome-soluble factor induces IP3 formation, intracellular Ca²⁺ mobilization and microfilament rearrangement in host cells. *J Cell Biol*. 1995; 129:1263–73. PMID: 7775573
45. Rodriguez A, Webster P, Ortego J, Andrews NW. Lysosomes behave as Ca²⁺-regulated exocytic vesicles in fibroblasts and epithelial cells. *J Cell Biol*. 1997; 137:93–104. PMID: 9105039

46. Granger B, Green SA, Gabel CA, Howe CL, Mellman I, Helenius A. Characterization and cloning of Igp 110, a lysosomal membrane glycoprotein from mouse and rat cells. *J Biol Chem.* 1990; 265:12036–43. PMID: [2142158](#)
47. Fukuda M. Lysosomal membrane glycoproteins. Structure, biosynthesis, and intracellular trafficking. *J Biol Chem.* 1991; 266(32):21327–30. PMID: [1939168](#).
48. Schenkman S, Diaz C, Nussenzweig V. Attachment of *Trypanosoma cruzi* trypomastigotes to receptors at restricted cell surface domains. *Exp Parasitol.* 1991; 72(1):76–86. PMID: [1993466](#)
49. Huynh KK, Eskelinen EL, Scott CC, Malevanets A, Saftig P, Grinstein S. LAMP proteins are required for fusion of lysosomes with phagosomes. *EMBO J.* 2007; 26(2):313–24. Epub 2007/01/25. doi: 7601511 [pii] <https://doi.org/10.1038/sj.emboj.7601511> PMID: [17245426](#); PubMed Central PMCID: PMC1783450.
50. Schneede A, Schmidt CK, Holtta-Vuori M, Heeren J, Willenborg M, Blanz J, et al. Role for LAMP-2 in endosomal cholesterol transport. *J Cell Mol Med.* 2011; 15(2):280–95. <https://doi.org/10.1111/j.1582-4934.2009.00973.x> PMID: [19929948](#); PubMed Central PMCID: PMC3822795.
51. Li J, Pfeffer SR. Lysosomal membrane glycoproteins bind cholesterol and contribute to lysosomal cholesterol export. *eLife.* 2016; 5. <https://doi.org/10.7554/eLife.21635> PMID: [27664420](#); PubMed Central PMCID: PMC5068966.
52. Byfield FJ, Aranda-Espinoza H, Romanenko VG, Rothblat GH, Levitan I. Cholesterol depletion increases membrane stiffness of aortic endothelial cells. *Biophys J.* 2004; 87(5):3336–43. Epub 2004/09/07. <https://doi.org/10.1529/biophysj.104.040634> S0006-3495(04)73800-X [pii]. PMID: [15347591](#).
53. Binker MG, Cosen-Binker LI, Terebiznik MR, Mallo GV, McCaw SE, Eskelinen EL, et al. Arrested maturation of *Neisseria*-containing phagosomes in the absence of the lysosome-associated membrane proteins, LAMP-1 and LAMP-2. *Cell Microbiol.* 2007; 9(9):2153–66. Epub 2007/05/18. doi: CMI946 [pii] <https://doi.org/10.1111/j.1462-5822.2007.00946.x> PMID: [17506821](#).
54. Corrotte M, Almeida PE, Tam C, Castro-Gomes T, Fernandes MC, Millis BA, et al. Caveolae internalization repairs wounded cells and muscle fibers. *eLife.* 2013; 2:e00926. <https://doi.org/10.7554/eLife.00926> PMID: [24052812](#); PubMed Central PMCID: PMC3776555.
55. Mundy DI, Li WP, Luby-Phelps K, Anderson RG. Caveolin targeting to late endosome/lysosomal membranes is induced by perturbations of lysosomal pH and cholesterol content. *Mol Biol Cell.* 2012; 23(5):864–80. <https://doi.org/10.1091/mbc.E11-07-0598> PMID: [22238363](#); PubMed Central PMCID: PMC3290645.
56. Hayer A, Stoeber M, Bissig C, Helenius A. Biogenesis of caveolae: stepwise assembly of large caveolin and cavin complexes. *Traffic.* 2010; 11(3):361–82. <https://doi.org/10.1111/j.1600-0854.2009.01023.x> PMID: [20070607](#).



OxLDL alterations in endothelial cell membrane dynamics leads to changes in vesicle trafficking and increases cell susceptibility to injury

Natália Fernanda Couto^a, Luisa Rezende^a, Wesley Fernandes-Braga^b, Ana Paula Alves^c, Ubirajara Agero^c, Jacqueline Alvarez-Leite^b, Nágila Raquel Teixeira Damasceno^d, Thiago Castro-Gomes^e, Luciana O. Andrade^{a,*}

^a Department of Morphology, Federal University of Minas Gerais, Belo Horizonte, MG, Brazil

^b Department of Biochemistry and Immunology, Federal University of Minas Gerais, Belo Horizonte, MG, Brazil

^c Department of Physics, Federal University of Minas Gerais, Belo Horizonte, MG, Brazil

^d Department of Nutrition, University of São Paulo, São Paulo, SP, Brazil

^e Department of Parasitology, Federal University of Minas Gerais, Belo Horizonte, MG, Brazil

ARTICLE INFO

Keywords:

Cholesterol
Oxidized LDL
Endothelial cell
Membrane repair

ABSTRACT

Plasma membrane repair (PMR) is an important process for cell homeostasis, especially for cells under constant physical stress. Repair involves a sequence of Ca^{2+} -dependent events, including lysosomal exocytosis and subsequent compensatory endocytosis. Cholesterol sequestration from plasma membrane causes actin cytoskeleton reorganization and polymerization, increasing cell stiffness, which leads to exocytosis and reduction of a peripheral pool of lysosomes involved in PMR. These changes in mechanical properties are similar to those observed in cells exposed to oxidized Low Density Lipoprotein (oxLDL), a key molecule during atherosclerosis development. Using a human umbilical vein endothelial cell line (EAH926) we evaluated the influence of mechanical modulation induced by oxLDL in PMR and its effect in endothelial fragility. Similar to M β CD (a drug capable of sequestering cholesterol) treatment, oxLDL exposure led to actin reorganization and *de novo* polymerization, as well as an increase in cell rigidity and lysosomal exocytosis. Additionally, for both M β CD and oxLDL treated cells, there was an initial increase in endocytic events, likely triggered by the peak of exocytosis induced by both treatments. However, no further endocytic events were observed, suggesting that constitutive endocytosis is blocked upon treatment and that the reorganized cytoskeleton function as a mechanical barrier to membrane traffic. Finally, the increase in cell rigidity renders cells more prone to mechanical injury. Together, these data show that mechanical modulation induced by oxLDL exposure not only alters membrane traffic in cells, but also makes them more susceptible to mechanical injury, which may likely contribute to the initial steps of atherosclerosis development.

1. Introduction

The plasma membrane is a complex structure formed by a lipid bilayer that confers fluidity to the cell membrane and acts as a barrier between the extracellular environment and the cytosol. Lipids in the plasma membrane can naturally aggregate forming specialized regions in the form of microdomains, which play a key role on several cell membrane functions. Cholesterol enriched membrane microdomains, also called membrane rafts, are small domains (10–200 nm), rich in sterols and sphingolipids, which are present on the cell surface and are responsible for several cellular functions [1,2]. Cholesterol is an essential molecule for the organization and structuring of these

membrane rafts. It confers special biophysical properties to the cell membrane by increasing the cohesion and packing of their lipids, thereby forming platforms containing proteins with which they have affinity [2]. Regulation of cholesterol content at the plasma membrane interferes with membrane rafts organization and, consequently, may influence several cellular processes, including membrane trafficking events and cell cytoskeleton organization [3–6].

Recently, we have shown that cholesterol sequestration from plasma membrane and consequently rafts disruption lead to a massive unregulated exocytosis of a peripheral pool of lysosomes. Cell membrane cholesterol depletion induced by methyl-beta cyclodextrin (M β CD), a well-known cholesterol sequestering drug, triggered lysosomal

* Corresponding author.

E-mail address: landrade@icb.ufmg.br (L.O. Andrade).

<https://doi.org/10.1016/j.bbamem.2019.183139>

Received 24 July 2019; Received in revised form 14 November 2019; Accepted 27 November 2019

Available online 05 December 2019

0005-2736/© 2019 Elsevier B.V. All rights reserved.

exocytosis as early as 10 min of cell treatment [7]. It has also been suggested in this work that the lysosomal exocytic events were elicited by the increase in cell surface tension and stiffness, caused by changes in actin cytoskeleton organization and polymerization induced by cholesterol depletion [6]. On the other hand, these changes in actin cytoskeleton organization may also create a peripheral barrier for new membrane trafficking events from or to the plasma membrane [8,9].

Plasma membrane repair (PMR) is an important process for cell homeostasis, especially for cells under constant physical stress, such as endothelial cells (ECs). It has been shown that repair involves a sequence of Ca^{2+} -dependent processes, including lysosomal exocytosis and subsequent compensatory endocytic events [10]. Briefly, when the cell is submitted to plasma membrane injury, extracellular Ca^{2+} flows into cells through the injured sites and triggers exocytosis of lysosomes. Upon exocytosis, acid sphingomyelinase, a lysosomal enzyme, is delivered to the external surface of the plasma membrane, where it converts sphingomyelin into ceramide. Ceramide is believed to self-associate inducing a curvature in the cell surface that results in the internalization of the wounded membrane in a process called compensatory endocytosis. This process carries the injury into the cell, resealing the membrane [10]. Therefore, changes in membrane rafts organization and their consequent alterations in cell membrane mechanical properties could affect PMR mechanisms.

Other scenarios induce rafts disorganization, such as the exposure of ECs to an oxidized form of the Low Density Lipoprotein (oxLDL), which is found accumulated in the early stages of atherosclerotic lesions [11]. OxLDL exposure also causes modifications in the mechanical properties of ECs by changing actin cytoskeleton organization and increasing membrane stiffness [12–14]. It is well known that OxLDL binding to its receptors is able to enhance endothelial dysfunction and permeability, as well as RhoA activation [15–17], but how the mechanical changes induced by endothelial cell exposure to oxLDL interfere with this process it is still poorly understood.

Since cholesterol sequestration and rafts disruption induces the formation of an actin cytoskeleton barrier at cell cortex and considerably diminishes the peripheral pool of lysosomes, we decided to study the effects of oxLDL-induced actin reorganization in vesicular traffic and PMR processes.

2. Materials and methods

2.1. Cell culture

The endothelial cell line EAhy926, derived from Human Umbilical Vein Endothelial Cells (HUVEC) was used for all experiments (passages 2–10). Endothelial cells (ECs) were maintained in high-glucose Dulbecco's Modified Eagle's Medium (DMEM; Gibco), supplemented with 10% fetal bovine serum (FBS; GIBCO) and 1% penicillin/streptomycin (100 U/mL and 100 $\mu\text{g}/\text{mL}$, respectively) (GIBCO) at 37 °C in a humidified atmosphere containing 5% CO_2 .

2.2. Isolation and oxidation of LDL

Blood from health individuals was collected and plasma separated by centrifugation. Potassium Bromide (KBr) solution at the density of 1.019 g/mL was added to the plasma and the latter was submitted to ultracentrifugation at 236.500 $\times g$ for 7 h using Sorvall Ultra Pro 80 ultracentrifuge. Following, the supernatant containing VLDL was discarded. The infranatant was resuspended, its density was adjusted to 1.063 g/mL with KBr, and then submitted to a new ultracentrifugation cycle at 236.5 $\times g$ for 6 h. After this cycle, LDL was collected and dialyzed overnight in PBS with gentle agitation in a cold chamber. LDL concentration was determined by evaluating protein concentration using Lowry's method. After that, a cocktail of protease inhibitors and antioxidants composed of PMSF (5 $\mu\text{mol}/\text{L}$ plasma), Benzamidine (10 $\mu\text{mol}/\text{L}$ plasma), BHT (100 $\mu\text{mol}/\text{L}$ plasma) and aprotinin

(10 $\mu\text{mol}/\text{L}$ plasma) was added to the LDL fraction. This portion of LDL, which will be referred to as nLDL, was filtered through a 0.22 μm filter unity and held at -80 °C, protected from light, until use.

For LDL oxidation (oxLDL), after determining protein concentration, LDL was incubated for 18 h at 37 °C with 20 μM CuSO_4/mg of protein. To stop the oxidation reaction, the cocktail of inhibitors and antioxidants was added only at the end. OxLDL was then filtered through a 0.22 μm filter unity and stored at -80 °C, protected from light, until use. Lipid oxidation was detected by TBARS assay (in fresh and thawed samples) and the results expressed by the ratio of malondialdehyde (MDA) / protein concentration. Preparations used in the experiments presented the following values: nLDL = 0.602 nmol of MDA/mg of protein; oxLDL = 24,401 nmol of MDA/mg of protein (extensively oxidized LDL). In order to ensure that LDL samples were not degraded with the freezing and thawing processes, we have performed SDS-PAGE electrophoresis of nLDL (1 mg/mL) and oxLDL (0.4 mg/mL) (data not shown).

2.3. Cell treatment

ECs were washed three times with serum free DMEM and exposed to oxidized LDL for 24 h in a working concentration of 50 $\mu\text{g}/\text{mL}$, a standard concentration used in several studies [12,18,19] In these assays, native LDL (50 $\mu\text{g}/\text{mL}$) was used as negative control. As an additional control, cells were washed and incubated with serum-free DMEM for 24 h.

For some experiments plasma membrane cholesterol sequestration was performed by washing cells three times with serum free DMEM with subsequent incubation with 5 mM methyl-beta cyclodextrin (M β CD; Sigma-Aldrich), a well-known cholesterol-sequestering drug, for 10–40 min. As negative control, cells were incubated with 5 mM of an inactive analog, hydroxypropyl-gamma cyclodextrin (H γ CD; Sigma-Aldrich), in the same experimental conditions.

2.4. Labeling of polymerized actin

Cells were plated on 24 well plates containing 13 mm round coverslips at a density of 4×10^4 cells/well, 24 h before the assay. Cells were then treated and fixed with formaldehyde 3.7% for 20 min at room temperature. To analyze *de novo* polymerization, cells were previously treated with 95 μM Latrunculin-A (LAT-A; Sigma-Aldrich) for 1 h, followed by the different treatments and fixation.

After fixation, coverslips with attached cells were washed three times in Phosphate Buffered Saline (PBS) and permeabilized with Triton X-100 0.5% (Sigma-Aldrich) for 15 min. For polymerized actin labeling, cells were incubated with Phalloidin-Alexa Fluor 546 (Invitrogen) using a 1:40 dilution in PBS at room temperature followed by three additional washes. Subsequently, the DNA of cells was stained for 1 min with DAPI (Sigma), mounted, and examined on a Zeiss ApoTome.2 microscope.

2.5. Defocusing microscopy

In order to measure parameters able to characterize the biomechanical properties of the complex plasma-membrane-cytoskeleton of endothelial cells during treatment, we used Defocusing Microscopy (DM) technique as previously described [20]. DM is an optical technique which has been applied to obtain quantitative parameters which characterize membrane surface dynamics of living cells using a bright field microscope [21,22]. Briefly, cells were plated on glass coverslips in 35 mm dishes at a density of 8×10^4 cells/dish 24 h before the assay. To evaluate the effects of oxLDL exposure, cells were treated for 24 h and then recorded by DM in serum free DMEM for 10 min. For the experiments in which cholesterol sequestration was performed, ECs were recorded by DM in serum free DMEM for 10 min (control), then M β CD was added to the medium and cells continued to be recorded for another 40 min. These assays were performed in triplicate and at least 5

different cells were analyzed.

In order to obtain parameters that evaluate drug treatment as a function of time we analyzed slightly defocused captured movies. The contrast of the defocused images is proportional to cell surface curvature [20]. The analysis has been done by the temporal autocorrelation of the contrast adjusted by a single exponential as a function of time, as shown in Eq. (1),

$$\langle C(t_0)C(t_0 + t) \rangle = Ae^{-\frac{t}{\tau}} \quad (1)$$

The amplitude, A , is proportional to the oscillations amplitude, and τ , represents the relaxation time of membrane fluctuations. The mathematical model that describes the autocorrelation function to image contrast is shown by Agero and coworkers (2003) [20].

All experiments were analyzed using ImageJ Plugins that correct for background and calculate the temporal autocorrelation function among frames. These temporal autocorrelation functions were adjusted in Kaleida Graph Software (Synergy Software, Essex Junction, VT, USA) using single exponential decay curves that carry information about their time characteristics (relaxation time) and amplitude of curvature. The experiments were performed in a Nikon Eclipse TI inverted microscope equipped with a 530 nm wavelength green filter, a stage-heated oil immersion objective Nikon Apo TIRF 100 \times , NA 1.49 (Nikon, Japan), and an environmental chamber (model Chamlyde ICCU: 109, Live Cell Instrument, Nowan-gu, Korea) which provides a 5% CO₂ atmosphere, 37 °C temperature and 50% humidity. The images were captured using a 12 bit monochrome Uniq camera (model 1800 CL) (Epix Inc., Buffalo Grove, IL, USA, 4096 Gy levels and 0.064 mm of pixel square side), with a gain of 11.04 db and a capture rate of 1 frame per second. The focal distance was controlled during the entire experiment by a Nikon Perfect Focus System (PFS) apparatus and the camera gray level calibration was performed as previously described [21].

2.6. Cell viability assay

Cells were plated on 6 well plates at a density of 1×10^5 cells/well in triplicates. After 24 h, cells were treated, washed twice with PBS – / – (Ca²⁺ and Mg²⁺ free), trypsinized, pelleted and incubated with a solution of Propidium Iodide (10 μ g/mL) in Hanks' Balanced Salt Solution (HBSS; Sigma-Aldrich). The PI fluorescence of 30,000 individual cells in each replica was measured using a Becton Dickinson FACSscan or Accuri C6 (BD Biosciences, USA) and data were analyzed using FlowJo v10.1 software (Tree Star, Inc.). Three independent experiments were performed.

2.7. β -Hexosaminidase assay

To evaluate lysosomal exocytosis, a β -hexosaminidase secretion assay was performed according to previous work [23]. Briefly, EAhy.926 cells were plated in triplicates in 24-well plates at a density of 4×10^4 cells/well 24 h before the assay. ECs were then treated with oxLDL or nLDL (50 μ g/mL) for 24 h or 10 μ M Ionomycin (Calbiochem) for 10 min at 37 °C. After treatment, the supernatant was collected and attached cells were lysed with Triton x-100 (Sigma-Aldrich) 1% in PBS. Cell supernatant and cell lysates were incubated with 50 μ L of β -hexosaminidase substrate, 6 mM 4-methylumbelliferyl-N-acetyl-B-D-glucosaminide (Sigma M2133), dissolved in Na-citrate-PO₂ buffer (pH 4.5). After 15 min of incubation at 37 °C, the reactions were stopped by adding 100 μ L of stop buffer solution (2 M Na₂CO₃-H₂O, 1.1 M glycine) followed by reading in a spectrofluorimeter at 365 nm excitation and 450 nm emission (Synergy 2, Biotek). Several independent experiments were performed.

2.8. Compensatory endocytosis assay

Compensatory endocytic events triggered by lysosomal exocytosis as well as constitutive endocytosis were measured for each treatment.

In order to measure compensatory endocytosis upon M β CD treatment, 2×10^6 cells were kept in suspension and the outer leaflet of the plasma membrane was labeled with 1 μ g/mL wheat germ agglutinin (WGA) – Alexa Fluor 488 for 1 min at 4 °C, followed by two washes with HBSS. After membrane labeling, cells were exposed or not to M β CD at 37 °C (as described above), resuspended in 0.2% trypan blue (Sigma-Aldrich), washed with HBSS and fixed with formaldehyde 3.7% before FACS analysis. WGA-Alexa Fluor 488 fluorescence of 10,000 individual cells was measured using BD FACSscan and analyzed using FlowJo v10.1 software. Due to WGA-Alexa Fluor 488 susceptibility to quenching by the membrane impermeable trypan blue, Alexa Fluor 488 fluorescence measurement will correspond to the amount of membrane endocytosed after trypan blue exposure.

For nLDL/oxLDL treatment, due to the long period of incubation and WGA degradation with time, we used an alternative method to evaluate compensatory endocytosis. For this, cells were plated on 13 mm round coverslips at a density of 4×10^4 cells/well 24 h before the assay. Then, cells were incubated with oxLDL for 0, 1, 4, 8, 12, 16, and 24 h in the presence of Texas-Red Dextran, a membrane impermeable fluorescent dye. At each time point, cells were washed to eliminate extracellular Texas-Red Dextran, fixed with Paraformaldehyde 4% and cell nuclei labeled with DAPI. The fluorescence of the endocytosed fluorophore was evaluated by fluorescence microscopy using Zeiss Axio Vert.A1. To quantify the distribution of Texas-Red Dextran labeled vesicles in each cell, first the mean nucleus' radius (R) was measured in order to determine the perinuclear area. Next, the distances between labeled vesicles (D) and the center of cell nuclei were also measured, and the ratio D/R determined. Values closer to one indicate vesicles located closer to the perinuclear area, whereas values higher than one indicate locations further from the cell center and nearer the cell borders.

For oxLDL treatment, we also measured compensatory endocytosis induced by plasma membrane repair after injury. For this, we used a scrape wound assay as previously described [24]. ECs were grown in 10 cm plates, subjected to oxLDL exposure, and washed with HBSS containing or not 1.8 mM Ca²⁺. Cells were then labeled on the plasma membrane with 1 μ g/mL WGA–Alexa Fluor 488 for 1 min at 4 °C, washed twice with HBSS, wounded by scraping in the presence or absence of Ca²⁺, and incubated for 2 min at 37 °C with 0.2% trypan blue before washing and FACS analysis. Internalized WGA-Alexa Fluor 488 fluorescence of 30,000 individual cells was measured using BD Accuri C6 and data analyzed using FlowJo v10.1 software.

2.9. Cell scraping-induced membrane injury and PM repair assay

ECs were cultured in 35 mm culture dishes in high glucose DMEM supplemented with 10% FBS and 1% penicillin/streptomycin at 37 °C and 5% CO₂. After 24 h, cell monolayers (3×10^5 cells/dish) were subjected or not to oxLDL/nLDL treatments and washed with Calcium-free PBS. To measure the amount of membrane injury (hitting control), treated cells were incubated with Ca²⁺-free HBSS at 4 °C, wounded by scraping in the presence of PI (10 μ g/mL), and then incubated for 5 min at 37 °C. To measure membrane resealing and injury recovery, treated cells were incubated with HBSS containing Ca²⁺, wounded by scraping, and incubated for 5 min in the presence of Ca²⁺ to allow for PM repair. After the addition of 10 μ g/mL propidium iodide, 30,000 individual cells were analyzed by flow cytometry using BD Accuri C6 and data analyzed using FlowJo v10.1 software.

2.10. Orbital shear stress induced membrane injury assay

3×10^5 cells were seeded on 6-well plates until reaching confluence. Cells were then submitted to treatment of oxLDL or nLDL and

placed on a 37 °C incubator with orbital shaker at 160 rpm and rotation radius of 1cm² to obtain a shear stress of approximately 7 dyne/cm². The shear stress was calculated as previously described [25]. After 1 h of rotation in serum free media, cells were put in the presence of propidium iodide (PI) 10 µg/mL. PI positive cells were counted within 16 fields at the well periphery.

3. Results

3.1. OxLDL exposure, induces reorganization of cell actin, *de novo* polymerization and changes in cell mechanical properties

Alterations in cell membrane cholesterol content and consequently membrane rafts disruption by treatment with a well-known cholesterol sequestering drug (MβCD) has been shown to have significant effects on actin cytoskeleton reorganization in different cell types, including endothelial cells [6,26,27]. Recently, our group has also shown that cholesterol sequestration and rafts disruption using MβCD, besides reorganizing cell actin cytoskeleton, also induce *de novo* actin polymerization in fibroblasts [6]. Both events lead to altered cell mechanical properties [6,27]. Exposure of endothelial cells (ECs) to oxLDL, similarly to cholesterol sequestration using MβCD, has also been shown to induce rafts disorganization and consequently change actin cytoskeleton organization [13,28]. We then decided to investigate whether oxLDL treatment would also induce *de novo* actin polymerization in ECs by using a cell lineage of human umbilical vein endothelial cells (EAhy926).

In order to confirm the effect of oxLDL on actin reorganization in this cell lineage we first submitted these ECs to treatment with oxLDL or nLDL and compared their effects on actin cytoskeleton organization by labeling cells with Alexa 546-conjugated phalloidin (Fig. 1A). As expected, we observed considerable changes in actin filaments structural organization after treatment with oxLDL when compared to control groups. A significant increase in actin fluorescence intensity was observed upon oxLDL treatment in relation to control or nLDL treated cells (Fig. 1C). As a consequence of actin reorganization, we also observed changes in cell morphology. Similar results were obtained when this cell lineage was treated with MβCD (Supplementary Fig. 1A).

In parallel, we analyzed the ability of these cells in polymerizing new actin filaments upon treatment. In this regard, cells were previously treated with Latrunculin-A (Lat-A), a toxin able to disrupt actin filaments through its binding to actin monomers, blocking their association into microfilaments. After Lat-A exposure and cytoskeleton disruption, cells were washed and exposed or not to the different treatments. As previously shown for fibroblasts [6], treatment of ECs with MβCD, after Lat-A incubation, also induced *de novo* actin polymerization with reconstruction of actin fibers, whereas the same was not observed for cells pre-treated with Lat-A and incubated with serum-free medium (Supplementary Fig. 1B). We further tested if this was also the case for ECs pre-treated with Lat-A and then exposed to oxLDL. Similar to what was observed for MβCD, pre-treatment of these cells with Lat-A followed by treatment with oxLDL seemed to induce *de novo* actin polymerization, as noticed by the actin cytoskeleton organization in the different conditions (Fig. 1B). However, since the exposure to oxLDL was performed for an extended period of time (24 h) after treatment with Lat-A, new actin filaments were also observed in the control groups (non-treated and treated with nLDL for the same 24 h after Lat-A treatment). Even so, a significant increase in actin labeling fluorescence intensity was observed for Lat-A + oxLDL in relation to Lat-A + DMEM treated cells, indicating that in the Lat-A + oxLDL condition cells reconstructed their actin cytoskeleton more efficiently (Fig. 1D). Although no statistically significant increase in labeling was observed between Lat-A + nLDL and Lat-A + oxLDL treatments (Fig. 1D), it was possible to observe qualitatively that Lat-A + oxLDL cells seem different from Lat-A + nLDL treated cells (Fig. 1B) and that quantitatively there is a tendency to a higher fluorescence intensity for

Lat-A + oxLDL treated cells (Fig. 1D). This again indicates that the Lat-A + oxLDL condition seems still more efficient in reconstructing their actin cytoskeleton (Fig. 1B).

Additionally to cell actin reorganization, the literature shows that rafts disruption upon cholesterol depletion or oxLDL exposure also affects the biomechanical properties of the complex cytoskeleton-membrane, thereby increasing cell stiffness [6,12–14]. To confirm this, we evaluated actin reorganization effects on biomechanical properties of endothelial cells after oxLDL exposure. In order to characterize the mechanical dynamics on cell membrane we used DM technique to follow the treatment as a function of time. The analysis of the autocorrelation function as a function of time allows us to measure relaxation time and the amplitude of membrane fluctuation, which characterize the changes on cellular membrane curvature over time, considering the interface cytoskeleton-membrane, as previously described [21].

In this assay, cells were exposed to oxLDL for 24 h and then recorded for 10 min (Supplementary Video 1). As control, cells were exposed to either nLDL treatment or serum free DMEM for 24 h and then recorded for 10 min (Supplementary Videos 2 and 3, respectively). All experiments were analyzed using ImageJ Plugins that correct for background and calculate the temporal autocorrelation function among frames, as described in the methods section.

Representative frames are shown in Fig. 2, revealing the non-treated control images and images from nLDL or oxLDL treated cells (Fig. 2A). Temporal correlation fits are shown below each frame and were used to determine the values of the relaxation time and amplitude of curvature (Fig. 2B and C, respectively). Similar to cholesterol depletion upon MβCD treatment of fibroblasts, cells exposed to oxLDL have an increase in cell stiffness, demonstrated by the increase in relaxation time (Fig. 2A–B and Supplementary Fig. 2A), which corroborates previous data from the literature [12–14]. Exposure to nLDL (Supplementary Video 2) did not change cell stiffness, as observed by the similar values of relaxation time obtained for control and non-treated cells. We did not observe any changes on the amplitude of curvature among treatments (Fig. 2C and Supplementary Fig. 2B and D). The absence of changes in membrane stiffness in nLDL treated cells confirmed previous results showing that this treatment is not able to induce stress fibers formation and therefore has no impact on cellular mechanical properties. This result reinforces that the effects observed for oxLDL treatment is due to rafts disruption, as described previously [12–14].

3.2. ECs exposure to oxLDL triggers deregulated lysosomal exocytosis

It has been shown that changes in cell mechanical properties upon membrane cholesterol sequestration also triggers unregulated lysosomal exocytic events [7]. These exocytic events were shown to happen in the absence of extracellular Ca²⁺ and to be most likely induced by actin reorganization, which would push lysosomes against the cytosolic face of the plasma membrane contributing to its fusion. These events seem to compromise a peripheral pool of lysosomes, which are thought to be engaged with plasma membrane repair (PMR). Thus, we first tested whether this was also true for ECs treated with MβCD and then whether treatment with oxLDL would trigger the same effect.

Lysosomal exocytosis upon treatment was quantified using a β-hexosaminidase secretion assay [23]. Briefly, cells were exposed to MβCD for 10–40 min or oxLDL / nLDL for 24 h and β-hexosaminidase activity measures in the supernatant and cells lysates. As positive control, cells were exposed to 10 mM Ionomycin for 10 min.

Exposure of ECs to both oxLDL (Fig. 3A) or MβCD (Fig. 3B) led to an increase in the levels of β-hexosaminidase activity in the cell supernatants. MβCD treatment doubled enzyme activity in the cell supernatant when compared to non-treated controls. These exocytic events were observed as early as 10 min of treatment (Fig. 3B). For oxLDL treated cells, an increase of about 50% in β-hexosaminidase secretion in relation to control (non-treated) or nLDL treated cells was obtained

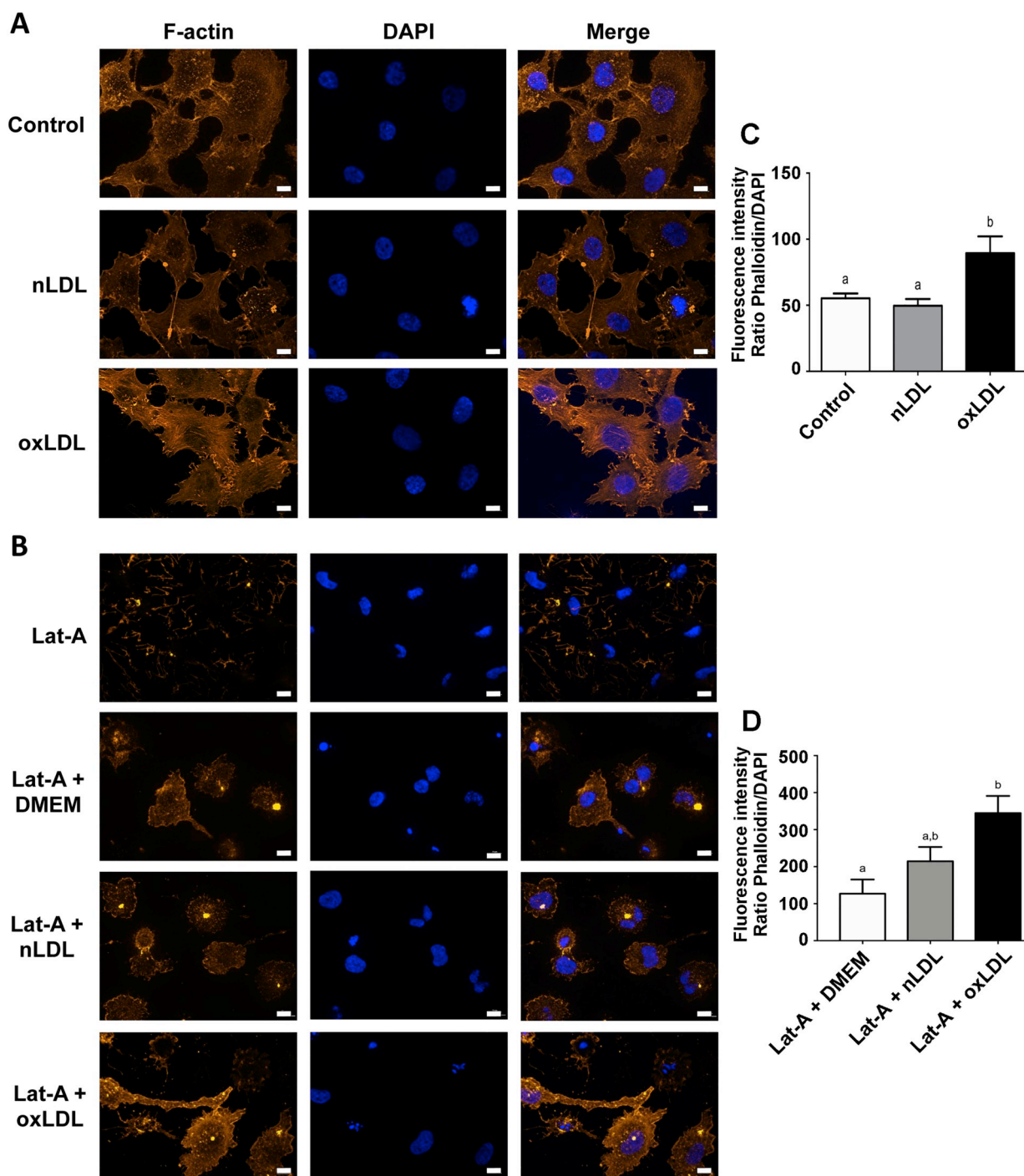


Fig. 1. Actin cytoskeleton organization of endothelial cells upon treatment with oxLDL. (A) Representative images of cells treated or not with oxLDL or nLDL (50 μ g/mL) for 24 h and labeled with Phalloidin-Alexa Fluor 546 to reveal F-actin filaments organization (left panels) and DAPI to reveal cell nuclei (middle panel). Right panels show a merge of the first two panels. Control cells were maintained in serum free DMEM for the same amount of time. (B) Representative images of cells treated with 95 μ M of Lat-A for 1 h followed by treatment or not with oxLDL or nLDL (50 μ g/mL) for 24 h. Cells were also labeled with Phalloidin-Alexa Fluor 546 (left panels), DAPI (middle panel). Right panels show a merge of the first two panels. Control cells were pre-treated with Lat-A and incubated with serum free DMEM for the same amount of time (24 h). Images were captured in a Zeiss Axio Imager.Z2 (ApoTome.2 structured illumination system) fluorescence microscope using the 40 \times objective and the most representative images of the assay were shown. Scale bars: 20 μ m. (C) Graph shows Phalloidin- Alexa Fluor 546 fluorescence intensity of control non-treated cells, as well as oxLDL and nLDL treated cells. (D) Graph shows Phalloidin- Alexa Fluor 546 fluorescence intensity of cells previously treated with Lat-A followed by treatment or not with oxLDL or nLDL. Different letters above bars indicate statistically significant differences ($p < 0,05$ using One-way ANOVA and Newman-Keuls post-test).

(Fig. 3A).

In order to confirm that the increase in β -hexosaminidase activity observed for oxLDL treated cells was really due to lysosome exocytosis and not due to cell death, a cell viability assay was performed. The cell

viability assay was performed by exposing control non-treated and treated (M β CD, nLDL or oxLDL) cells to Propidium Iodide. As expected, no significant differences in the percentage of PI labeled cells was observed between controls (non-treated and H $_7$ CD treated cells) and

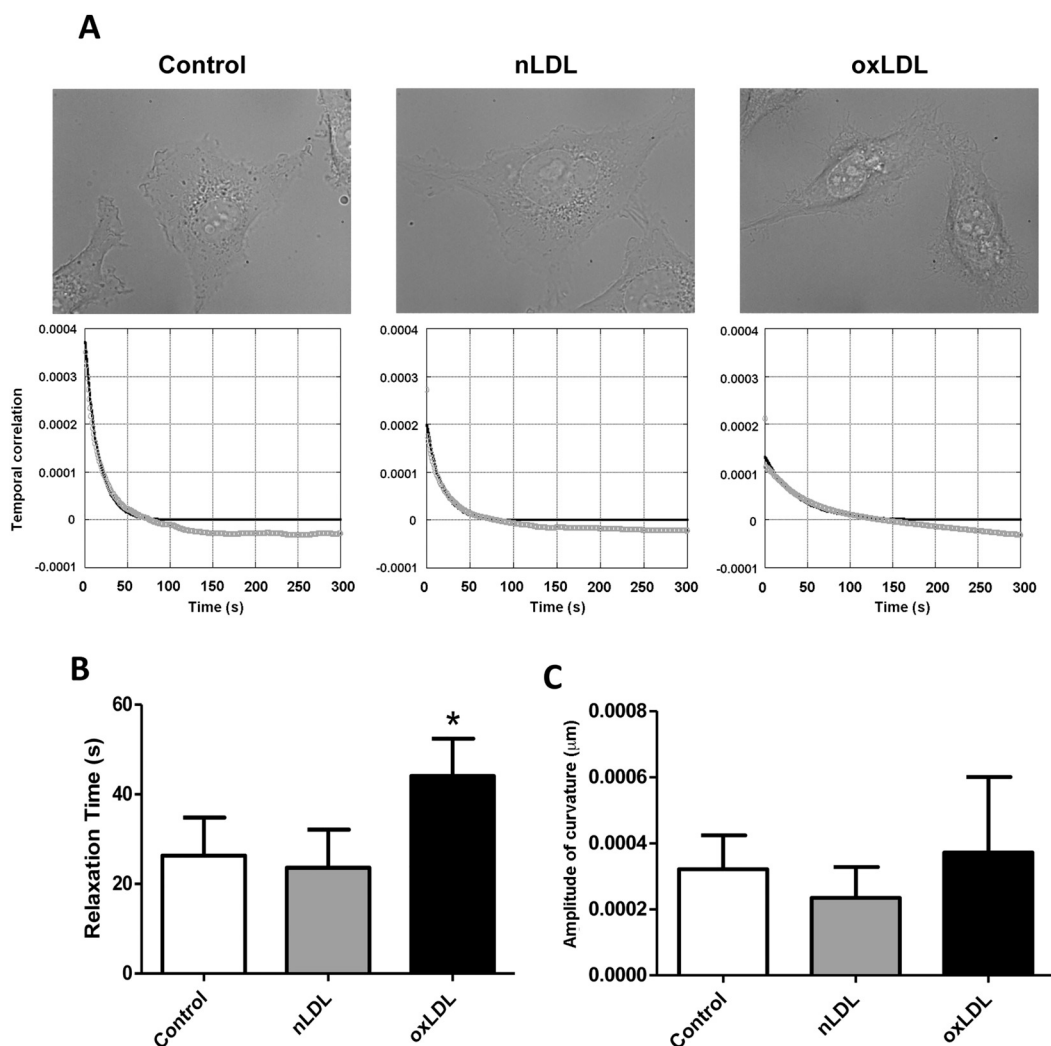


Fig. 2. Defocusing microscopy of endothelial cells upon oxLDL treatment. (A) Representative DM images showing control untreated EC as well as nLDL and oxLDL treated cells (50 $\mu\text{g}/\text{mL}$ for 24 h). Control cells were kept in serum-free medium for 24 h before being recorded. Temporal correlation functions for each condition is also displayed under each representative images. (B) Relaxation time of control non-treated cells, as well as nLDL and oxLDL treated cells. (C) Amplitude of curvature of control non-treated cells, as well as treated cells. Different letters above bars indicate statistically significant differences ($p < 0,05$ using One-way ANOVA and Newman-Keuls post-test).

M β CD treated cells (Fig. 3C). For assays, using LDL treated cells, non-treated controls showed $< 3\%$ of PI labeled cells (2.56%), and similar values were observed for nLDL and oxLDL treated cells (2.22% and 3.71% of PI labeled cells, respectively) (Fig. 3D). These results confirm that none of the treatments induce cell death and that the high amount of enzyme activity observed was indeed due to lysosomal exocytosis induced by M β CD and oxLDL treatment.

3.3. OxLDL exposure impaired constitutive endocytosis in endothelial cells

It is well known that every exocytic event is accompanied by compensatory endocytosis in order to maintain cell volume. Lysosomal exocytosis is no exception. On the other hand, cytoskeleton reorganization with an increase in peripheral actin stress fibers may compromise membrane trafficking especially at cell periphery [29]. We then evaluated whether actin rearrangements induced by ECs exposure to M β CD or oxLDL would compromise compensatory endocytic events following lysosome exocytosis.

We first evaluated compensatory endocytic events following lysosomal exocytosis induced by M β CD treatment. For this we performed a previously described compensatory endocytosis assay using a fluorophore conjugated Wheat Germ Agglutinin (WGA) [24]. Briefly, the

plasma membrane of a suspension of endothelial cells was labeled with WGA-Alexa Fluor 488, followed by treatment with M β CD for 10 to 40 min, after the quenching of the extracellular fluorescence with trypan blue, the intracellular fluorescence correspondent to the endocytosed dye was quantified by flow cytometry. After 10 min of incubation with M β CD, non-treated cells showed higher levels of endocytosis when compared to cells treated with M β CD. However, between 10 and 20 min of treatment, a significant increase in compensatory endocytosis was observed for M β CD treated in relation to non-treated control cells, as indicated by the 1.37-fold increase in WGA-Alexa Fluor 488 fluorescence intensity in these cells when compared to non-treated controls (Fig. 4A and B). It is noteworthy that the increase in endocytic events occurs right after the peak of lysosomal exocytosis observed 10 min post treatment with M β CD in endothelial cells (see Fig. 3B). This result shows that compensatory endocytosis triggered by M β CD-induced exocytosis was not impaired. Nonetheless, we have observed that constitutive endocytosis events in later time points, derived from pinocytosis, a very common process in ECs, are impaired in cells treated with the drug. Indeed, while control non-treated cells increased intracellular WGA-Alexa Fluor 488 fluorescence over time, M β CD-treated cells maintained a similar amount of fluorescence observed after 10 to 20 min of exposure to the drug, leading to a decrease

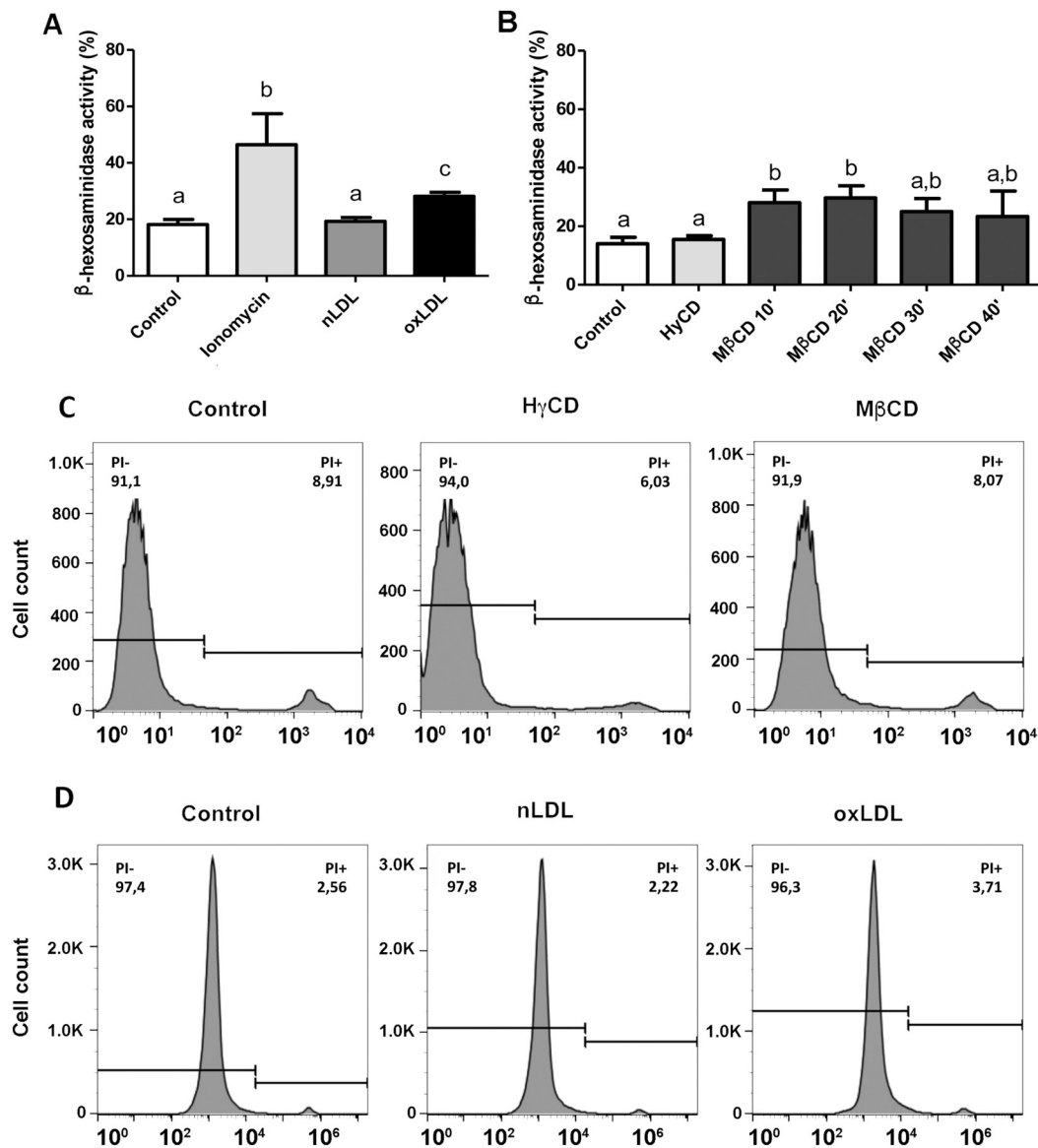


Fig. 3. Quantification of lysosomal exocytosis through activity of β -hexosaminidase in cell culture supernatant. (A) Graph shows the percentage of β -hexosaminidase activity in the supernatant of EC cultures incubated for 24 h in serum-free medium alone (non-treated control cells) or containing 50 μ g/mL nLDL or oxLDL. Results are expressed as percentage of the enzyme found in the supernatant in relation to total amount of the enzyme. (B) Graph shows the percentage of β -hexosaminidase activity found in supernatant of EC cultures incubated in serum-free medium alone (control non-treated cells) or containing HyCD (5 mM) for 40 min, or serum-free medium containing M β CD (5 mM) for different periods (10 to 40 min.). Different letters above bars indicate statistically significant differences ($p < 0,05$ using One-way ANOVA and Newman-Keuls post-test). (C-D) Analysis of cell viability through Propidium Iodide (PI) exclusion. ECs were treated with serum-free medium (control non-treated cells), M β CD or HyCD (5 mM) for 40 min (C) and nLDL or oxLDL for 24 h (D), then labeled with PI (10 μ g/mL) and analyzed by flow cytometry. Histograms show the number of viable cells (PI-) and the number of non-viable cells (PI+).

in the difference between M β CD and control non treated cells WGA-Alexa Fluor 488 fluorescence intensity (Fig. 4A and B).

In order to evaluate compensatory endocytic events following lysosomal exocytosis induced by oxLDL treatment we used an alternative assay. Because of the long period of exposure to oxLDL, endocytosis was evaluated by incubating cells for a period of 24 h in the presence of Texas-Red Dextran, a fluorescent dye membrane impermeable. At determined time points during the 24-h treatment, cells were washed to eliminate extracellular dextran-conjugated fluorophore, fixed and cell nuclei labeled with DAPI for further fluorescence microscopy analysis. Therefore, only the endocytosed fluorophore would be evaluated. As shown in Fig. 4C and Supplementary Fig. 3A, in all conditions it is possible to note a time-dependent increase in fluorescence intensity, indicating the occurrence of endocytic events. However the distribution of Texas-Red Dextran labeled vesicles seemed to differ when cells were

exposed to oxLDL, when compared to control non-treated or nLDL treated cells (Fig. 4C and Suppl. Fig. 3A). While non-treated and nLDL-treated cells exhibit Texas-Red Dextran labeled vesicles disperse all over the cytoplasm throughout the different incubation times, vesicles from oxLDL-treated cells were accumulated in the perinuclear region, especially at later time points. To further address this difference, we decided to perform a quantitative assay to measure vesicle dispersion using an approach previously described for lysosomes dispersion analyses [6]. Briefly, for each isolated nucleus it was calculated the mean distance between labeled vesicles (D) relative to the mean nucleus' radius (R), defined as the ratio D/R. Values closer to one indicated vesicles located closer to the perinuclear area, whereas values higher than one indicated locations further from the cell center and nearer the cell borders. The graphs show the percentage of vesicles located at a specific D/R value (Fig. 4D). As shown in the graphs for control and

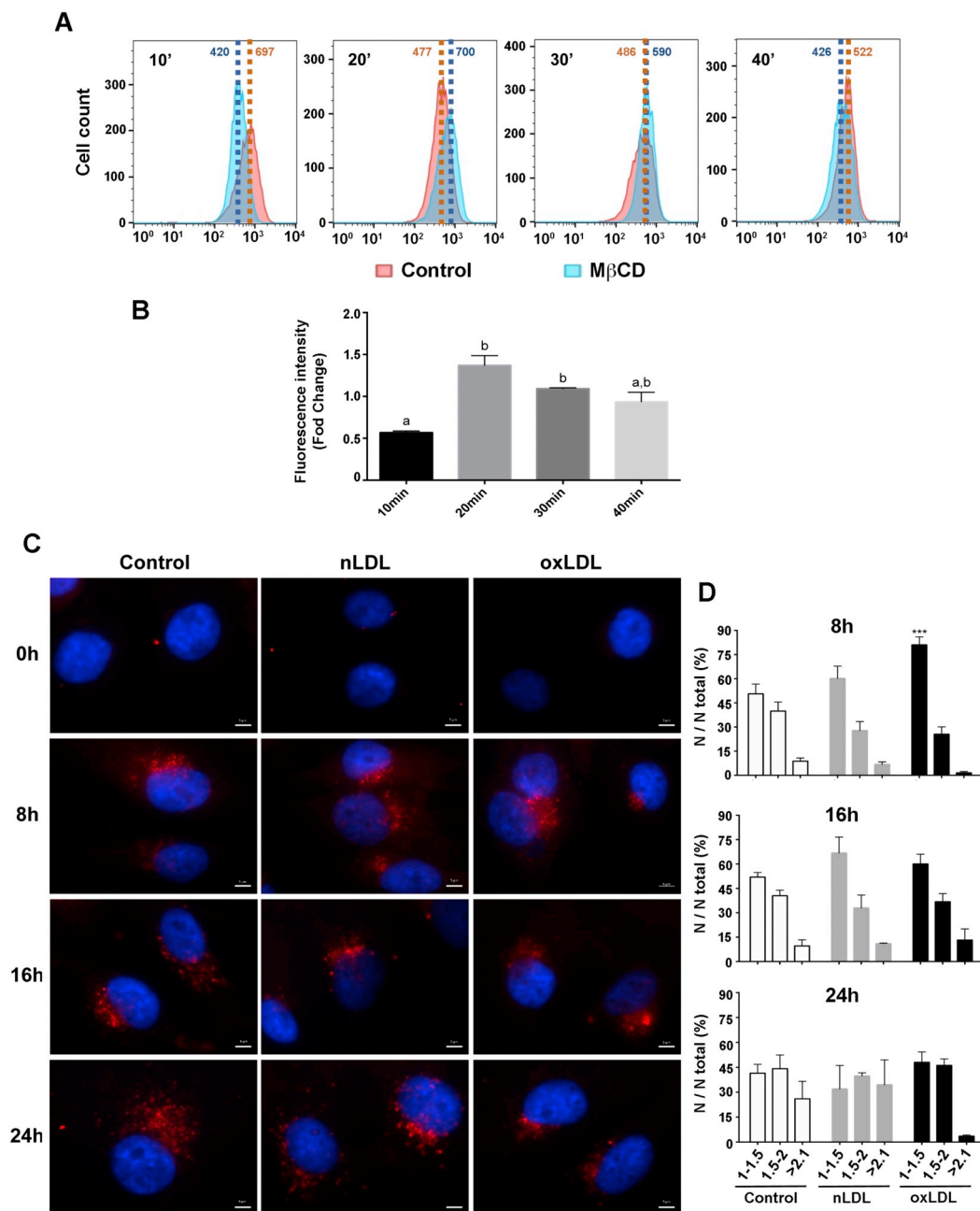


Fig. 4. Quantitative analysis of endocytic events induced by the treatment alone. (A) ECs were labeled with WGA-Alexa Fluor 488 and treated with MβCD for 10 to 40 min. After treatment, plasma membrane fluorescence was quenched with trypan blue 0.2%, so that only fluorescence from endocytic vesicles would remain. Cells were then fixed and analyzed by flow cytometry. Histograms show the number, as well as WGA-Alexa Fluor 488 fluorescence intensity, of control non-treated (red) or MβCD treated cells (blue). The higher the fluorescence, the higher the number of endocytic events. (B) Graph shows the fold-change of WGA-Alexa Fluor 488 mean fluorescence intensity in MβCD treated cells in relation to non-treated control cells. Different letters above bars indicate statistically significant differences ($p < 0,05$ using One-way ANOVA and Newman-Keuls post-test). (C) ECs were exposed or not (control cells) to oxLDL or nLDL for 8, 16 or 24 h in the presence of Texas-Red Dextran, a membrane impermeable fluorescent compound, washed, fixed, labeled with DAPI and analyzed in the fluorescence microscope Zeiss Axio Vert.A1 using a 100 × objective. Panels show intracellular vesicles containing Texas-Red Dextran (red) and cell nuclei (blue). (D) Quantitative analysis of Texas-Red Dextran labeled vesicle distribution, relative to cell nuclei, in control non-treated and nLDL or oxLDL treated cells. The mean distance between a vesicle and its respective nuclei center is represented by letter D and the mean vesicle distance relative to the mean nucleus' radius (R) was defined as the ratio D/R. Data are expressed as the percentage of vesicles from total (N/N total) located at a specific D/R. Asterisks indicate statistically significant differences ($p < 0,05$ using One-way ANOVA and Newman-Keuls post-test).

nLDL treated cells it is possible to observe a high dispersion of vesicles throughout the cytoplasm in all times analyzed. This, as mentioned above, may indicate that these cells are able to endocytose during the entire period of the experiment. On the other hand, for oxLDL treated cells it is possible to observe a change in vesicle dispersion throughout time. Eight hours post treatment, Texas-Red Dextran labeled vesicles in

oxLDL treated cells seem less dispersed than vesicles from control and nLDL treated cells and show a very high percentage of vesicles close to the nuclei (Fig. 4C and D). This probably corresponds to endocytic events triggered by lysosomal exocytosis observed upon oxLDL treatment. At 16 h of oxLDL exposure, vesicle dispersion in these cells increase with a larger number of vesicles located at regions further from

the cell nuclei and more similar to the distribution observed for control and nLDL treated cells (Fig. 4C and D). Then a shift back to cell nuclei is observed upon 24 h of treatment, showing a noteworthy difference from their control and nLDL treated counterparts, even though not statistically significant (Fig. 4C and D). These results suggest that in oxLDL treated cells there are fewer events of endocytosis at later exposure times when compared to controls, indicating that new endocytic events might be compromised upon oxLDL treatment.

3.4. OxLDL treated endothelial cells became more prone to mechanical injury

It has been shown before by our group that M β CD induced cholesterol depletion leads to the exocytosis of a peripheral pool of lysosomes [7], which has then been proposed to be the first one to exocytose upon signaling and thus more prone to participate in PMR [6]. Therefore both exocytosis and endocytosis are crucial steps for PMR. We have shown in the present work that cell exposure to oxLDL, as well as to M β CD, leads to lysosomal exocytosis and compensatory endocytic events, likely triggered by the latter. However, we have also shown that cells exposure to oxLDL may compromise subsequent membrane trafficking events between cytoplasm and plasma membrane, likely due to the barrier formed by actin cytoskeleton rearrangement. This could then interfere with cells ability to perform PMR. In fact, Idone and collaborators (2008) had shown that M β CD treatment inhibit plasma membrane repair by compromising compensatory endocytosis, in a concentration-dependent manner [30]. Unexpectedly though, oxLDL-treated cells exhibited a significant increase in compensatory endocytosis upon scraping, indicating that these events are not impaired by the treatment with the lipoprotein (Supplementary Fig. 3B). However, it was also possible to observe in this experiment that cell counting was much smaller for oxLDL treated cells, when scraped in the absence of calcium, reflecting cell loss. This indicates that cells exposed to oxLDL are more prone to mechanical injury, which could be a consequence of the increase in cell stiffness upon treatment.

We then set out to investigate whether cells exposure to oxLDL would in fact affect cell's ability to perform plasma membrane repair. For this, we first performed a specific assay to address the amount of injury caused by cell scraping from the plate, as described previously [24]. Briefly, cells were treated with oxLDL for 24 h and scraped from the surface they were adhered in the presence of PI. Next, cells were allowed to recover from injury for 5 min at 37 °C, followed by FACS analysis. In this model, since cell membrane is impermeable to PI, in the absence of plasma membrane rupture PI labeling would be prevented, characterizing the PI-negative peak in the histograms. In parallel, the PI-positive peak in the histograms provided the amount of cells injured by scraping from plates.

For non-treated cells, which rested in serum-free culture medium for the equivalent time as cells exposed to oxLDL (24 h), about 30% of injured cells was obtained upon scraping (Fig. 5A and C). A similar amount of injured cells was found when cells were previously exposed to nLDL for 24 h (33.5%) (Fig. 5A and C). However, when cells were exposed to oxLDL for 24 h and then scraped from the plate, approximately 50% of the cells were injured, representing an increase of 20% in the amount of injured cells when compared to control or nLDL treated cells (Fig. 5A and C). These results strongly suggest that oxLDL treatment makes cells more prone to mechanical injury.

We further investigated whether oxLDL treated cells were as efficient as non-treated or nLDL treated cells in performing PMR upon injury. For this, PI was only added after cells were scraped off the plate and allowed to repair. Using this approach, only cells that were not able to repair from injury would be labeled by PI. For control non-treated cells, 12.2% of injured cells were not able to repair (Fig. 5B and D). This result indicates that in control conditions about 58.5% of injured cells were able to recover from mechanical injury caused by scraping (Fig. 5E). Similar results were obtained for cells treated with nLDL. In

the latter, about 12.8% of the cells were PI positive (Fig. 5B and D), which represents about 61.8% efficiency in repair (Fig. 5E). For oxLDL treated cells, the percentage of total cells that were not able to recover from injury was significantly higher (25.4%) when compared to the other two groups (Fig. 5B and C). Additionally, a smaller percentage of cells recovered from injury (about 48.6%) when compared to control non-treated or nLDL treated cells (Fig. 5E). These results reinforce that exposure to oxLDL make cells more susceptible to membrane injury.

Since cell scraping is very aggressive we decided to use also a less disruptive assay to measure cell susceptibility to injury and PMR in the different conditions. For this, cells (treated or not) were submitted to a shear stress of approximately 7 dyne/cm² in an orbital shaker. Subsequently, cells were incubated with PI in order to stain cells that were not able to repair from injury. PI stained cells were then counted in a microscope. For control non-treated cells, we observed 290.25 \pm 90.5 PI positive cells after orbital flow exposure. A similar amount of PI-positive cells were found in nLDL-treated cells (259 \pm 57.7). Cells exposed to oxLDL, on the other hand, revealed to be significantly more susceptible to the flow-induced injury, showing a 2.4-fold increase in PI-positive cells (693.25 \pm 200.6) when compared to the control group (Fig. 5F and G). Using this approach, cells exposed to oxLDL showed once again to be more susceptible to injury.

Even though the decrease in the relative efficiency of PMR was not statistically significantly different when cells were exposed to oxLDL, our results indicate that cell susceptibility to mechanical injury is enhanced in this condition and the absolute values of cells that are not able to recover from this extensive injury is significantly higher.

4. Discussion

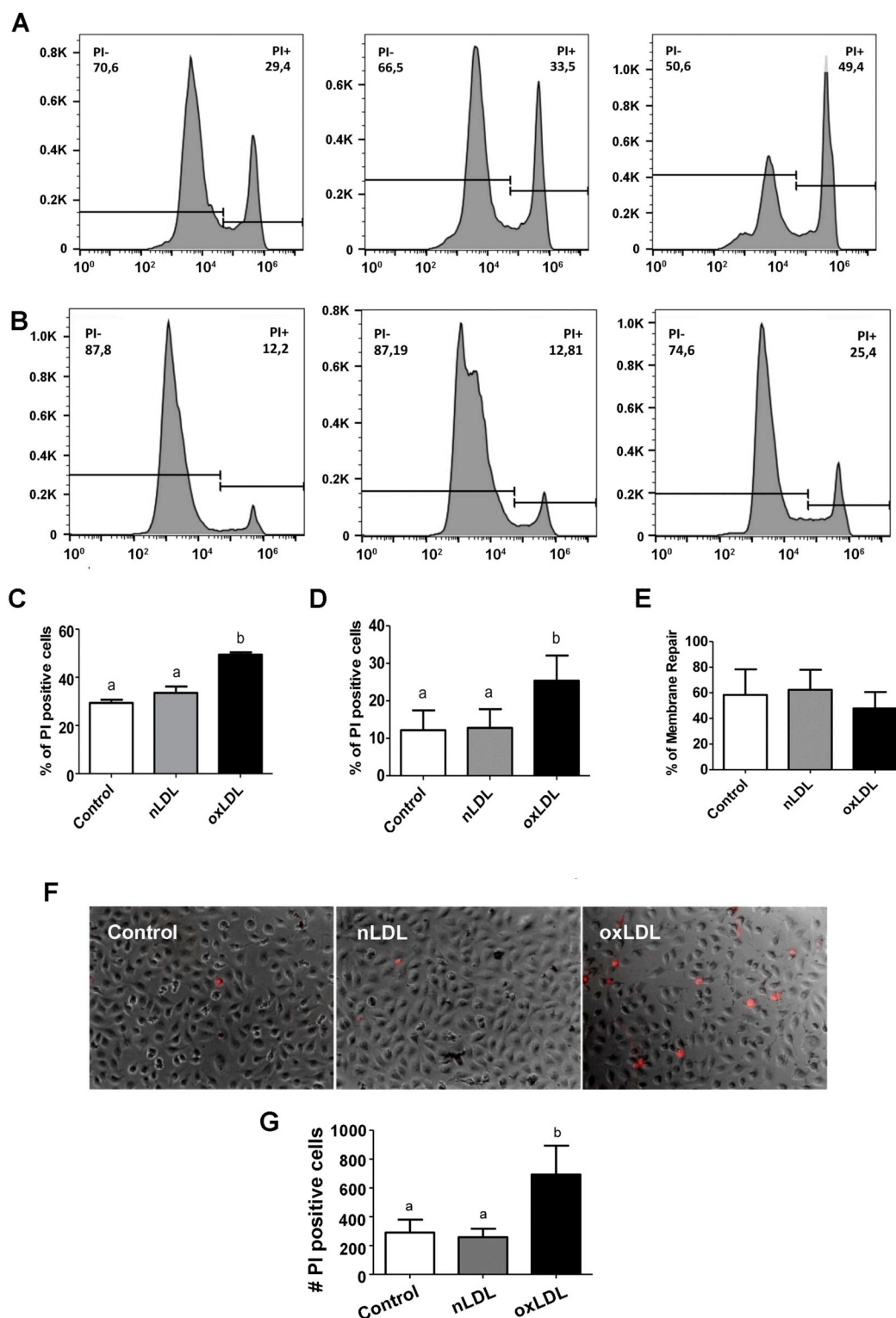
Cholesterol content at the cell plasma membrane has long been known to interfere with membrane organization and consequently in diverse cellular processes [3–6]. Most recently, a series of studies have implicated plasma membrane cholesterol levels and cholesterol enriched membrane microdomains, also known as membrane rafts, in actin cytoskeleton organization at the cell periphery, significantly controlling cellular biomechanics [6,28,31]. In parallel, previous studies from our group have shown that cholesterol sequestration induces a massive exocytosis of peripheral lysosomes, which was correlated to actin rearrangement and mechanical alterations at the cell surface [6,7]. Localization of lysosomes throughout cell cytoplasm and more specifically its positioning at the cell periphery may influence their function in different cellular processes. Among them, the delivery of different molecules to the plasma membrane or to the extracellular space, as well as PMR, are particularly important for cell function and viability [10,32–34]. Therefore comprehending membrane trafficking events at the cell surface level upon disorganization of rafts structures, especially when considering PMR, is of major importance.

ECs are continually submitted to mechanical stress due to blood flow and, consequently, PMR mechanisms should be expected to play an important role for cell maintenance. Therefore, we used an EC model to study the effects of rafts disruption upon treatment with M β CD or the oxidized form of LDL particles in membrane trafficking events involved with PMR. In PMR, both exocytosis and endocytosis are primordial steps. The influx of Ca²⁺ through wound sites at plasma membrane stimulates local fusion and exocytosis of lysosomes. The delivery of lysosomal enzymes to the extracellular milieu induces and regulates a compensatory endocytic event responsible to reseal the membrane [10,24,35,36]. Thereby, changes on cell cholesterol content and its consequent effect on exocytosis and actin organization could interfere with membrane repair mechanisms, affecting cell viability.

Our results confirmed previous reports showing that disruption of ECs rafts upon cholesterol sequestration or exposure to oxLDL leads to actin cytoskeleton reorganization, increased cell stiffness and lysosomal exocytosis [6,27,37]. It has been shown before that oxLDL treatment interferes with rafts organization, especially regions enriched in

cholesterol and caveolin [28,38,39] reinforcing the role not only of cholesterol, but most importantly of rafts, in the regulation of these processes. Additionally, both treatments induced *de novo* actin polymerization, showing that disruption of membrane rafts without complete cholesterol sequestration is equally able to induce formation of new actin fibers. Although it has been shown that oxLDL treatment is able to induce Rho/Rock activation [19], to the best of our knowledge, this is the first evidence for *de novo* actin polymerization, as well as

lysosomal exocytosis upon treatment of ECs with oxLDL. Also, contrary to MβCD, we did not observe any difference in the amplitude of curvature upon oxLDL treatment when compared to control non-treated or nLDL treated cells. We speculate that the change in amplitude of curvature might be somehow compensated by changes in the areas of fluctuation, but further investigation is necessary to support this hypothesis. Interestingly though, for oxLDL treated cells we have observed a wider distribution of the amplitude of curvature values, which may



(caption on next page)

Fig. 5. Quantitative analysis of injury level and PMR ability of ECs submitted to mechanical injury. (A) Analysis of injury level caused by cell scraping in the different conditions (control non-treated, 50 $\mu\text{g}/\text{mL}$ nLDL or oxLDL treated cells). ECs were incubated for 24 h in serum-free medium alone (control non-treated cells) or containing 50 $\mu\text{g}/\text{mL}$ nLDL or oxLDL, submitted to injury by scrapping in the presence of Propidium Iodide (PI - 10 $\mu\text{g}/\text{mL}$) and analyzed by flow cytometry. Histograms show the number of non-injured cells (PI-) and the number of injured cells (PI+). (B) Analysis of ECs PMR ability upon mechanical injury in the different conditions (control non-treated, 50 $\mu\text{g}/\text{mL}$ nLDL or oxLDL treated cells). ECs were incubated for 24 h in serum-free medium alone (non-treated control cells) or containing 50 $\mu\text{g}/\text{mL}$ nLDL or oxLDL, submitted to injury by scrapping, allowed to recover from injury and then incubated with PI (10 $\mu\text{g}/\text{mL}$) before flow cytometry analysis. Histograms show the number of non-injured cells as well as cells that recovered from injury cells (PI-) and the number of injured cells that were not able to recover from injury (PI+). (C) Graph shows the quantitative analysis from three different experiments of the percentage of cells that were injured upon scraping in the different conditions. (D) Graph shows the quantitative analysis from three different experiments of the percentage of cells that did not recover from injury upon scraping in the different conditions. (E) Graph shows the percentage of membrane repair after injury in the different conditions relative to the total injury induced by scrapping. Different letters above bars indicate statistically significant differences ($p < 0,05$ using One-way ANOVA and Newman-Keuls post-test). (F) Analysis of the injured cells number upon orbital flow in the different conditions (control non-treated, 50 $\mu\text{g}/\text{mL}$ nLDL or oxLDL treated cells). ECs were incubated for 24 h in serum-free medium alone (control non-treated cells) or containing 50 $\mu\text{g}/\text{mL}$ nLDL or oxLDL, submitted to injury by inducing a flow in a horizontal shaker for 1 h. Cells were allowed to recover from injury and then incubated with PI (10 $\mu\text{g}/\text{mL}$) before fluorescence microscope analysis. Panels show representative merged images of ECs in brightfield and PI+ cells (red). (G) Graph shows the number of injured cells (PI+) in each condition. Different letters above bars indicate statistically significant differences ($p < 0,05$ using One-way ANOVA and Newman-Keuls post-test).

indicate that oxLDL and M β CD effects on rafts organization may differ from each other. Nevertheless, both treatments led to the same effect on actin polymerization and cell rigidity.

Previous studies demonstrated that actin cytoskeleton reorganization acts, on one hand, as a stimuli to vesicle fusion and exocytosis and, on the other hand, as a barrier to new traffic of vesicles localized more internally in the cell [29,40–43]. Here we showed that ECs treatment with oxLDL or M β CD induces a massive lysosome exocytosis, most likely due to actin rearrangement and polymerization as suggested before for M β CD treatment of cardiomyocytes [7]. In both oxLDL and M β CD treatments a peak of endocytosis following lysosome exocytic events is also observed, certainly corresponding to compensatory endocytosis induced by lysosome fusion with the plasma membrane. However, for both treatments it was also observed a reduction in new constitutive endocytic events, typical of these cells. It is plausible to suggest that there may be a window between the initial actin rearrangement, important for exocytosis, and its complete reorganization that allows for compensatory endocytosis to occur. However, once actin

is completely rearranged at the cell periphery, new membrane trafficking events are compromised (Fig. 6A and B). One evidence that corroborates this hypothesis is that non treated cells, as well as nLDL treated cells, continue to display small amounts of constitutive endocytic events, probably arising from pinocytosis, a common process in ECs. This is demonstrated by the presence of vesicles dispersed all over the cytosol even at later time points, indicating the existence of new endocytic events. These results suggest that, in contrast to what was previously proposed [6], lysosomal exocytic events occur during the initial steps of actin remodeling and not after its complete rearrangement and that, in this last scenario, membrane trafficking is indeed compromised. In fact, this corroborates with the dual role, mentioned before, of actin cytoskeleton during secretion of vesicles in chromaffin cells. Although it was first demonstrated that actin formed a network at the cell periphery and vesicle secretion was seen only at sites of actin reorganization, later it was shown that there were secretory vesicles localized in between cortical actin filaments, which could also participate in vesicle transport during secretion [29,44–48]. The same is

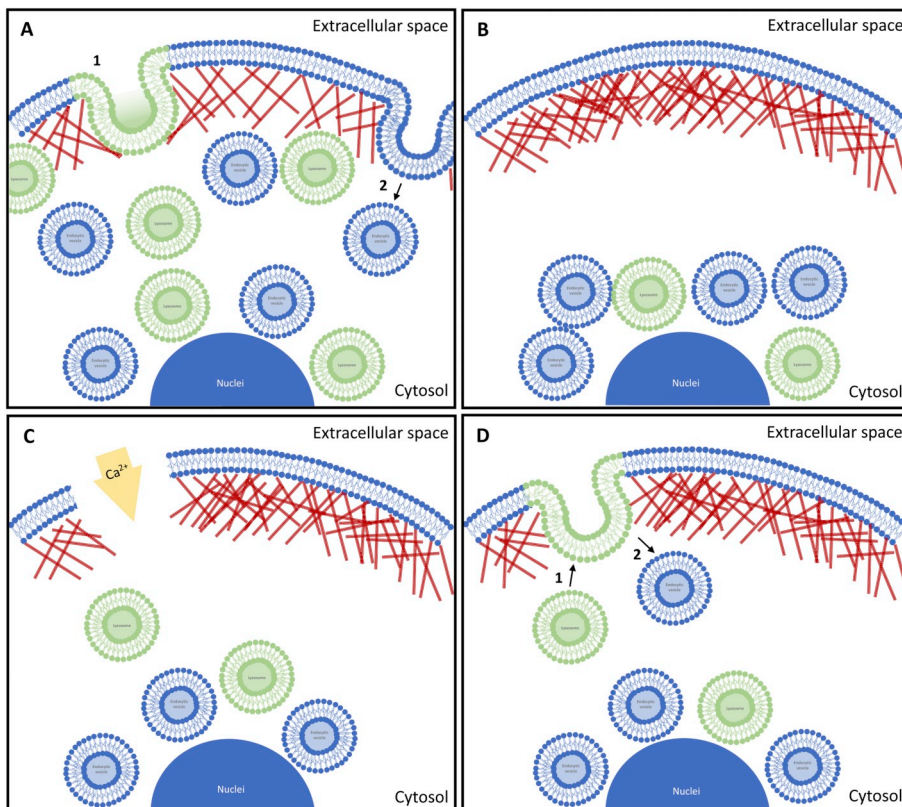


Fig. 6. Schematic illustration of the hypothesis. (A) During the first hours of oxLDL exposure, EC presents a window between the initial actin rearrangement, which stimulates lysosomal exocytosis (1), and its complete reorganization that allows for compensatory endocytosis (2) to occur. (B) Once actin cytoskeleton is completely rearranged at the cell periphery, new membrane trafficking events are compromised. (C) Upon enhanced stiffness, mechanical injury causes disruption of local actin filaments, thereby breaking cytoskeleton barrier, allowing Ca^{2+} influx. (D) The increase in Ca^{2+} cytosolic concentration, stimulates the membrane trafficking at the cell periphery important to PMR, once lysosomal exocytosis (1) and its subsequent compensatory endocytosis (2) are allowed to happen, therefore resealing the plasma membrane.

observed for endocytosis, where actin might present as a barrier, but also work as active participants in endocytic pathways (reviewed by [8,49]).

Interestingly, PMR evaluation through PI labeling after cell mechanical injury and repair showed that oxLDL treated cells do not lose their ability in repairing their membrane wounds. We speculate that, upon enhanced stiffness, mechanical injury causes disruption of local actin filaments, thereby breaking cytoskeleton barrier and allowing membrane trafficking at the cell periphery to occur and, therefore, PMR (Fig. 6C and D). It has been shown recently by Chen and coworkers (2014) that single-site sonoporation episodes induced by ultrasound-triggered collapse of a single targeted microbubble leads to rupture of filamentous actin (F-actin) at the sonoporation membrane injury site [50]. Additionally, it has been shown that increase in calcium due to its influx from the extracellular to the intracellular milieu caused by membrane rupture may also contribute to actin depolymerization at the site of injury [51,52]. It is then plausible to assume that, even though actin polymerization and reorganization induced by oxLDL treatment may interfere with membrane trafficking at cellular surface, upon mechanical injury actin cytoskeleton may be locally disrupted allowing new exocytic and endocytic events to occur. Nonetheless, it is noteworthy that the amount of injured cells after oxLDL exposure increases notoriously. Also, even though the relative efficiency of PMR in these cells is similar when compared to controls, the amount of PI positive cells after injury is significantly higher, which might have an important physiological impact in the endothelial barrier restoration. This is probably a result of the amount of injury caused by scraping in these mechanically stiffer cells.

The present work has a substantial impact in the understanding of cholesterol and rafts regulation in membrane trafficking events, especially membrane susceptibility to injury and PMR ability. Abnormal cholesterol metabolism and delivery to the plasma membrane has been implicated in various diseases [53–56]. However, possible links between disease and defects in vesicle trafficking processes or with membrane susceptibility to injury have not been explored before. In this scenario, the effects of endothelial dysfunction in the first steps of atherosclerosis establishment, may be directly related to the mechanical alterations and injury susceptibility upon oxLDL exposure. Since endothelial cells are in constant mechanical stress generated by the blood flow, it is possible that biomechanical changes induced by endothelial cell exposure to oxLDL are responsible for injuries and alterations in cell viability previously observed by Liao & Granger (1995) [57]. Different scavenger receptors, such as LOX-1 and CD36, which recognize and bind oxLDL have been shown to induce the activation of different pathways including RhoA activation, which may then lead to the actin cytoskeleton rearrangements shown here (Sugimoto et al., 2009; Chen, 2012; Oh et al., 2016; Balzan, 2018). Further studies are needed to address this matter.

Finally, other scenarios that influence cholesterol metabolism and its content at the plasma membrane level may also be affected by the events studied herein. Therefore, we believe that our results contribute to better understand the biological and pathological roles of membrane cholesterol in cellular biomechanics and PMR.

Supplementary data to this article can be found online at <https://doi.org/10.1016/j.bbmem.2019.183139>.

Transparency document

The Transparency document associated with this article can be found, in online version.

Declaration of competing interest

The manuscript has no Conflict of Interest. I would like to add that the funders had no role in study design, data collection and analysis, decision to publish, or preparation of the manuscript.

Acknowledgements

We are especially grateful to all the funding Agencies: Conselho Nacional de Desenvolvimento Científico e Tecnológico - CNPq (INCT-FCx 465259/2014-6), Fundação de Amparo à Pesquisa do Estado de Minas Gerais (FAPEMIG - APQ-02974-17) and Coordenação de Aperfeiçoamento de Pessoal de Nível Superior. We are also grateful to Centro de Aquisição e Processamento de Imagens (CAPI/ICB) and Centro de Microscopia da UFMG for the use of microscopes and imaging processing systems, as well as to Centro de Laboratórios Multiusuários do ICB (CELAM - ICB)/UFMG and Center for Gastrointestinal Biology in the name of Dr. Gustavo Batista de Menezes for the use of FACS equipment.

DATA statement

All relevant data are contained within the paper and its Supporting Information files.

At the moment we do not have a repository at the university for data collection.

However, all raw data will be available upon request.

References

- [1] L.J. Pike, Rafts defined: a report on the keystone symposium on lipid rafts and cell function, *J. Lipid Res.* 47 (2006) 1597–1598.
- [2] E. Ikonen, Cellular cholesterol trafficking and compartmentalization, *Nat Rev Mol Cell Biol* 9 (2008) 125–138.
- [3] D.A. Brown, E. London, Structure and function of sphingolipid- and cholesterol-rich membrane rafts, *J. Biol. Chem.* 275 (2000) 17221–17224.
- [4] V.I. Chubinskiy-Nadezhdin, Y.A. Negulyaev, E.A. Morachevskaya, Cholesterol depletion-induced inhibition of stretch-activated channels is mediated via actin rearrangement, *Biochem. Biophys. Res. Commun.* 412 (2011) 80–85.
- [5] M. Sun, N. Northup, F. Marga, T. Huber, F.J. Byfield, I. Levitan, G. Forgacs, The effect of cellular cholesterol on membrane-cytoskeleton adhesion, *J. Cell Sci.* 120 (2007) 2223–2231.
- [6] B. Hissa, B. Pontes, P.M. Roma, A.P. Alves, C.D. Rocha, T.M. Valverde, P.H. Aguiar, F.P. Almeida, A.J. Guimaraes, C. Guatimosim, A.M. Silva, M.C. Fernandes, N.W. Andrews, N.B. Viana, O.N. Mesquita, U. Agero, L.O. Andrade, Membrane cholesterol removal changes mechanical properties of cells and induces secretion of a specific pool of lysosomes, *PLoS One* 8 (2013) e82988.
- [7] B. Hissa, J.G. Duarte, L.F. Kelles, F.P. Santos, H.L. del Puerto, P.H. Gazzinelli-Guimaraes, A.M. de Paula, U. Agero, O.N. Mesquita, C. Guatimosim, E. Chiari, L.O. Andrade, Membrane cholesterol regulates lysosome-plasma membrane fusion events and modulates *Trypanosoma cruzi* invasion of host cells, *PLoS Negl. Trop. Dis.* 6 (2012) e1583.
- [8] E. Smythe, K.R. Ayscough, Actin regulation in endocytosis, *J. Cell Sci.* 119 (2006) 4589–4598.
- [9] A. Gil-Krzewska, M.B. Saeed, A. Oszmiana, E.R. Fischer, K. Lagrue, W.A. Gahl, W.J. Introne, J.E. Coligan, D.M. Davis, K. Krzewski, An actin cytoskeletal barrier inhibits lytic granule release from natural killer cells in patients with Chediak-Higashi syndrome, *J. Allergy Clin. Immunol.* 142 (2018) 914–927 (e916).
- [10] C. Tam, V. Idone, C. Devlin, M.C. Fernandes, A. Flannery, X. He, E. Schuchman, I. Tabas, N.W. Andrews, Exocytosis of acid sphingomyelinase by wounded cells promotes endocytosis and plasma membrane repair, *J. Cell Biol.* 189 (2010) 1027–1038.
- [11] S. Yla-Herttuala, W. Palinski, M.E. Rosenfeld, S. Parthasarathy, T.E. Carew, S. Butler, J.L. Witztum, D. Steinberg, Evidence for the presence of oxidatively modified low density lipoprotein in atherosclerotic lesions of rabbit and man, *J. Clin. Invest.* 84 (1989) 1086–1095.
- [12] F.J. Byfield, S. Tikku, G.H. Rothblat, K.J. Gooch, I. Levitan, OxLDL increases endothelial stiffness, force generation, and network formation, *J. Lipid Res.* 47 (2006) 715–723.
- [13] J.A. Chouinard, G. Grenier, A. Khalil, P. Vermette, Oxidized-LDL induce morphological changes and increase stiffness of endothelial cells, *Exp. Cell Res.* 314 (2008) 3007–3016.
- [14] G.B. Kowalsky, F.J. Byfield, I. Levitan, oxLDL facilitates flow-induced realignment of aortic endothelial cells, *Am J Physiol Cell Physiol* 295 (2008) C332–C340.
- [15] M. Chen, T. Masaki, T. Sawamura, LOX-1, the receptor for oxidized low-density lipoprotein identified from endothelial cells: implications in endothelial dysfunction and atherosclerosis, *Pharmacol. Ther.* 95 (2002) 89–100.
- [16] K. Sugimoto, T. Ishibashi, T. Sawamura, N. Inoue, M. Kamioka, H. Uekita, H. Ohkawara, T. Sakamoto, N. Sakamoto, Y. Okamoto, Y. Takuwa, A. Kakino, Y. Fujita, T. Tanaka, T. Teramoto, Y. Maruyama, Y. Takeishi, LOX-1-MT1-MMP axis is crucial for RhoA and Rac1 activation induced by oxidized low-density lipoprotein in endothelial cells, *Cardiovasc. Res.* 84 (2009) 127–136.
- [17] H.J. Oh, M. Kato, S. Deshpande, E. Zhang, S. Das, L. Lanting, M. Wang, R. Natarajan, Inhibition of the processing of miR-25 by HIPK2-phosphorylated-

- MeCP2 induces NOX4 in early diabetic nephropathy, *Sci. Rep.* 6 (2016) 38789.
- [18] M.J. Oh, C. Zhang, E. LeMaster, C. Adamos, E. Berdyshev, Y. Bogachkov, E.E. Kohler, J. Baruah, Y. Fang, D.E. Schraufnagel, K.K. Wary, I. Levitan, Oxidized LDL signals through Rho-GTPase to induce endothelial cell stiffening and promote capillary formation, *J. Lipid Res.* 57 (2016) 791–808.
- [19] C. Zhang, C. Adamos, M.J. Oh, J. Baruah, M.A.A. Ayee, D. Mehta, K.K. Wary, I. Levitan, oxLDL induces endothelial cell proliferation via Rho/ROCK/Akt/p27(kip1) signaling: opposite effects of oxLDL and cholesterol loading, *Am J Physiol Cell Physiol* 313 (2017) C340–C351.
- [20] U. Agero, C.H. Monken, C. Ropert, R.T. Gazzinelli, O.N. Mesquita, Cell surface fluctuations studied with defocusing microscopy, *Phys. Rev. E Stat. Nonlinear Soft Matter Phys.* 67 (2003) 51904.
- [21] U. Agero, L.G. Mesquita, B.R. Neves, R.T. Gazzinelli, O.N. Mesquita, Defocusing microscopy, *Microsc. Res. Tech.* 65 (2004) 159–165.
- [22] J. Coelho Neto, U. Agero, R.T. Gazzinelli, O.N. Mesquita, Measuring optical and mechanical properties of a living cell with defocusing microscopy, *Biophys. J.* 91 (2006) 1108–1115.
- [23] I. Martinez, S. Chakrabarti, T. Hellevik, J. Morehead, K. Fowler, N.W. Andrews, Synaptotagmin VII regulates Ca²⁺-dependent exocytosis of lysosomes in fibroblasts, *J. Cell Biol.* 148 (2000) 1141–1149.
- [24] V. Idone, C. Tam, J.W. Goss, D. Toomre, M. Pypaert, N.W. Andrews, Repair of injured plasma membrane by rapid Ca²⁺-dependent endocytosis, *J. Cell Biol.* 180 (2008) 905–914.
- [25] A. Dardik, L. Chen, J. Frattini, H. Asada, F. Aziz, F.A. Kudo, B.E. Sumpio, Differential effects of orbital and laminar shear stress on endothelial cells, *J. Vasc. Surg.* 41 (2005) 869–880.
- [26] J. Kwik, S. Boyle, D. Fooksman, L. Margolis, M.P. Sheetz, M. Edidin, Membrane cholesterol, lateral mobility, and the phosphatidylinositol 4,5-bisphosphate-dependent organization of cell actin, *Proc. Natl. Acad. Sci. U. S. A.* 100 (2003) 13964–13969.
- [27] F.J. Byfield, H. Aranda-Espinoza, V.G. Romanenko, G.H. Rothblat, I. Levitan, Cholesterol depletion increases membrane stiffness of aortic endothelial cells, *Biophys. J.* 87 (2004) 3336–3343.
- [28] T.P. Shentu, I. Titushkin, D.K. Singh, K.J. Gooch, P.V. Subbaiah, M. Cho, I. Levitan, oxLDL-induced decrease in lipid order of membrane domains is inversely correlated with endothelial stiffness and network formation, *Am J Physiol Cell Physiol* 299 (2010) C218–C229.
- [29] D. Aunis, M.F. Bader, The cytoskeleton as a barrier to exocytosis in secretory cells, *J. Exp. Biol.* 139 (1988) 253–266.
- [30] V. Idone, C. Tam, N.W. Andrews, Two-way traffic on the road to plasma membrane repair, *Trends Cell Biol.* 18 (2008) 552–559.
- [31] T.P. Shentu, D.K. Singh, M.J. Oh, S. Sun, L. Sadaat, A. Makino, T. Mazzone, P.V. Subbaiah, M. Cho, I. Levitan, The role of oxysterols in control of endothelial stiffness, *J. Lipid Res.* 53 (2012) 1348–1358.
- [32] A. Reddy, E. Caler, N. Andrews, Plasma membrane repair is mediated by Ca²⁺-regulated exocytosis of lysosomes, *Cell* 106 (2001) 157–169.
- [33] J. Pu, C. Schindler, R. Jia, M. Jarnik, P. Backlund, J.S. Bonifacino, BORC, a multisubunit complex that regulates lysosome positioning, *Dev. Cell* 33 (2015) 176–188.
- [34] M. Encarnacao, L. Espada, C. Escreveante, D. Mateus, J. Ramalho, X. Michelet, I. Santarino, V.W. Hsu, M.B. Brenner, D.C. Barral, O.V. Vieira, A Rab3a-dependent complex essential for lysosome positioning and plasma membrane repair, *J. Cell Biol.* 213 (2016) 631–640.
- [35] N.W. Andrews, P.E. Almeida, M. Corrotte, Damage control: cellular mechanisms of plasma membrane repair, *Trends Cell Biol.* 24 (2014) 734–742.
- [36] T. Castro-Gomes, M. Corrotte, C. Tam, N.W. Andrews, Plasma membrane repair is regulated Extracellularly by proteases released from lysosomes, *PLoS One* 11 (2016) e0152583.
- [37] Z. Hong, M.C. Staiculescu, P. Hampel, I. Levitan, G. Forgacs, How cholesterol regulates endothelial biomechanics, *Front. Physiol.* 3 (2012) 426.
- [38] A. Blair, P.W. Shaul, I.S. Yuhanna, P.A. Conrad, E.J. Smart, Oxidized low density lipoprotein displaces endothelial nitric-oxide synthase (eNOS) from plasmalemmal caveolae and impairs eNOS activation, *J. Biol. Chem.* 274 (1999) 32512–32519.
- [39] I. Levitan, T.P. Shentu, Impact of oxLDL on cholesterol-rich membrane rafts, *J. Lipids* 2011 (2011) 730209.
- [40] T. Nakata, N. Hirokawa, Organization of cortical cytoskeleton of cultured chromaffin cells and involvement in secretion as revealed by quick-freeze, deep-etching, and double-label immunoelectron microscopy, *J. Neurosci.* 12 (1992) 2186–2197.
- [41] S. Muallen, K. Kwiatkowska, X. Xu, H.L. Yin, Actin filament disassembly is a sufficient trigger for exocytosis in non-excitable cells, *J. Cell Biol.* 128 (1995) 589–598.
- [42] A. Pendleton, A. Koffer, Effects of latrunculin reveal requirements for the actin cytoskeleton during secretion from mast cells, *Cell Motil. Cytoskeleton* 48 (2001) 37–51.
- [43] P. Miklavc, O.H. Wittekindt, E. Felder, P. Dietl, Ca²⁺-dependent actin coating of lamellar bodies after exocytotic fusion: a prerequisite for content release or kiss-and-run, *Ann. N. Y. Acad. Sci.* 1152 (2009) 43–52.
- [44] D. Aunis, B. Guerold, M.F. Bader, J. Cieselski-Treska, Immunocytochemical and biochemical demonstration of contractile proteins in chromaffin cells in culture, *Neuroscience* 5 (1980) 2261–2277.
- [45] T.R. Cheek, R.D. Burgoyne, Nicotine-evoked disassembly of cortical actin filaments in adrenal chromaffin cells, *FEBS Lett.* 207 (1986) 110–114.
- [46] R.D. Burgoyne, T.R. Cheek, Reorganisation of peripheral actin filaments as a prelude to exocytosis, *Biosci. Rep.* 7 (1987) 281–288.
- [47] T. Lang, I. Wacker, I. Wunderlich, A. Rohrbach, G. Giese, T. Soldati, W. Almers, Role of actin cortex in the subplasmalemmal transport of secretory granules in PC-12 cells, *Biophys. J.* 78 (2000) 2863–2877.
- [48] R. Rudolf, T. Kogel, S.A. Kuznetsov, T. Salm, O. Schlicker, A. Hellwig, J.A. Hammer 3rd, H.H. Gerdes, Myosin Va facilitates the distribution of secretory granules in the F-actin rich cortex of PC12 cells, *J. Cell Sci.* 116 (2003) 1339–1348.
- [49] M. Skrzynny, T. Brach, R. Ciuffa, S. Rybina, M. Wachsmuth, M. Kaksonen, Molecular basis for coupling the plasma membrane to the actin cytoskeleton during clathrin-mediated endocytosis, *Proc. Natl. Acad. Sci. U. S. A.* 109 (2012) E2533–E2542.
- [50] X. Chen, R.S. Leow, Y. Hu, J.M. Wan, A.C. Yu, Single-site sonoporation disrupts actin cytoskeleton organization, *J. R. Soc. Interface* 11 (2014) 20140071.
- [51] K. Zechel, Stability differences of muscle F-actin in formamide in the presence of Mg²⁺ and Ca²⁺, *Biochim. Biophys. Acta* 742 (1983) 135–141.
- [52] E. Boucher, C.A. Mandato, Plasma membrane and cytoskeleton dynamics during single-cell wound healing, *Biochim. Biophys. Acta* 1853 (2015) 2649–2661.
- [53] K. Simons, R. Ehehalt, Cholesterol, lipid rafts, and disease, *J. Clin. Invest.* 110 (2002) 597–603.
- [54] I.J. Martins, T. Berger, M.J. Sharman, G. Verdile, S.J. Fuller, R.N. Martins, Cholesterol metabolism and transport in the pathogenesis of Alzheimer's disease, *J. Neurochem.* 111 (2009) 1275–1308.
- [55] J. Zhang, Q. Liu, Cholesterol metabolism and homeostasis in the brain, *Protein Cell* 6 (2015) 254–264.
- [56] J. Li, S.R. Pfeffer, Lysosomal membrane glycoproteins bind cholesterol and contribute to lysosomal cholesterol export, *eLife* 5 (2016).
- [57] L. Liao, D.N. Granger, Modulation of oxidized low-density lipoprotein-induced microvascular dysfunction by nitric oxide, *Am. J. Phys.* 268 (1995) H1643–H1650.

Measuring Intracellular Vesicle Density and Dispersion Using Fluorescence Microscopy and ImageJ/FIJI

Natália Fernanda do Couto¹, Thamires Queiroz-Oliveira², Maria Fátima Horta³,
Thiago Castro-Gomes² * and Luciana Oliveira Andrade¹ *

¹Departamento de Morfologia, Instituto de Ciências Biológicas, Universidade Federal de Minas Gerais, Belo Horizonte, Brasil; ²Departamento de Parasitologia, Instituto de Ciências Biológicas, Universidade Federal de Minas Gerais, Belo Horizonte, Brasil; ³Departamento de Bioquímica e Imunologia, Instituto de Ciências Biológicas, Universidade Federal de Minas Gerais, Belo Horizonte, Brasil

*For correspondence: luoandrade@gmail.com; tcg@icb.ufmg.br

[Abstract] Cell signalling, cell secretion, and plasma membrane repair are processes that critically rely on intracellular vesicles, important components of the endocytic and secretory pathways. More specifically, the strategic distribution of intracellular vesicles is important for diverse cellular processes. The method presented here is a simple, affordable, and efficient tool to analyze the distribution of intracellular vesicles such as lysosomes, endosomes, Golgi vesicles or secretory granules under different experimental conditions. The method is an accessible way to analyze the density and dispersion of intracellular vesicles by combining immunofluorescence with pixel-based quantification software (e.g., ImageJ/FIJI). This protocol can be used widely within the scientific community because it utilizes ImageJ/FIJI, an open source software that is free. By tracking fluorescent vesicles based on their position relative to cell nuclei we are able to quantify and analyze their distribution throughout the cell.

Keywords: Intracellular vesicles, Vesicle dispersion, Endocytic vesicles, Lysosomal dispersion, ImageJ/FIJI, Fluorescence microscopy

[Background] Intracellular vesicles are important components of the endocytic and secretory pathways, which are responsible for maintaining several critical cellular functions. For this reason, many studies have focused on the pathways that regulate the distribution of vesicles in both physiological and pathological conditions, while others have examined the consequences of aberrant vesicle distribution in many important cellular processes.

In 1988, Aunis and Bader showed that two pools of secretory vesicles exist in secretory cells (Aunis and Bader, 1988). The first pool was located just below the plasma membrane and the secretion of this pool was not regulated by the cytoskeleton, but attached to the plasma membrane as a result of being bound to elements of the cytoskeleton; the second pool was attached to actin filaments, slightly away from the membrane, which could be mobilized to the inner leaflet of the plasma membrane after the depletion of the first pool. This was achieved by depolarization of the membrane, rearrangement of the actin filaments and dissolution of the cytoskeleton barrier, leading to its detachment from the cytoskeleton to reach the exocytic sites.

Koseoglu *et al.* (2011) also provided evidence for the existence of different pools of secretory vesicles and that membrane cholesterol content is important for exocytosis of these pools. The authors observed that membrane cholesterol sequestration from chromaffin cells of the adrenal medulla did not alter either the kinetics or the amount of release of the first pool of vesicles, which was already pre-anchored to the plasma membrane. However, the subsequent release of the remaining vesicles, belonging to the second slow-releasing pool, also called the reserve pool, was compromised by changes in membrane cholesterol levels. The authors further suggested that the change in the polymerization of actin filaments induced by cholesterol depletion could be compromising the mobilization of the slow releasing or reserve vesicles.

Mobilization of lysosome pools is described in several situations (Brito *et al.*, 2019; Lawrence and Zoncu, 2019). One example is plasma membrane repair (PMR), a mechanism widely used by nucleated cells to maintain plasma membrane integrity. Briefly, when a cell suffers a micro-injury, its membrane must be sealed to avoid depolarization, cytoplasm leakage and cell death. Upon injury, extracellular Ca^{2+} flows through the lesions into the cytoplasm, increasing cytoplasmic Ca^{2+} concentration, which in turn induces lysosomal exocytosis. Lysosomal exocytosis is then followed by a massive endocytosis, which reseals the plasma membrane by carrying wounded portions in endosomes into the cell. The whole process involves the participation of lysosomal hydrolases, which act on the extracellular leaflet of the plasma membrane and facilitates the endocytic process by inducing plasma membrane invagination and its inward budding (Idone *et al.*, 2008; Tam *et al.*, 2010; Castro-Gomes *et al.*, 2016).

Some parasites, such as *Trypanosoma cruzi* and *Leishmania amazonensis*, can subvert PMR to invade different host cells (Horta *et al.*, 2020). Tardieux *et al.* (1992) verified that the mobilization of lysosomes is a key event for effective cell infection by *T. cruzi*, which subverts PMR mechanism to invade cells. Hissa *et al.* (2012), studying how the protozoan parasite *T. cruzi* enters cardiomyocytes, showed that depletion of membrane cholesterol led to a decrease in host cell invasion by interfering with lysosome recruitment and fusion during parasite-host cell interaction. More recently, Cavalcante-Costa *et al.* (2019) showed that lysosomal positioning is also crucial for *L. amazonensis* invasion to non-phagocytic cells, using basically the same mechanism previously described for *T. cruzi*.

Therefore, lysosomal positioning is crucial for PMR and cell invasion by some pathogens, as well as many other cellular mechanisms. These vesicles can be found around cell nuclei or spread throughout the cell, moving fast along cell microtubules towards the cell periphery in a stop-and-go manner (Cabukusta and Neefjes, 2018), depending on cell type or special conditions, such as the presence of certain drugs or plasma membrane injury by cytotoxins. Since lysosomes function as Ca^{2+} sensitive vesicles (Rodriguez *et al.*, 1997), their positioning and exocytosis are finely regulated by the presence of this ion in the cytosol.

The examples above show that the distribution of intracellular vesicles can be disturbed by several conditions and that their correct positioning is pivotal for physiological cellular functions. Thus, it is critical to have a reliable method to measure the distribution and movement of intracellular vesicles. Here we describe a method to quantify lysosomes in cells that takes advantage of immunofluorescence, a commonly-used technique, and open source software ImageJ/FIJI (Schneider *et al.*, 2012; Schindelin

et al., 2012). This protocol provides a way for researchers to compare changes in the distribution of lysosomes in diverse processes and it can be adapted to studies involving different types of intracellular vesicles such as endosomes, Golgi vesicles or secretory granules.

Materials and Reagents

1. 13 mm round coverslips (Perfecta, catalog number: 10210013CE)
2. 24-well plates
3. Primary antibody: rat anti-LAMP1 IgG (1:50, 1D4B) or rat anti-LAMP2 IgG (1:50, ABL-93) (obtained from Developmental Studies Hybridoma Bank–DSHB–University of Iowa) or any marker of the desired vesicle
4. Alexa-Fluor-488-conjugated equivalent anti-rat secondary antibodies (Life Technologies, catalog number: A11006)
5. Texas Red Dextran (Thermo Fisher Scientific, catalog number: D1863)
6. Phosphate Buffered Saline (PBS) (Sigma-Aldrich, catalog number: P3813)
7. Bovine Serum Albumin (BSA) (Sigma-Aldrich, catalog number: A7906)
8. Saponin (Sigma-Aldrich, catalog number: S4521)
9. 4',6-Diamidino-2'-phenylindole dihydrochloride (DAPI) (Thermo Fisher Scientific, catalog number: D1306)
10. Paraformaldehyde (Vetec, catalog number: 694)

Equipment

1. Epifluorescence or confocal microscope

Software

1. ImageJ (NIH/<https://imagej.nih.gov/ij/download.html>) or "FIJI Is Just ImageJ" FIJI (NIH/<http://fiji.sc/Fiji>)

Procedure

Cell labeling:

A. Labeling of lysosomes

1. For this assay, we start with subconfluent cell monolayers. We use mouse embryonic fibroblasts (MEF) in this assay. To get subconfluent cell monolayers 24 h before the assay, we plate cells on 13 mm round coverslips at a density of 4×10^4 cells/well in 24-well plates. Treat each cell-containing well as follows.
2. Fix with 4% paraformaldehyde for 15 min.

3. Rinse 3 times with 500 μ l of PBS.
4. Block and permeabilize cells by incubating them in 500 μ l of PBS containing 2% BSA and 0.5% saponin (PBS/BSA/Saponin) for 20 min.
5. Incubate for 45 min with any of the following primary antibodies: rat anti-LAMP1 IgG (1:50, 1D4B); rat anti-LAMP2 IgG (1:50, ABL-93) (obtained from Developmental Studies Hybridoma Bank) or any desired marker.

Note: Antibodies must be diluted in PBS/BSA/Saponin solution.

6. Rinse 3 times with 500 μ l of PBS/BSA/Saponin to remove wash primary antibody.
7. Incubate for 30 min with Alexa-Fluor-488-conjugated equivalent secondary antibodies (Life Technologies), in a dilution of 1:250 in PBS/BSA/Saponin, or any appropriate labeled secondary antibody.
8. Rinse 3 times with 500 μ l of PBS/BSA/Saponin to wash secondary antibody.
9. Stain with DAPI (10 μ g/ml) to visualize cell nuclei.
10. Rinse 3 times with 500 μ l of PBS.
11. Mount coverslips on microscope slides using anti-fading mounting medium. Let the microscope slides dry overnight.
12. Analyze slides by fluorescence microscopy, acquiring images of representative cells.

Note: Use 60x and/or 100x objectives to acquire images of the entire cell. Prefer individual cells, rather than groups of cells (an alternative method for analyzing a group of cells is explained below).

B. Labeling of endocytic vesicles

1. Obtain subconfluent monolayers by plating cells on 13 mm round coverslips at a density of 4×10^4 cells/well in 24-well plates 24 h before assay.
2. At selected time points, incubate cells with Texas Red-Dextran (0.25 mg/ml) (or any other labeled dextran), a membrane impermeable fluorescent dye.

Note: If you intend to study whether a treatment or another condition can stimulate or compromise endocytosis, perform the stimuli in the presence of Texas Red-Dextran.

3. At the researcher-determined time points of treatment, rinse at least 3 times with 500 μ l of PBS to eliminate extracellular Texas-Red Dextran. This is a crucial step to avoid high background staining. Treat each cell-containing well as follows.
4. Fix with 4% paraformaldehyde (500 μ l) for 15 min.
5. Rinse 3 times with 500 μ l of PBS.
6. Follow Steps A9-A12.

Data analysis

- A. Density of lysosomes and dispersion of fluorescence intensity in perinuclear and pericellular regions
By labeling the lysosomes as described, it is possible to distinguish two regions in the cytoplasm

and measure the fluorescence intensity of labeled vesicles in these regions. The first region surrounds the nucleus, and will be referred to as the perinuclear region, which can be defined as having 0.5 of the nuclei radius. Since it is common for the nucleus to be an irregular size, or oval, a short (r) and a long (R) radius have to be defined to define the perinuclear region accordingly (adapted from Nabavi *et al.*, 2008 and as illustrated in Figure 1). Measurements will be made throughout the whole area defined by the perimeter traced around the nucleus considering the starting point from the center of the nuclei to $r + 0.5r$ or $R + 0.5R$, removing the DAPI channel. The second region (pericellular) is determined as the cell periphery ranging from the end of the perinuclear region to the border of the cell. These measurements can be made using ImageJ/FIJI software or similar. Just remember to calibrate the software to provide measurements in μm instead of pixels. To calibrate, open an image that has been taken using the same microscope (with the same objective) of an element of a well-known size, for instance a scale bar or a ruler with a micrometric scale. Using the line selection tool, draw a line with the same measures of the known element, press analyze > set scale. ImageJ/FIJI will provide the distance in pixels. Complete blank fields with the known distance and the unit (μm). The calibration can be applied to the open image or it can be applied to other images by checking the "Global" option.

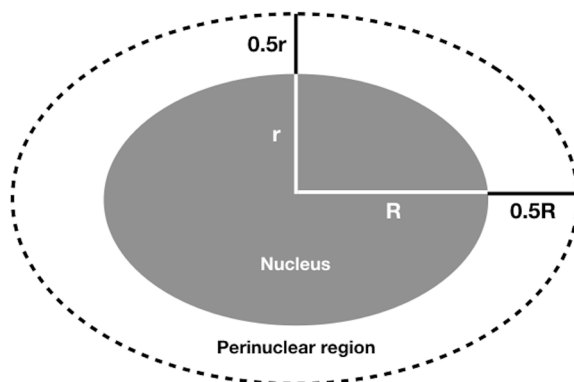


Figure 1. Definition of the perinuclear region used to quantify fluorescence-labeled vesicles distribution around an oval-shaped nucleus. r is the nucleus short radius, R is the nucleus long radius. Perinuclear region radii are calculated starting from the nuclei center as $r + 0.5r$ and $R + 0.5R$ for short and large radius, respectively, to define the area inside the perimeter obtained.

1. Using ImageJ/FIJI, open an image of the DAPI-labeled nuclei. Determine the diameters of the nucleus ($2R$ and $2r$). To do so, use the DAPI channel image, choose the Line Selection Tool to draw a line from one border to the opposite border of the DAPI staining, and measure the length of the line (make sure the parameter "Length" is set in the "Set Measurements" dialog box, then press Analyze > Measure).
2. Calculate the radii (r and R) of the nucleus.
3. Open an image of Alexa488 or Texas Red-labeled vesicles.
4. Determine the perinuclear region, as described and indicated in Figure 1.

Note: Use the composite image of DAPI and Alexa488 or Texas Red-labeled vesicle to determine the radius of the perinuclear region.

5. Once the perinuclear region sizes are established, measure fluorescence intensity inside this gated area, exclude the DAPI channel. Consider these values as Integrated Density (ID).

Note: Performed measurements can be specified in the "Set Measurements" dialog box (Analyze > Set measurements). Check "Area", "Mean Gray Value" and "Integrated Density" boxes. To create the statistics according to the defined parameters, press Analyze > Measure.

6. Measure fluorescence intensity of the whole cell image (ID).
7. Measure fluorescence intensity in at least 4 areas of the background (use Area Selection Tools) and calculate the mean gray value (mean background) of these areas.
8. Correct the Fluorescence Intensity (IDcor) of the Perinuclear region and of the whole image subtracting the mean gray value of the background (mean background) from the ID using the equation below:

$$\text{IDcor} = \text{ID} - (\text{area} \times \text{mean background})$$

9. After correcting the fluorescence intensity, determine the pericellular region using the equation below.

$$\text{Pericellular region} = \text{IDcor}_{\text{whole image}} - \text{IDcor}_{\text{perinuclear region}}$$

10. If the image contains more than one cell, use the addition of all IDcor_{perinuclear region} for the equation above. Then, normalize the result by the number of cells.
11. Plot the values as preferred.
12. When a particular effect in the distribution of the vesicles has been observed and quantified as explained above, a typical representation of the effect can be shown choosing a typical cell and obtaining the mean fluorescence intensity along a line drawn from the middle of the nuclei to cell periphery (Figure 2).

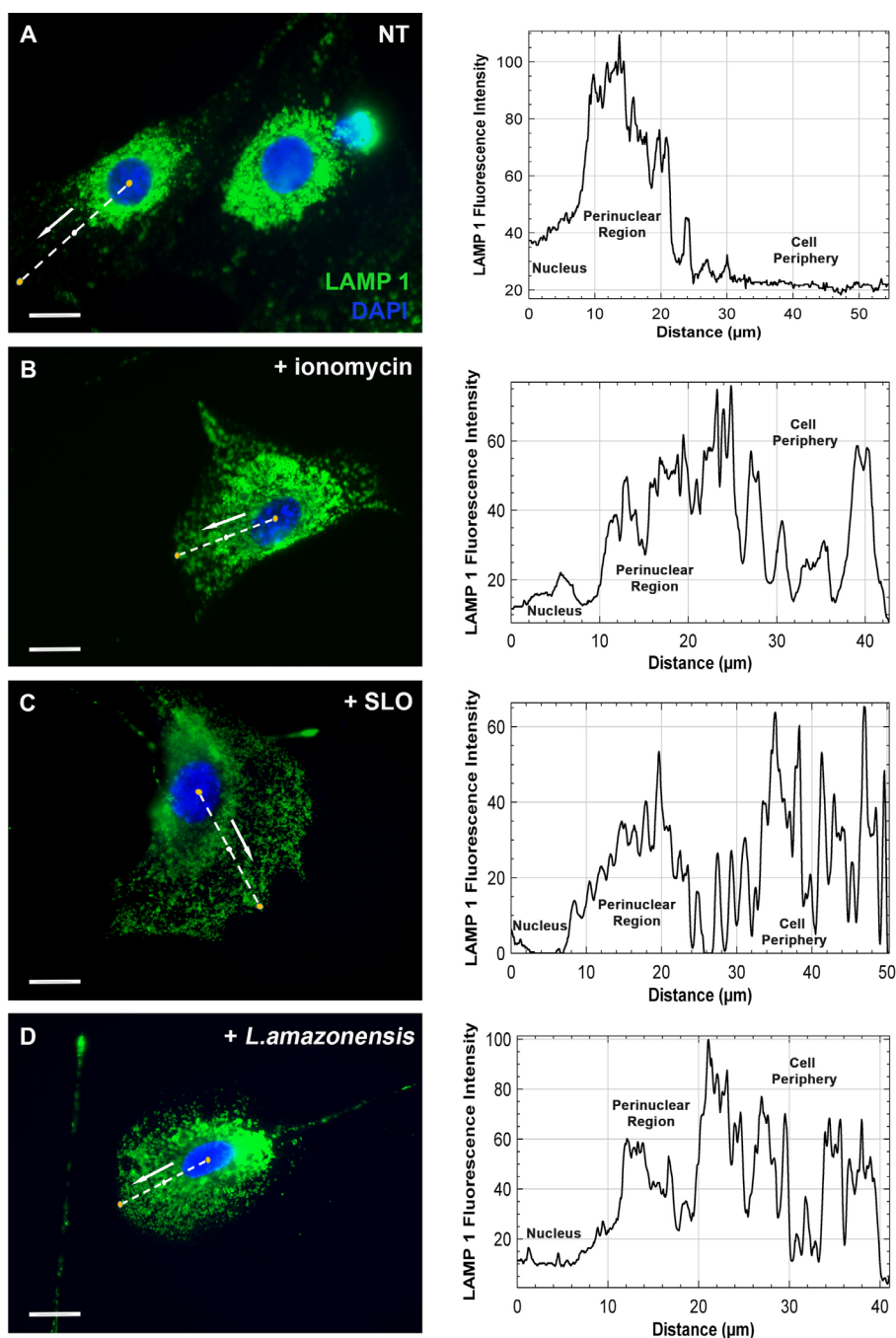


Figure 2. Lysosomes distribution in fibroblasts under different treatments. MEF cells were cultivated, treated as indicated in each image, fixed and labeled as described. Green, lysosomes (LAMP1), blue, nuclei (DAPI). **A.** Non-treated cells with its typical perinuclear cloud of lysosomes. Cells pre-treated with **B** 10 μ M ionomycin or **C** 100 ng/ml streptolysin-O (SLO), to induce Ca^{2+} influx and lysosome spread, or **D** parasite *Leishmania amazonensis* (10 per MEF) which induces Ca^{2+} -dependent lysosome spread towards the plasma membrane. For each indicated typical cell, a line was drawn from the middle of the nuclei to the edge of the cell and the fluorescence along this line is shown at the side of each image to visualize the re-distribution of the vesicles from the nuclear cloud located at the perinuclear region to cell periphery. Bars = 20 μ m.

B. Dispersion of labeled endosomal vesicles along the cell—calculating the number of vesicles from the perinuclear region to cell periphery

With this approach, it is possible to assess the distance between labeled vesicles and the center of the cell nuclei. Consequently, it generates an overview of the cell and the areas where labeled vesicles accumulate. This method is an interesting alternative to follow the occurrence of new endocytosis over time, for instance.

1. On ImageJ/FIJI, open image of the DAPI-labeled nuclei.
2. Measure mean nucleus' radius (R), or radii (r and R) when the shape of the nucleus is irregular, using the same approach described previously in steps A1-A2 of Data analysis.
3. Determine approximate center of the nucleus.
4. Open an image of the Alexa488 or Texas Red-labeled vesicles.
5. Determine the regions of interest (ROIs) around the nucleus using the area selection tools (rings) with known mean distances arising from the approximate nucleus center (D), as shown in the figure (Figure 3).

Note: To hold multiple ROIs, and manipulate them separately, select the first ROI, press Analyze > Tools > ROI Manager and press "Add". Select a second ROI and add to the ROI Manager. Repeat these steps to continue adding ROIs to the image.

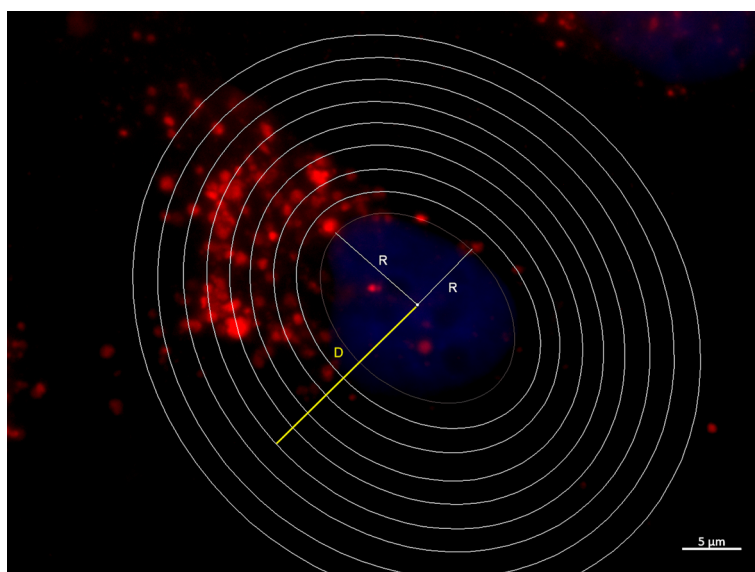


Figure 3. Definition of the areas around the nuclei used to quantify fluorescence-labeled vesicles distribution. Measurement of mean nucleus radius (R) and areas around the nuclei with a known distance (D) starting from the center of cell nucleus. The nucleus is stained with DAPI (blue) and endocytic vesicles are labeled with Texas-Red Dextran (red).

6. Determine the D/R ratio. Values close to one indicate vesicles located closer to the perinuclear area, whereas values higher than one indicate locations further from the cell center and nearer the cell border.

- Count the number of labeled vesicles (if countable) or measure the fluorescence intensity inside of each ring.

Note: Counting vesicles can be done manually or automatically by choosing the desired image and channel (type RGB or 8-bit), adjusting the threshold (Image > Adjust > Threshold) to define a better adjustment for a B&W image. Then press Process > Binary > Convert to mask (in case of touching particles, separate them by pressing Process > Binary > Watershed) and, finally, proceed to counting: Analyze > Analyze particles. In cases where you are measuring the fluorescence intensity, consider values of ID, correcting for background, as shown previously in items 5 to 8 of the alternative method described above.

- Plot values as number of vesicles (% of total) or fluorescence intensity versus D/R, as shown in figure (Figure 4).

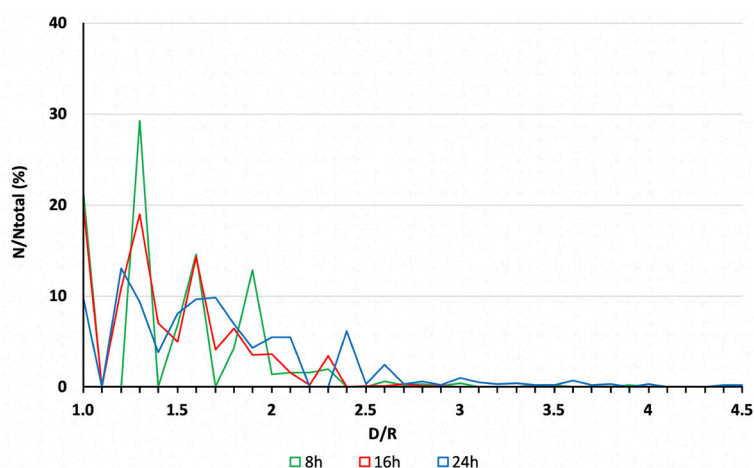


Figure 4. Example of plot. Quantitative analysis of Texas-Red Dextran labeled vesicle distribution, relative to cell nuclei, in endothelial cells (Eahy.926) over 24 h. The mean distance between a vesicle and its respective nuclei center is represented by the letter D and the mean vesicle distance relative to the mean nucleus' radius (R) was defined as the ratio of D/R. Data are expressed as the percentage of vesicles from total (N/N total) located at a specific D/R.

Acknowledgments

We acknowledge Fundação de Amparo à Pesquisa do Estado de Minas Gerais (FAPEMIG), Coordenação de Aperfeiçoamento de Pessoal de Nível Superior (CAPES), Conselho Nacional de Desenvolvimento Científico e Tecnológico (CNPq) and Instituto Nacional de Ciência e Tecnologia de Fluidos Complexos (INCT/FCx) for supporting this work and Centro de Aquisição e Processamento de Imagens (CAPI / ICB) for the fluorescence equipments. We also acknowledge the previous work of Hissa *et al.* (2012 and 2013) from which this protocol was adapted.

Competing interests

The manuscript has no conflict of interest. The funders had no role in the study design, data collection and analysis, decision to publish, or preparation of the manuscript.

References

1. Aunis, D. and Bader, M. F. (1988). [The cytoskeleton as a barrier to exocytosis in secretory cells.](#) *J Exp Biol* 139: 253-266.
2. Brito, C., Cabanes, D., Sarmiento Mesquita, F. and Sousa, S. (2019). [Mechanisms protecting host cells against bacterial pore-forming toxins.](#) *Cell Mol Life Sci* 76(7): 1319-1339.
3. Cabukusta, B. and Neefjes, J. (2018). [Mechanisms of lysosomal positioning and movement.](#) *Wiley Traffic* 19(10): 761-769.
4. Castro-Gomes, T., Corrotte, M., Tam, C. and Andrews, N. W. (2016). [Plasma Membrane Repair Is Regulated Extracellularly by Proteases Released from Lysosomes.](#) *PLoS ONE* 11(3): e0152583.
5. Cavalcante-Costa, V. S., Costa-Reginaldo, M., Queiroz-Oliveira, T., Oliveira, A. C. S., Couto, N. F., Dos Anjos, D. O., Lima-Santos, J., Andrade, L. O., Horta, M. F. and Castro-Gomes, T. (2019). [Leishmania amazonensis hijacks host cell lysosomes involved in plasma membrane repair to induce invasion in fibroblasts.](#) *J Cell Sci* 132(6).
6. Hissa, B., Duarte, J. G., Kelles, L. F., Santos, F. P., del Puerto, H. L., Gazzinelli-Guimaraes, P. H., de Paula, A. M., Agero, U., Mesquita, O. N., Guatimosim, C., Chiari, E. and Andrade, L. O. (2012). [Membrane cholesterol regulates lysosome-plasma membrane fusion events and modulates Trypanosoma cruzi invasion of host cells.](#) *PLoS Negl Trop Dis* 6(3): e1583.
7. Hissa, B., Pontes, B., Roma, P. M., Alves, A. P., Rocha, C. D., Valverde, T. M., Aguiar, P. H., Almeida, F. P., Guimaraes, A. J., Guatimosim, C., Silva, A. M., Fernandes, M. C., Andrews, N. W., Viana, N. B., Mesquita, O. N., Agero, U. and Andrade, L. O. (2013). [Membrane cholesterol removal changes mechanical properties of cells and induces secretion of a specific pool of lysosomes.](#) *PLoS One* 8(12): e82988.
8. Horta M. F. , Andrade L. O., Martins-Duarte É. S., Castro-Gomes T. (2020). [Cell invasion by intracellular parasites - the many roads to infection.](#) *J Cell Sci* 133(4): jcs232488.
9. Idone, V., Tam, C., Goss, J. W., Toomre, D., Pypaert, M. and Andrews, N. W. (2008). [Repair of injured plasma membrane by rapid Ca²⁺-dependent endocytosis.](#) *J Cell Biol* 180(5): 905-914.
10. Koseoglu, S., Love, S. A. and Haynes, C. L. (2011). [Cholesterol effects on vesicle pools in chromaffin cells revealed by carbon-fiber microelectrode amperometry.](#) *Anal Bioanal Chem* 400(9): 2963-2971.
11. Lawrence, R. E. and Zoncu, R. (2019). [The lysosome as a cellular centre for signalling, metabolism and quality control.](#) *Nat Cell Biol* 21(2): 133-142.

12. Nabavi, N., Urukova, Y., Cardelli, M., Aubin, J. E. and Harrison, R. E. (2008). [Lysosome dispersion in osteoblasts accommodates enhanced collagen production during differentiation.](#) *J Biol Chem* 283(28): 19678-19690.
13. Rodriguez, A., Webster, P., Ortego, J., Andrews, N (1997). [Lysosomes behave as Ca²⁺-regulated exocytic vesicles in fibroblasts and epithelial cells.](#) *The Journal of Cell Biology* 137 (1): 93-104.
14. Schindelin, J., Arganda-Carreras, I., Frise, E., Kaynig, V., Longair, M., Pietzsch, T., Preibisch, S., Rueden, C., Saalfeld, S., Schmid, B., Tinevez, J. Y., White, D. J., Hartenstein, V., Eliceiri, K., Tomancak, P. and Cardona, A. (2012). [Fiji: an open-source platform for biological-image analysis.](#) *Nat Methods* 9(7): 676-682.
15. Schneider, C. A., Rasband, W. S. and Eliceiri, K. W. (2012). [NIH Image to ImageJ: 25 years of image analysis.](#) *Nat Methods* 9(7): 671-675.
16. Tam, C., Idone, V., Devlin, C., Fernandes, M. C., Flannery, A., He, X., Schuchman, E., Tabas, I. and Andrews, N. W. (2010). [Exocytosis of acid sphingomyelinase by wounded cells promotes endocytosis and plasma membrane repair.](#) *J Cell Biol* 189(6): 1027-1038.
17. Tardieux, I., Webster, P., Ravestloot, J., Boron, W., Lunn, J. A., Heuser, J. E. and Andrews, N. W. (1992). [Lysosome recruitment and fusion are early events required for trypanosome invasion of mammalian cells.](#) *Cell* 71(7): 1117-1130.

9. REFERENCES

Agero, U.; Monken, C.H.; Ropert, C.; Gazzinelli, R.T.; Mesquita, O.N. Cell surface fluctuations studied with defocusing microscopy, *Phys. Rev. E Stat. Nonlinear Soft Matter Phys.* 67, 2003.

Agero, U.; Mesquita L.G.; Neves, B.R.; Gazzinelli, R.T.; Mesquita, O.N. Defocusing microscopy. *Microsc Res Tech.* v.65, n.3, p. 159-165, 2004.

Alberts B, Johnson A, Lewis J, et al. *Molecular Biology of the Cell.* 5ª Edição. New York: Garland Science; 2002.

Allen, J.A; Halverson-Tamboli, R.A; Rasenick, M.M. Lipid raft microdomains and neurotransmitter signaling. *Nature Reviews Neuroscience.* v.8, 2007.

Andrews, N.W.; Almeida, P.E.; Corotte, M. Damage control: cellular mechanisms of plasma membrane repair. *Trends in Cell Biology.* p.1–9, 2014.

Aunis, D.; Bader, M.F. The cytoskeleton as a barrier to exocytosis in secretory cells. *J. Exp Biol.* v.139, p.253–266, 1988.

Aunis, D.; Guerold, B.; Bader, M.F.; Cieselski-Treska, J. Immunocytochemical and biochemical demonstration of contractile proteins in chromaffin cells in culture, *Neuroscience* 5, p. 2261–2277, 1980.

Aviram, M. Modified forms of low density lipoprotein and atherosclerosis. *Atherosclerosis*, 98, p. 1-9, 1993.

Balzan S, Lubrano V. LOX-1 receptor: A potential link in atherosclerosis and cancer. *Life Sci.*v. 198, p.79-86, 2018

Berliner, J. A.; Watson, A.D. A role for oxidized phospholipids in atherosclerosis. *N Engl J Med.* v.353, n.1, p.9-11, 2005.

Blair, A.; Shaul, P.W.; Yuhanna, I.S.; Conrad, P.A.; Smart, E.J. Oxidized low density lipoprotein displaces endothelial nitric-oxide synthase (eNOS) from plasmalemmal caveolae and impairs eNOS activation, *J. Biol. Chem.* 274, p. 32512–32519, 1999.

Byfield, F. J., Aranda-Espinoza, H.; Romanenko, V. G.; Rothblat, G. H.; Levitan, I. Cholesterol depletion increases membrane stiffness of aortic endothelial cells. *Biophys J.* v.87, n.5, p.3336-3343, 2004.

Byfield, F. J., S. Tikku, G. H. Rothblat, K. J. Gooch and I. Levitan. OxLDL increases endothelial stiffness, force generation, and network formation. *J Lipid Res.* v.47, n.4, p. 715-723, 2006.

Brown, D.A., London, E. Structure and function of sphingolipid- and cholesterol-rich membrane rafts, *J. Biol. Chem.* 275, p.17221–17224, 2000.

- Boucher, E.; Mandato, C.A. Plasma membrane and cytoskeleton dynamics during single-cell wound healing, *Biochim. Biophys. Acta* 1853, p. 2649–2661, 2015.
- Burgoyne, R.D.; Cheek, T.R. Reorganisation of peripheral actin filaments as a prelude to exocytosis, *Biosci. Rep.* 7, p. 281–288, 1987.
- Cabukusta, B.; Neefjes, J. Mechanisms of lysosomal positioning and movement. *Traffic*.19:761–769, 2018.
- Castro-Gomes, T.; Corrotte, M.; Tam, C.; Andrews, N.W. Plasma membrane repair is regulated Extracellularly by proteases released from lysosomes, *PLoS One* 11, 2016.
- Cheek, T.R.; Burgoyne, R.D. Nicotine-evoked disassembly of cortical actin filaments in adrenal chromaffin cells, *FEBS Lett.* 207p. 110–114, 1986.
- Chen, X.; Leow, R.S.; Hu, Y.; Wan, J.M.; Yu, A.C. Single-site sonoporation disrupts actin cytoskeleton organization, *J. R. Soc. Interface* 11, 2014.
- Cheng C, Tempel D, van Haperen R, et al. Atherosclerotic lesion size and vulnerability are determined by patterns of fluid shear stress. *Circulation.* v. 113, p. 2744-53, 2006.
- Cheng C, Tempel D, van Haperen R, et al. Shear stress-induced changes in atherosclerotic plaque composition are modulated by chemokines. *J Clin Invest.* v. 117, n. 3, p. 616-626, 2007.
- Chouinard, J.A., Grenier, G.; Khalil, A.; Vermette, P. Oxidized-LDL induce morphological changes and increase stiffness of endothelial cells. *Exp Cell Res* v.314, n.16., p. 3007-3016, 2008.
- Chubinskiy-Nadezhdin, V.I.; Negulyaev, Y.A.; Morachevskaya, E.A. Cholesterol depletion-induced inhibition of stretch-activated channels is mediated via actin re-arrangement, *Biochem. Biophys. Res. Commun.* 412, p. 80–85, 2011.
- Coelho Neto, J.; Agero, U.; Gazzinelli, R.T.; Mesquita, O.N. Measuring optical and mechanical properties of a living cell with defocusing microscopy, *Biophys. J.* 91, p. 1108–1115, 2006.
- Couto, NF; Queiroz-Oliveira, T.; Horta, M.F; Castro-Gomes, T.; Andrade, L.O. Measuring intracellular vesicle density and dispersion using fluorescence labeling. *Bio-Protocol*, v.10, n. 15, 2020.
- Cremesti, A.E.; Goni, F.M.; Kolesnick, R. Role of sphingomyelinase and ceramide in modulating rafts: do biophysical properties determine biologic outcome? *FEBS Lett.* v.531, p.47–53, 2002.
- Criqui, M.H. Epidemiology of atherosclerosis: an updated overview. *Am J Cardiol*, v. 57 p. 18C-23C, 1988.

Dardik, A.; Chen, L.; Frattini, J.; Asada, H.; Aziz, F.; Kudo, F.A.; Sumpio, B.E. Differential effects of orbital and laminar shear stress on endothelial cells, *J. Vasc. Surg.* 41, p.869–880, 2005.

De Flora, S.; Izzotti, A.; Walsh, D.; Degan, P.; Petrilli, G.L.; Lewtas, J. Molecular epidemiology of atherosclerosis. *The FASEB Journal*, v.11, 1997.

De Wilde D, Trachet B, De Meyer GRY, Segers P. Shear Stress Metrics and Their Relation to Atherosclerosis: An In Vivo Follow-up Study in Atherosclerotic Mice. *Annals of Biomedical Engineering.* v. 44, n. 8, p. 2327–2338, 2015,

Fisher AB *et al.* Endothelial cellular response to altered shear stress. *Am J Physiol Lung Cell Mol Physiol.* v. 281, p. L529–L533, 2001.

Fraga-Silva RA, Savergnini SQ, Montecucco F, Nencioni A, Caffa I, Soncini D, Costa-Fraga FP, De Sousa FB, Sinisterra RD, Capettini LA, Lenglet S, Galan K, Pelli G, Bertolotto M, Pende A, Spinella G, Pane B, Dallegri F, Palombo D, Mach F, Stergiopoulos N, Santos RA, da Silva RF. Treatment with Angiotensin-(1-7) reduces inflammation in carotid atherosclerotic plaques. *Thromb Haemost.* 2014 Feb 6;111(4).

Gil, C.; Soler-Jover, A.; Blasi, J.; Aguilera, J. Synaptic proteins and SNARE complexes are localized in lipid rafts from rat brain synaptosomes. *Biochemical and Biophysical Research Communications.* v.329, n.1, p.117–124, 2005.

Hansson, G. K.; Robertson, A. K., Soderberg-Naucler, C. Inflammation and atherosclerosis. *Annual Review of Pathology.* v. 1, p. 297–329, 2006.

Hanzal-Bayer, M.F.; Hancock, J.F. Lipid rafts and membrane traffic. *FEBS Letters.* v.581, n.11, p.2098–2104, 2007.

Head, B.P.; Patel, H.H.; Insel, P.A. Interaction of membrane/lipid rafts with the cytoskeleton: Impact on signaling and function: Membrane/lipid rafts, mediators of cytoskeletal arrangement and cell signaling. *Biochimica et Biophysica Acta – Biomembranes.* v.1838, n.2, p.532–545, 2014.

Hissa, B., Duarte, J.G.; Kelles, L.F.; Santos, F.P.; del Puerto, H.L.; Gazzinelli-Guimaraes, P.H.; de Paula, A.M.; Agero, U.; Mesquita, O.N.; Guatimosim, C.; Chiari, E.; Andrade, L.O. Membrane cholesterol regulates lysosome-plasma membrane fusion events and modulates *Trypanosoma cruzi* invasion of host cells. *PLoS Negl Trop Dis.* v.6, n.3, e1583, 2012.

Hissa, B., Pontes, B.; Roma, P.M.; Alves, A.P.; Rocha, C.D.; Valverde, T.M.; Aguiar, P.H.; Almeida, F.P.; Guimaraes, A. J.; Guatimosim, C.; Silva, A.M.; Fernandes, M.C.; Andrews, N.W.; Viana, N.B.; Mesquita, O.N.; Agero, U.; Andrade, L.O. Membrane cholesterol removal changes mechanical properties of cells and induces secretion of a specific pool of lysosomes. *PLoS One.* v.8, n. 12, e82988, 2013.

Hofmann A, Brunssen C, Morawietz H. Contribution of lectin-like oxidized low-density lipoprotein receptor-1 and LOX-1 modulating compounds to vascular diseases. *Vascul Pharmacol.* pii: S1537-1891(17)30171-4, 2017.

- Hong, Z.; Staiculescu, M. C.; Hampel, P.; Levitan, I.; Forgacs, G. How cholesterol regulates endothelial biomechanics. *Frontiers in Physiology*. v.3, 2012.
- Idone, V.; Tam, C.; Goss, J.W.; Toomre, D.; Pypaert, M.; Andrews, N.W. Repair of injured plasma membrane by rapid Ca²⁺-dependent endocytosis. *J Cell Biol*. v.180, n.5, p.905-914, 2008.
- Idone, V.; Tam, C.; Andrews, N.W. Two-way traffic on the road to plasma membrane repair, *Trends Cell Biol*. 18, p. 552–559, 2008.
- Ikonen, E. Cellular cholesterol trafficking and compartmentalization. *Nature Reviews Molecular Cell Biology*. v.9, p. 125-138, 2008.
- Koseoglu, S.; Love, S.A.; Haynes, C.L. Cholesterol effects on vesicle pools in chromaffin cells revealed by carbon-fiber microelectrode amperometry. *Anal Bioanal Chem*. v.400, p.2963–2971, 2011.
- Kowalsky, G. B.; Byfield, F. J.; Levitan, I. (2008). oxLDL facilitates flow-induced realignment of aortic endothelial cells. *Am J Physiol Cell Physiol*. v.295, n.2, p. 332-340.
- Kwik, J.; Boyle, S.; Fooksman, D.; Margolis, L. et al. Membrane cholesterol, lateral mobility and the phosphatidylinositol 4,5 biphosphate –dependent organization of cell actin. *PNAS*. v.100,n.24, p.13964- 13969, 2003.
- Lafont, F.; van der Goot, F. G. Bacterial invasion via lipid rafts. *Cellular Microbiology*, v.7, n.5, p.613–620, 2005.
- Lang, T et al. SNAREs are concentrated in cholesterol-dependent clusters that define docking and fusion sites for exocytosis. *EMBO J*. 20(9): 2202–2213, 2001.
- Lang, T.; Wacker, I.; Wunderlich, I.; Rohrbach, A.; Giese, G.; Soldati, T.; Almers, W. Role of actin cortex in the subplasmalemmal transport of secretory granules in PC-12 cells, *Biophys. J*. 78, p.2863–2877, 2000.
- Lange, Y.; Steck, T.L. Active membrane cholesterol as a physiological effector. *Chem. Phys. Lipids*, 2016.
- Levitan, I.; Gooch, K.J. Lipid rafts in membrane- cytoskeleton interactions and control of cellular biomechanics: actions of oxLDL. *Antioxidants and Redox Signaling*, v.9, n. 9, p. 1519-1534, 2007.
- Levitan, I.; Shentu, T.P. Impact of oxLDL on cholesterol-rich membrane rafts, *J Lipids* 2011.
- Li, J.; Pfeffer, S.R. Lysosomal membrane glycoproteins bind cholesterol and contribute to lysosomal cholesterol export, *eLife* 5, 2016.
- Liao, L.; Granger, D. N. Modulation of oxidized low-density lipoprotein-induced microvascular dysfunction by nitric oxide. *Am J Physiol*. v.268, p.1643-1650, 1995.

- Libby, P.; Ridker, P.M.; Hansson, G.K. Progress and challenges in translating the biology of atherosclerosis. *Nature*. v.473, n. 7347, p.317-325, 2011.
- Libby, P.; Ridker, P.M.; Maseri, A. Inflammation and Atherosclerosis. *Circulation*, n. 105, p.1135-1143, 2002.
- Malek AM *et al.* Hemodynamic shear stress and its role in atherosclerosis. *JAMA* v. 282, p. 2035–2042, 1999.
- Martinez, I.; Chakrabarti, S.; Hellevik, T.; Morehead, J.; Fowler, K.; Andrews, N.W. Synaptotagmin VII regulates Ca(2+)-dependent exocytosis of lysosomes in fibroblasts, *J. Cell Biol.* 148, p. 1141–1149, 2000.
- Martins, I.J.; Berger, T.; Sharman, M.J.; Verdile, G.; Fuller, S.J.; Martins, R.N. Cholesterol metabolism and transport in the pathogenesis of Alzheimer's disease, *J. Neurochem.* 111, p.1275–1308, 2009.
- McNeil, P.L.; Miyake, K.; Vogel, S.S. The endomembrane requirement for cell surface repair. *Proc. Natl. Acad. Sci. USA* . v.100, p.4592 – 4597, 2003.
- Miklavc, P.; Wittekindt, O.H.; Felder, E.; Dietl, P. Ca²⁺-dependent actin coating of lamellar bodies after exocytotic fusion: a prerequisite for content release or kiss-and-run. *Ann N Y Acad Sci.* v.1152, p.43–52, 2009.
- Moore, K.; Tabas, I. Macrophages in the Pathogenesis of Atherosclerosis. *Cell*, n. 145, April 29, 2011.
- Muallen, S.; Kwiatkowska, K.; Xu, X.; Yin, H.L. Actin filament disassembly is a sufficient trigger for exocytosis in non-excitabile cells. *J Cell Biol.* v.128, p.589–598, 1995.
- Murray, D.; Tamm, L.K. Clustering of Syntaxin-1A in Model Membranes is Modulated by Phosphatidylinositol-4,5-bisphosphate and Cholesterol. *Biochemistry.* v.48, n.21, p. 4617–4625, 2009.
- Nakata, T.; Hirokawa, N. Organization of cortical cytoskeleton of cultured chromaffin cells and involvement in secretion as revealed by quick-freeze, deepetching, and double-label immunoelectron microscopy. *J Neurosci.* v.12, p. 2186–2197, 1992.
- Pendleton, A.; Koffer, A. Effects of latrunculin reveal requirements for the actin cytoskeleton during secretion from mast cells. *Cell Motil Cytoskeleton.* v.48, p. 37–51, 2001.
- Pike, L.J. Rafts defined: a report on the Keystone Symposium on Lipid Rafts and Cell Function. *Journal of Lipid Research.* v.47, n.7, p.1597-1598, 2006.
- Pike, L.J.; Miller, J.M. Cholesterol depletion delocalizes phosphatidylinositol bisphosphate and inhibits hormone-stimulated phosphatidylinositol turnover. *J Biol Chem.* v. 273, n. 35, p.22298-304, 1998.
- Pirillo, A.; Norata, G.D.; Catapano, A.L. LOX-1, OxLDL, and Atherosclerosis. *Mediators of Inflammation*, 2013.

Pomorski, T.; Hrafnadóttir, S.; Devaux, P.F.; Van Meer, G. Lipid distribution and transport across cellular membranes. *Cell & Developmental Biology*, v. 12, p. 139–148, 2001.

Oh MJ, C. Zhang, E. LeMaster, C. Adamos, E. Berdyshev, Y. Bogachkov, E.E. Kohler, J. Baruah, Y. Fang, D.E. Schraufnagel, K.K. Wary, I. Levitan, Oxidized LDL signals through Rho-GTPase to induce endothelial cell stiffening and promote capillary formation, *J Lipid Res*, 57 (2016) 791-808.

Qi, M.; Liu, Y.; Freeman, M.R.; Solomon, K.R. Cholesterol-Regulated Stress Fiber run. *Ann N Y Acad Sci*. v.1152, p. 43–52, 2009.

Reddy, A.; Caler, E.; Andrews, N. Plasma membrane repair is mediated by Ca²⁺-regulated exocytosis of lysosomes. *Cell*. v.106, p.157-169, 2001.

Rodriguez-Flores, M.; Rodriguez-Saldaña, J.; Cantú-Brito, C.; Aguirre-Garcia, J.; Alejandro, G.G. Prevalence and severity of atherosclerosis in different arterial territories and its relation with obesity. *Cardiovascular Pathology*. v.22, p. 332–338, 2013.

Rudolf, R.; Kogel, T.; Kuznetsov, S.A.; Salm, T.; Schlicker, O.; Hellwig, A.; Hammer 3rd, J.A.; Gerdes, H.H. Myosin Va facilitates the distribution of secretory granules in the F-actin rich cortex of PC12 cells, *J. Cell Sci*. 116 p. 1339–1348, 2003.

Sampath R, Kukielka GL, Smith CW, Eskin SG, McIntire LV. Shear stress-mediated changes in the expression of leukocyte adhesion receptors on human umbilical vein endothelial cells in vitro. *Ann Biomed Eng*. v. 23, p. 247-256, 1995.

Sawamura T., et al. An endothelial receptor for oxidized low-density lipoprotein, *Nature* 386(6620)73-7, 1997.

Segers D., J.A. Lipton, P.J.M. Leenen, C. Cheng, D. Tempel, H.J. Duckers, G. Pasterkamp, F.L. Moll, R. de Crom, R. Krams. Atherosclerotic Plaque Stability is Affected by the Chemokine CXCL10 in Both Mice and Humans. *Int J Inflam*. 2011;2011:936109.

Shentu, T.P; Titushkin, I.; Singh, D.K.; Gooch, K.J.; Subbaiah, P.V; Cho, M.; Levitan, I. oxLDL-induced decrease in lipid order of membrane domains is inversely correlated with endothelial stiffness and network formation. *Am J Physiol Cell Physiol*. v. 299, n.2, C218–C229, 2010.

Shentu, T.P.; Singh, D. K.; Oh, M.J.; Sun, S.; Sadaat, L.; Makino, A.; Mazzone, T.; Suabbaiah, P.V.; Cho, M.; Levitan, I. The role of oxysterols in control of endothelial stiffness. *J Lipid Res.*, v. 53, n. 7, p. 1348–1358, 2012.

Simons, K.; Ehehalt, R. Cholesterol, lipid rafts, and disease, *J. Clin. Invest*. 110 p.597–603, 2002.

Skruzny, M.; Brach, T.; Ciuffa, R.; Rybina, S.; Wachsmuth, M.; Kaksonen, M. Molecular basis for coupling the plasma membrane to the actin cytoskeleton

during clathrin-mediated endocytosis, *Proc. Natl. Acad. Sci. U. S. A.* 109, E2533–E2542, 2012.

Smythe, E.; Ayscough, K.R. Actin regulation in endocytosis, *J. Cell Sci.* 119 p. 4589–4598, 2006.

Strydom HC, Chandler AB, Dinsmore RE, Fuster V, Glagov S, Insull W, Rosenfeld ME, Schwartz CJ, Wagner WD, Wissler RW. A definition of advanced types of atherosclerotic lesions and a histological classification of atherosclerosis. A report from the committee on vascular lesions of the council on arteriosclerosis, American Heart Association. *Arterioscler Thromb Vasc Biol.* 1995;15:1512-1531

Strydom HC. Natural history and histological classification of atherosclerotic lesions: An update. *Arterioscler Thromb Vasc Biol.* 2000;20:1177-1178

Steinberg, D. The LDL modification hypothesis of atherogenesis: an update. *J Lipid Res.* v.50, p.376-381, 2009.

Steinberg, D.; Witztum, J.L. Oxidized low-density lipoprotein and atherosclerosis. *Arterioscler Thromb Vasc Biol.* v.30, n.12, p.2311-2316, 2010.

Steinbrecher, U.P.; Zhang, H.; Loughheed, M. Role of oxidatively modified LDL in atherosclerosis. *Free Radical Biology & Medicine*, v. 9, p. 155-168, 1990.

Suciu CF, Prete M, Ruscitti P, Favoino E, Giacomelli R, Perosa F. Oxidized low density lipoproteins: The bridge between atherosclerosis and autoimmunity. *Autoimmunity Reviews*, v. 17, Issue 4, p. 366-375, 2018.

Sun, M.; Northrup, N.; Marga, F.; Huber, T.; Byfield, F.J.; Levitan, I.; Forgacs, G. The effect of cellular cholesterol on membrane-cytoskeleton adhesion, *J. Cell Sci.* 120, p.2223–2231, 2007.

Tam et al. Exocytosis of acid sphingomyelinase by wounded cells promotes endocytosis and plasma membrane repair. *J. Cell Biol.* v.189, n. 6, p.1027–1038, 2010.

Van De Graaff, K.M. *Human Anatomy*. McGraw-Hill Company, 6ª edição, 2001.

Van Meer, G.; Voelker, D.R.; Feigenson, G.W. Membrane lipids: where they are and how they behave. *Nat Rev Mol Cell Biol*, 2009.

Walker, H.K.; Hall, W. D.; Hurst, J.W. *Clinical Methods: The History, Physical, and Laboratory Examinations*. Emory University School of Medicine, Atlanta, Georgia. Boston: Butterworths; 3ª edição, 1990.

Walpola PL, Gotlieb AI, Langille BL. Monocyte adhesion and changes in endothelial cell number, morphology, and F-actin distribution elicited by low shear stress in vivo. *Am J Pathol.* v. 142, p. 1392-1400, 1993.

Walpola PL, Gotlieb AI, Cybulsky MI, Langille BL. Expression of icam-1 and vcam-1 and monocyte adherence in arteries exposed to altered shear stress. *Arterioscler Thromb Vasc Biol.* v. 15, p. 2-10, 1995.

World Health Organization. Cardiovascular diseases [Internet]. Access in January 2015. Available at: <http://www.who.int/mediacentre/factsheets/fs317/en/>.

Zechel, K. Stability differences of muscle F-actin in formamide in the presence of Mg²⁺ and Ca²⁺, *Biochim. Biophys. Acta* 742, p.135–141, 1983.

Zhang, J.; Liu, Q. Cholesterol metabolism and homeostasis in the brain, *Protein Cell* 6, p.254–264, 2015).

Ziegler T, Silacci P, Harrison VJ, Hayoz D. Nitric oxide synthase expression in endothelial cells exposed to mechanical forces. *Hypertension* 32, p.351-355, 1998

Ziegler T, Bouzourene K, Harrison VJ, Brunner HR, Hayoz D. Influence of oscillatory and unidirectional flow environments on the expression of endothelin and nitric oxide synthase in cultured endothelial cells. *Arterioscler Thromb Vasc Biol.* 18, p.686-692, 1998.